
Dephasing in disordered systems at low temperatures

Maximilian Treiber



München 2013

Dephasing in disordered systems at low temperatures

Maximilian Treiber

Dissertation
an der Fakultät für Physik
der Ludwig–Maximilians–Universität
München

vorgelegt von
Maximilian Treiber
aus Göttingen

München, den 25.04.2013

Erstgutachter: Prof. Dr. Jan von Delft
Zweitgutachter: Prof. Dr. Igor V. Lerner
Tag der mündlichen Prüfung: 06.06.2013

Table of Contents

Deutsche Zusammenfassung	1
List of publications	3
1 Introduction, motivation and overview	5
2 Dephasing in disordered systems	9
2.1 Electrons in disordered systems	9
2.1.1 Diagrammatic approach to disorder	10
2.1.2 Disorder averaged correlation functions	11
2.1.3 Magnetic field dependence and time-reversal symmetry	19
2.1.4 Validity of the loop-expansion	21
2.1.5 Field theoretical approaches	22
2.1.6 Comparison with random matrix theory	23
2.2 Dephasing due to electron interactions	28
2.2.1 Keldysh perturbation theory	28
2.2.2 Electron interactions in disordered systems	29
2.2.3 Quasi-particle lifetime of electrons in disordered systems	32
2.2.4 Diagrammatic calculation of the dephasing time	37
2.2.5 Regimes of dephasing	43
2.2.6 Electronic noise and the semi-classical picture of dephasing	45
2.3 To be published: Two-loop calculation of the generalized diffusion propagator	49
2.3.1 Dimensional regularization	49
2.3.2 Ballistic regularization	52
2.3.3 Conclusions	57
2.4 Publication: Thermal noise and dephasing due to electron interactions in nontrivial geometries	61
3 Quantum corrections to the conductance	71
3.1 The conductance of disordered metals	71
3.1.1 The classical conductance	71
3.1.2 Quantum corrections to the conductance: weak localization	75
3.1.3 Universal conductance fluctuations	78
3.2 The random matrix theory of quantum transport	80
3.2.1 Conductance as a scattering problem	80
3.2.2 Quantum corrections	81
3.2.3 Models of dephasing	83
3.3 Dephasing in non-trivial geometries	84

3.3.1	Confined geometries	85
3.3.2	Networks of wires	86
3.4	Publication: Dimensional crossover of the dephasing time in disordered mesoscopic rings	91
3.5	Publication: Dimensional Crossover of the Dephasing Time in Disordered Mesoscopic Rings: From Diffusive through Ergodic to 0D Behavior	97
3.6	Publication: Transport and dephasing in a quantum dot: Multiply connected graph model	125
4	Quantum corrections to the polarizability	137
4.1	Isolated systems: Realizing the canonical ensemble	137
4.2	The polarizability in the random phase approximation	139
4.3	Results from RMT and the sigma-model	140
4.4	Overview of recent experiments	146
4.5	Preprint: Quantum Corrections to the Polarizability of Isolated Disordered Metals	149
5	Summary and conclusions	163
A	Source code listings	167
A.1	Calculation of the two-loop Hikami boxes	167
	Bibliography	177
	Acknowledgments	187
	Curriculum vitae	189

Abstract

The transition from quantum to classical behavior of complex systems, known as *dephasing*, has fascinated physicists during the last decades. Disordered systems provide an insightful environment to study the *dephasing time* τ_φ , since electron interference leads to quantum corrections to classical quantities, such as the weak-localization correction Δg to the conductance, whose magnitude is governed by τ_φ . In this thesis, we study one of the fundamental questions in this field: How does *Pauli blocking* influence the interaction-induced dephasing time at low temperatures? In general, Pauli blocking limits the energy transfer ω of electron interactions to $\omega \ll T$, which leads to an increase of τ_φ . However, the so-called 0D regime of dephasing, reached at $T \ll E_{\text{Th}}$, is practically the only relevant regime, in which Pauli blocking significantly influences the temperature dependence of τ_φ . Despite of its fundamental physical importance, 0D dephasing has not been observed experimentally in the past. We investigate several possible scenarios for verifying its existence: (1) We analyze the temperature dependence of Δg in open and confined systems and give detailed instructions on how the crossover to 0D dephasing can be reliably detected. Two concrete examples are studied: an almost isolated ring and a new quantum dot model. However, we conclude that in transport experiments, 0D dephasing unavoidably occurs in the universal regime, in which all quantum corrections to the conductance depend only weakly on τ_φ , and hence carry only weak signatures of 0D dephasing. (2) We study the quantum corrections to the polarizability $\Delta\alpha$ of isolated systems, and derive their dependence on τ_φ and temperature. We show that 0D dephasing occurs in a temperature range, in which $\Delta\alpha$ depends strongly (as a power-law) on τ_φ , making the quantum corrections to the polarizability an ideal candidate to study dephasing at low temperatures and the influence of Pauli blocking.

A detailed summary of the of the contents of this thesis may be found at the end of Chapter 1, and in the concluding Chapter 5.

Deutsche Zusammenfassung

Diese Doktorarbeit beschäftigt sich mit der Theorie der Dephasierung in ungeordneten mesoskopischen Systemen. Bei niedrigen Temperaturen wird das Pauli'sche Ausschlussprinzip wichtig und bewirkt eine Schwächung der Wirkung von Elektronenwechselwirkungen, da Streuprozesse mit Energien $\omega \ll T$ aufgrund des Nichtvorhandenseins möglicher Streuzustände ausgeschlossen sind. Wir analysieren den Einfluss des Pauli-Prinzips auf die wechselwirkungsinduzierte Dephasierungsrate γ und diskutieren mögliche Experimente, die den Einfluss des Pauli-Prinzips demonstrieren.

Die Arbeit ist in 4 Kapitel aufgeteilt, in denen wir zunächst den aktuellen Stand der Forschung beschreiben und eine kurze Zusammenfassung unserer Ergebnisse präsentieren. Details unserer Ergebnisse finden sich in Veröffentlichungen am Ende jedes Kapitels. Eine graphische Zusammenfassung unserer Hauptkenntnisse findet sich in dem abschliessenden Kapitel 5, siehe Fig. 5.1.

Kapitel 1 beinhaltet eine allgemeine Einführung in die Thematik, gefolgt von einer Diskussion unserer Motivation. Des Weiteren findet sich hier eine kurze Darstellung der Gliederung dieser Arbeit.

In Kapitel 2 stellen wir die Standardmethoden der mesoskopischen Physik vor: die perturbative Schleifenentwicklung in diffusiven Propagatoren und die nicht-perturbative Theorie der Zufallsmatrizen. Wir besprechen die üblichen Herleitungen der Dephasierungsrate: (1) mittels einer Störungstheorie in der Elektronenwechselwirkung und (2) mittels eines Pfadintegrals mit effektivem Rauschpotential. Wir kommen zu dem Schluss, dass die Temperaturabhängigkeit der Dephasierungsrate durch eine einfache selbstkonsistente Integralgleichung hinreichend beschrieben wird. Des Weiteren stellen wir fest, dass nur in dem sog. 0D Dephasierungsregime, erreicht bei Temperaturen $T \ll E_{\text{Th}}$, das Pauli-Prinzip einen signifikanten Einfluss auf das Temperaturverhalten der Dephasierungsrate hat. Dieses 0D Regime konnte jedoch trotz zahlreicher Versuche bisher nicht experimentell nachgewiesen werden. Im Folgenden haben wir uns daher auf die Beschreibung eines solchen Nachweises konzentriert. Von besonderer Bedeutung sind die folgenden Eigenschaften des 0D Regimes: (1) Es beschreibt ein System mit diskreten Energieniveaus, welches im Allgemeinen nicht mehr mit Hilfe der Schleifenentwicklung beschrieben werden kann. (2) Die 0D Dephasierungsrate ist so klein, dass die relevanten Elektronentrajektorien das ganze System ausfüllen und daher von der Geometrie des Systems abhängig werden. Unser erstes Hauptergebnis in diesem Kapitel ist die Berechnung der Zwei-Schleifen-Korrektur zum verallgemeinerten Diffusionspropagator, in der wir eine neue Methode zur Berechnung der kurzreichweitigen Teile (die sogenannten Hikami-Boxen) der zugehörigen Diagramme vorschlagen. Die neue Methode kann direkt auf die Berechnung von Diagrammen höherer Ordnung und verwandte physikalische Probleme ausgedehnt werden. Unser zweites Hauptergebnis ist die Herleitung eines neuartigen Dephasierungsratenfunktional, welches Dephasierung bei beliebigen Temperaturen und in nicht-trivialen Geometrien, insbesondere Netzwerken von Drähten, beschreibt.

Kapitel 3 befasst sich mit der Leitwertkorrektur Δg aufgrund von schwacher Lokalisierung, welche in offenen Systemen einen universellen Wert ~ 1 annimmt, sobald $\gamma \ll E_{\text{Th}}$. Da zudem $T \ll \gamma$ gilt, liegt das 0D Dephasierungsregime in einem Temperaturbereich, in dem Δg praktisch nicht mehr von

γ abhängt. Nichtsdestotrotz kann ein Nachweis von 0D Dephasierung in solchen Systemen gelingen, indem die Kurve $\Delta g(T)$ vom universellen Leitwert bei $T \rightarrow 0$ abgezogen wird. Wir argumentieren, dass ein verhältnismäßig kleiner Leitwert in Verbindung mit stark absorbierenden Zuleitungen einen Nachweis von 0D Dephasierung ermöglichen könnte. Des weiteren befassen wir uns mit der Transporttheorie der Zufallsmatrizen, welche "eingeschlossene" Systeme beschreibt, in denen die Elektronentrajektorien den gesamten Raum des Systems ergodisch ausfüllen. Solche Systeme lassen sich mit Hilfe einer sogenannten Verweilzeit τ_{dw} beschreiben, und wir schlagen ein Modell vor, welches Dephasierung in annähernd isolierten Systemen beschreibt. Unser erstes Hauptergebnis in diesem Kapitel ist eine detaillierte Beschreibung der Temperaturabhängigkeit von Δg eines annähernd isolierten Rings. Wir zeigen, dass die Ringgeometrie besonders gut geeignet ist, um den Übergang zu 0D Verhalten zu untersuchen, da aufgrund des Aharonov-Bohm-Effekts die Beiträge zum Leitwert vom Ring von den störenden Beiträgen der Zuleitungen getrennt werden können. Unser zweites Hauptergebnis ist die Beschreibung der Dephasierung in einem Quantenpunktmodell, welches (1) auf der Theorie der Diffusion in Graphen und (2) auf dem Dephasierungsratenfunktional, hergeleitet in Kapitel 2, basiert. Unser Modell beschreibt die Leitwertkorrektur aufgrund von schwacher Lokalisierung bei beliebigen Temperaturen und kann ohne Umschweife auf kompliziertere Geometrien erweitert werden. Wir folgern, dass eingeschlossene Systeme sich besser eignen, um den Übergang zu 0D Verhalten zu untersuchen, jedoch tritt 0D Dephasierung unausweichlich im universellen Regime auf, solange der Leitwert der Kontakte zu den Zuleitungen größer als 1 ist.

In Kapitel 4 beschäftigen wir uns mit isolierten Systemen, in denen $\tau_{dw} \rightarrow \infty$. Insbesondere befassen wir uns mit den Quantenkorrekturen zur Polarisierbarkeit $\Delta\alpha$ eines Ensembles von isolierten und geordneten Metallen. Bisherige Beschreibungen von $\Delta\alpha$, die auf einer Kombination der Theorie der Zufallsmatrizen und dem nicht-linearen σ -Modell basierten, konnten die Frequenzabhängigkeit erklären, beschrieben jedoch nicht die Dephasierung bei endlichen Temperaturen. Unser Hauptergebnis ist eine Herleitung von $\Delta\alpha$ mittels der Schleifenentwicklung, welche uns ermöglicht, die Temperaturabhängigkeit zu beschreiben, und welche sowohl für verbundene (Großkanonisches Ensemble) als auch isolierte (Kanonisches Ensemble) Systeme anwendbar ist. Wir konnten zeigen, dass, im Gegensatz zu Δg , der Übergang zum 0D Regime in einem Temperaturbereich auftritt, in dem $\Delta\alpha$ einem Potenzgesetz in γ folgt. Unsere Ergebnisse stimmen gut mit vorherigen Experimenten überein und legen nahe, dass 0D Dephasierung in den beobachteten Magnetooszillationen gefunden wurde. Aufgrund der kleinen Zahl an relevanten Datenpunkten bleibt dies jedoch derzeit eine Hypothese, die erst in zukünftigen Experimenten hinreichend belegt werden kann. Nichtsdestotrotz folgern wir, dass sich die Quantenkorrekturen zur Polarisierbarkeit besonders für die Untersuchung von Dephasierung bei niedrigen Temperaturen eignen. Insbesondere lässt sich der Übergang zum 0D Regime und der Einfluss des Pauli-Prinzips hervorragend untersuchen. Es bleibt zu hoffen, dass unsere theoretischen Ergebnisse zu neuen Experimenten in dieser Richtung führen werden.

List of publications

During the work for this thesis the following articles have been published in peer-reviewed journals, as a chapter in a book, or made available as preprints:

1. *Dimensional crossover of the dephasing time in disordered mesoscopic rings*, MT, O. M. Yevtushenko, F. Marquardt, J. von Delft, and I. V. Lerner, published in *Physical Review B* **80**, 201305(R) (2009), see Section 3.4.
2. *Dimensional Crossover of the Dephasing Time in Disordered Mesoscopic Rings: From Diffusive through Ergodic to 0D Behavior*, MT, O. M. Yevtushenko, F. Marquardt, J. von Delft, and I. V. Lerner, published as Chapter 20 in the book *Perspectives of Mesoscopic Physics: Dedicated to Yoseph Imry's 70th Birthday*, edited by A. Aharony and O. Entin-Wohlman (World Scientific, Singapore, 2010), see Section 3.5.
3. *Thermal noise and dephasing due to electron interactions in nontrivial geometries*, MT, C. Texier, O. M. Yevtushenko, J. von Delft, and I. V. Lerner, published in *Physical Review B* **84**, 054204 (2011), see Section 2.4.
4. *Transport and dephasing in a quantum dot: Multiply connected graph model*, MT, O. M. Yevtushenko, F. Marquardt, J. von Delft, and I. V. Lerner, published in *Annalen der Physik (Berlin)* **524**, 188 (2012), see Section 3.6.
5. *Quantum Corrections to the Polarizability and Dephasing in Isolated Disordered Metals*, MT, P. M. Ostrovsky, O. M. Yevtushenko, J. von Delft, and I. V. Lerner, available as preprint at [arXiv:1304.4342](https://arxiv.org/abs/1304.4342), see Section 4.5.

Chapter 1

Introduction, motivation and overview

The interest in disordered systems was initiated by the pioneering work of P.W. Anderson in the late 1950ies, who realized that in “certain random lattices” the diffusion of quantum particles is substantially inhibited [Anderson, 1958]. He established a concept nowadays known as *Anderson Localization*: quantum particles become increasingly localized in the presence of disorder until their wavefunctions have typically exponentially small overlap, making transport impossible (see Fig. 1.1(a)). Soon after, the discovery of divergences in the perturbation theory of the conductance of a normal metal in the impurity concentration [Langer and Neal, 1966] confirmed his predictions, and ultimately lead to one of the keystones of solid state physics: the *scaling theory of localization* for the conductance [Abrahams *et al.*, 1979].

In solid-state experiments, traces of localization were first discovered in the 1970ies, when a negative “dip” in the magneto-resistance of metallic thin-films at zero field and low temperatures was observed (see the review by Bergmann (1984)) (see Fig. 1.1(b)). The dip was attributed to a reduction of the diffusion probability by quantum interference of the electrons, leading to so-called *weak localization* (WL). It was soon realized that transport experiments at the onset of the localization transition were essentially time-of-flight experiments of the conduction electrons interfering at impurities [Bergmann, 1983], similar in spirit to the groundbreaking double-slit experiments. This established a new powerful method to determine characteristic time scales of the system. In particular, being a quantum mechanical effect, WL requires phase coherence of the participating electrons, and thus gives a direct way to measure the so-called *dephasing time*.

With the discovery of several related effects, such as the observation of the *Aharonov-Bohm effect* in metallic rings and cylinders [Sharvin and Sharvin, 1981; Webb *et al.*, 1985], *persistent currents* [Lévy *et al.*, 1990; Chandrasekhar *et al.*, 1991], and *universal conductance fluctuations* [Stone, 1985; Altshuler, 1985; Lee *et al.*, 1987] (see Fig. 1.1(c)), the study of phase-coherent systems developed in the 1980ies into its own field called *mesoscopic physics*. It has been shown that the most important aspects of these effects can be understood through a certain perturbation theory, the so-called *loop-expansion* in diffusive propagators, which is essentially a perturbation theory in the inverse dimensionless conductance. Several introductory books on the subject are available, such as Imry (1986) and Akkermans and Montambaux (2007). Today, many areas outside of solid state physics, e.g. quantum optics, quantum chaos, and the physics of cold atoms, benefit from the numerous insights gained in mesoscopics.

Results from phase-coherent disordered systems often display a remarkable *universality*. One example is that the fluctuations of the dimensionless conductance of a disordered metal are always of a magnitude ~ 1 as soon as the thermal length exceeds the system size, and independent of the impurity concentration, the geometry, or the dimensionality of the system. Such universal results called for a proper mathematical model, provided by the *random matrix theory* (RMT), which had been initially

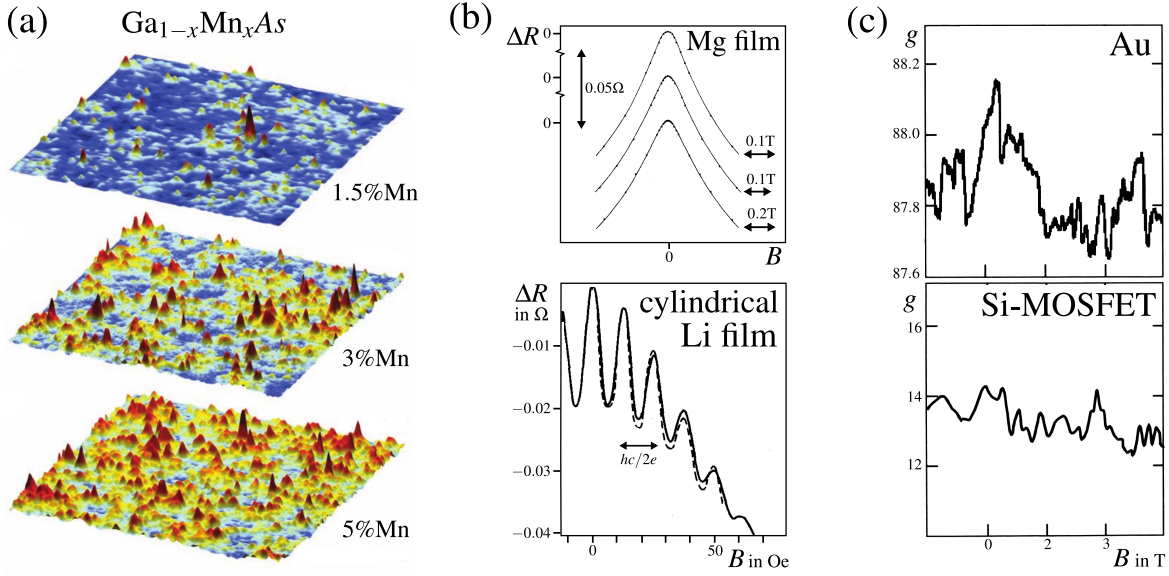


Figure 1.1: Effects in disordered systems:

(a) STM images of GaMnAs for different Mn concentrations, showing the evolution of the local density of states (LDOS) close to the *Anderson transition*: from weakly insulating (1.5%) to relatively conducting (5%). [picture from [Richardella et al. \(2010\)](#)]

(b) The resistance of metallic films decreases as a function of the external magnetic field due to a reduction of the *weak localization* effect. In the geometry of a cylinder with perpendicular magnetic field (lower picture), oscillations with a flux-period of $hc/2e$ are superimposed due to the Aharonov-Bohm effect. (In this context they are also called Altshuler-Aronov-Spivak oscillations [[Altshuler et al., 1981b](#)]) [pictures from [Bergmann \(1984\)](#) and [Altshuler et al. \(1982b\)](#)]

(c) The dimensionless conductance g (G in units of e/h) of two samples in the mesoscopic regime shows *universal conductance fluctuations* as a function of magnetic field: Although the samples shown are totally different in shape and material, and their conductance differs by almost one order of magnitude, the fluctuations are ~ 1 . [pictures from [Lee et al. \(1987\)](#)]

used in the study of nuclear energy levels. Using RMT, exact universal results for quantities, such as the energy level correlation function, have been found. These results had been known from the loop-expansion only in some restricted parameter range.

This thesis deals with disordered electronic systems at low temperatures. Such systems can be considered as being at the edge of mesoscopic universality since the dephasing time increases with decreasing temperature. This is due to the fact that the temperature determines the magnitude of the environmental noise of the electrons, which in turn determines the inelastic scattering rate responsible for randomizing the phase of the electrons.

In a seminal work, [Altshuler et al. \(1982a\)](#) determined the dephasing time of electrons in a classical Johnson-Nyquist noise environment (i.e. assuming white noise) using a path integral approach. Soon after, their results were confirmed by [Fukuyama and Abrahams \(1983\)](#) by means of a diagrammatic perturbation theory in the screened electron interaction propagators. Since then, numerous experiments have shown their predicted dependence of the dephasing time on temperature, namely $\tau_\phi \sim T^{-2/3}$ for 1D - and $\tau_\phi \sim T^{-1}$ for 2D -systems. However, both calculations assumed that the temperature is still relatively high, so that the dephasing length is shorter than the system size.

At lower temperatures, a *0D regime* of dephasing has been predicted by [Sivan et al. \(1994\)](#), where

dephasing is substantially weaker and the dephasing time depends on temperature as $\tau_\phi \sim T^{-2}$. It is called “0D ” since it is reached independently of the geometry and real dimensionality of the system, while the results of [Altshuler *et al.* \(1982a\)](#); [Fukuyama and Abrahams \(1983\)](#) show a distinct dependence on dimensionality. The increase of the dephasing time in this regime is essentially due to the Pauli principle. The Pauli principle prevents the electrons from exchanging energies larger than temperature with their environment, and thus reduces the scattering rate. An environment where such a behavior is observed is often referred to as *quantum noise*, and in contrast to classical white noise, it is characterized by a finite correlation time $\tau_T \sim 1/T$. However, despite of its physical importance, attempts to observe this 0D regime experimentally in mesoscopic systems have been unsuccessful so far. From a fundamental point of view, this is somewhat unsatisfactory: since the difference between classical and quantum noise has a very fundamental origin, namely the Pauli principle, our understanding of dephasing is incomplete as long as the “deep quantum limit”, in which Pauli blocking influences dephasing in an essential way, remains hidden from experimental observation. An experimental verification of the existence of the 0D regime has been identified by [Aleiner *et al.* \(2002\)](#) as one of the major open challenges in the physics of disordered systems.

Therefore, the overall goal of this thesis is to theoretically analyze experimental scenarios that would allow the difference between classical and quantum noise to be probed experimentally.

In the following, we give a brief overview of the contents of this thesis. It is organized in three main chapters, with our original results presented in publications at the end of each of them:

- Chapter 2 starts with a review of the disordered systems in general. We give a detailed derivation of the perturbative loop-expansion of quantum-corrections to important correlation functions, discuss their dependence on time-reversal symmetry, and give a comparison to non-perturbative results from RMT. We then introduce the concept of dephasing in this setting. Based on the approach developed by [von Delft *et al.* \(2007\)](#), which uses the Keldysh diagrammatic technique and takes into account Pauli blocking, we discuss the influence of quantum noise on dephasing due to electron interactions. By generalizing the calculations to arbitrary system sizes, we show how all known regimes of the dephasing time, and in particular the 0D regime, can be described on an equal footing.

We will see that for closed systems and in the absence of other sources of dephasing (besides electron interactions), the weakness of dephasing in the 0D regime necessarily leads to a formal breakdown of the loop-expansion, which is characterized by the onset of a discreteness in the energy levels of the system. We provide a better understanding of the crossover regime, by calculating the two-loop correction to the generalized diffusion propagator.

For transport experiments in open systems, we establish that 0D dephasing always occurs at the edge of the universal regime, where the quantum corrections depend only weakly on the dephasing time. To make quantitative predictions on the dephasing time in this parameter range, one has to model the geometry of the system explicitly.

To achieve this, we derive the noise correlations for multiply-connected systems and use this result in order to develop a theory of dephasing by electronic noise applicable for arbitrary geometries and arbitrary temperatures, which we formulate in terms of a trajectory-dependent functional.

- Chapter 3 is devoted to quantum corrections to the conductivity of disordered metals. After giving a detailed derivation of the WL correction using the loop-expansion, we analyze its dependence on the dephasing time. Moreover, we review the RMT of quantum transport and discuss the currently-known possibilities to incorporate dephasing in this theory.

In order to analyze the possibility to observe 0D dephasing in a conductance experiment, we discuss two concrete scenarios:

(1) For a ring weakly coupled to leads in an external magnetic field, we show that 0D dephasing also governs the magnitude of the Altshuler-Aronov-Spivak oscillations at sufficiently low temperatures. This allows signatures of dephasing in the ring to be cleanly extracted by filtering out those of the leads.

(2) We propose a novel quantum dot model based on results from the theory of *diffusion in graphs*, and using the functional derived in Chapter 2. We will see that in this model, which is complementary to the RMT models, interaction-induced dephasing can be accounted for in detail, and we make qualitative predictions on the observability of 0D dephasing.

- In Chapter 4, we investigate the polarizability α of isolated metals. After briefly discussing the implications of the fixed particle number in isolated systems, and the role of screening in this problem, we derive an expression for the quantum corrections of α .

In contrast to previous approaches which used a model based on RMT, we show how the corrections can be calculated by means of the loop-expansion. Using the two-loop correction to the generalized diffusion propagator derived in Chapter 2, we show that this perturbative calculation adequately reproduces the RMT result in the zero temperature limit. Importantly, our approach also allows us to determine the dependence of α on the dephasing time, the temperature and the magnetic field, and we compare our findings with recent experiments.

Finally, we show that quantum corrections to the polarizability might be the key to eventually observe 0D dephasing in an experiment.

Chapter 2

Dephasing in disordered systems

2.1 Electrons in disordered systems

The goal of this section is a description of the electron dynamics in a disordered metal. Remarkably, an approximation in terms of free particles with kinetic energy H_0 in a static disorder potential V (to be specified further below) of the form

$$H = H_0 + V, \quad (2.1)$$

is usually sufficient. This is mainly due to two profound achievements of solid state theory, namely *electronic band theory*, which describes the influence of the periodic lattice potential of an underlying crystal, see e.g. [Madelung \(1978\)](#), and *Landau-Fermi liquid theory*, which includes the interactions between the electrons, see e.g. [Pines and Nozieres \(1989\)](#). It is shown that most of the effects of the lattice-potential and the interactions can be accounted for, by shifting and rescaling parameters of the dispersion relation $\varepsilon(\mathbf{k})$ of the electrons. As a result, the system is formally described by free *quasi-particles* with a finite lifetime, which have, however, essentially the same properties as free electrons.¹ Importantly, due to the fermionic statistics of the quasi-particles, all excitations occur in the vicinity of the Fermi edge, characterized by a *Fermi energy* ε_F . In metals, ε_F is very large compared to the typical excitation energies, which are usually of the order of temperature [$\varepsilon_F \gtrsim 10^4 K$]. In fact, in the following, we will always assume that ε_F is the largest energy scale, and we will measure particle energies relative to ε_F .

For the disorder potential, we assume that at each point in space $V(\mathbf{x})$ is an independent real Gaussian random variable characterized by the probability distribution

$$P[V] = \frac{1}{\mathcal{Z}} \int DV \exp\left(-\frac{1}{2\gamma} \int d^d \mathbf{x} [V(\mathbf{x})]^2\right), \quad (2.2)$$

where γ is a measure of the disorder strength and \mathcal{Z} is a normalization constant. We denote the *disorder average* of a quantity “ A ” with respect to the probability distribution function (2.2) by “ \overline{A} ”. In particular, the lowest order correlation functions of V are given by

$$\overline{V(\mathbf{x})} = 0, \quad \overline{V(\mathbf{x})V(\mathbf{y})} = \gamma\delta(\mathbf{x} - \mathbf{y}), \quad (2.3)$$

and all higher correlation functions can be obtained from Eq. (2.3) using *Wick’s theorem*. A random potential characterized by Eq. (2.3) is also called *white noise*.

1. We will discuss the lifetime τ_{ee} of the quasi-particles in more details in Section 2.2, and simply assume that τ_{ee} is sufficiently large in the following.

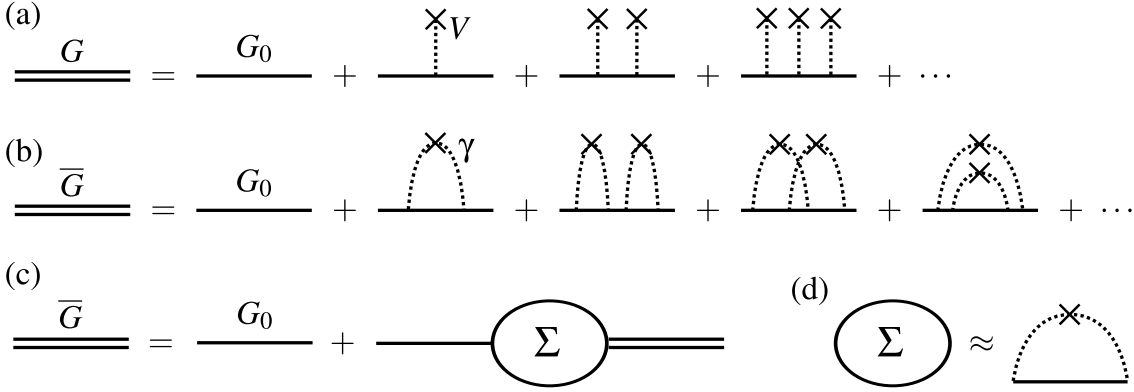


Figure 2.1: Diagrammatic representation of Eq. (2.6) and Eq. (2.7).

Eq. (2.2) is the simplest possible model of disorder, nevertheless, it accurately describes the long-range physics of many disordered systems. For a metal, it can be justified from a microscopic point of view as follows: Assume that N impurities with potential $u(\mathbf{x})$ are distributed randomly in the system (so-called *Edwards model*). E.g. $u(\mathbf{x})$ might describe the real microscopic potential of impurities, dislocations, vacancies, etc. Then the total disorder potential is given by

$$V(\mathbf{x}) = \sum_{i=1}^N u(\mathbf{x} - \mathbf{x}_i). \quad (2.4)$$

On scales larger than the range of u , the position \mathbf{x}_i of the microscopic potential should be irrelevant. After taking an average over all \mathbf{x}_i and taking the limit of a high density ($N/V \rightarrow \infty$) of weak scatterers ($u \rightarrow 0$), one recovers Eq. (2.3), up to a shift of the electron energy.

A powerful tool to describe the dynamics of the system are the resolvents of the corresponding Schrödinger equation, called *retarded/advanced Green's functions*, which are given for $V = 0$ by

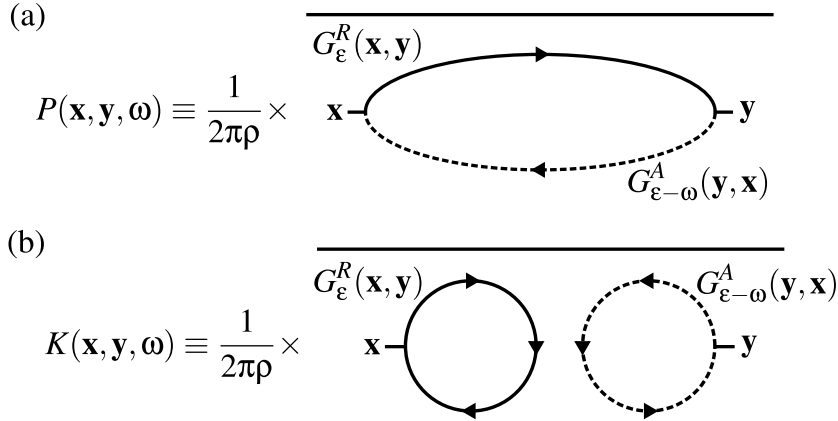
$$G_{\varepsilon}^{R/A}(\mathbf{k}) = \frac{1}{\varepsilon - \varepsilon(\mathbf{k}) \pm i0}. \quad (2.5)$$

The regularizer, $\pm i0$, is added to ensure that the Fourier transform of G^R vanishes for times $t < 0$, while G^A vanishes for $t > 0$. In the following we will calculate the disorder average of Eq. (2.5) and see how important correlation functions can be calculated by using $G^{R/A}$.

2.1.1 Diagrammatic approach to disorder

The standard way to study the system described by Eq. (2.1) is a perturbation theory in the disorder potential. A detailed derivation of all results given in this section can be found, for example, in [Lee and Ramakrishnan \(1985\)](#) or [Akkermans and Montambaux \(2007\)](#). Diagrammatically expanding the retarded or advanced Green's functions in powers of V results in the diagram shown in Fig. 2.1(a). Upon averaging according to Eq. (2.3), the term linear in V , as well as all other odd power terms vanish, while the even terms are paired according to Wick's theorem. Each pair of potentials is represented by a dotted line in Fig. 2.1(b), called *impurity line*, and brings an additional factor of γ , according to Eq. (2.3). Formally, we can sum up all diagrams using Dyson's equation shown in Fig. 2.1(c), with the result

$$\bar{G}_{\varepsilon}^{R/A}(\mathbf{k}) = \frac{1}{\varepsilon - \varepsilon(\mathbf{k}) \pm i/2\tau}, \quad (2.6)$$

Figure 2.2: Diagrammatic representation of the correlation functions P and K .

where $-1/2\tau$ is defined as the imaginary part of the irreducible self-energy Σ . [The real part gives an unimportant shift of the electron energy.] The calculation of the self-energy is in principle a difficult problem since it contains an infinite number of terms. In the so-called first *Born approximation*, it is given by the diagram shown in Fig. 2.1(d). It is given by a momentum sum over an electron Green's function (G^R) and an impurity line (γ):

$$\frac{1}{2\tau} = -\text{Im}[\Sigma_\epsilon^R(\mathbf{k})] \approx -\text{Im}\left[\frac{1}{V} \sum_{\mathbf{k}'} G_\epsilon^R(\mathbf{k}-\mathbf{k}')\gamma\right] = \pi\rho_\epsilon\gamma. \quad (2.7)$$

One can show that the higher order diagrams, which involve crossed and nested impurity lines, are small in terms of the parameter $(\epsilon_F\tau)^{-1}$. Note that in Eq. (2.6), τ determines the lifetime of the electron in a momentum eigen-state \mathbf{k} , and is often called *momentum relaxation time* or *impurity scattering time*. The corresponding length scale, defined via $\ell = v_F\tau$, where v_F is the Fermi velocity of the electrons, is called the *mean free path*. Thus, $(\epsilon_F\tau)^{-1} \ll 1$ describes a “classical limit” where the wavelength of the electrons is much shorter than the distance between two scattering events, which is usually the case in a disordered metal.

In Eq. (2.7), we have introduced the density of states per unit volume,

$$\rho_\epsilon \equiv \frac{1}{V} \sum_{\mathbf{k}} \delta(\epsilon - \epsilon_{\mathbf{k}}) \quad (2.8)$$

$$= -\frac{1}{\pi V} \sum_{\mathbf{k}} \text{Im}[G_\epsilon^R(\mathbf{k})] = \frac{i}{2\pi} [G_\epsilon^R(\mathbf{x}, \mathbf{x}) - G_\epsilon^A(\mathbf{x}, \mathbf{x})]. \quad (2.9)$$

For a continuous energy spectrum, ρ_ϵ is typically a slowly varying function of energy. Thus, in the following we will often neglect its energy dependence and simply denote it by $\rho \equiv \rho_0$. Furthermore, we see from substituting Eq. (2.6) in Eq. (2.9), that the density of states itself depends only weakly on disorder for $(\epsilon_F\tau)^{-1} \ll 1$, such that $\overline{\rho_\epsilon} \approx \rho$.

2.1.2 Disorder averaged correlation functions

In a classical disordered system, particle propagation in a random potential is diffusive for distances larger than ℓ and times larger than τ . To see that the same characteristic behavior survives in the quantum picture, we consider the probability of an electron of energy ϵ to propagate from \mathbf{x} to \mathbf{y} in

$$\begin{aligned}
P_d(\mathbf{q}, \omega) &= \frac{1}{2\pi\rho} \times \sum_{N=0}^{\infty} \text{Diagram} \\
&\hat{=} \frac{1}{2\pi\rho} \times \text{Wavy Line} \hat{=} \frac{1}{2\pi\rho} \times \frac{1}{\gamma^2} \times \text{Wavy Line} \\
&\approx \frac{1}{D\mathbf{q}^2 - i\omega}
\end{aligned}$$

Figure 2.3: The ladder approximation to the generalized diffusion propagator.

time t . For large ε , it can be expressed as follows in terms of a correlation function of the retarded and advanced Green's functions [Akkermans and Montambaux, 2007]:¹

$$P(\mathbf{x}, \mathbf{y}, t) = \int_{-\infty}^{\infty} \frac{d\omega}{2\pi} e^{-i\omega t} \frac{1}{2\pi\rho} \overline{G_{\varepsilon}^R(\mathbf{x}, \mathbf{y}) G_{\varepsilon-\omega}^A(\mathbf{y}, \mathbf{x})}. \quad (2.10)$$

P is also called the *generalized diffusion propagator*, and plays an important role in the description of the transport properties of the metal, such as the conductivity considered in Chapter 3. Diagrammatically, we can represent Eq. (2.10) as a bubble shown in Fig. 2.2(a).

The second important correlation function which we consider here is shown in Fig. 2.2(b) and defined as

$$K(\mathbf{x}, \mathbf{y}, t) = \int_{-\infty}^{\infty} \frac{d\omega}{2\pi} e^{-i\omega t} \frac{1}{2\pi\rho} \overline{G_{\varepsilon}^R(\mathbf{x}, \mathbf{x}) G_{\varepsilon-\omega}^A(\mathbf{y}, \mathbf{y})}. \quad (2.11)$$

Evidently, K is directly related to the fluctuations of the density of states, cf. Eq. (2.8). Thus, it describes spectral characteristics of the metal, such as the energy level correlations.

Note that we have suppressed the argument ε in the definitions of P and K , since the disorder averaged product of Green's functions depends only weakly on their common energy, see e.g. Eq. (2.18) below.

Generalized diffusion propagator

Let us first consider P in a disordered system. The "classical" contribution to Eq. (2.10) is given by the so-called *ladder diagram*, shown in Fig. 2.3. It is called "classical" due to the following argument: P can be interpreted as the interfering amplitudes of an electron, G_{ε}^R , and a hole, $G_{\varepsilon-\omega}^A$, propagating through a disorder landscape. In the limit $(\varepsilon_F \tau)^{-1} \ll 1$, their wavelengths are much shorter than the mean free path, and we may visualize their trajectories as being two independent random walks changing directions only at impurity positions. After averaging over the random disorder potential $V(\mathbf{x})$, the quantum-mechanical phase difference of electron and hole is randomized. However, constructive interference is guaranteed if both, electron and hole, scatter at the same impurities in the same order. This process is precisely described by Fig. 2.3.

1. Formally, Eq. (2.10) follows from a description of the electron as wave-packed with energy-width $\Delta\varepsilon$ in the limit $\Delta\varepsilon \ll \varepsilon_F$.

The diagram shown in Fig. 2.3 is called a ladder diagram, since it consists of N equal building blocks, which look like “steps” of a ladder. Evidently, each of these building blocks describes the scattering of the electron and the hole at one and the same impurity, and is given by the following expression:

$$d_{\mathbf{q},\omega} \equiv \gamma \frac{1}{V} \sum_{\mathbf{k}} \overline{G}_{\varepsilon}^R(\mathbf{k} + \mathbf{q}) \overline{G}_{\varepsilon-\omega}^A(\mathbf{k}). \quad (2.12)$$

We are interested only in the long-range, and long-time behavior of P . Thus, we expand the Green's functions in \mathbf{q} and ω as follows

$$\overline{G}_{\varepsilon+\omega}^{R/A}(\mathbf{k} + \mathbf{q}) \approx \overline{G}_{\varepsilon}^{R/A}(\mathbf{k}) + \omega \left[\overline{G}_{\varepsilon}^{R/A}(\mathbf{k}) \right]^2 + \mathbf{v}_{\mathbf{k}} \mathbf{q} \left[\overline{G}_{\varepsilon}^{R/A}(\mathbf{k}) \right]^2 + (\mathbf{v}_{\mathbf{k}} \mathbf{q})^2 \left[\overline{G}_{\varepsilon}^{R/A}(\mathbf{k}) \right]^3, \quad (2.13)$$

where $\mathbf{v}_{\mathbf{k}} = \partial_{\mathbf{k}} \varepsilon(\mathbf{k}) \approx v_F \hat{\mathbf{v}}_{\mathbf{k}}$. Note that due to the pole structure, the sum of Green's functions of equal retardation is much smaller than that of different retardations, e.g.

$$\sum_{\mathbf{k}} \overline{G}_{\varepsilon}^R(\mathbf{k}) \overline{G}_{\varepsilon}^R(\mathbf{k}) \ll \sum_{\mathbf{k}} \overline{G}_{\varepsilon}^R(\mathbf{k}) \overline{G}_{\varepsilon}^A(\mathbf{k}). \quad (2.14)$$

In combination with the identity

$$\overline{G}_{\varepsilon}^R(\mathbf{k}) \overline{G}_{\varepsilon}^A(\mathbf{k}) = -2\tau \text{Im} \overline{G}_{\varepsilon}^R(\mathbf{k}), = i\tau \left[\overline{G}_{\varepsilon}^R(\mathbf{k}) - \overline{G}_{\varepsilon}^A(\mathbf{k}) \right], \quad (2.15)$$

and the definition of the density of states, Eq. (2.8), we can recursively determine the leading behavior of momentum sums of arbitrary powers of Green's functions:

$$\gamma \frac{1}{V} \sum_{\mathbf{k}} \left[\overline{G}_{\varepsilon}^R(\mathbf{k}) \right]^m \left[\overline{G}_{\varepsilon}^A(\mathbf{k}) \right]^n = i^{n-m} \frac{(n+m-2)!}{(n-1)!(m-1)!} \tau^{n+m-2}, \quad (2.16)$$

for all $n, m \in \mathbb{Z} > 0$. Substituting Eq. (2.13) in Eq. (2.12), and using Eq. (2.16), we find for the “step” of the ladder diagram

$$d_{\mathbf{q},\omega} \approx 1 - \tau D \mathbf{q}^2 + i\tau \omega, \quad (2.17)$$

where $D = v_F^2 \tau / d$ is the diffusion constant and d is the dimensionality of the systems.¹ Note that $d_{\mathbf{q},\omega}$ is a short-ranged object on the scale ℓ , since Eq. (2.17) depends only weakly on momentum for $\mathbf{q} \ell \ll 1$.

The diagram shown in Fig. 2.3 consists of N impurity lines. Summing over all possible numbers of impurity lines gives the generalized diffusion propagator in the ladder approximation:

$$P(\mathbf{q}, \omega) \approx P_d(\mathbf{q}, \omega) = \sum_{N=0}^{\infty} \frac{1}{2\pi\rho} \frac{1}{\gamma} (d_{\mathbf{q},\omega})^{N+1} = \frac{\tau}{1 - d_{\mathbf{q},\omega}} = \frac{1}{D\mathbf{q}^2 - i\omega}. \quad (2.18)$$

Note that it is independent of ε and long-ranged. In the following we will denote the averaged product $\overline{G}_{\varepsilon}^R(\mathbf{x}, \mathbf{y}) \overline{G}_{\varepsilon-\omega}^A(\mathbf{y}, \mathbf{x})$ in the ladder approximation as a double wavy line, shown in the second line of Fig. 2.3. Moreover, we defined the so-called *impurity structure factor* Γ_d in Fig. 2.3. Γ_d is obtained from the ladder diagram for P_d , after removing the two vertices and the four Green's functions directly attached to them, which give an additional factor of γ^2 , cf. Eq. (2.16). It is given by

$$\Gamma_d(\mathbf{q}, \omega) = \gamma \sum_{N=0}^{\infty} (d_{\mathbf{q},\omega})^{N+1} = 2\pi\rho\gamma^2 P_d(\mathbf{q}, \omega) = \frac{1}{2\pi\rho\tau^2} \frac{1}{D\mathbf{q}^2 - i\omega}. \quad (2.19)$$

1. The factor $1/d$ stems from angular averaging $\int d\alpha (\mathbf{v}_{\mathbf{k}} \mathbf{q})^2 = v_F^2 \mathbf{q}^2 / d$, where α is the normalized solid angle determined by the two vectors \mathbf{q} and \mathbf{k} .

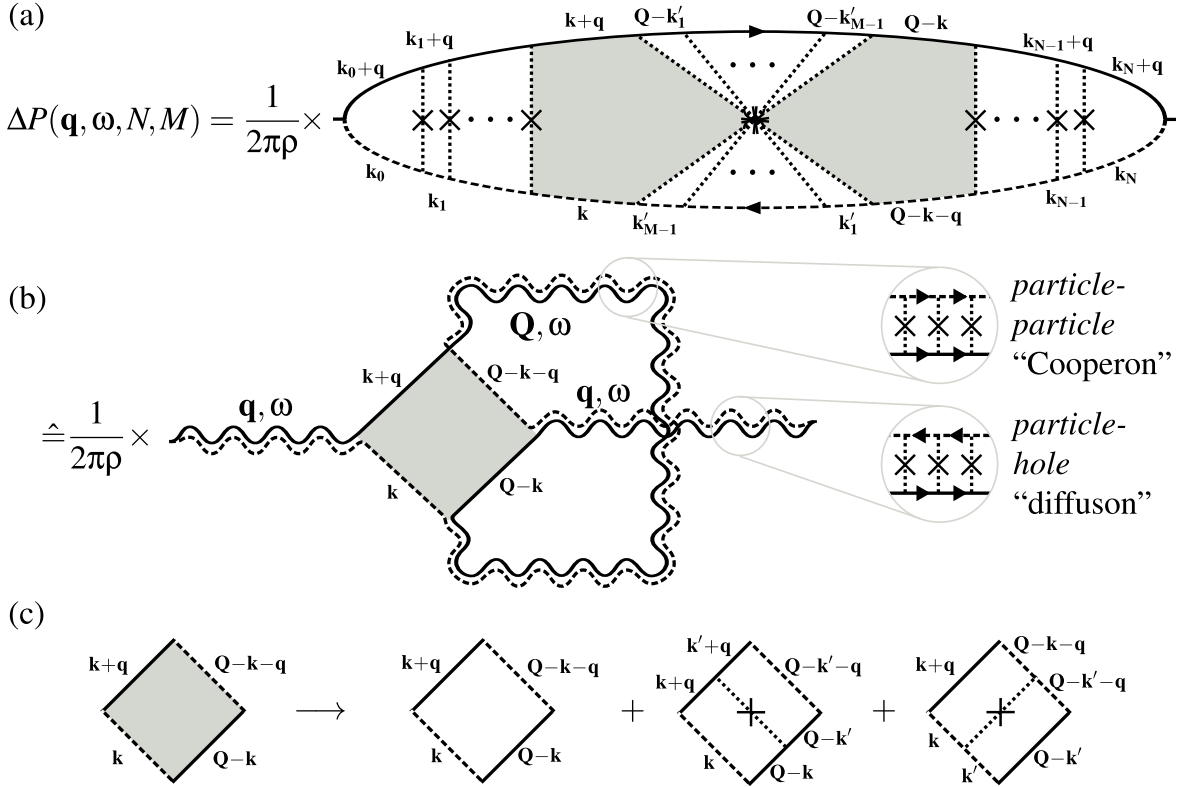


Figure 2.4: (a) and (b): maximally crossed diagrams. (c): 4-point Hikami box.

We will need Γ_d in the following as a “building block” for more complicated diagrams.

The Fourier transform of P_d , defined in Eq. (2.18), is the solution of the diffusion equation

$$[\partial_t - D\Delta] P_d(\mathbf{x}, \mathbf{y}, t) = \delta(\mathbf{x} - \mathbf{y})\delta(t). \quad (2.20)$$

Thus, we will refer to P_d as *diffusion propagator* in the following. For a closed system, it is normalized: $\int d^d \mathbf{y} P_d(\mathbf{x}, \mathbf{y}, t > 0) = 1$. This normalization also holds for P in total, which can be checked directly from its definition (2.10) in terms of the Green’s functions using the normalization of the wave-functions. Since P describes the propagation of a particle, its normalization reflects particle number conservation. It follows that all additional contributions to P beyond P_d have to vanish in the limit $\mathbf{q} \rightarrow 0$.

Quantum corrections to the generalized diffusion propagator in the limit $(\epsilon_F \tau)^{-1} \ll 1$ are obtained by inserting so-called *maximally-crossed* impurity ladders into the ladder diagram, as shown in Fig. 2.4(a). In analogy to the argument given for P_d , the maximally-crossed ladder can be interpreted as the interfering amplitudes of an electron and a hole scattering at the same impurities, but in *exactly opposite order*. Evidently, constructive interference is also guaranteed for this process, provided that the system is symmetric under time-reversal. As in Fig. 2.3, we can represent the impurity ladders of Fig. 2.4(a) by wavy lines, leading to the diagram shown in Fig. 2.4(b). Due to the structure of this diagram, its contribution is also called the *one-loop correction*. It is clear that inserting additional maximally-crossed and non-crossed impurity ladders leads to a *loop-expansion* (see Section 2.3 for a depiction of the two-loop diagrams).

We will see in the following, by summing up the infinite number of diagrams of the maximally crossed ladder, that the contribution of each loop is formally infrared (IR) divergent at $\omega \rightarrow 0$ in

dimensions $d < 3$ [Langer and Neal, 1966]. Thus the loop-expansion can be considered as a grouping of all possible crossed and non-crossed impurity lines in the most divergent contributions. We give a detailed discussion of this divergence and the validity of the loop-expansion in Section 2.1.4. For now, we simply *assume* that the contribution of each loop gives rise to a small factor, and that the leading correction to $P \approx P_d$ is given by the one-loop diagram shown in Fig. 2.4(a/b).

In Fig. 2.4(b), we see that the direction of the Green's functions in the maximally-crossed impurity ladder constituting the inner loop are reversed: This ladder thus expresses propagation in the so-called *particle-particle channel*, and is described by the so-called *Cooperon propagator* P_c (a notation adopted from superconductivity). This is in contrast to the diffuson propagator P_d , calculated in Eq. (2.18), which describes propagation in the *particle-hole channel*. Correspondingly, we denote each ‘‘step’’ of an impurity ladder in the particle-particle channel as $d_{\mathbf{q},\omega}^c$, and note that it is given by $d_{\mathbf{q},\omega}$, calculated in Eq. (2.17), only if the system has time-reversal symmetry.

In the representation of Fig. 2.4(b), the short range part connecting the crossed to the regular impurity ladders is highlighted as a shaded square consisting of two retarded and two advanced averaged Green's functions. This short-range part of the diagram is called *Hikami box* [Hikami, 1981]. Adding a single impurity line connecting two of the Green's functions of equal retardation (also called *dressing* of the Hikami box), as shown in Fig. 2.4(c), one finds two more diagrams of the same order in $(\epsilon_F \tau)^{-1} \ll 1$. Denoting this short-range part by H_4 , we find for the diagram shown in Fig. 2.4(a):

$$\Delta P(\mathbf{q}, \omega, N, M) = \frac{1}{2\pi\rho_\epsilon} \times (d_{\mathbf{q},\omega})^N \times \frac{1}{V} \sum_{\mathbf{Q}} \gamma(d_{\mathbf{Q},\omega}^c)^{M-1} \times H_4(\mathbf{q}, \mathbf{Q}, \omega). \quad (2.21)$$

Summing over all possible numbers of impurities and positions of the crossed ladder ($N + 1$ possibilities), we find

$$\begin{aligned} \Delta P(\mathbf{q}, \omega) &= \sum_{N=0}^{\infty} \sum_{M=1}^{\infty} (N+1) \Delta P(\mathbf{q}, \omega, N, M) \\ &= \frac{1}{2\pi\rho} \frac{1}{(1-d_{\mathbf{q},\omega})^2} \frac{1}{V} \sum_{\mathbf{Q}} \frac{\gamma}{1-d_{\mathbf{Q},\omega}^c} \times H_4(\mathbf{q}, \mathbf{Q}, \omega) \\ &\approx \frac{1}{2\pi\rho} \frac{1}{(D\mathbf{q}^2 - i\omega)^2} \frac{1}{V} \sum_{\mathbf{Q}} P_c(\mathbf{Q}, \omega) \times \frac{1}{2\pi\rho\tau^4} H_4(\mathbf{q}, \mathbf{Q}, \omega), \end{aligned} \quad (2.22)$$

where $P_c(\mathbf{Q}, \omega) = P_d(\mathbf{Q}, \omega) = (D\mathbf{Q}^2 - i\omega)^{-1}$ only if the system has time-reversal symmetry. We will discuss the \mathbf{Q} -sum and appropriate cutoffs in more detail in Section 2.1.4 below.

Let us now turn to a calculation of the Hikami box first. Naively writing down the expression following from the diagram in Fig. 2.4(c), it is given by the following sum of Green's functions:

$$\begin{aligned} H_4(\mathbf{q}, \mathbf{Q}, \omega) &\stackrel{?}{=} \sum_{\mathbf{k}} \bar{G}_{\epsilon-\omega}^A(\mathbf{k}) \bar{G}_{\epsilon}^R(\mathbf{k}+\mathbf{q}) \bar{G}_{\epsilon-\omega}^A(\mathbf{Q}-\mathbf{k}-\mathbf{q}) \bar{G}_{\epsilon}^R(\mathbf{Q}-\mathbf{k}) \\ &\quad + \sum_{\mathbf{k}} \bar{G}_{\epsilon}^R(\mathbf{Q}-\mathbf{k}) \bar{G}_{\epsilon-\omega}^A(\mathbf{k}) \bar{G}_{\epsilon}^R(\mathbf{k}+\mathbf{q}) \sum_{\mathbf{k}'} \bar{G}_{\epsilon}^R(\mathbf{k}'+\mathbf{q}) \bar{G}_{\epsilon-\omega}^A(\mathbf{Q}-\mathbf{k}'-\mathbf{q}) \bar{G}_{\epsilon}^R(\mathbf{Q}-\mathbf{k}') \\ &\quad + \sum_{\mathbf{k}} \bar{G}_{\epsilon-\omega}^A(\mathbf{Q}-\mathbf{k}-\mathbf{q}) \bar{G}_{\epsilon}^R(\mathbf{Q}-\mathbf{k}) \bar{G}_{\epsilon-\omega}^A(\mathbf{k}) \bar{G}_{\epsilon}^R(\mathbf{k}+\mathbf{q}) \sum_{\mathbf{k}'} \bar{G}_{\epsilon}^R(\mathbf{Q}-\mathbf{k}') \bar{G}_{\epsilon-\omega}^A(\mathbf{k}'). \end{aligned} \quad (2.23)$$

Expanding in the transferred momenta and energies $(\mathbf{q}, \mathbf{Q}, \omega)$, using Eq. (2.13), and calculating the sums using Eq. (2.16) shows that all three diagrams are of the same order in $\tau D\mathbf{q}^2$, $\tau D\mathbf{Q}^2$, and $\tau\omega$,

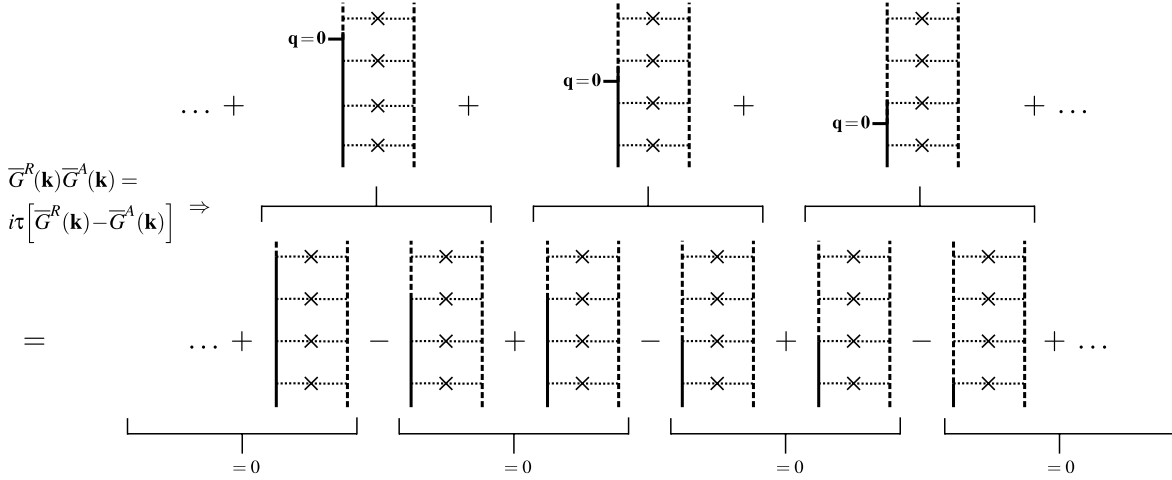


Figure 2.5: Illustration of the idea of [Hastings et al. \(1994\)](#): Moving a vertex with $\mathbf{q} = 0$ around an impurity ladder generates a set of diagrams that cancels each other.

and that the leading terms cancel each other:

$$\text{WRONG : } H_4(\mathbf{q}, \mathbf{Q}) \approx (2\pi\rho\tau^3) [2 - 2\tau D(\mathbf{q}^2 + \mathbf{Q}^2) + 6i\tau\omega] \quad (2.24)$$

$$\begin{aligned} &+ (2\pi\rho\tau^3) [-1 + 2\tau D(\mathbf{q}^2 + \mathbf{q}\mathbf{Q} + \mathbf{Q}^2) - 4i\tau\omega] \\ &+ (2\pi\rho\tau^3) [-1 + 2\tau D(\mathbf{q}^2 - \mathbf{q}\mathbf{Q} + \mathbf{Q}^2) - 4i\tau\omega] \\ &\approx 4\pi\rho\tau^4 [D\mathbf{q}^2 + D\mathbf{Q}^2 - i\omega]. \end{aligned} \quad (2.25)$$

Evidently, Eq. (2.23) has to be wrong, since inserting Eq. (2.25) in Eq. (2.22) leads to an UV-divergent \mathbf{Q} -sum in any dimension. Moreover, the terms $[D\mathbf{Q}^2 - i\omega]$ violate particle number conservation, since they give a non-zero contribution to the generalized diffusion propagator at $\mathbf{q} = 0$.

The problem can be resolved by the following argument: We assumed in Eq. (2.22), that the maximally crossed impurity ladder can have only one single impurity line ($M = 1$). However, a single line together with an undressed Hikami box gives no new contribution to P , since it is already included in the diffusion propagator P_d . On the other hand, a single line does give a new contribution, if the Hikami box is dressed! Thus, the maximally crossed ladder has an additional “step” whenever the Hikami box is undressed. Consequently, the first diagram of Fig. 2.4(c) should be multiplied by an additional factor of $d_{\mathbf{Q},\omega} \approx 1 - \tau D\mathbf{Q}^2 + i\tau\omega$. Multiplying the first line of Eq. (2.24) by $d_{\mathbf{Q},\omega}$, and collecting terms to lowest order in τ gives instead of Eq. (2.25):¹

$$\text{CORRECT : } H_4(\mathbf{q}, \mathbf{Q}) \approx 4\pi\rho\tau^4 D\mathbf{q}^2. \quad (2.26)$$

Finally, substituting Eq. (2.26) in Eq. (2.22) gives the leading quantum correction to the generalized diffusion propagator:

$$\Delta P(\mathbf{q}, \omega) \approx \frac{1}{\pi\rho} \frac{D\mathbf{q}^2}{(D\mathbf{q}^2 - i\omega)^2} \frac{1}{V} \sum_{\mathbf{Q}} P_c(\mathbf{Q}, \omega). \quad (2.27)$$

Note that $\Delta P(\mathbf{q} \rightarrow \mathbf{0}, \omega) = 0$ as expected.

1. Remarkably, our argument for the calculation of H_4 cannot, to the best of our knowledge, be found in the literature, albeit the final result for ΔP is well-known, see e.g. [Aleiner et al. \(1999\)](#).

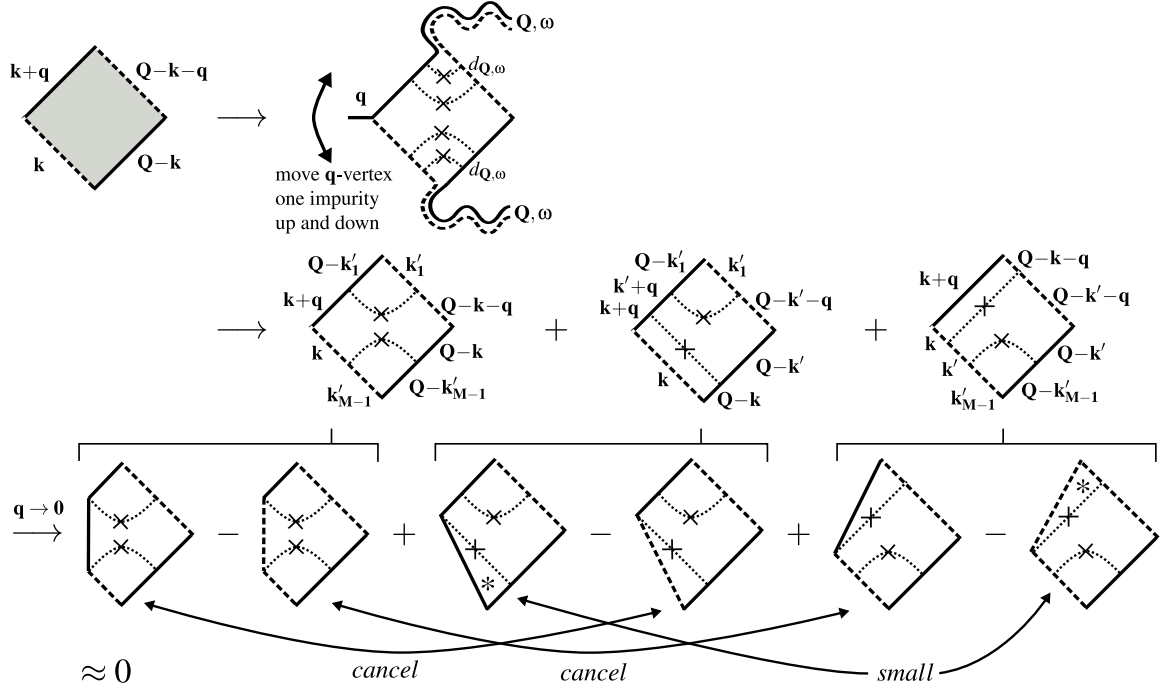


Figure 2.6: Dressing of the Hikami box by moving the vertex one impurity up and down into the attached impurity ladder. In the limit $\mathbf{q} \rightarrow \mathbf{0}$ the Hikami box vanishes by construction: Using $\overline{G}^R(\mathbf{k})\overline{G}^A(\mathbf{k}) = i\tau [\overline{G}^R(\mathbf{k}) - \overline{G}^A(\mathbf{k})]$, we see that all diagrams cancel to leading order in $(\epsilon_F\tau)^{-1} \ll 1$. (Parts of the diagrams marked with “*” are small in $(\epsilon_F\tau)^{-1} \ll 1$ due to Eq. (2.14).)

Unfortunately, for the Hikami boxes appearing in higher order diagrams, the same UV-divergences appear and there is no straightforward generalization of the above simple argument due to ambiguities in the “few impurity” diagrams. An alternative, physically motivated way to arrive at Eq. (2.26) is to start from the requirement $H_4(\mathbf{q} \rightarrow \mathbf{0}) = 0$, motivated by the particle conservation law for P . At $\mathbf{q} \rightarrow \mathbf{0}$ the two Green’s functions at the vertex are simply given by the product $G^R(\mathbf{k})G^A(\mathbf{k})$, which can be rewritten as the difference $\sim [G^R(\mathbf{k}) - G^A(\mathbf{k})]$ using Eq. (2.15). It follows that for $\mathbf{q} \rightarrow \mathbf{0}$ by *moving the vertex around the maximally crossed impurity ladder*, a set of diagrams is generated which cancels each other, and thus restores the particle conservation law, see Fig. 2.5. We note that a similar idea has been discussed by [Hastings et al. \(1994\)](#) to derive a current-conserving non-local conductivity. We illustrate how this procedure is applied for the Hikami box of Fig. 2.4(b) in Fig. 2.6: Instead of dressing the Hikami box by inserting additional impurity lines, we move the (“diffuson-dressed”) \mathbf{q} -vertex one impurity up and down into the maximally crossed ladder. Moving it further would give a subleading diagram in $(\epsilon_F\tau)^{-1} \ll 1$. This naturally “generates” the dressing, while keeping the total number of impurities of the diagram fixed. Summing up the 3 diagrams shown in the second line of Fig. 2.6 also leads to Eq. (2.26). We will use this method to obtain one of the main results of our work, which we discuss in Section 2.3: The calculation of the two-loop correction to the generalized diffusion propagator.

We have now established that the generalized diffusion propagator including the one-loop correction is given by the sum of Eqs. (2.18, 2.27):

$$P(\mathbf{q}, \omega) \approx \frac{1}{D\mathbf{q}^2 - i\omega} + \frac{1}{\pi\rho_\epsilon} \frac{D\mathbf{q}^2}{(D\mathbf{q}^2 - i\omega)^2} \frac{1}{V} \sum_{\mathbf{Q}} P_c(\mathbf{Q}, \omega). \quad (2.28)$$

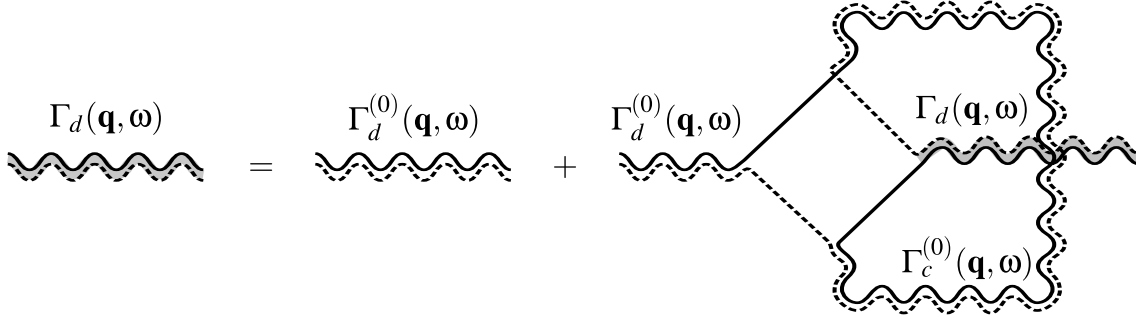


Figure 2.7: Renormalization of the diffusion constant.

A better approximation is possible by summing up an infinite number of diagrams using Dyson's equation [Vollhardt and Wölfle, 1980b,a]. We illustrate this equation for the impurity structure factor in Fig. 2.7. It corresponds to the following equation:

$$\Gamma_d(\mathbf{q}, \omega) = \Gamma_d^{(0)}(\mathbf{q}, \omega) \left[1 + \left(D\mathbf{q}^2 \frac{2\tau^2}{V} \sum_{\mathbf{Q}} P_c(\mathbf{q}, \omega) \right) \Gamma_d^{(0)}(\mathbf{q}, \omega) \right], \quad (2.29)$$

with $\Gamma_d^{(0)}(\mathbf{q}, \omega)$ given by Eq. (2.19). The solution of Eq. (2.29) reads

$$\Gamma_d(\mathbf{q}, \omega) = \frac{1}{2\pi\rho\tau^2} \frac{1}{D^*(\omega) \mathbf{q}^2 - i\omega}, \quad D^*(\omega) \equiv D \left[1 - \frac{1}{\pi\rho V} \sum_{\mathbf{Q}} \frac{1}{D\mathbf{Q}^2 - i\omega} \right]. \quad (2.30)$$

The corresponding generalized diffusion propagator is thus a solution to a diffusion equation with renormalized, frequency-dependent diffusion constant:

$$P(\mathbf{q}, \omega) \approx \frac{1}{D^*(\omega) \mathbf{q}^2 - i\omega}. \quad (2.31)$$

We see that the *quantum corrections reduce the diffusion constant* of the system. This reduction is responsible for the decrease of the conductance of disordered quantum systems mentioned in the introduction, and which we will discuss in more details in Chapter 3.

Fluctuations of the density of states

The dimensionless fluctuations of the density of states are also called the *two-level correlation function* R_2 . According to Eq. (2.8) they are given by

$$\begin{aligned} \delta R_2(\omega) &\equiv \frac{\overline{\rho_\varepsilon \rho_{\varepsilon-\omega}}}{\rho^2} - 1 = \frac{1}{(\rho V)^2} \sum_{\mathbf{k}, \mathbf{k}'} \delta(\varepsilon - \varepsilon_{\mathbf{k}}) \delta(\varepsilon - \omega - \varepsilon_{\mathbf{k}'}) - 1 \\ &= -\frac{1}{(2\pi\rho V)^2} \int d^d \mathbf{x} \int d^d \mathbf{y} [\overline{G_\varepsilon^R(\mathbf{x}, \mathbf{x}) - G_\varepsilon^A(\mathbf{x}, \mathbf{x})}] [\overline{G_{\varepsilon-\omega}^R(\mathbf{y}, \mathbf{y}) - G_{\varepsilon-\omega}^A(\mathbf{y}, \mathbf{y})}] - 1. \end{aligned} \quad (2.32)$$

Evidently, δR_2 is directly related to the correlation function K , defined in Eq. (2.11), since the products $G^R G^R$ and $G^A G^A$ have no non-trivial dependence on disorder:¹

$$\delta R_2(\omega) = \frac{1}{V^2} \int d^d \mathbf{x} \int d^d \mathbf{y} \frac{1}{\pi\rho} \text{Re}[\delta K(\mathbf{x}, \mathbf{y}, \omega)] = \frac{1}{\pi\rho V} \text{Re}[\delta K(\mathbf{q} = 0, \omega)]. \quad (2.33)$$

1. Due to Eq. (2.14), we have $\gamma \sum_{\mathbf{k}} G_\varepsilon^R(\mathbf{k}) G_{\varepsilon-\omega}^R(\mathbf{k}) \ll 1$ in contrast to Eq. (2.17). It follows that diagrams with impurity lines between G_ε^R and $G_{\varepsilon-\omega}^R$ are small: $\overline{G^R G^R} \approx \overline{G^R} \overline{G^R}$.

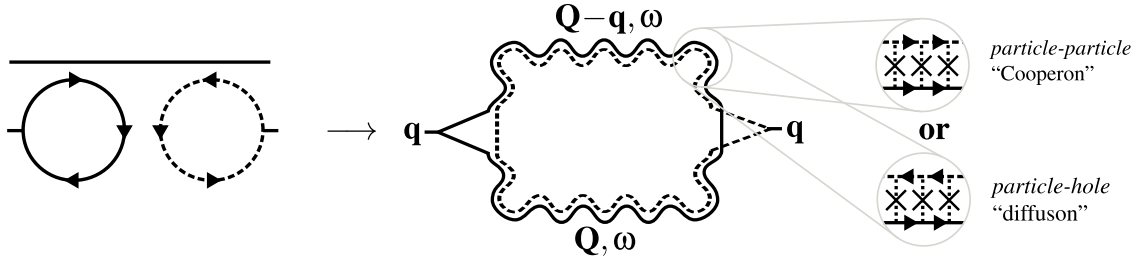


Figure 2.8: The loop-expansion applied to the correlation function K , defined in Eq. (2.11). The impurity ladders (wavy double-lines) describe multiple scattering in either the particle-hole (diffuson) or the particle-particle (Cooperon) channel.

The one-loop correction to this quantity has been calculated by Altshuler and Shklovskii (1986). For small $Dq^2\tau$, $\omega\tau$, we apply the loop-expansion and obtain to leading order the diagram shown in Fig. 2.8. It corresponds to the expression

$$\delta K(\mathbf{q}, \omega) = \frac{1}{2\pi\rho V} \sum_{\mathbf{Q}} [P_d(\mathbf{Q}, \omega)P_d(\mathbf{Q} - \mathbf{q}, \omega) + P_c(\mathbf{Q}, \omega)P_c(\mathbf{Q} - \mathbf{q}, \omega)]. \quad (2.34)$$

Note that the relative direction of the Green's functions can be chosen freely. Thus, diagrams with diffusion- *and* Cooperon-propagators have to be considered. Using Eq. (2.34) in Eq. (2.33), we find

$$\delta R_2(\omega) = \frac{1}{2(\pi\rho V)^2} \sum_{\mathbf{Q}} \text{Re} [P_d(\mathbf{Q}, \omega)^2 + P_c(\mathbf{Q}, \omega)^2]. \quad (2.35)$$

Note that higher order loop diagrams can be calculated by substituting the renormalized diffusion constant, Eq. (2.30), into Eq. (2.35).

2.1.3 Magnetic field dependence and time-reversal symmetry

In the previous section we have established that physical properties of disordered systems can be expressed in terms of correlation functions of Green's functions, such as the functions P and K defined in Eqs. (2.10, 2.11). Furthermore, we showed how they can be expressed in terms diffusive propagators using a loop-expansion. Two different types of propagators have been identified, diffusons P_d and Cooperons P_c , which differ by their alignment of the direction of the Green's functions.

In the discussion before Eq. (2.22), we have argued that $P_c = P_d$ if the time-reversal symmetry holds, and $P_c = 0$ if broken. Thus, as a first step, we may introduce a parameter β ,

$$\beta = \begin{cases} 1 & \text{system has time reversal symmetry} \\ 2 & \text{time reversal symmetry is broken} \end{cases}, \quad (2.36)$$

to express the correlation functions in a consistent way. E.g. using Eq. (2.36), the two-level correlation function R_2 , Eq. (2.34), can be written as

$$R_2(\omega) = 1 + \frac{1}{\beta\pi^2(\rho V)^2} \sum_{\mathbf{Q}} \text{Re} \frac{1}{(DQ^2 - i\omega)^2}. \quad (2.37)$$

However, the usual way to quantitatively account for the crossover between the two cases described by Eq. (2.36), is to introduce a ‘‘mass’’ term to the Cooperon propagator of the form

$$P_c(\mathbf{q}, \omega) = \frac{1}{Dq^2 - i\omega} \longrightarrow \frac{1}{Dq^2 - i\omega + \gamma}, \quad (2.38)$$

or in real time:

$$P_c(\mathbf{q}, t) = \theta(t)e^{-D\mathbf{q}^2 t} \longrightarrow \theta(t)e^{-D\mathbf{q}^2 t} e^{-\gamma t}. \quad (2.39)$$

γ plays the role of an *infrared cutoff* to the sums appearing in the loop-expansion, such as Eq. (2.22). The diffuson propagator P_d calculated in Eq. (2.18), on the other hand, cannot acquire a mass due to the requirement of particle conservation.¹ Since the “mass” term γ describes the *dephasing* of the electron and the hole of the Cooperon it is called the *dephasing rate*, and the corresponding time-scale $\tau_\phi = 1/\gamma$ the *dephasing time*. In Section 2.2, we will calculate the contribution of electron interactions to the mass of the Cooperon.

To explicitly see how a finite value of γ can appear, it is instructive to consider the influence of a magnet field on P_d and P_c . The Hamiltonian for a free electron in a random potential and an external magnetic field described by the vector potential \mathbf{A} can be written as

$$H = -\frac{1}{2m} \left(\nabla + i\frac{e}{c}\mathbf{A} \right)^2 + V(\mathbf{x}). \quad (2.40)$$

Assuming that the magnetic field is sufficiently weak, such that it does not affect the dynamics of the electron², it’s sole effect is to modify the phase of the wave functions. For a sufficiently slowly varying field, it can be shown that the Green’s functions acquire an additional phase factor (see e.g. the discussion in [Fetter and Walecka \(1971\)](#)):

$$\overline{G}_\varepsilon^{R/A}(\mathbf{x}, \mathbf{y}, \mathbf{A}) = \overline{G}_\varepsilon^{R/A}(\mathbf{x}, \mathbf{y}) e^{i\phi(\mathbf{x}, \mathbf{y})}, \quad (2.41)$$

where the phase ϕ is given by a line integral over the vector potential:

$$\phi(\mathbf{x}, \mathbf{y}) = -e \oint_{\mathbf{x}}^{\mathbf{y}} d\mathbf{z} \cdot \mathbf{A}(\mathbf{z}). \quad (2.42)$$

For diffuson propagators, which are given by geometric series of the products $\overline{G}^R(\mathbf{x}, \mathbf{y})\overline{G}^A(\mathbf{y}, \mathbf{x})$, the phase factors of Eq. (2.41) cancel exactly, such that P_d is unaffected by the magnetic field, and still described by the diffusion equation Eq. (2.20). For Cooperon propagators, on the other hand, which are described by the products $\overline{G}^R(\mathbf{x}, \mathbf{y})\overline{G}^A(\mathbf{x}, \mathbf{y})$, the phases add up and lead to a total phase difference of 2ϕ . Thus, the Cooperon in a magnetic field obeys a covariant diffusion equation given by

$$\left[-i\omega - D(\nabla_{\mathbf{y}} + 2ieA(\mathbf{y}))^2 \right] P_c(\mathbf{x}, \mathbf{y}, \omega) = \delta(\mathbf{x} - \mathbf{y}), \quad (2.43)$$

see [Aronov and Sharvin \(1987\)](#) for details. One consequence of the substitution $\nabla \rightarrow \nabla + 2ieA$ is that in the geometry of a ring or a cylinder with perpendicular magnetic field \mathbf{B} , the Cooperon becomes a $\phi_0/2$ -periodic function of the flux, where $\phi_0 = 2\pi c/e$ is the flux quantum [[Altshuler et al., 1981a](#)]. Furthermore, the phase difference leads to a decay of the Cooperon at sufficiently large \mathbf{B} . The characteristic time of the decay, τ_B , can be estimated from the condition

$$\Delta\phi = \frac{BA(\tau_B)}{\phi_0} \simeq 1, \quad (2.44)$$

where $A(t)$ is the typical area perpendicular to the magnetic field strength B , which is covered by the electron trajectory in time t . For an infinite plane $A(t) \propto (\sqrt{Dt})^2$, such that $\tau_B \propto 1/B$ [[Altshuler et al.](#),

1. The situation is different for the diffuson propagators appearing in the calculation of fluctuations, such as Eq. (2.34). In this case, the Green’s functions correspond to measurements of the density of states *at different times* and thus correspond to different realizations of disorder.

2. This is the case for $r_c \ll \ell$, where $r_c = mv_F/eB$ is the cyclotron radius.

1980]. The case of a longitudinal magnetic field \mathbf{B} , as well as quasi-1D wires, have been investigated by Altshuler *et al.* (1980). The corresponding Cooperon propagator is thus of the form suggested in Eq. (2.38):

$$P_c(\mathbf{q}, \omega) = \frac{1}{D\mathbf{q}^2 - i\omega + 1/\tau_B}. \quad (2.45)$$

2.1.4 Validity of the loop-expansion

The one-loop quantum correction to the diffusion constant, Eq. (2.30), breaks down if

$$\frac{1}{\rho V \pi} \sum_{\mathbf{Q}} \frac{1}{D\mathbf{Q}^2 - i\omega + \gamma} \gg 1, \quad (2.46)$$

where we used expression (2.38) for the Cooperon propagator with a dephasing rate γ . Note that the prefactor of the sum, the inverse density of states, is often called *level spacing*:

$$\Delta \equiv \frac{1}{\rho V}. \quad (2.47)$$

Evidently, including higher order loop diagrams leads to additional terms on the l.h.s of Eq. (2.46) which are of the same form as the one-loop term, albeit raised to a higher power¹, cf. Section 2.3. Moreover, the quantum corrections to other correlation functions, such as K , can be constructed by substituting the renormalized diffusion constant for D . Thus, the criterion (2.46) applies to the loop-expansion in general.

The summation in Eq. (2.46) runs over all diffusive modes $Q_{\alpha,n}$, where $\alpha = x, y, z$ and $n \in \mathbb{Z}$. For example, in an open (not confined, connected) system of size L_α in direction α , the modes are $Q_{\alpha,n} \sim \frac{n}{L_\alpha}$. Evidently, the sum is dominated by large momenta (UV) in dimensions $d \geq 2$ and by small momenta (IR) in $d \leq 2$.² Thus, we do not consider the case $d = 3$ in the following, where quantum corrections are generally weak and independent of γ . Furthermore, we follow the general practice to introduce an upper cutoff $1/\ell$ for $d = 2$, effectively assuming no quantum corrections from ballistic scales. The IR behavior on the other hand, is governed by ω and γ for a closed system. For connected systems, the sum has no zero mode in the connected direction and may also be dominated by the so-called *Thouless energy* $E_{\text{Th}} = D/L^2$, representing the smallest diffusive mode. The inverse of the Thouless energy, the so-called *Thouless time* $\tau_{\text{Th}} = L^2/D$ is the average time needed to diffusively traverse the whole sample.

The implications of these findings to two types of experiments, typical conducted with disordered systems, are as follows:

- In transport experiments on open systems, which we will analyze (along with confined systems) in more detail in Chapter 3, the energy ω corresponds to the AC-frequency of the current source, and is typically small. In this case, for weak dephasing $\gamma \ll E_{\text{Th}}$, the quantum corrections are controlled by the small parameter

$$\frac{1}{g} \equiv \frac{\Delta}{2\pi E_{\text{Th}}} \ll 1, \quad (2.48)$$

1. Note that the Cooperon propagator in Eq. (2.46) may be replaced by a diffuson propagator in higher loops. But since the diffusion propagator has no dependence on a magnetic field, see Section 2.1.3, and quantum effects in disordered systems are often measured via the magnetic field dependent parts of observables, this is usually not a problem.

2. Note that d is the effective ‘‘quasi’’ dimension of the diffusive process, for which ℓ is the shortest length scale. The dimension of the underlying electronic system might be larger.

where g is the so-called *dimensionless conductance* of the system, which is always large for a disordered metal (see Eq. (3.21)), implying that the loop-expansion is always valid. This regime is often called *mesoscopic*, since the sample is completely phase coherent due to $\tau_\phi \gg \tau_{\text{Th}}$. Simultaneously, this regime is often called *universal*, since the quantum corrections to the conductance g become $g \times \frac{1}{g} \sim 1$.

For strong dephasing $E_{\text{Th}} \ll \gamma$, on the other hand, the corrections are controlled by the ratio Δ/γ . In this regime, the temperature dependence of the dephasing time can be determined directly from the amplitude of the quantum corrections.

- Isolated systems can be studied by measuring their response to external electric or magnetic fields, and we will give a detailed discussion of the polarizability of disordered metals in Chapter 4. In this case, ω is the frequency of the external field, and the quantum corrections are controlled by the parameter $\Delta/\max(\gamma, \omega)$. Evidently, at sufficiently low temperatures and frequencies, the loop-expansion can break down in this case. Since the level broadening γ becomes smaller than the level spacing Δ in this limit, it can be interpreted as a transition to a *discrete level* regime. The preferred theoretical method to study systems in this regime is the so-called random matrix theory (RMT), which we discuss briefly in Section 2.1.6. However, there is no straightforward way to include dephasing in RMT.

2.1.5 Field theoretical approaches

The field theoretical approach to disordered systems starts from a representation of the Green's function of Eq. (2.1) as an integral over a complex vector field $\phi(\mathbf{x})$, see [Feynman and Hibbs \(1965\)](#):

$$G_\varepsilon^R(\mathbf{x}, \mathbf{y}) = \langle \mathbf{x} | \frac{1}{\varepsilon - \hat{H}_0 - \hat{V} \pm i0} | \mathbf{y} \rangle = -i \frac{\int D\phi D\phi^* (\phi(\mathbf{x})\phi^*(\mathbf{y})) \exp(iS[\phi^*, \phi])}{\int D\phi D\phi^* \exp(iS[\phi^*, \phi])}, \quad (2.49)$$

with the action

$$S[\phi^*, \phi] = \int d^d \mathbf{z} \phi^*(\mathbf{z}) [(\varepsilon + i0) - \hat{H}_0 - \hat{V}] \phi(\mathbf{z}). \quad (2.50)$$

Averaging over the random potential V with the probability distribution function (2.2) presents a technical challenge often called the *problem of denominator*: Due to the appearance of V in the numerator and the denominator, the integral over fluctuating variables is largely intractable (see e.g. the discussion in [Altland and Simons \(2006\)](#)). Different approaches have been identified to circumvent this problem, the most prominent being the *replica trick* [[Edwards and Anderson, 1975](#)], the *Keldysh technique* [[Kamenev, 2005](#)], and the *supersymmetry approach* [[Efetov, 1983, 1997](#)]. They share the feature that the propagator, Eq. (2.49), is expressed as a field-integral without the necessity of a normalization factor in the denominator. As a result the disorder average is doable and leads to a quartic term in the fields of the following form:

$$S[\psi^*, \psi] \longrightarrow \bar{S}[\psi^*, \psi] = \int d^d \mathbf{z} \psi^*(\mathbf{z}) [(\varepsilon + i0) - \hat{H}_0] \psi(\mathbf{z}) + \frac{\gamma}{2} [\psi^*(\mathbf{z})\psi(\mathbf{z})]^2. \quad (2.51)$$

In Eq. (2.51), we wrote ψ instead of ϕ to make clear that this field must have a non-trivial internal structure to avoid the denominator, e.g. in the replica formalism it carries an additional *replica index* and in the supersymmetry approach it is a so-called *supervector* field which includes bosonic and fermionic degrees of freedom. The usual strategy to describe systems far from localization is now to decouple the disorder-generated quartic term by the *Hubbard-Stratonovich* transformation [[Hubbard,](#)

1959]. This is done by introducing an auxiliary field $Q(\mathbf{x})$ and applying the identity

$$\exp\left(-\frac{1}{2}[\Psi^*(\mathbf{z})\Psi(\mathbf{z})]^2\right) = \sqrt{\frac{1}{2\pi}} \int DQ \exp\left(-\frac{1}{2}Q(\mathbf{z})^2 - iQ(\mathbf{z})\Psi^*(\mathbf{z})\Psi(\mathbf{z})\right) \quad (2.52)$$

to the quartic term of Eq. (2.51). Importantly, due to the structure of the field Ψ , the Hubbard-Stratonovich field Q must be *matrix valued*. After this transformation, the Ψ field can be integrated out and one obtains an effective action that depends only on Q . However, minimizing this effective action is not straightforward, since it is characterized by a whole *manifold* of saddle points such that Q and has to obey *non-linear constraints*. Performing a gradient expansion and expanding in excitation energy ω to linear order and integrating out massive modes, one can derive an action describing the low-lying excitations, which is known as the *non-linear sigma model*:

$$S_\omega[Q] \sim \int d^d \mathbf{z} \operatorname{Tr}[-D[\nabla Q(\mathbf{z})]^2 - 2i\omega Q(\mathbf{z})], \quad \text{with } Q(\mathbf{z})^2 = \mathbb{1}. \quad (2.53)$$

In the context of the replica trick Eq. (2.53) was first derived by Schäfer and Wegner (1980); Efetov *et al.* (1980), and in the context of the supersymmetric technique by Efetov (1983).

The results for correlation functions calculated by using this low-energy field theory are identical to those discussed in the previous sections. In particular, a similar loop-expansion can be generated, and the same limitations as discussed in Section 2.1.4 apply. Furthermore, Hikami (1981) has shown that a certain parametrization of the Q matrix field exists, where the results of the Hikami boxes are identical to those obtained in perturbation theory, including the unphysical divergences discussed after Eq. (2.24). In the field theoretical representation, a *dimensional regularization* scheme is usually applied (see Brezin *et al.* (1980)) to obtain the physical results, and we show in Section 2.3, that the results obtained in this way are identical, up to and including the second loop, to those obtained by the “moving vertex”-procedure discussed in Fig. 2.6.

2.1.6 Comparison with random matrix theory

We have seen in the previous sections that only perturbative results for correlation functions of the Green’s functions of our Hamiltonian (2.1) are known. In this section, we consider a simpler system where non-perturbative results can be found: We assume that the Hamiltonian is simply given by a random matrix \mathbf{H} . In comparison to Eq. (2.1), this means that all spatial degrees of freedom in the problem are neglected. Strictly speaking, these results are only relevant for effectively 0D systems, such as isolated quantum-dots. Nevertheless, we will discuss such a system here to gain insights on the validity of the loop-expansion.

Random matrix theory (RMT) is a broad topic with an extremely wide range of applications in physics and mathematics, such as: condensed matter physics, chaotic systems, spectra of complex nuclei, number theory, quantum gravity, traffic networks, stock movement in the financial markets, etc. An overview on the main ideas, results and applications can be found in Mehta (2004). However, the literature on this topic is often very mathematically oriented, for which reason we find it necessary to discuss several aspects of RMT related to our work in this section.

The celebrated Gaussian random matrix ensemble of Wigner and Dyson is defined by the probability distribution function (cf. Eq. (2.2))

$$P(\mathbf{H}) \propto \prod_{n,m=1}^N \exp(-a|\mathbf{H}_{nm}|^2). \quad (2.54)$$

Eq. (2.54) describes $N \times N$ hermitian matrices $\mathbf{H} = \mathbf{H}^\dagger$, where each entry is an independent Gaussian random variable. \mathbf{H} is identified as the Hamiltonian of a system, having N energy levels. Depending on the global symmetry, the matrix elements \mathbf{H}_{nm} are restricted: with time reversal symmetry, $\mathbf{H}_{nm} \in \mathbb{R}$, while $\mathbf{H}_{nm} \in \mathbb{C}$, if time reversal symmetry is broken. The symmetry is usually encoded in the parameter β as follows

$$\beta = \begin{cases} 1 & \text{for } \mathbf{H}_{nm} \in \mathbb{R} \quad \text{Gaussian orthogonal ensemble (GOE)} \\ 2 & \text{for } \mathbf{H}_{nm} \in \mathbb{C} \quad \text{Gaussian unitary ensemble (GUE)} \end{cases}, \quad (2.55)$$

which is in analogy to the parameter introduced in Eq. (2.55). Note that the situation is more complicated if spin degrees of freedom are considered, but we restrict ourselves here to the symmetry classes defined in Eq. (2.55).

Other probability distribution functions than Eq. (2.54) are the subject of active research. In particular, the model originally devised by Anderson (1958) to describe the localization transition can be studied by a *banded* RMT, where the matrix elements in the exponential of Eq. (2.54) are weighted with respect to their distance to the diagonal. Remarkably, many of these models can be solved in a broad range of parameters, see e.g. Fyodorov and Mirlin (1991); Bunder *et al.* (2007); Yevtushenko and Kravtsov (2003); Yevtushenko and Ossipov (2007).

In the following we derive the density of states and the n -level correlation functions (loosely following Kravtsov (2009)), which will be used in Chapter 4. We use the so-called *method of orthogonal polynomials* here, and note that the same results can be obtained from a field-theoretical approach, namely, a 0D limit of the non-linear sigma model, see e.g. Mirlin (2000). We restrict our derivation to the simpler unitary ensemble ($\beta = 2$), and then discuss briefly the generalization to $\beta = 1$. As a first step, we rewrite the probability distribution function (2.54) in terms of the eigen-energies $\{\epsilon_n\}$ of \mathbf{H} as follows

$$P(\{\epsilon_n\}) = C \cdot \mathcal{J}(\epsilon_n) \cdot \exp\left(-a \sum_{i=1}^N \epsilon_i^2\right). \quad (2.56)$$

where C is a normalization constant, and \mathcal{J} is the Jacobian of the transformation $\mathbf{H} = \mathbf{U}\mathbf{D}\mathbf{U}^\dagger$, where \mathbf{U} is a unitary matrix and \mathbf{D} is a diagonal matrix containing the eigen-energies. The Jacobian is given by the square of the so-called *Vandermonde determinant* V_N :

$$\mathcal{J} = |V_N|^\beta, \quad V_N = \prod_{1 \leq i < j \leq N} |\epsilon_i - \epsilon_j| = \begin{vmatrix} 1 & 1 & \dots & 1 \\ \epsilon_1 & \epsilon_2 & \dots & \epsilon_N \\ \epsilon_1^2 & \epsilon_2^2 & \dots & \epsilon_N^2 \\ \dots & \dots & \dots & \dots \\ \epsilon_1^N & \epsilon_2^N & \dots & \epsilon_N^N \end{vmatrix}. \quad (2.57)$$

The result (2.57) can be explained by the following two arguments: (1) \mathcal{J} must be a polynomial of degree $N(N-1)$ since \mathbf{U} has $N(N-1)/2$ independent complex variables, with independent real and imaginary part, and (2), since the Jacobian is a determinant, which is an alternating form, \mathcal{J} has to vanish whenever two eigen-values are identical. The latter is a fundamental property of random matrices called *level repulsion*.

Using Eq. (2.56), we can directly evaluate quantities such as the averaged density of states $\overline{\rho_\epsilon}$, which is defined in analogy to Eq. (2.8) as

$$\overline{\rho_\epsilon} = \overline{\sum_{n=1}^N \delta(\epsilon - \epsilon_n)}, \quad (2.58)$$

with the average being now calculated with respect to probability distribution (2.54). To do this, we consider a seemingly unrelated problem: The wave-function of a system of N non-interacting 1D fermions in a parabolic potential $V(x) \propto x^2$ is given by the *Slater determinant*:

$$\Psi(\{x_n\}) \propto \begin{vmatrix} \varphi_0(x_1) & \varphi_0(x_2) & \dots & \varphi_0(x_N) \\ \varphi_1(x_1) & \varphi_1(x_2) & \dots & \varphi_1(x_N) \\ \dots & \dots & \dots & \dots \\ \varphi_N(x_1) & \varphi_N(x_2) & \dots & \varphi_N(x_N) \end{vmatrix}, \quad (2.59)$$

where $\varphi_n(x) = H_n(x) \exp(-x^2/2)$ and $H_n(x)$ are the *Hermite polynomials*. As orthogonal polynomials, they can be defined via a three-term recursive relation:

$$H_0(x) = 1, \quad H_1(x) = x, \quad H_{n+1}(x) = 2xH_n(x) - 2nH_{n-1}(x). \quad (2.60)$$

We immediately note the similarity between the Slater determinant (2.59) and the Vandermonde determinant (2.57). In fact, using Eq. (2.60) it is easy to show that the absolute value squared of the wave-function (2.59) is equal to the probability density function (2.56), after substituting the coordinates x_n by ε_n :

$$P(\{\varepsilon_n\}) = |\Psi(\{\varepsilon_n\})|^2. \quad (2.61)$$

In the language of non-interacting fermions, the density of states (2.58) is nothing but the expectation value of the N -particle density operator $\hat{n}(x) = \sum_{i=1}^N \delta(x - x_i)$. In its second quantized form it is given by $\hat{n}(x) = \hat{\Psi}^\dagger(x)\hat{\Psi}(x)$, where the field operators are defined as $\hat{\Psi}(x) \equiv \sum_n \varphi_n(x)\hat{a}_n$ and $\hat{\Psi}^\dagger(x) \equiv \sum_n \varphi_n(x)\hat{a}_n^\dagger$. Thus, the expectation value of $\hat{\Psi}^\dagger(x)\hat{\Psi}(x)$ in the N -particle ground state described by $\Psi(\{\varepsilon_n\})$ is equal to the density of states averaged with respect to the probability distribution function $P(\{\varepsilon_n\})$. It directly follows that

$$\overline{\rho_\varepsilon} = \sum_{n=0}^{N-1} \varphi_n(\varepsilon)^2. \quad (2.62)$$

Eq. (2.62) relates the density of states of a unitary random matrix to a sum of products of orthogonal polynomials. The advantage of this representation is due to the famous *Christoffel-Darboux formula*, which allows to calculate sums of this type very efficiently:

$$K_N(x, y) \equiv \sum_{n=0}^{N-1} \varphi_n(x)\varphi_n(y) = \sqrt{\frac{N}{2}} \frac{\varphi_{N-1}(x)\varphi_N(y) - \varphi_{N-1}(y)\varphi_N(x)}{x - y}. \quad (2.63)$$

The large- n limit of the Hermite polynomials is well-known in the physical literature, in particular in the context of the WKB approximation [Schwabl, 2002]:

$$\lim_{\substack{n \rightarrow \infty \\ x \rightarrow 0}} (-1)^n n^{1/4} \varphi_{2n}(x) = \frac{\cos(2n^{1/2}x)}{\sqrt{\pi}}, \quad \lim_{\substack{n \rightarrow \infty \\ x \rightarrow 0}} (-1)^n n^{1/4} \varphi_{2n+1}(x) = \frac{\sin(2n^{1/2}x)}{\sqrt{\pi}}. \quad (2.64)$$

Using Eq. (2.64) in Eq. (2.63) for large N , we immediately obtain

$$K_{N \rightarrow \infty}(x, y) = \frac{1}{\pi} \frac{\sin(\sqrt{2N}(x - y))}{x - y}. \quad (2.65)$$

As a result the density of states of a unitary random matrix with large N and ε close to the band center is given by:¹

$$\overline{\rho_\varepsilon} = K_{N \rightarrow \infty}(\varepsilon, \varepsilon) = \frac{1}{\pi} \sqrt{2N}, \quad (2.66)$$

independent of ε , in full analogy to the density of states at the Fermi energy considered in Eq. (2.8). In the following we will denote it simply as $\rho \equiv \overline{\rho_\varepsilon}$.

Correlation functions of higher order can be calculated in the same way: For example, the two-level correlation function R_2 can be expressed by four fermionic field operators, $\hat{\Psi}^\dagger(x)\hat{\Psi}(x)\hat{\Psi}^\dagger(y)\hat{\Psi}(y)$, and thus, can also be represented in terms of the wave-functions φ_n and the functions K_N defined in Eq. (2.63):²

$$R_2(\varepsilon, \varepsilon') = \frac{\overline{\rho_\varepsilon \rho_{\varepsilon'}}}{\rho^2} = \frac{1}{\rho^2} \sum_{n=0}^{N-1} \sum_{m=0}^{N-1} [\varphi_n^2(\varepsilon)\varphi_m^2(\varepsilon') - \varphi_n(\varepsilon)\varphi_n(\varepsilon')\varphi_m(\varepsilon')\varphi_m(\varepsilon)] \quad (2.67)$$

$$= \frac{1}{\rho^2} [K_N(\varepsilon, \varepsilon)K_N(\varepsilon', \varepsilon') - K_N^2(\varepsilon, \varepsilon')]. \quad (2.68)$$

It is easy to show that the general n -level correlation function is given by the following determinant:

$$R_n(\varepsilon_1, \varepsilon_2, \dots, \varepsilon_n) = \frac{1}{\rho^n} \begin{vmatrix} K_N(\varepsilon_1, \varepsilon_1) & K_N(\varepsilon_1, \varepsilon_2) & \dots & K_N(\varepsilon_1, \varepsilon_n) \\ K_N(\varepsilon_2, \varepsilon_1) & K_N(\varepsilon_2, \varepsilon_2) & \dots & K_N(\varepsilon_2, \varepsilon_n) \\ \dots & \dots & \dots & \dots \\ K_N(\varepsilon_n, \varepsilon_1) & K_N(\varepsilon_n, \varepsilon_2) & \dots & K_N(\varepsilon_n, \varepsilon_n) \end{vmatrix}. \quad (2.69)$$

Using Eq. (2.65) in Eq. (2.68) we find R_2 in the limit $N \rightarrow \infty$

$$R_2^{GUE}(\varepsilon, \varepsilon') = 1 - \frac{\sin^2(\pi s)}{(\pi s)^2}, \quad s \equiv \frac{\varepsilon - \varepsilon'}{\Delta}, \quad (2.70)$$

where the mean level spacing is defined in analogy to Eq. (2.47) as $\Delta = 1/\rho = \pi/\sqrt{2N}$.

In the orthogonal ensemble ($\beta = 1$), the Jacobian \mathcal{J} in Eq. (2.56) is proportional to $|V_D|$ instead of $|V_D|^2$. In this case, there is a similar analogy to interacting particles: the so-called *Calogero-Sutherland model* [García-García and Verbaarschot, 2003]. However, instead of orthogonal polynomials (such as the Hermite polynomials), so-called skew-orthogonal polynomials of real type have to be considered [Mehta, 2004]. Nevertheless it can be shown that the average density of states and the n -level correlation functions are still given by Eqs. (2.66, 2.69), when replacing the real-valued function K_N with a different, biquaternion³-valued function. The result for the two-level correlation function in the orthogonal ensemble is

$$R_2^{GOE}(\varepsilon, \varepsilon') = 1 - \frac{\sin^2(\pi s)}{(\pi s)^2} - \left[\int_s^\infty du \frac{\sin(\pi u)}{\pi u} \right] \left[\frac{d}{ds} \frac{\sin(\pi s)}{\pi s} \right]. \quad (2.71)$$

In the limits of large energy separations, the envelope of Eqs. (2.70, 2.71) yield

$$R_2(\omega/\Delta \rightarrow \infty) = 1 - \frac{\Delta^2}{\beta\pi^2\omega^2}. \quad (2.72)$$

-
1. Since the limits $N \rightarrow \infty$ and $x \rightarrow y$ in Eq. (2.63) do not commute, Eq. (2.66) is only valid for $2N \gg \varepsilon^2$. For arbitrary N , the result for ρ_ε is Wigner's celebrated *semi-circle*: $\rho_\varepsilon = \sqrt{2N - \varepsilon^2}/\pi$, see Mehta (2004).
 2. In Eq. (2.67) and further expressions for R_2 we assume $\varepsilon \neq \varepsilon'$, and neglect a trivial contribution $R_2(\varepsilon, \varepsilon') \propto \delta(\varepsilon - \varepsilon')$ stemming from one and the same level n in Eq. (2.58).
 3. Biquaternions are quaternions where all 4 coefficients are complex numbers.

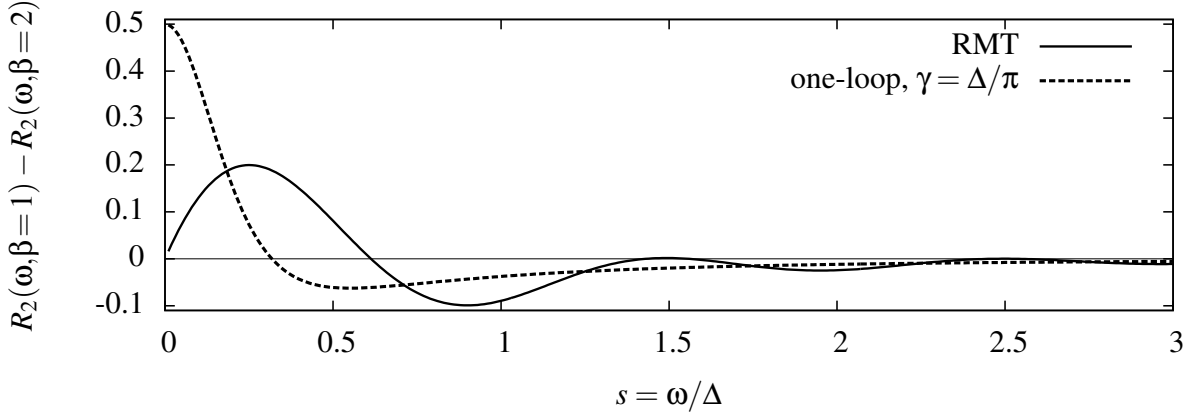


Figure 2.9: The GUE-GOE difference of the two-level correlation functions: Comparison of the perturbative one-loop result with the non-perturbative RMT result.

in full agreement with the perturbative result (2.37). Moreover, they show *non-perturbative* oscillations with a period of Δ .

To further compare the RMT results with the loop-expansion (“LE”), we consider the 0D limit of Eq. (2.33) obtained by retaining only the zero-mode of the internal sum:

$$R_2^{\text{LE}}(\omega) = 1 + \frac{\Delta^2}{\pi^2\beta} \text{Re} \frac{1}{(\gamma - i\omega)^2}. \quad (2.73)$$

We remind the reader that the RMT results cannot describe a γ dependence, while the perturbative results are valid only if either γ or ω is larger than Δ . Thus, to compare the ω dependence of R_2 at $\omega \sim \Delta$, we set $\gamma = \Delta/\pi$ in Eq. (2.73). The result is shown in Fig. 2.9. Note that apart from the non-perturbative oscillations, the one-loop correction qualitatively reproduces the exact result correctly at $\omega \gtrsim \Delta$.

2.2 Dephasing due to electron interactions

We have argued in Section 2.1.3, that all processes that break the time-reversal symmetry of the system lead to a reduction of the quantum corrections described by Cooperon propagators. Moreover, we have introduced the dephasing time τ_ϕ in terms of the inverse ‘‘Cooperon mass’’ $\gamma = 1/\tau_\phi$ in Eq. (2.38). The goal of this section is a description of dephasing due to inelastic scattering events.

Inelastic scattering of electrons in a disordered metal is typically due to interactions with phonons or other electrons. However, experiments in mesoscopic systems are usually conducted at temperatures $T \lesssim 1K$, where the lattice vibrations of the underlying crystal are effectively ‘‘frozen’’ [Altshuler *et al.*, 1981c]. Thus, in the following, we will concentrate solely on electron interactions and neglect the influence of phonons.

2.2.1 Keldysh perturbation theory

In contrast to the perturbation theory in the static potential $V(\mathbf{x})$ used in the first part of this Chapter, electron interactions in disordered metals are time-dependent due to *dynamical screening*, which we will discuss in the following section. Moreover, we have so far not accounted for the influence of temperature, which plays an important role in the description of inelastic scattering.

Two well-established formalisms have been developed to describe problems of this type: The *Matsubara* technique and the *Keldysh* technique. Both have their advantages and disadvantages (see e.g. Zagoskin (1998) for a detailed comparison): The former introduces discrete Matsubara frequencies, and requires to calculate a non-trivial analytic continuation to real frequencies in the end. In the latter, which we will employ here, the propagators become matrices. The reason for the matrix structure in the Keldysh technique is that the time evolution of the field operators is calculated by integrating the Hamiltonian over times along a closed contour from $-\infty$ to $+\infty$ and back to $-\infty$. This is in contrast to the integration over an inverse temperature interval in the Matsubara formalism or the real axis for $T = 0$. Since one needs to keep track of the location of the time arguments of the field operators in the perturbative expansions, and since each of them can be on the forward or backward contour, this leads to a 2×2 matrix structure for the propagators. The main advantages of the Keldysh technique are (i) that it can describe non-equilibrium situations, (ii) that the occurrence of a normalization factor (partition function) is avoided, and (iii) that a finite temperature is automatically accounted for. Note that the Keldysh technique has been developed primarily to deal with non-equilibrium processes, but we will restrict ourselves exclusively to *thermal equilibrium* in the following.

However, we will not give a detailed discussion or derivation of the Keldysh technique here and restrict ourselves purely to the ‘‘user perspective’’. The interested reader is referred to the books by Rammer (2007) and Kamenev (2011). Note that the matrix structure is not unique and many different conventions can be found in the literature. In the following, we strictly follow the notations of Rammer and Smith (1986), who use a representation originally introduced by Larkin and Ovchinnikov (1975).

In Section 2.1 we have introduced the retarded and advanced Green’s functions as electron propagators, and argued that they have a simple perturbative expansion in a static potential $V(\mathbf{x})$, cf. Eq. (2.1). In the Keldysh perturbation theory, the propagators of the electrons \underline{G} and electron interactions \underline{U} are represented as upper triangular matrices, defined as:

$$\underline{G}_\varepsilon(\mathbf{x}, \mathbf{y}) = \begin{pmatrix} G_\varepsilon^R(\mathbf{x}, \mathbf{y}) & G_\varepsilon^K(\mathbf{x}, \mathbf{y}) \\ 0 & G_\varepsilon^A(\mathbf{x}, \mathbf{y}) \end{pmatrix}, \quad \underline{U}_\omega(\mathbf{x}, \mathbf{y}) = \begin{pmatrix} U_\omega^R(\mathbf{x}, \mathbf{y}) & U_\omega^K(\mathbf{x}, \mathbf{y}) \\ 0 & U_\omega^A(\mathbf{x}, \mathbf{y}) \end{pmatrix}, \quad (2.74)$$

where the so-called *Keldysh Green’s functions* are given in thermal equilibrium by

$$G_\varepsilon^K(\mathbf{x}, \mathbf{y}) = h_\varepsilon [G_\varepsilon^R(\mathbf{x}, \mathbf{y}) - G_\varepsilon^A(\mathbf{x}, \mathbf{y})], \quad U_\omega^K(\mathbf{x}, \mathbf{y}) = g_\omega [U_\omega^R(\mathbf{x}, \mathbf{y}) - U_\omega^A(\mathbf{x}, \mathbf{y})], \quad (2.75)$$

with

$$h_\varepsilon = \tanh\left(\frac{\varepsilon}{2T}\right), \quad g_\omega = \coth\left(\frac{\omega}{2T}\right). \quad (2.76)$$

The information on the occupation of the energy levels at temperature T is fully contained in the functions h and g , defined in Eq. (2.76).

The relations of Eq. (2.75) are also known as *fluctuation dissipation theorem* (FDT), since the Keldysh Green's function effectively describes the fluctuations of the electron field operators, while the retarded and advanced functions describe their response to an external perturbation.

Let us now briefly summarize the rules of this perturbation theory: The perturbation expansion of the propagators (as described by Wick's theorem) at finite temperature is equivalent to the usual Feynman diagrams at $T = 0$, when replacing the time ordered Green's functions by the matrices defined in Eq. (2.74). In particular, multiplying Green's functions and expanding in scalar potentials is represented by the usual matrix multiplication. However, interaction vertices have to be distinguished by absorption, $\underline{\gamma}_a^i$ and emission $\underline{\gamma}_e^j$ vertices, and they have a tensor structure with the additional indices $i, j \in \{1, 2\}$ denoting the i, j 'th component of the matrix \underline{U} to which the Green's functions \underline{G} couple:

$$\underline{\gamma}_a^1 = \underline{\gamma}_e^2 = \frac{1}{\sqrt{2}} \begin{pmatrix} 1 & 0 \\ 0 & 1 \end{pmatrix}, \quad \underline{\gamma}_a^2 = \underline{\gamma}_e^1 = \frac{1}{\sqrt{2}} \begin{pmatrix} 0 & 1 \\ 1 & 0 \end{pmatrix}. \quad (2.77)$$

Moreover, matrix multiplication has to be carried out opposite to the propagation direction, which we will denote by arrows on the propagators. The tensor structure will become more clear in the examples below, see e.g. Eqs. (2.82, 2.113). The other rules are identical to the $T = 0$ theory. In particular, the diagrammatic n 'th order expansion of the electron Green's function in interaction propagators is multiplied by $i^n(-1)^F$, where F is the number of electron loops [Abrikosov *et al.*, 1965].

2.2.2 Electron interactions in disordered systems

In this section, we will begin our discussion of electron interactions by analyzing the influence of diffusive screening. Interactions between free electrons are described by a potential U_0 given by Coulomb's law [Jackson, 1962]:¹

$$U_0(\mathbf{x}, \mathbf{y}) = \frac{e^2}{|\mathbf{x} - \mathbf{y}|}, \quad U_0(\mathbf{q}) = \begin{cases} 4\pi e^2/|\mathbf{q}|^2 & (d = 3) \\ 2\pi e^2/|\mathbf{q}| & (d = 2) \\ -2e^2 \ln|\mathbf{q}|W & (d = 1) \end{cases}. \quad (2.78)$$

In a metal, the interaction is substantially screened due to the high electron density. This is usually accounted for in the *random phase approximation* (RPA), where the creation and annihilation of electron-hole pairs by the interaction are taken into account [Gell-Mann and Brueckner, 1957] (see e.g. Bruus and Flensberg (2004) for a detailed discussion). As a result, the effective Coulomb potential becomes short ranged:

$$U(\mathbf{x}, \mathbf{y}) = U_0(\mathbf{x}, \mathbf{y})e^{-\kappa|\mathbf{x} - \mathbf{y}|}, \quad (2.79)$$

where the *Thomas-Fermi screening wave-vector* is given by

$$\kappa = \begin{cases} \sqrt{8\pi e^2 \rho} & (d = 3) \\ 4\pi e^2 \rho & (d = 2) \end{cases}. \quad (2.80)$$

1. We follow the usual sign convention in Eq. (2.78). As a result, all diagrams are multiplied by $(-1)^I$, where I is the number of interaction lines.

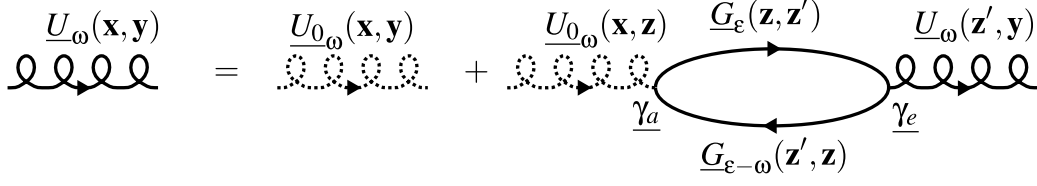


Figure 2.10: The interaction propagator in the random phase approximation (RPA).

For a metal, screening is very efficient and the corresponding screening length $\lambda_s = 1/\kappa$ is typically of the order of the Fermi wavelength, $\lambda_s \sim \lambda_F$.

In the presence of disorder, the RPA diagrams are modified and lead to a time dependence of the effective electron interaction, which we will calculate in the following. Accounting for the creation of electron-hole pairs, the electron interaction is given by the Dyson equation shown in Fig. 2.10, which corresponds to the expression

$$\underline{U}_\omega^{ij}(\mathbf{x}, \mathbf{y}) = \underline{U}_{0\omega}^{ij}(\mathbf{x}, \mathbf{y}) + 2 \int d^d \mathbf{z} d^d \mathbf{z}' \underline{U}_{0\omega}^{ik}(\mathbf{z}', \mathbf{y}) \underline{\Pi}_\omega^{kl}(\mathbf{z}, \mathbf{z}') \underline{U}_\omega^{lj}(\mathbf{x}, \mathbf{z}), \quad (2.81)$$

where \underline{A}^{ij} denotes the i, j -th component of the 2×2 matrix \underline{A} , and summation of repeated indices is implied. The factor “2” in Eq. (2.81) is due to spin degeneracy. Furthermore, we introduced the so-called *polarization function*¹²

$$\underline{\Pi}_\omega^{kl}(\mathbf{x}, \mathbf{y}) = i \int \frac{d\epsilon}{2\pi} \underline{\gamma}_a^{ij,k} \underline{G}_{\epsilon-\omega}^{jm}(\mathbf{y}, \mathbf{x}) \underline{\gamma}_e^{mn,l} \underline{G}_\epsilon^{ni}(\mathbf{x}, \mathbf{y}) \quad (2.82)$$

$$= \frac{i}{2} \int \frac{d\epsilon}{2\pi} \begin{pmatrix} G_\epsilon^R(\mathbf{x}, \mathbf{y}) G_{\epsilon-\omega}^K(\mathbf{y}, \mathbf{x}) & G_\epsilon^A(\mathbf{x}, \mathbf{y}) G_{\epsilon-\omega}^R(\mathbf{y}, \mathbf{x}) + G_\epsilon^R(\mathbf{x}, \mathbf{y}) G_{\epsilon-\omega}^A(\mathbf{y}, \mathbf{x}) \\ + G_\epsilon^K(\mathbf{x}, \mathbf{y}) G_{\epsilon-\omega}^A(\mathbf{y}, \mathbf{x}) & + G_\epsilon^K(\mathbf{x}, \mathbf{y}) G_{\epsilon-\omega}^K(\mathbf{y}, \mathbf{x}) \\ G_\epsilon^R(\mathbf{x}, \mathbf{y}) G_{\epsilon-\omega}^R(\mathbf{y}, \mathbf{x}) & G_\epsilon^K(\mathbf{x}, \mathbf{y}) G_{\epsilon-\omega}^R(\mathbf{y}, \mathbf{x}) \\ + G_\epsilon^A(\mathbf{x}, \mathbf{y}) G_{\epsilon-\omega}^A(\mathbf{y}, \mathbf{x}) & + G_\epsilon^A(\mathbf{x}, \mathbf{y}) G_{\epsilon-\omega}^K(\mathbf{y}, \mathbf{x}) \end{pmatrix} \quad (2.83)$$

$$\equiv \begin{pmatrix} \Pi_\omega^R(\mathbf{x}, \mathbf{y}) & \Pi_\omega^K(\mathbf{x}, \mathbf{y}) \\ 0 & \Pi_\omega^A(\mathbf{x}, \mathbf{y}) \end{pmatrix},$$

where we used the absorption and emission vertices defined in Eq. (2.77). We will show in Chapter 4, that $\Pi^{R/A}$ describes the linear response of the electron charge density to an external electric potential. Using Eq. (2.75) in Eq. (2.83), we find:

$$\begin{aligned} \Pi_\omega^R(\mathbf{x}, \mathbf{y}) &= (\Pi_\omega^A(\mathbf{x}, \mathbf{y}))^* \\ &= \frac{i}{2} \int_{-\infty}^{\infty} \frac{d\epsilon}{2\pi} [h_\epsilon - h_{\epsilon-\omega}] G_\epsilon^R(\mathbf{x}, \mathbf{y}) G_{\epsilon-\omega}^A(\mathbf{y}, \mathbf{x}) + h_{\epsilon-\omega} G_\epsilon^R(\mathbf{x}, \mathbf{y}) G_{\epsilon-\omega}^R(\mathbf{y}, \mathbf{x}) - h_\epsilon G_\epsilon^A(\mathbf{x}, \mathbf{y}) G_{\epsilon-\omega}^A(\mathbf{y}, \mathbf{x}), \end{aligned} \quad (2.84)$$

and for the Keldysh component the FDT holds true:

$$\Pi_\omega^K(\mathbf{x}, \mathbf{y}) = g_\omega [\Pi_\omega^R(\mathbf{x}, \mathbf{y}) - \Pi_\omega^A(\mathbf{x}, \mathbf{y})]. \quad (2.85)$$

Let us now calculate the disorder average of Eq. (2.84): the first term is of the form of the correlation function P , defined in Eq. (2.10), and can be calculated using the loop-expansion. Moreover, we

1. The summation over the repeated index i in Eq. (2.82) corresponds to a “trace” operation in the 2×2 Keldysh space.
2. $\underline{\Pi}^{21} = 0$ follows from $G^R(t)G^R(-t) = G^A(t)G^A(-t) = 0$.

found in Eq. (2.18) that it does not depend on energy ε . Thus, averaging the first term of Eq. (2.84) gives

$$\frac{i}{2} \overline{G_\varepsilon^R(\mathbf{x}, \mathbf{y}) G_{\varepsilon-\omega}^A(\mathbf{y}, \mathbf{x})} \int_{-\infty}^{\infty} \frac{d\varepsilon}{2\pi} [h_\varepsilon - h_{\varepsilon-\omega}] \approx \rho i\omega P_d(\mathbf{x}, \mathbf{y}, \omega). \quad (2.86)$$

The disorder average of the second term factorizes, see the discussion before Eq. (2.33), and after a Fourier transform, we obtain

$$\frac{i}{2} \int_{-\infty}^{\infty} d\varepsilon h_{\varepsilon-\omega} \sum_{\mathbf{k}} \overline{G_\varepsilon^R(\mathbf{k} + \mathbf{q}) G_{\varepsilon-\omega}^R(\mathbf{k})} \approx \frac{i}{2} \int_0^{\infty} \frac{d\varepsilon}{2\pi} \sum_{\mathbf{k}} \overline{G_\varepsilon^R(\mathbf{k}) G_\varepsilon^R(\mathbf{k})} = \frac{i}{2\pi} \sum_{\mathbf{k}} \overline{G_0^R(\mathbf{k})} \quad (2.87)$$

where we shifted $h_{\varepsilon-\omega}$ by a constant term ($+1/2$) which gives no contribution to the integral, took the limit $T \rightarrow 0^1$, expanded in \mathbf{q}, ω , and used $[\overline{G_\varepsilon^R(\mathbf{k})}]^2 = -\frac{\partial}{\partial \varepsilon} \overline{G_\varepsilon^R(\mathbf{k})}$. Comparing Eq. (2.87) with Eq. (2.8), we see that the sum of the second and third term simply yield the average density of states ρ . Thus, to leading order in the loop-expansion $\overline{\Pi}^R$ reads:

$$\overline{\Pi}_\omega^R(\mathbf{q}) = \rho [1 + i\omega P_d(\mathbf{q}, \omega)] = \rho \frac{D\mathbf{q}^2}{D\mathbf{q}^2 - i\omega}. \quad (2.88)$$

Note that $\overline{\Pi}_\omega^R(\mathbf{q} \rightarrow 0) = 0$, reflecting particle number conservation. Moreover, disorder averaging restores translational symmetry, such that the Dyson equation (2.81) simply becomes

$$\begin{pmatrix} \overline{U}_\omega^R(\mathbf{q}) & \overline{U}_\omega^K(\mathbf{q}) \\ 0 & \overline{U}_\omega^A(\mathbf{q}) \end{pmatrix} = \begin{pmatrix} U_0(\mathbf{q}) + 2U_0(\mathbf{q})\overline{\Pi}_\omega^R(\mathbf{q})\overline{U}_\omega^R(\mathbf{q}) & 2U_0(\mathbf{q})\overline{\Pi}_\omega^R(\mathbf{q})\overline{U}_\omega^K(\mathbf{q}) + 2U_0(\mathbf{q})\overline{\Pi}_\omega^K(\mathbf{q})\overline{U}_\omega^A(\mathbf{q}) \\ 0 & U_0(\mathbf{q}) + 2U_0(\mathbf{q})\overline{\Pi}_\omega^A(\mathbf{q})\overline{U}_\omega^A(\mathbf{q}) \end{pmatrix}, \quad (2.89)$$

and is solved by

$$\overline{U}_\omega^R(\mathbf{q}) = \frac{U_0(\mathbf{q})}{1 - 2U_0(\mathbf{q})\overline{\Pi}_\omega^R(\mathbf{q})} = U_0(\mathbf{q}) \frac{D\mathbf{q}^2 - i\omega}{D\mathbf{q}^2 - i\omega - D\mathbf{q}^2 [2U_0(\mathbf{q})\rho]}, \quad (2.90)$$

$$\overline{U}_\omega^A(\mathbf{q}) = \left(\overline{U}_\omega^R(\mathbf{q})\right)^*, \quad (2.91)$$

$$\overline{U}_\omega^K(\mathbf{q}) = 2i g_\omega \text{Im} \overline{U}_\omega^R(\mathbf{q}). \quad (2.92)$$

Note that the last term in the denominator of Eq. (2.90) dominates in the diffusive limit $\omega\tau \ll 1$, $\ell\mathbf{q} \ll 1$, since the screening length is much shorter than ℓ . In particular in $d=3$, we find from Eqs. (2.78, 2.80) that $D\mathbf{q}^2 [2U_0(\mathbf{q})\rho] = D\kappa^2$. Thus, we can approximate Eq. (2.90) by neglecting the term “1” in the denominator in the following. This approximation is called *unitary limit* in the literature, and given by

$$\overline{U}_\omega^R(\mathbf{q}) = \left(\overline{U}_\omega^A(\mathbf{q})\right)^* = -\frac{1}{2\overline{\Pi}_\omega^R(\mathbf{q})} = -\frac{1}{2\rho} \frac{D\mathbf{q}^2 - i\omega}{D\mathbf{q}^2}, \quad \text{and} \quad \overline{U}_\omega^K(\mathbf{q}) = \frac{g_\omega}{\rho} \frac{i\omega}{D\mathbf{q}^2}. \quad (2.93)$$

We will now analyze the quasi-particle lifetime in the presence of the time dependent interaction described by Eq. (2.90).

1. Taking into account a finite temperature $T \ll \varepsilon_F$ leads to the same conclusions, since ρ_ε depends weakly on ε at $\varepsilon \ll \varepsilon_F$

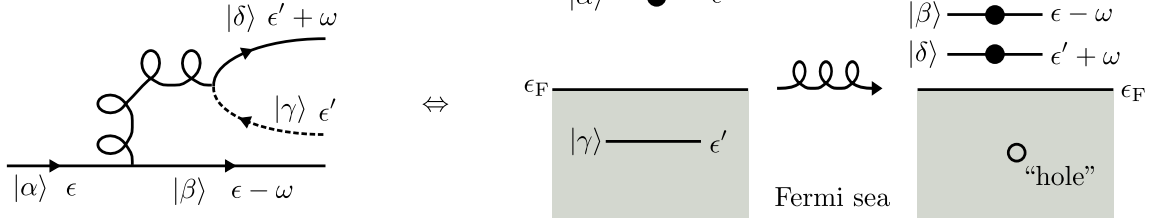


Figure 2.11: Fermi's golden rule for electron interactions in a disordered metal.

2.2.3 Quasi-particle lifetime of electrons in disordered systems

In the previous section, we have discussed that electron interactions in a metal are substantially screened due to the creation of electron-hole pairs. These pairs constitute a so-called screening cloud around the electrons [Pines and Nozieres, 1989]. Remarkably, Landau has shown that electrons (close to the Fermi surface) surrounded by such a cloud can be considered as quasi-particles, which have almost the same properties as non-interacting electrons. However, they have renormalized physical parameters (such as an effective mass) and decay after a finite lifetime $\tau_{ee}^{(0)}$ due to inelastic scattering. The quasi-particle picture holds if this lifetime is sufficiently large. For quasi-particles with an excitation energy ε at temperature T the lifetime is given by [Abrikosov *et al.*, 1975]

$$\frac{1}{\tau_{ee}^{(0)}(\varepsilon)} \simeq \frac{\max(\varepsilon, T)^2}{\varepsilon_F}. \quad (2.94)$$

Importantly, at $T = 0$ and close to the Fermi level (in the limit $\varepsilon \rightarrow 0$) the decay rate associated with this lifetime, $1/\tau_{ee}^{(0)}$, vanishes faster than the excitation energy ε , such that quasi-particles are well defined. In the following, we review the situation in disordered metals using two approaches: We analyze the relevant processes using Fermi's golden rule, and we calculate the electron self-energy to first order in the interaction propagators.

According to the discussion in the previous section, electron interactions are governed by the process shown in Fig. 2.11, where a (quasi-)particle in a state α decays via the Coulomb interaction into two particles (in states β, δ) and one hole (in state γ). From Fermi's golden rule, one obtains for such a process a transition probability [Schwabl, 2002]:

$$P_{\alpha}^{\text{GR}} = 4\pi \sum_{\beta\gamma\delta} |\langle \alpha\gamma | U | \beta\delta \rangle|^2 \delta(\varepsilon_{\alpha} + \varepsilon_{\gamma} - \varepsilon_{\beta} - \varepsilon_{\delta}), \quad (2.95)$$

Assuming that the quasi-particle is in a state with energy ε , we can estimate its lifetime in a disordered system as

$$\frac{1}{\tau_{ee}(\varepsilon)} = \sum_{\alpha} \overline{\delta(\varepsilon - \varepsilon_{\alpha}) P_{\alpha}^{\text{GR}}} = \frac{4\pi}{\rho V} \sum_{\alpha\beta\gamma\delta} \overline{|\langle \alpha\gamma | U | \beta\delta \rangle|^2 \delta(\varepsilon_{\alpha} + \varepsilon_{\gamma} - \varepsilon_{\beta} - \varepsilon_{\delta}) \delta(\varepsilon - \varepsilon_{\alpha})}. \quad (2.96)$$

In thermal equilibrium, the occupation of the energy levels at temperature T is governed by the Fermi distribution function:

$$f_{\varepsilon} = \frac{1}{e^{\varepsilon/T} + 1}. \quad (2.97)$$

Thus, the occupation of states required for this process (and the inverse process) can be determined from the function [Altshuler and Aronov, 1985]

$$F(\varepsilon, \varepsilon', \omega) = f_{\varepsilon'}(1 - f_{\varepsilon - \omega})(1 - f_{\varepsilon' + \omega}) + (1 - f_{\varepsilon'})f_{\varepsilon - \omega}f_{\varepsilon' + \omega}. \quad (2.98)$$

Denoting the energy of state γ by ε' and the energy-transfer by ω , energy conservation requires the energy of the final states β, δ to be $\varepsilon - \omega$ and $\varepsilon' + \omega$. Using Eq. (2.98), we obtain the quasi-particle lifetime at finite temperature:

$$\frac{1}{\tau_{ee}(\varepsilon, T)} = 4\pi(\rho V)^3 \int_{-\infty}^{\infty} d\omega d\varepsilon' F(\varepsilon, \varepsilon', \omega) \overline{|\mathcal{M}|^2}(\varepsilon, \varepsilon', \omega), \quad (2.99)$$

where the modulus squared of the disorder averaged transition matrix element is given by

$$\overline{|\mathcal{M}|^2}(\varepsilon, \varepsilon', \omega) = \frac{1}{(\rho V)^4} \sum_{\alpha\beta\gamma\delta} \overline{|\langle \alpha\gamma | U | \beta\delta \rangle|^2 \delta(\varepsilon - \varepsilon_\alpha) \delta(\varepsilon' - \varepsilon_\gamma) \delta(\varepsilon - \omega - \varepsilon_\beta) \delta(\varepsilon' + \omega - \varepsilon_\delta)}. \quad (2.100)$$

To calculate $\overline{|\mathcal{M}|^2}$, it is convenient to express it in terms of the eigen-function $\phi_\alpha(\mathbf{x})$ of the Hamiltonian:

$$\langle \alpha\gamma | U | \beta\delta \rangle = \int d^d \mathbf{x} d^d \mathbf{y} \phi_\alpha^*(\mathbf{x}) \phi_\gamma^*(\mathbf{y}) \phi_\beta(\mathbf{x}) \phi_\delta(\mathbf{y}) U_\omega^R(\mathbf{x}, \mathbf{y}). \quad (2.101)$$

Now we can use the identity

$$\sum_\alpha \phi_\alpha^*(\mathbf{y}) \phi_\alpha(\mathbf{x}) \delta(\varepsilon - \varepsilon_\alpha) = \frac{i}{2\pi} [G_\varepsilon^R(\mathbf{y}, \mathbf{x}) - G_\varepsilon^A(\mathbf{y}, \mathbf{x})], \quad (2.102)$$

to write Eq. (2.100) in terms of Green's functions:

$$\begin{aligned} \overline{|\mathcal{M}|^2}(\varepsilon, \varepsilon', \omega) &= \frac{1}{(2\pi\rho V)^4} \int d^d \mathbf{x} d^d \mathbf{y} d^d \mathbf{x}' d^d \mathbf{y}' \overline{U_\omega^R(\mathbf{x} - \mathbf{y}) U_\omega^A(\mathbf{y}' - \mathbf{x}')} \\ &\quad \times \overline{[G_\varepsilon^R(\mathbf{x}, \mathbf{x}') - G_\varepsilon^A(\mathbf{x}, \mathbf{x}')] [G_{\varepsilon - \omega}^R(\mathbf{x}', \mathbf{x}) - G_{\varepsilon - \omega}^A(\mathbf{x}', \mathbf{x})]} \\ &\quad \times \overline{[G_{\varepsilon'}^R(\mathbf{y}, \mathbf{y}') - G_{\varepsilon'}^A(\mathbf{y}, \mathbf{y}')] [G_{\varepsilon' + \omega}^R(\mathbf{y}', \mathbf{y}) - G_{\varepsilon' + \omega}^A(\mathbf{y}', \mathbf{y})]}, \end{aligned} \quad (2.103)$$

where the average over four Green's functions has been decoupled into a product of two averages.¹ To leading order in the loop-expansion, we find that the disorder dependent part² of $\overline{|\mathcal{M}|^2}$ depends only on ω and is given by

$$\overline{|\mathcal{M}|^2}(\omega) = \frac{1}{(\pi\rho)^2 V^4} \int d^d \mathbf{x} d^d \mathbf{y} d^d \mathbf{x}' d^d \mathbf{y}' \overline{U_\omega^R(\mathbf{x} - \mathbf{y}) U_\omega^A(\mathbf{y}' - \mathbf{x}') \text{Re}P_d(\mathbf{x}, \mathbf{x}', \omega) \text{Re}P_d(\mathbf{y}, \mathbf{y}', -\omega)}.$$

After a Fourier transform, and using Eq. (2.93) for the disorder averaged screened Coulomb interaction, we finally obtain

$$\overline{|\mathcal{M}|^2}(\omega) = \frac{1}{4\pi^2(\rho V)^4} \sum_{\mathbf{q} \neq \mathbf{0}} \frac{1}{(D\mathbf{q}^2)^2 + \omega^2}. \quad (2.104)$$

Note that the $\mathbf{q} = \mathbf{0}$ mode does not contribute since $\text{Re}P_d$ vanishes at $\mathbf{q} \rightarrow 0$ due to particle conservation, while the interaction propagator has to remain finite in this limit due to screening. As a result, the matrix element (2.104) is independent of ω at $\omega \ll E_{\text{Th}}$:

$$\overline{|\mathcal{M}|^2}(\omega) \stackrel{E_{\text{Th}} \gg \omega}{\approx} \frac{c'}{4\pi^2(\rho V)^4 E_{\text{Th}}^2}, \quad c' = \sum_{\mathbf{q} \neq \mathbf{0}} \frac{1}{(D\mathbf{q}^2/E_{\text{Th}})^2}, \quad (2.105)$$

1. There is an additional contribution to Eq. (2.103) involving averaged products of Green's functions of the form $G_\varepsilon^R(\mathbf{x}, \mathbf{x}') G_\varepsilon^A(\mathbf{y}, \mathbf{y}')$ and $G_{\varepsilon - \omega}^R(\mathbf{x}', \mathbf{x}) G_{\varepsilon' + \omega}^A(\mathbf{y}', \mathbf{y})$, which is small in the limit $\ell \gg \lambda_s$, see Altshuler and Aronov (1985).

2. The disorder independent part, including the contributions from $G^R G^R$ and $G^A G^A$, leads to Landau's result, Eq. (2.94).

where c' is a constant which depends on dimensionality and boundary conditions. E.g. for an isolated quasi-1D ring where $q = 2\pi n/L$ with $n \in \mathbb{Z}$ we have $c' = 1/720$. For $\omega \gg E_{\text{Th}}$, on the other hand, the sum can be approximated by an integral:

$$\overline{|\mathcal{M}|^2}(\omega) \stackrel{\omega \gg E_{\text{Th}}}{\approx} \frac{c_d}{4\pi^2(\rho V)^4} \frac{1}{\omega^2} \left(\frac{\omega}{E_{\text{Th}}} \right)^{d/2}, \quad c_d = \begin{cases} 1/\sqrt{8} & d = 1 \\ 1/8 & d = 2 \end{cases}. \quad (2.106)$$

We remind the reader that we will not consider the case $d = 3$ in the following, see the discussion after Eq. (2.47).

Let us first consider the case $T = 0$ for a particle with $\varepsilon > 0$. In this limit, the quasi-particle lifetime, Eq. (2.99), becomes

$$\frac{1}{\tau_{\text{ee}}(\varepsilon, 0)} = 4\pi(\rho V)^3 \int_0^\varepsilon d\omega \int_{-\omega}^0 d\varepsilon' \overline{|\mathcal{M}|^2}(\varepsilon, \varepsilon', \omega). \quad (2.107)$$

Using Eq. (2.104) in Eq. (2.107), we identify two regimes ($\Delta = 1/\rho V$, cf. Eq. (2.47)):

$$\frac{1}{\tau_{\text{ee}}(\varepsilon, 0)} \simeq \begin{cases} \Delta \left(\frac{\varepsilon}{E_{\text{Th}}} \right)^{d/2} & \varepsilon \gg E_{\text{Th}} \\ \Delta \left(\frac{\varepsilon}{E_{\text{Th}}} \right)^2 & E_{\text{Th}} \gg \varepsilon \end{cases}. \quad (2.108)$$

The later regime at $E_{\text{Th}} \gg \varepsilon$ is called the *0D regime* [Sivan *et al.*, 1994], since it is reached at small system sizes independent of the real dimensionality. Importantly, the Fermi liquid theory remains valid as long as the system is in the metallic regime, since $g = 2\pi E_{\text{Th}}/\Delta \gg 1$ implies $1/\tau_{\text{ee}}(\varepsilon, 0) \ll \varepsilon$, such that quasi-particles are well defined [Aleiner and Blanter, 2002].

As an aside, we note that Schmid (1974) and Altshuler and Aronov (1979) have analyzed the *energy relaxation time* τ_{E} ¹ in a disordered metal using the kinetic equation approach. τ_{E} corresponds to the time needed for an electron with energy $\varepsilon > 0$ injected into the system to relax towards thermal equilibrium. They found that at $T = 0$ it is essentially given by Eq. (2.108), $\tau_{\text{E}}(\varepsilon, 0) = \tau_{\text{ee}}(\varepsilon, 0)$. At finite T one usually assumes that τ_{E} is symmetric with respect to interchanging $\varepsilon \leftrightarrow T$, such that $\tau_{\text{E}}(\varepsilon, T) \simeq \tau_{\text{E}}(\max(\varepsilon, T))$, in analogy to Landau's result for clean systems (see Altshuler and Aronov (1985) for details).

Let us now return to the quasi-particle lifetime at finite temperature, given by Eq. (2.99) with (2.98).² Since the matrix element, Eq. (2.104), is independent of ε' , we can integrate over ε' in Eq. (2.99). This yields

$$\frac{1}{\tau_{\text{ee}}(\varepsilon, T)} = 4\pi(\rho V)^3 \int_{-\infty}^{\infty} d\omega \omega f_{\varepsilon-\omega} \frac{e^{\beta\varepsilon} + 1}{e^{\beta\omega} - 1} \overline{|\mathcal{M}|^2} \quad (2.109)$$

$$= \frac{1}{2\pi\rho} \int_{-\infty}^{\infty} d\omega \omega [g_\omega + h_{\varepsilon-\omega}] \frac{1}{V} \sum_{\mathbf{q} \neq \mathbf{0}} \frac{1}{(D\mathbf{q}^2)^2 + \omega^2}, \quad (2.110)$$

where we used the identity

$$\omega f_{\varepsilon-\omega} \frac{e^{\beta\varepsilon} + 1}{e^{\beta\omega} - 1} = \frac{1}{2} \omega [g_\omega + h_{\varepsilon-\omega}]. \quad (2.111)$$

1. Schmid calls τ_{E} the *inelastic collision time*.

2. Note that $\tau_{\text{ee}}(\varepsilon, T)$ has no direct analogy in terms of a *relaxation time*. Instead, it rather corresponds to an electron-hole-symmetrized version of the *out-scattering rate* in the kinetic equation approach [Aleiner and Blanter, 2002]. (See Blanter (1996) for a detailed discussion.)

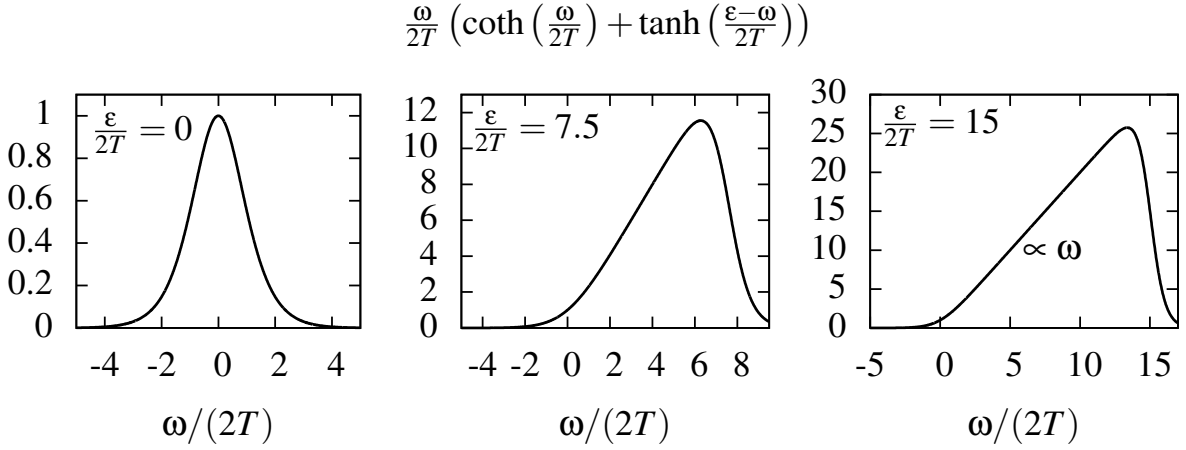


Figure 2.12: Plot of the Fermi factors appearing in the probability (2.110).

$$\underline{G}_\varepsilon(\mathbf{x}, \mathbf{y}) = \underline{G}_{0\varepsilon}(\mathbf{x}, \mathbf{y}) + \underline{G}_{0\varepsilon}(\mathbf{x}, \mathbf{z}) \underbrace{\begin{array}{c} \text{---} U_\omega(\mathbf{z}, \mathbf{z}') \text{---} \\ \text{---} G_{0\varepsilon-\omega}(\mathbf{z}, \mathbf{z}') \text{---} \\ \gamma_e \qquad \qquad \gamma_a \end{array}} \underline{G}_\varepsilon(\mathbf{z}', \mathbf{y})$$

Figure 2.13: Keldysh representation of the Dyson equation for the electron Green's function.

We see that Eq. (2.110) is in general not symmetric w.r.t. interchanging $\varepsilon \leftrightarrow T$ due to the Fermi factors (2.111), which we show in Fig. 2.12. For electrons close to the Fermi level, $\varepsilon \rightarrow 0$ (see Fig. 2.12 left), the Fermi factors limit the energy transfer to $\omega \lesssim T$ due to the unavailability of final scattering states, expressing so-called *Pauli blocking*. Only in the 0D limit, when $\max(\varepsilon, T) \ll E_{\text{Th}}$, we recover $1/\tau_{\text{ee}}(\varepsilon, T) \sim \max(\varepsilon, T)^2$. For an infinite system size, on the other hand, substituting Eq. (2.106) in Eq. (2.110), we see that the ω -integral is IR-divergent in 1D and 2D for any $T > 0$. Apparently, an appropriate low-energy cutoff has to be introduced. However, before analyzing Eq. (2.110) in more details, let us see how the same expression for the quasi-particle lifetime can be obtained from the electron interaction self energy.

We have argued in Section 2.1.1 that a lifetime can be associated with the imaginary part of the self-energy Σ . Expanding the electron Green's function in the Keldysh representation in the interaction \underline{U} yields the Dyson equation shown in Fig. 2.13.¹ It corresponds to the expression

$$\underline{G}_\varepsilon^{ij}(\mathbf{x}, \mathbf{y}) = \underline{G}_{0\varepsilon}^{ij}(\mathbf{x}, \mathbf{y}) + \int d^d \mathbf{z} d^d \mathbf{z}' \underline{G}_{0\varepsilon}^{ik}(\mathbf{z}', \mathbf{y}) \underline{\Sigma}_\varepsilon^{kl}(\mathbf{z}, \mathbf{z}') \underline{G}_\varepsilon^{lj}(\mathbf{x}, \mathbf{z}), \quad (2.112)$$

1. We neglect crossed interaction lines, which are small in the limit of a high electron density, and consider only the so-called *Fock* term. Moreover, it is known that the so-called *Hartree* term, given by a tadpole-shaped diagram, gives no contribution to the imaginary part of the self-energy. See e.g. Bruus and Flensberg (2004) for a detailed discussion of the diagrammatic selection rules.

where the self-energy $\underline{\Sigma}$ is given by¹

$$\underline{\Sigma}_{\varepsilon}^{kl}(\mathbf{x}, \mathbf{y}) = -i \int \frac{d\omega}{2\pi} \underline{\gamma}_a^{km,i} \underline{G}_{0\varepsilon-\omega}^{mn}(\mathbf{x}, \mathbf{y}) \underline{U}_{\omega}^{ij}(\mathbf{x}, \mathbf{y}) \underline{\gamma}_e^{nl,j} \quad (2.113)$$

$$= -\frac{i}{2} \int \frac{d\omega}{2\pi} \begin{pmatrix} G_{0\varepsilon-\omega}^R(\mathbf{x}, \mathbf{y}) U_{\omega}^K(\mathbf{x}, \mathbf{y}) & G_{0\varepsilon-\omega}^A(\mathbf{x}, \mathbf{y}) U_{\omega}^A(\mathbf{x}, \mathbf{y}) + G_{0\varepsilon-\omega}^R(\mathbf{x}, \mathbf{y}) U_{\omega}^R(\mathbf{x}, \mathbf{y}) \\ + G_{0\varepsilon-\omega}^K(\mathbf{x}, \mathbf{y}) U_{\omega}^R(\mathbf{x}, \mathbf{y}) & + G_{0\varepsilon-\omega}^K(\mathbf{x}, \mathbf{y}) U_{\omega}^K(\mathbf{x}, \mathbf{y}) \\ G_{0\varepsilon-\omega}^R(\mathbf{x}, \mathbf{y}) U_{\omega}^A(\mathbf{x}, \mathbf{y}) & G_{0\varepsilon-\omega}^A(\mathbf{x}, \mathbf{y}) U_{\omega}^K(\mathbf{x}, \mathbf{y}) \\ + G_{0\varepsilon-\omega}^A(\mathbf{x}, \mathbf{y}) U_{\omega}^R(\mathbf{x}, \mathbf{y}) & + G_{0\varepsilon-\omega}^K(\mathbf{x}, \mathbf{y}) U_{\omega}^A(\mathbf{x}, \mathbf{y}) \end{pmatrix}_{kl} \quad (2.114)$$

$$\equiv \begin{pmatrix} \Sigma_{\varepsilon}^R(\mathbf{x}, \mathbf{y}) & \Sigma_{\varepsilon}^K(\mathbf{x}, \mathbf{y}) \\ 0 & \Sigma_{\varepsilon}^A(\mathbf{x}, \mathbf{y}) \end{pmatrix}_{kl}.$$

Using Eq. (2.75), we find the imaginary part of the retarded self-energy:

$$\text{Im} [\Sigma_{\varepsilon}^R(\mathbf{x}, \mathbf{y})] = \text{Im} \left[-\frac{i}{2} \int \frac{d\omega}{2\pi} G_{0\varepsilon-\omega}^R(\mathbf{x}, \mathbf{y}) U_{\omega}^K(\mathbf{x}, \mathbf{y}) + G_{0\varepsilon-\omega}^K(\mathbf{x}, \mathbf{y}) U_{\omega}^R(\mathbf{x}, \mathbf{y}) \right] \quad (2.115)$$

$$= -\frac{i}{2} \int \frac{d\omega}{2\pi} [g_{\omega} + h_{\varepsilon-\omega}] [G_{0\varepsilon-\omega}^R(\mathbf{x}, \mathbf{y}) - G_{0\varepsilon-\omega}^A(\mathbf{x}, \mathbf{y})] \text{Im} U_{\omega}^R(\mathbf{x}, \mathbf{y}). \quad (2.116)$$

$\text{Im} [\Sigma_{\varepsilon}^R(\mathbf{x}, \mathbf{y})]$ determines the lifetime of a quasi-particle of energy ε propagating from \mathbf{x} to \mathbf{y} . We are interested in the average lifetime of *any* quasi-particle in a state α having the energy $\varepsilon_{\alpha} = \varepsilon$. Following [Abrahams *et al.* \(1981\)](#); [dos Santos \(1983\)](#), we define

$$-\frac{1}{2\tau_{\text{ee}}(\varepsilon)} \equiv \frac{1}{\rho V} \int d^d \mathbf{x} d^d \mathbf{y} \sum_{\alpha} \overline{\delta(\varepsilon - \varepsilon_{\alpha}) \phi_{\alpha}(\mathbf{x}) \text{Im} [\Sigma_{\varepsilon}^R(\mathbf{x}, \mathbf{y})] \phi_{\alpha}(\mathbf{y})^*} \quad (2.117)$$

$$= \frac{i}{2\pi\rho V} \int d^d \mathbf{x} d^d \mathbf{y} \overline{[G_{0\varepsilon}^R(\mathbf{y}, \mathbf{x}) - G_{0\varepsilon}^A(\mathbf{y}, \mathbf{x})] \text{Im} [\Sigma_{\varepsilon}^R(\mathbf{x}, \mathbf{y})]}, \quad (2.118)$$

where we used the identity (2.102). Evidently, using Eq. (2.116) in Eq. (2.118) we obtain a contribution proportional to the correlation function $P(\mathbf{x}, \mathbf{y}, \omega)$ defined in Eq. (2.10). Thus, using Eq. (2.18) and Eq. (2.93), the disorder dependent part of Eq. (2.117) reads

$$\frac{1}{\tau_{\text{ee}}(\varepsilon)} = \frac{2}{V} \int \frac{d\omega}{2\pi} [g_{\omega} + h_{\varepsilon-\omega}] \int d^d \mathbf{x} d^d \mathbf{y} \text{Re} P_d(\mathbf{x}, \mathbf{y}, \omega) \text{Im} \overline{U_{\omega}^R(\mathbf{x}, \mathbf{y})} \quad (2.119)$$

$$\approx \frac{1}{2\pi\rho} \int d\omega \omega [g_{\omega} + h_{\varepsilon-\omega}] \frac{1}{V} \sum_{\mathbf{q} \neq 0} \frac{1}{(D\mathbf{q}^2)^2 + \omega^2}. \quad (2.120)$$

As expected, Eq. (2.120) is identical to the lifetime obtained from Fermi's golden rule, Eq. (2.110). In particular, we come across the same IR-divergence for infinite systems. [Abrahams *et al.* \(1981\)](#) argue that this divergence is cured by including higher order diagrams and propose a way to include their effect by a shift of the particle energies. [dos Santos \(1983\)](#), on the other hand, proposes a self-consistent renormalization of the electron propagator in the self-energy, with similar results in 2D.

For our purposes, namely the understanding of electron interactions in disordered systems at energies close to the Fermi level ($\varepsilon \rightarrow 0$), we have gained three important insights: (1) The energy transfers ω of the interactions is always restricted by $\omega \lesssim T$ due to Pauli blocking, (2) at $T \gg E_{\text{Th}}$ the energy transfers are dominated by small frequencies and momenta in 1D and 2D, and (3) at $\omega \ll E_{\text{Th}}$ the scattering matrix element is independent of energy in any dimension, such that large energy transfers $\omega \simeq T$ dominate the interactions.

We will see in the next section that an expression similar to Eq. (2.120) can be derived for the dephasing time. However, for the dephasing time, the IR-cutoff is provided by including the so-called *vertex diagrams*, which do not appear in the calculation of the quasi-particle lifetime.

1. $\underline{\Sigma}^{21} = 0$ follows from $G^R(t)U^A(t) = G^A(t)U^R(t) = 0$.

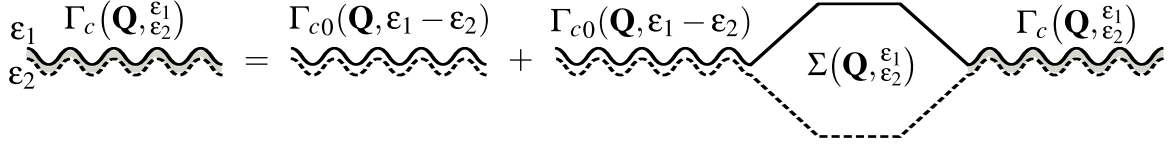


Figure 2.14: Cooperon with self-energy.

2.2.4 Diagrammatic calculation of the dephasing time

In this section, we calculate the dephasing rate, defined as the Cooperon mass in Section 2.1.3, using a perturbation theory in the (diffusively screened) electron interaction which was developed by [von Delft *et al.* \(2007\)](#). However, in contrast to [von Delft *et al.* \(2007\)](#), we avoid making any reference to the conductivity, emphasizing the generality of the obtained results.

The diagrams contributing to the Cooperon mass have been identified first by [Fukuyama and Abrahams \(1983\)](#). In the simplest approach, only diagrams are considered where the energy transferred by the interaction is conserved separately for electron and hole of the Cooperon propagator.¹ In this case a Dyson equation for the Cooperon structure factor (cf. Eq. (2.19)) can be set up and is shown in Fig. 2.14. We assume that the retarded electron Green's function representing the electron has energy ε_1 and the advanced electron Green's function representing the hole has energy ε_2 . Since there is no energy transfer between electron and hole, Fig. 2.14 corresponds to the equation

$$\Gamma_c(\mathbf{Q}, \varepsilon_1, \varepsilon_2) = \Gamma_{c0}(\mathbf{Q}, \varepsilon_1 - \varepsilon_2) + \Gamma_{c0}(\mathbf{Q}, \varepsilon_1 - \varepsilon_2) \Sigma(\mathbf{Q}, \varepsilon_1) \Gamma_c(\mathbf{Q}, \varepsilon_1, \varepsilon_2), \quad (2.121)$$

where $\Gamma_{c0} = \Gamma_d$ is the Cooperon structure factor in the absence of interactions.² Eq. (2.121) is solved by

$$\Gamma_c(\mathbf{Q}, \varepsilon_1, \varepsilon_2) = \frac{1}{1/\Gamma_{c0}(\mathbf{Q}, \varepsilon_1 - \varepsilon_2) - \Sigma(\mathbf{Q}, \varepsilon_1)} = \frac{1}{2\pi\rho\tau^2} \frac{1}{D\mathbf{Q}^2 - i(\varepsilon_1 - \varepsilon_2) - \frac{1}{2\pi\rho\tau^2} \Sigma(\mathbf{Q}, \varepsilon_1)}. \quad (2.122)$$

Evidently, the real part of the self-energy Σ in Eq. (2.122) plays the role of a Cooperon mass as in Eq. (2.38), while the imaginary part leads to a shift in the relative energies, which we do not consider here. We have seen in Eq. (2.113), that the self-energy of $G_{\varepsilon_1}^R$ and $G_{\varepsilon_2}^A$ can be written as

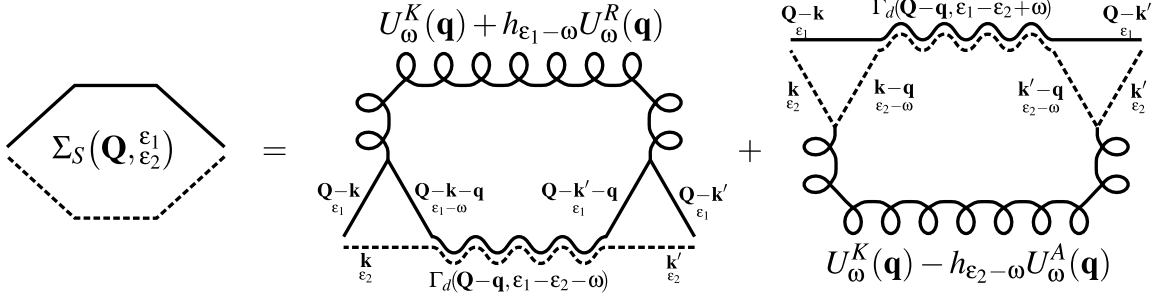
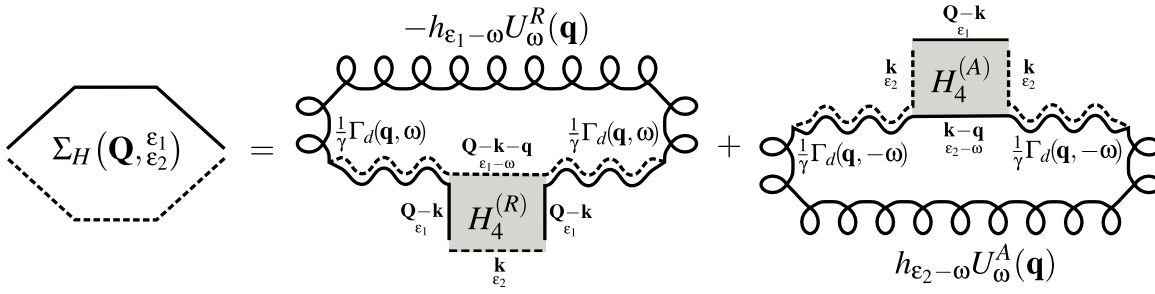
$$\Sigma_{\varepsilon_1}^R(\mathbf{x}, \mathbf{y}) = -\frac{i}{2} \int_{-\infty}^{\infty} d\omega G_{\varepsilon_1-\omega}^R(\mathbf{x}, \mathbf{y}) [U_{\omega}^K(\mathbf{x}, \mathbf{y}) + h_{\varepsilon_1-\omega} U_{\omega}^R(\mathbf{x}, \mathbf{y})] - G_{\varepsilon_1-\omega}^A(\mathbf{x}, \mathbf{y}) [h_{\varepsilon_1-\omega} U_{\omega}^R(\mathbf{x}, \mathbf{y})] \quad (2.123)$$

$$\Sigma_{\varepsilon_2}^A(\mathbf{x}, \mathbf{y}) = -\frac{i}{2} \int_{-\infty}^{\infty} d\omega G_{\varepsilon_2-\omega}^A(\mathbf{x}, \mathbf{y}) [U_{\omega}^K(\mathbf{x}, \mathbf{y}) - h_{\varepsilon_2-\omega} U_{\omega}^A(\mathbf{x}, \mathbf{y})] + G_{\varepsilon_2-\omega}^R(\mathbf{x}, \mathbf{y}) [h_{\varepsilon_2-\omega} U_{\omega}^A(\mathbf{x}, \mathbf{y})], \quad (2.124)$$

where we used Eq. (2.75) and grouped the resulting terms $\propto G^R$ and $\propto G^A$. Eqs. (2.123, 2.124) give rise to two different types of contributions to the Cooperon self-energy: (1) the contributions where the retardation of the Green's function is preserved at the interaction vertices (denoted Σ_S), and (2) the contribution where the retardation is changed (denoted Σ_H). Let us first consider the contribution Σ_S , resulting from the terms $\sim G^R$ in Eq. (2.123) and the terms $\sim G^A$ in Eq. (2.124). After impurity

1. In the following we call the G^R propagator of the Cooperon “electron” and the G^A propagator “hole”. However, we emphasize that the hole is propagating backwards in time, such that the Cooperon corresponds to propagation in the particle-particle channel.

2. To keep the notations simple, we assume in this section that no other mechanisms of dephasing, such as a magnetic field, are present.

Figure 2.15: The contribution Σ_S of the Cooperon self-energy.Figure 2.16: The contribution Σ_H of the Cooperon self-energy.

averaging in the loop-expansion, we obtain two diagrams shown in Fig. 2.15. Both diagrams include two 3-point Hikami boxes, which are given by a momentum-sum over three Green's functions and, in contrast to the 4-point Hikami boxes discussed in Eq. (2.23), they cannot be dressed by adding single impurity lines. Assuming small $DQ^2\tau$, $(\varepsilon_1 - \varepsilon_2)\tau$, and $\omega\tau$, we use Eqs. (2.13, 2.16) and obtain

$$\begin{aligned} \frac{1}{V} \sum_{\mathbf{k}} \bar{G}_{\varepsilon_1}^R(\mathbf{Q}-\mathbf{k}) \bar{G}_{\varepsilon_1-\omega}^R(\mathbf{Q}-\mathbf{k}-\mathbf{q}) \bar{G}_{\varepsilon_2}^A(\mathbf{k}) &\approx -i2\pi\rho\tau^2 \\ \frac{1}{V} \sum_{\mathbf{k}} \bar{G}_{\varepsilon_1}^R(\mathbf{Q}-\mathbf{k}) \bar{G}_{\varepsilon_2}^A(\mathbf{k}) \bar{G}_{\varepsilon_2-\omega}^A(\mathbf{k}-\mathbf{q}) &\approx i2\pi\rho\tau^2. \end{aligned} \quad (2.125)$$

Thus, the answer for Σ_S reads:

$$\begin{aligned} -\frac{1}{2\pi\rho\tau^2} \Sigma_S(\mathbf{Q}, \varepsilon_1, \varepsilon_2) &= -\frac{i}{2} \int_{-\infty}^{\infty} \frac{d\omega}{2\pi} \frac{1}{V} \sum_{\mathbf{q}} P_d(\mathbf{q}-\mathbf{Q}, \varepsilon_1 - \varepsilon_2 - \omega) \\ &\quad \times [2U_{\omega}^K(\mathbf{q}) + (h_{\varepsilon_1-\omega} - h_{\varepsilon_2+\omega})U_{\omega}^R(\mathbf{q})] \end{aligned} \quad (2.126)$$

where we used $2\pi\rho\tau^2\Gamma_d(\mathbf{x}, \mathbf{y}, \omega) = P_d(\mathbf{x}, \mathbf{y}, \omega)$, see Eq. (2.19), and used the relations $\bar{U}_{\omega}^A = \bar{U}_{-\omega}^R$ and $\bar{U}_{\omega}^K = \bar{U}_{-\omega}^K$ from Eq. (2.93).

Let us now consider the contribution to the self-energy resulting from the terms $\sim G^A$ of Eq. (2.123) and $\sim G^R$ of Eq. (2.124), which correspond to Σ_H . After impurity averaging we obtain the diagrams shown in Fig. 2.16. They include a 4-point Hikami box, which can be calculated straightforwardly as in Section 2.1.2. In contrast to Eq. (2.24), there is no unphysical UV-divergence here and the Cooperon is not protected by particle conservation. In full analogy with the calculation in Eq. (2.24),

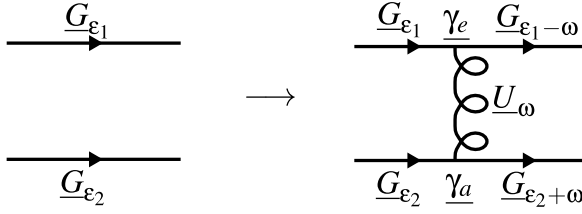


Figure 2.17: Vertex contribution.

we obtain

$$\begin{aligned} H_4^{(R)} &\approx 2\pi\rho\tau^4 [D(\mathbf{Q}-\mathbf{q})^2 - i\omega - i(\epsilon_1 - \epsilon_2)] \\ H_4^{(A)} &\approx 2\pi\rho\tau^4 [D(\mathbf{Q}-\mathbf{q})^2 + i\omega - i(\epsilon_1 - \epsilon_2)]. \end{aligned} \quad (2.127)$$

In total, the answer for Σ_H reads

$$\begin{aligned} -\frac{1}{2\pi\rho\tau^2}\Sigma_H(\mathbf{Q}, \epsilon_1, \epsilon_2) & \\ &= -\frac{i}{2}\int_{-\infty}^{\infty}\frac{d\omega}{2\pi}\frac{1}{V}\sum_{\mathbf{q}}P_d(\mathbf{q}, \omega)^2 [D(\mathbf{q}-\mathbf{Q})^2 - i\omega - i(\epsilon_1 - \epsilon_2)] [(h_{\epsilon_1-\omega} - h_{\epsilon_2+\omega})U_{\omega}^R(\mathbf{q})]. \end{aligned} \quad (2.128)$$

The total Cooperon self-energy, neglecting energy transfers between particle and hole, is given by $\Sigma_{SE} = \Sigma_S + \Sigma_V$. To simplify the discussion of this quantity, let us consider the spatial average $\frac{1}{V}\int d\mathbf{x}\Sigma_{SE}(\mathbf{x})$ of the self-energy, given by the limit $\mathbf{Q} \rightarrow 0$. Inserting the expression (2.93) for the screened interaction propagator in Eq. (2.126) and Eq. (2.128), we find

$$\begin{aligned} -\frac{1}{2\pi\rho\tau^2}\Sigma_{SE}(\epsilon_1, \epsilon_2) &= \frac{i}{2}\int_{-\infty}^{\infty}\frac{d\omega}{2\pi}\frac{1}{V}\sum_{\mathbf{q}}P_d(\mathbf{q}, \omega) \times \\ &\left[-2U_{\epsilon_1-\epsilon_2-\omega}^K(\mathbf{q}) + (h_{\epsilon_2+\omega} - h_{\epsilon_1-\omega}) \left(U_{\epsilon_1-\epsilon_2-\omega}^R(\mathbf{q}) - \frac{D\mathbf{q}^2 - i\omega - i(\epsilon_1 - \epsilon_2)}{D\mathbf{q}^2 - i\omega} U_{\omega}^R(\mathbf{q}) \right) \right] \\ &= \frac{1}{\rho}\int_{-\infty}^{\infty}\frac{d\omega}{2\pi}\frac{1}{V}\sum_{\mathbf{q}\neq 0}P_d(\mathbf{q}, \omega)\frac{1}{D\mathbf{q}^2} \left[(\epsilon_1 - \epsilon_2 - \omega)g_{\epsilon_1-\epsilon_2-\omega} - \frac{\omega}{2}(h_{\epsilon_2+\omega} - h_{\epsilon_1-\omega}) \right]. \end{aligned} \quad (2.130)$$

We have argued that the real part of Eq. (2.130) corresponds to the Cooperon mass. Remarkably, for particle and hole at the Fermi energy ($\epsilon_1 \rightarrow 0$ and $\epsilon_2 \rightarrow 0$), we find the same expression as in Eqs. (2.120, 2.110):

$$\gamma_{SE} \approx -\frac{1}{2\pi\rho\tau^2}\text{Re}\Sigma_{SE}(0) = \frac{1}{2\pi\rho}\int_{-\infty}^{\infty}d\omega\omega[g_{\omega} + h_{-\omega}]\frac{1}{V}\sum_{\mathbf{q}\neq 0}\frac{1}{(D\mathbf{q}^2)^2 + \omega^2}. \quad (2.131)$$

Note that, similar to the discussion in the previous section, we see that Eq. (2.131) is IR-divergent in the limit of an infinite system size.

The case of a finite energy difference ($\epsilon_1 - \epsilon_2$) in Eq. (2.130), together with a self-consistent cutoff scheme, has been studied in a master's thesis co-supervised by the present author. It has been found that the influence is sub-leading as long as $|\epsilon_1 - \epsilon_2| \ll \gamma$, and all relevant correction terms have been evaluated [Schäffer, 2012]. In the opposite regime, $\gamma \ll |\epsilon_1 - \epsilon_2|$, on the other hand, the quantum corrections are dominated by $|\epsilon_1 - \epsilon_2|$ itself, such that the influence of γ is weak, cf. Section 2.1.4.

von Delft *et al.* (2007) have shown that the IR-divergence in Eq. (2.131) is cured by the contribution of the diagrams with energy transfer between electron and hole of the Cooperon. We will give

$$\begin{aligned}
& U_{\omega}^K(\mathbf{q}) + h_{\varepsilon_1 - \omega} U_{\omega}^R(\mathbf{q}) - h_{\varepsilon_2} U_{\omega}^A(\mathbf{q}) \\
& \Sigma_{VX}(\mathbf{Q}, \varepsilon_1, \varepsilon_2) = \text{Diagram 1} + \text{Diagram 2} \\
& U_{\omega}^K(\mathbf{q}) + h_{\varepsilon_1 + \omega} U_{\omega}^R(\mathbf{q}) - h_{\varepsilon_2} U_{\omega}^A(\mathbf{q})
\end{aligned}$$

Figure 2.18: Vertex contribution.

a brief summary of their calculation in the following: The structure of such an energy transfer in Keldysh space is shown in Fig. 2.17. It can be written as follows:

$$\underline{G}_{\varepsilon_1}^{ij} \underline{G}_{\varepsilon_2}^{kl} \rightarrow i \left(\underline{G}_{\varepsilon_1 - \omega}^{im} \underline{\gamma}_e^{mn,r} \underline{G}_{\varepsilon_1}^{nj} \right) \left(\underline{G}_{\varepsilon_2 + \omega}^{kp} \underline{\gamma}_a^{pq,s} \underline{G}_{\varepsilon_2}^{ql} \right) \underline{U}_{\omega}^{sr}. \quad (2.132)$$

In particular for the electron and hole, represented by $G_{\varepsilon_1}^R$ and $G_{\varepsilon_2}^A$, one obtains:

$$\begin{aligned}
G_{\varepsilon_1}^R G_{\varepsilon_2}^A & \rightarrow \frac{i}{2} \left[(G_{\varepsilon_1}^R G_{\varepsilon_1 - \omega}^K) (G_{\varepsilon_2}^A G_{\varepsilon_2 + \omega}^A) U_{\omega}^R \right. \\
& \quad + (G_{\varepsilon_1}^R G_{\varepsilon_1 - \omega}^R) (G_{\varepsilon_2}^K G_{\varepsilon_2 + \omega}^A) U_{\omega}^A \\
& \quad \left. + (G_{\varepsilon_1}^R G_{\varepsilon_1 - \omega}^R) (G_{\varepsilon_2}^A G_{\varepsilon_2 + \omega}^A) U_{\omega}^K \right] \\
& \rightarrow \frac{i}{2} (G_{\varepsilon_1}^R G_{\varepsilon_1 - \omega}^R) (G_{\varepsilon_2}^A G_{\varepsilon_2 + \omega}^A) [U_{\omega}^K + h_{\varepsilon_1 - \omega} U_{\omega}^R - h_{\varepsilon_2} U_{\omega}^A]. \quad (2.134)
\end{aligned}$$

For the inverse process where absorption and emission are interchanged, we find:

$$G_{\varepsilon_1}^R G_{\varepsilon_2}^A \rightarrow \frac{i}{2} (G_{\varepsilon_1}^R G_{\varepsilon_1 + \omega}^R) (G_{\varepsilon_2}^A G_{\varepsilon_2 - \omega}^A) [U_{\omega}^K + h_{\varepsilon_1 + \omega} U_{\omega}^R - h_{\varepsilon_2} U_{\omega}^A]. \quad (2.135)$$

After impurity averaging, we obtain the diagrams shown in Fig. 2.18 which give a contribution denoted by Σ_{VX} :

$$\begin{aligned}
& -\frac{1}{2\pi\rho\tau^2} \Sigma_{VX}(\mathbf{Q}, \varepsilon_1, \varepsilon_2) \\
& = \frac{i}{2} \int_{-\infty}^{\infty} \frac{d\omega}{2\pi} \frac{1}{V} \sum_{\mathbf{q}} P(\mathbf{q} - \mathbf{Q}, \varepsilon_1 - \varepsilon_2 - \omega) [2U_{\omega}^K(\mathbf{q}) + (h_{\varepsilon_1 - \omega} - h_{\varepsilon_2})(U_{\omega}^R(\mathbf{q}) + U_{\omega}^A(\mathbf{q}))]
\end{aligned} \quad (2.136)$$

Calculating the spatial average, we find an expression rather similar to Eq. (2.130):

$$-\frac{1}{2\pi\rho\tau^2} \Sigma_{VX}(\varepsilon_1, \varepsilon_2) = \frac{1}{\rho} \int_{-\infty}^{\infty} \frac{d\omega}{2\pi} \frac{1}{V} \sum_{\mathbf{q} \neq 0} P(\mathbf{q}, \omega) \frac{1}{D\mathbf{q}^2} \left[-(\varepsilon_1 - \varepsilon_2 - \omega) g_{\varepsilon_1 - \varepsilon_2 - \omega} - \frac{iD\mathbf{q}^2}{2} (h_{\varepsilon_2 + \omega} - h_{\varepsilon_2}) \right]. \quad (2.137)$$

However, since energy is not conserved for each Green's function, we cannot formulate the problem in terms of a Dyson equation of the form Eq. (2.121) any more. Instead, the Cooperon structure factor is described by a so-called *Bethe-Salpether equation*,

$$\Gamma_c(\mathbf{Q}, \varepsilon_{21}^{\varepsilon_{11}\varepsilon_{22}}) = \Gamma_{c0}(\mathbf{Q}, \varepsilon_{21}^{\varepsilon_{11}}) \left[\delta(\varepsilon_{11} - \varepsilon_{12}) \delta(\varepsilon_{21} - \varepsilon_{22}) + \int_{-\infty}^{\infty} d\omega_1 d\omega_2 \Sigma(\varepsilon_{21}^{\varepsilon_{11}\omega_1}) \Gamma_c(\mathbf{Q}, \omega_2^{\varepsilon_{11}\varepsilon_{22}}) \right], \quad (2.138)$$

with a self-energy which depends on four energy arguments and is given by a combination of Eq. (2.130) and Eq. (2.137):

$$\begin{aligned} -\frac{1}{2\pi\rho\tau^2} \Sigma(\varepsilon_{21}^{\varepsilon_{11}\varepsilon_{22}}) &= \frac{1}{\rho} \int_{-\infty}^{\infty} \frac{d\omega}{2\pi} \frac{1}{V} \sum_{\mathbf{q} \neq 0} P_d(\mathbf{q}, \omega) \frac{1}{D\mathbf{q}^2} \\ &\times \left[\left((\varepsilon_{11} - \varepsilon_{21} - \omega) g_{\varepsilon_{11} - \varepsilon_{21} - \omega} - \frac{\omega}{2} (h_{\varepsilon_{21} + \omega} - h_{\varepsilon_{11} - \omega}) \right) \delta(\varepsilon_{11} - \varepsilon_{12}) \delta(\varepsilon_{21} - \varepsilon_{22}) \right. \\ &\left. + \left(-(\varepsilon_{11} - \varepsilon_{21} - \omega) g_{\varepsilon_{11} - \varepsilon_{21} - \omega} - \frac{iD\mathbf{q}^2}{2} (h_{\varepsilon_{21} + \omega} - h_{\varepsilon_{21}}) \right) \delta(\varepsilon_{11} - \varepsilon_{12} - \omega) \delta(\varepsilon_{21} - \varepsilon_{22} + \omega) \right]. \end{aligned} \quad (2.139)$$

In general, Eq. (2.138) with Eq. (2.139) cannot be solved exactly. However, we can make two important observations: (a) In the limit of small energy transfers, $\omega \rightarrow 0$, the contributions from Σ_{SE} and Σ_{VX} , represented by the second and third line of Eq. (2.139), cancel exactly. (b) As in Eq. (2.130), only energy transfers $\omega \lesssim T$ contribute to the real part of Eq. (2.139) at energies close to the Fermi energy ($\varepsilon_{11} \rightarrow 0$ and $\varepsilon_{21} \rightarrow 0$).¹

von Delft *et al.* (2007) have suggested to transform Eq. (2.138) to real space and time, and then to solve it approximately with an exponential ansatz. Since the corresponding calculation is rather lengthy, we restrict ourselves here to a discussion of the final results. For electron and hole at the Fermi level, the solution has the following form

$$\Gamma_c(\mathbf{x}, \mathbf{y}, t) = \Gamma_{c0}(\mathbf{x}, \mathbf{y}, t) \exp[-F(\mathbf{x}, \mathbf{y}, t)]. \quad (2.140)$$

F is called the *Cooperon decay function* and is given by

$$\begin{aligned} F(\mathbf{x}, \mathbf{y}, t) &= \int_0^t d\tau d\tau' \frac{1}{V} \int d^d \mathbf{z} d^d \mathbf{z}' K(\mathbf{z} - \mathbf{z}', \tau - \tau') \\ &\times \left[\underbrace{P_{\mathbf{x}, \mathbf{y}, t}(\mathbf{z}, \mathbf{z}', \tau, \tau')}_{\text{from } \Sigma_{SE}} - \underbrace{P_{\mathbf{x}, \mathbf{y}, t}(\mathbf{z}, \mathbf{z}', \tau, t - \tau')}_{\text{from } \Sigma_{VX}} \right], \end{aligned} \quad (2.141)$$

where the Fourier transform of K is given by

$$K(\mathbf{q}, \omega) = \frac{1}{2\rho} \frac{1}{D\mathbf{q}^2} \omega [g_\omega + h_{-\omega}] \quad (2.142)$$

and $P_{\mathbf{x}, \mathbf{y}, t}(\mathbf{z}, \mathbf{z}', \tau, \tau')$ corresponds to the probability of diffusive propagation from \mathbf{x} to \mathbf{y} in time t passing through point \mathbf{z} at time τ and point \mathbf{z}' at time τ' . For $0 < \tau < t$ and $\tau < \tau' < t$ it is given by:²

$$P_{\mathbf{x}, \mathbf{y}, t}(\mathbf{z}, \mathbf{z}', \tau, \tau') = \frac{P_d(\mathbf{x}, \mathbf{z}, 0, \tau) P_d(\mathbf{z}, \mathbf{z}', \tau, \tau') P_d(\mathbf{z}', \mathbf{y}, \tau', t)}{P_d(\mathbf{x}, \mathbf{y}, t)}. \quad (2.143)$$

1. Note that $\text{Re}[iP_d(\mathbf{q}, \omega)] = \frac{-\omega}{(D\mathbf{q}^2)^2 + \omega^2}$.

2. For $\tau' < \tau$, we should interchange (\mathbf{z}, τ) and (\mathbf{z}', τ') in Eq. (2.143).

We will recover a relation similar to Eq. (2.141) in the path integral approach discussed in Section 2.2.6. To see that Eq. (2.141) is free of infrared divergences it is instructive to approximate the probability (2.143), which is restricted to follow a trajectory from \mathbf{x} to \mathbf{y} in time t , by the unrestricted diffusion probability between \mathbf{z} and \mathbf{z}' :

$$\frac{1}{V} \int d^d \mathbf{z} d^d \mathbf{z}' e^{i\mathbf{q}(\mathbf{z}-\mathbf{z}')} P_{\mathbf{x},\mathbf{y},t}(\mathbf{z}, \mathbf{z}', \tau, \tau') \approx \frac{1}{V} \int d^d \mathbf{z} d^d \mathbf{z}' e^{i\mathbf{q}(\mathbf{z}-\mathbf{z}')} P_d(\mathbf{z}-\mathbf{z}', |\tau-\tau'|) = e^{-D\mathbf{q}^2|\tau'-\tau|}. \quad (2.144)$$

It has been shown that the approximation Eq. (2.144) merely leads to a different prefactor ~ 1 of the final result, see Marquardt *et al.* (2007) for a detailed discussion. In this approximation, the decay function becomes independent of coordinates:

$$F(t) = \int_0^t d\tau d\tau' \int \frac{d\omega}{2\pi} e^{i\omega(\tau-\tau')} \frac{1}{V} \sum_{\mathbf{q} \neq \mathbf{0}} K(\mathbf{q}, \omega) \left[e^{-D\mathbf{q}^2|\tau-\tau'|} - e^{-D\mathbf{q}^2|t-\tau-\tau'|} \right]. \quad (2.145)$$

After integrating over time one obtains a result similar to Eq. (2.131) [von Delft *et al.*, 2007; Akkermans and Montambaux, 2007]:

$$F(t) = \frac{t}{2\pi\rho} \int d\omega \omega [g_\omega + h_{-\omega}] \left(1 - \frac{\sin(\omega t)}{\omega t} \right) \frac{1}{V} \sum_{\mathbf{q} \neq \mathbf{0}} \frac{1}{(D\mathbf{q}^2)^2 + \omega^2} \quad (2.146)$$

However, Eq. (2.146) contains the additional factor $1 - \sin(\omega t)/(\omega t)$ which is absent in Eq. (2.131). It effectively cuts the ω integral in IR at $\omega \simeq 1/t$. Large energy transfers, on the other hand, are restricted to $\omega \lesssim T$ due to the factor $g_\omega + h_{-\omega}$, cf. Fig. 2.12. Extracting the corresponding dephasing time from the relation $F(\tau_\phi) \simeq 1$, we finally obtain the self-consistent equation

$$\frac{1}{\tau_\phi} \approx \frac{2T}{\pi\rho} \int_{1/\tau_\phi}^T d\omega \frac{1}{V} \sum_{\mathbf{q} \neq \mathbf{0}} \frac{1}{(D\mathbf{q}^2)^2 + \omega^2}. \quad (2.147)$$

We see that the IR-divergence is effectively cut by the inverse dephasing time itself. This corresponds to the very plausible assumption that energies cannot be transferred on time scales larger than the dephasing time.

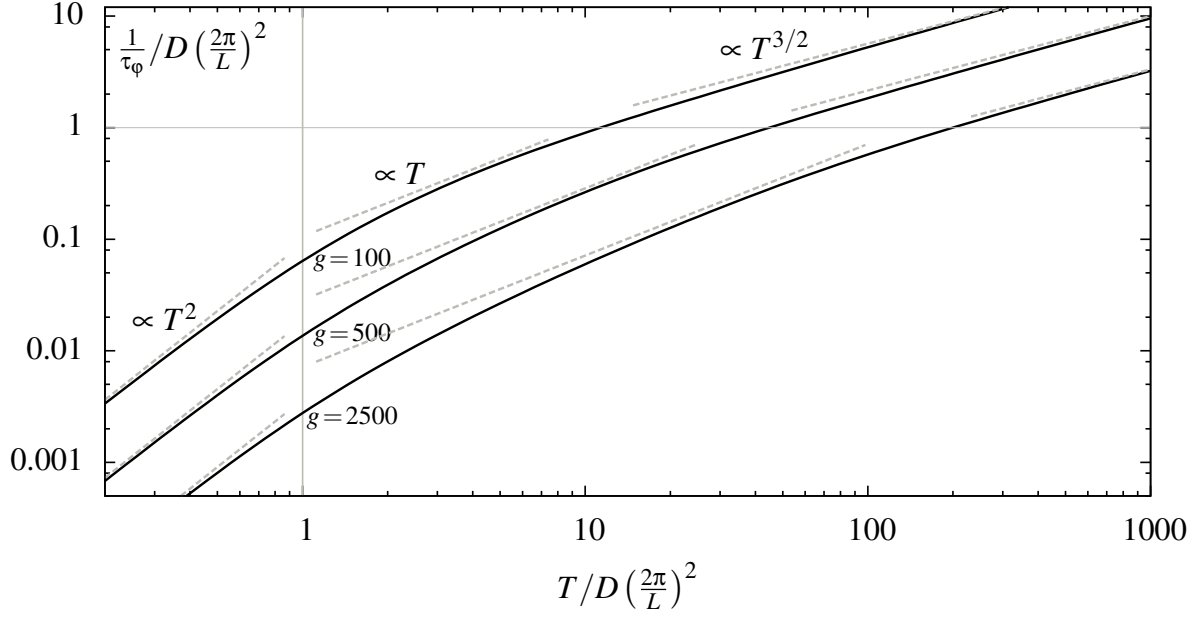


Figure 2.19: Numerical evaluation of τ_ϕ according to Eq. (2.148) for an isolated ring with circumference L for different values of $g \gg 1$.

2.2.5 Regimes of dephasing

In the previous section, we have discussed that the dephasing time τ_ϕ can be calculated from

$$\frac{1}{\tau_\phi} \approx \frac{4E_{\text{Th}}T}{g} \int_{1/\tau_\phi}^T d\omega \sum_{\mathbf{q} \neq 0} \frac{1}{(D\mathbf{q}^2)^2 + \omega^2}, \quad (2.148)$$

where we used $\rho V = g/(2\pi E_{\text{Th}})$ to express the lifetime in terms of the dimensionless conductance g and the Thouless energy $E_{\text{Th}} = D/L^2$, see Eqs. (2.47, 2.48). The temperature dependence of τ_ϕ is governed by the frequency dependence of the \mathbf{q} -sum. Recall that we have found the following limiting behavior, see Eqs. (2.105, 2.106):

$$\sum_{\mathbf{q} \neq 0} \frac{1}{(D\mathbf{q}^2)^2 + \omega^2} \approx \begin{cases} c' \frac{1}{E_{\text{Th}}^2} & \text{for } E_{\text{Th}} \gg \omega \\ c_d \frac{1}{\omega^2} \left(\frac{\omega}{E_{\text{Th}}} \right)^{d/2} & \text{for } \omega \gg E_{\text{Th}}. \end{cases} \quad (2.149)$$

We can now identify the leading temperature dependence of the dephasing time. For comparison, a numerical evaluation of τ_ϕ according to Eq. (2.148) for a quasi-1D ring is shown in Fig. 2.19. Note that we can rule out the case $T < 1/\tau_\phi$, since in this limit Eq. (2.148) shows that no energy ω can be transferred, such that no self-consistent solution can be found. We identify three regimes (see also our detailed discussion in Section 3.4):

- At $E_{\text{Th}} \ll 1/\tau_\phi \ll T$, we use Eq. (2.106) for $\omega \gg E_{\text{Th}}$ in Eq. (2.148) and solve self-consistently for $1/\tau_\phi$, with the result:

$$\frac{1}{\tau_\phi} \approx \begin{cases} \left(\frac{\sqrt{8} \sqrt{E_{\text{Th}}} T}{g} \right)^{2/3} & d = 1 \\ \frac{c_2}{2g} T \ln \left[\frac{g}{4c_2} \right] & d = 2 \end{cases}. \quad (2.150)$$

We call this the *diffusive regime* in the following, since the electron dynamics are governed by free diffusive trajectories much shorter than the system size.

Similar to the inelastic processes governing the quasi-particle lifetime, which we discussed in Section 2.2.3, dephasing is dominated by small energy and momentum transfers in this regime.

The diffusive regime has been first derived in the form of Eq. (2.150) by Altshuler *et al.* (1981c) by means of a dimensional estimation. The predicted temperature dependence, Eq. (2.150), has been observed in numerous experiments.

- At $1/\tau_\varphi \ll E_{\text{Th}} \ll T$, we split the ω integral into parts smaller and larger than E_{Th} , such that approximately

$$\frac{1}{\tau_\varphi} \approx \frac{4E_{\text{Th}}T}{g} \left[\int_{1/\tau_\varphi}^{E_{\text{Th}}} d\omega c' \frac{1}{E_{\text{Th}}^2} + \int_{E_{\text{Th}}}^T d\omega c_d \frac{1}{\omega^2} \left(\frac{\omega}{E_{\text{Th}}} \right)^{d/2} \right], \quad (2.151)$$

and find

$$\frac{1}{\tau_\varphi} \approx \begin{cases} \frac{4T}{g} [c' + 1/4] & d = 1 \\ \frac{4T}{g} [c' + c_2 \ln[T/E_{\text{Th}}]] & d = 2 \end{cases}. \quad (2.152)$$

We call this the *ergodic regime* in the following, since the quasi-particles explore the whole system before they dephase, $\tau_\varphi \gg 1/E_{\text{Th}}$. Note that the size of the temperature range where $1/\tau_\varphi \ll E_{\text{Th}} \ll T$ depends on g and the coefficients c' and c_d . We see in Fig. 2.19 that for a quasi-1D ring (without a magnetic field) a rather large conductance is required.

For open and unconfined systems, we have discussed in Section 2.1.4, that the quantum corrections are controlled by $\max(E_{\text{Th}}, 1/\tau_\varphi)$. At $1/\tau_\varphi \ll E_{\text{Th}}$, they become temperature independent and universal. Thus, a dephasing time of the form Eq. (2.152) can only contribute as a sub-leading correction in this case. However, we will see in Chapter 3, that the situation is different for confined systems, such as quantum dots.

The ergodic regime has been first discussed by Ludwig and Mirlin (2004) in the context of the Aharonov-Bohm effect: The trajectories contributing to dephasing of the AB-oscillations are always ergodic, such that the diffusive regime is absent. For the situation described here, it has been discussed first by Texier and Montambaux (2005). Moreover, it has been recently confirmed experimentally by Capron *et al.* (2013) (see also Ferrier *et al.* (2008)).

- At $1/\tau_\varphi \ll T \ll E_{\text{Th}}$, using Eq. (2.105) for $E_{\text{Th}} \gg \omega$ in Eq. (2.148), we find

$$\frac{1}{\tau_\varphi} \approx \frac{4c'}{gE_{\text{Th}}} T^2, \quad (2.153)$$

independent of dimensionality. This is the so-called *0D regime* first discussed in Sivan *et al.* (1994). Only in this regime, the upper limit of the integral in Eq. (2.148), which is due to Pauli blocking, has a significant influence on the temperature dependence of τ_φ . Thus, dephasing is governed by large energy transfers $\omega \simeq T$, cf. Section 2.2.3.

However, dephasing is even weaker than in the ergodic regime. As a result, the quantum corrections in open and unconfined systems depend only weakly on temperature. We will establish in Chapter 3, that even in confined geometries 0D dephasing can be observed in a transport experiment only as a sub-leading correction to the quantum corrections.

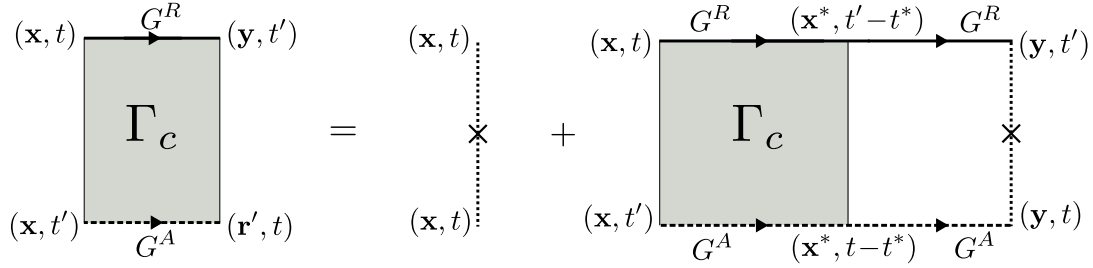


Figure 2.20: Time dependence of the Cooperon.

For isolated systems, we see from the definition $g = 2\pi E_{\text{Th}}/\Delta$ that

$$\gamma = \frac{1}{\tau_\phi} \approx \Delta \frac{2c'}{\pi} \left(\frac{T}{E_{\text{Th}}} \right)^2 \ll \Delta, \quad (2.154)$$

Thus, in the absence of other mechanisms of dephasing, the 0D regime is associated with a discrete energy spectrum $\gamma \ll \Delta$. In Section 2.1.6 we have argued that RMT is currently the only theory to describe quantum corrections in systems with a discrete spectrum. However, there is no straightforward method to introduce a dephasing time in this context. In general, the transition from the continuous to the discrete spectrum is still not well understood. Significant progress has been made by [Altshuler *et al.* \(1997\)](#), who have shown (by an analogy of localization in Fock space) that Eq. (2.153) remains valid in a parametrically large window (for $g \gg 1$) even at $\gamma \lesssim \Delta$.

Importantly, the 0D regime has so far eluded experimental observation, despite of several attempts, see e.g. [Huibers *et al.* \(1998b,a, 1999\)](#).

2.2.6 Electronic noise and the semi-classical picture of dephasing

In Section 2.1.2 we have analyzed the correlation functions P and K in the limit $\varepsilon_F \tau \gg 1$, and argued that their quantum corrections can be understood by means of a “semi-classical” picture of electron propagation. Since such a semi-classical picture often provides a more intuitive understanding, we will review the calculation of the dephasing time due to electron interactions in this framework in the following. Moreover, we have argued in Section 2.2.5 that the 0D regime of dephasing is practically impossible to observe in unconfined systems. We will see below that the semi-classical picture provides a powerful method to study systems with a more complicated geometry, which we will consider in Section 3.

Since this topic is rather broad, we will have to restrict our discussion to the key results necessary to understand our work. For details, we refer to the extensive review by [Chakravarty and Schmid \(1986\)](#), where the theory of disordered systems is put rigorously on a quasi-classical basis.

In Eq. (2.22), we have introduced the Cooperon propagator as a maximally crossed impurity ladder. In the absence of dephasing, it is the solution of the diffusion equation (2.20). In real space and time, the impurity ladder can be constructed by the Dyson equation shown in Fig. 2.20 for the Cooperon structure factor. Due to the non-local temporal structure of the Cooperon, Γ_c is in principle

a function of four time arguments, cf. Eq. (2.138):¹

$$\begin{aligned} \Gamma_c(\mathbf{x}, \mathbf{y}, t, t') &= \gamma \delta(\mathbf{x} - \mathbf{y}) \delta(t - t') \\ &+ \int d^d \mathbf{x}^* dt^* \Gamma_c(\mathbf{x}, \mathbf{x}^*, t, t') \bar{G}^R(\mathbf{x}^*, \mathbf{y}, t' - t^*, t') \bar{G}^A(\mathbf{x}^*, \mathbf{y}, t - t^*, t). \end{aligned} \quad (2.155)$$

The diffusive limit ($\mathbf{q}\ell \ll 1, \omega\tau \ll 1$) corresponds in real space and time to the assumptions that the Green's functions in Eq. (2.155) decay much faster than Γ_c , such that we can expand Γ_c in the integral around $\mathbf{x}^* \approx \mathbf{y}$ and $t^* \approx 0$. The term linear in $(\mathbf{x}^* - \mathbf{y})$ of the expansion vanishes due to symmetry, and after integrating over \mathbf{x}^* and t^* and a re-arrangement of the terms of Eq. (2.155) one obtains the diffusion equation for Γ_c ,

$$\tau(\partial_{t'} - D\Delta_{\mathbf{y}})\Gamma_c(\mathbf{x}, \mathbf{y}, t, t') = \gamma \delta(\mathbf{x} - \mathbf{y}) \delta(t - t'), \quad (2.156)$$

in full analogy to Eq. (2.19). Now, let us assume the presence of a slowly-varying smooth² time-dependent *noise potential* V , which describes the interactions with the surrounding electrons.³ In this case the Green's functions acquire an additional phase,

$$\bar{G}^R(\mathbf{x}, \mathbf{y}, t, t') \rightarrow \bar{G}^R(\mathbf{x}, \mathbf{y}, t, t') e^{i \int_t^{t'} d\tau V(\mathbf{x}, \tau)}, \quad (2.157)$$

and $\bar{G}^A(\mathbf{y}, \mathbf{x}, t', t)$ acquires the opposite phase. Thus, when deriving the diffusion equation (2.156), not only Γ_c , but also the phase-factor has to be expanded around (\mathbf{y}, t') . As a result, an additional term,

$$\frac{\partial}{\partial t} e^{i \int_t^{t'} d\tau V(\mathbf{x}, \tau)} \propto -iV(\mathbf{x}, t), \quad (2.158)$$

appears, and the diffusion equation becomes:

$$\gamma \delta(\mathbf{x} - \mathbf{y}) \delta(t - t') = \left(-\tau D\Delta_{\mathbf{y}} + \tau \partial_{t'} - i\tau \left[\underbrace{V(\mathbf{y}, t')}_{\text{from } G^R} - \underbrace{V(\mathbf{y}, t)}_{\text{from } G^A} \right] \right) \Gamma_c(\mathbf{x}, \mathbf{y}, t, t'). \quad (2.159)$$

It is important to note that the noise potential from the advanced Green's function enters this equation at time t and not t' , which is due to the time-reversed structure of the Cooperon, see Fig. 2.20. Thus, the difference of noise potentials, $\delta V \equiv -i[V(\mathbf{y}, t') - V(\mathbf{y}, t)]$, is local in space but not in time, and depends on the long-range nature of the Cooperon.

δV is directly associated with the *dephasing rate* $\gamma = 1/\tau_\varphi$, as we will see in the following: According to Feynman and Hibbs (1965), the solution to Eq. (2.159) can be written as a path-integral,

$$\begin{aligned} \frac{\tau}{\gamma} \Gamma_c(\mathbf{x}, \mathbf{y}, t, t') &= P_c(\mathbf{x}, \mathbf{y}, t - t') \\ &= \int_{\mathbf{z}(t)=\mathbf{x}}^{\mathbf{z}(t')=\mathbf{y}} D\mathbf{z} \exp \left(- \int_t^{t'} d\tau \left[\frac{\dot{\mathbf{z}}}{4D} - i(V(\mathbf{z}(\tau), \tau) - V(\mathbf{z}(\tau), t + t' - \tau)) \right] \right), \end{aligned} \quad (2.160)$$

where the noise potentials V in the action of Eq. (2.160) are taken at reversed times. Since V varies only slowly on the scale of the mean-free path, the path integral can be approximated by

$$P_c(\mathbf{x}, \mathbf{y}, t) \approx P_{c0}(\mathbf{x}, \mathbf{y}, t) \langle e^{i \int_0^t d\tau (V(\mathbf{z}(\tau), \tau) - V(\mathbf{z}(\tau), t - \tau))} \rangle_{\{\mathbf{z}(\tau)\}} \quad (2.161)$$

$$\equiv P_{c0}(\mathbf{x}, \mathbf{y}, t) \langle e^{-t\Gamma[\mathbf{z}(\tau)]} \rangle_{\{\mathbf{z}(\tau)\}}, \quad (2.162)$$

1. Note that in principle, two different times, τ_R^* for G^R , and τ_A^* for G^A , have to be considered, such that the second term on the r.h.s. of Eq. (2.155) comprises a double time integral. However, we have shown in the momentum-energy representation, Eq. (2.17), that the corresponding term is independent of the common energy ε , which is equivalent to setting $\tau_R^* = \tau_A^*$.

2. The noise potential V is assumed to be slowly varying on the scale of the mean free path ℓ , i.e. $V(x + \ell, t) \approx V(x, t)$.

3. $V(\mathbf{x}, t)$ should not be confused with the *static* disorder potential $V(\mathbf{x})$, introduced in Section 2.1.

where $\langle \dots \rangle_{\{\mathbf{z}(\tau)\}}$ denotes an average over diffusive trajectories from $\mathbf{z}(t) = \mathbf{x}$ to $\mathbf{z}(t') = \mathbf{y}$, and P_{c0} is the Cooperon in the absence of the noise potential. In Eq. (2.162), we have defined the *dephasing rate functional* $\Gamma[\mathbf{z}(\tau)]$, in full analogy to the dephasing rate in Eq. (2.39):

$$\Gamma[\mathbf{z}(\tau)] \equiv -i \frac{1}{t} \int_0^t d\tau (V(\mathbf{z}(\tau), \tau) - V(\mathbf{z}(\tau), t - \tau)). \quad (2.163)$$

Typically, the noise potential is a random function with Gaussian probability distribution. Averaging over the realizations of V and using $\langle \exp(i\Phi) \rangle_V = \exp(-\frac{1}{2}\langle \Phi^2 \rangle_V)$ we find

$$\Gamma[\mathbf{z}(\tau)] = \frac{1}{t} \int_0^t d\tau_1 d\tau_2 \left(\langle |V|^2 \rangle_V(\mathbf{z}(\tau_1), \mathbf{z}(\tau_2), t - \tau_1 - \tau_2) - \langle |V|^2 \rangle_V(\mathbf{z}(\tau_1), \mathbf{z}(\tau_2), \tau_1 - \tau_2) \right), \quad (2.164)$$

where we introduced the noise correlation function $\langle |V|^2 \rangle_V(\mathbf{x}, \mathbf{y}, t)$.

In Section 2.4 we give a detailed microscopic derivation of $\langle |V|^2 \rangle_V$. We will show that it is directly related to the interaction propagator in the random phase approximation, Eq. (2.93):

$$\langle |V|^2 \rangle_V(\mathbf{x}, \mathbf{y}, \omega) = F_\omega \text{Im} \left[\overline{U}_\omega^R(\mathbf{x}, \mathbf{y}) \right], \quad (2.165)$$

with an energy distribution function

$$F_\omega = \frac{2}{1 - e^{-\omega/T}}. \quad (2.166)$$

Moreover, we show that it can be expressed in terms of the solution of the diffusion equation of the system at $\omega = 0$:

$$\langle |V|^2 \rangle_V(\mathbf{x}, \mathbf{y}, \omega) = \frac{1}{2\rho} \omega F_\omega P_d(\mathbf{x}, \mathbf{y}, 0). \quad (2.167)$$

Powerful methods are available to calculate this quantity in systems with a non-homogeneous geometry. In Section 3.6, we will use Eq. (2.167) to describe dephasing in a confined system, namely a quantum dot.

In the limit of small frequencies, the distribution function is given by

$$\lim_{\omega/T \rightarrow 0} [\omega F_\omega] = 2T. \quad (2.168)$$

As a result, the r.h.s. of Eq. (2.167) becomes independent of frequency and describes *white noise* in time. In this limit, the average over random walks in Eq. (2.162) has been calculated exactly for an infinite quasi-1D wire by [Altshuler *et al.* \(1982a\)](#) and for a finite quasi-1D ring by [Texier and Montambaux \(2005\)](#).

The great advantage of a description of dephasing using Eq. (2.162) and Eq. (2.164) is that it is free of any IR-divergencies. We will show in Section 2.4 that this can be easily understood from the following argument: Due to the difference in noise correlators in Eq. (2.164), we can add any additional terms to Eq. (2.167), which do not depend on the difference in coordinates. In particular, we can substitute

$$P_d(\mathbf{x}, \mathbf{y}, 0) \rightarrow P_d(\mathbf{x}, \mathbf{y}, 0) - \frac{1}{2} [P_d(\mathbf{x}, \mathbf{x}, 0) + P_d(\mathbf{y}, \mathbf{y}, 0)] = -\frac{\sigma_0}{2D} \mathcal{R}(\mathbf{x}, \mathbf{y}), \quad (2.169)$$

where σ_0 is the Drude bulk conductivity and $\mathcal{R}(\mathbf{x}, \mathbf{y})$ is the classical dc resistance between the points \mathbf{x} and \mathbf{y} of the metal. Since the resistance $\mathcal{R}(\mathbf{x}, \mathbf{y})$ is not singular for any \mathbf{x} and \mathbf{y} and $\tau, \tau' \in [0, t]$, there cannot be an IR-divergence in Eq. (2.164).

However, at low temperatures $T \lesssim E_{\text{Th}}$, using Eq. (2.167) in Eq. (2.164) to calculate the dephasing rate cannot be correct, since energy transfers larger than temperature would be exchanged with the noise field due to $\lim_{\omega \rightarrow \infty} F_{\omega} = 2 \neq 0$. We have discussed in Section 2.2.3 and Section 2.2.4 that such processes are excluded due to Pauli blocking. The reason why Eqs. (2.167, 2.164) fail to describe this limit is clear: The path integral approach describes the Cooperon *in the presence of quantum noise, but in the absence of a Fermi sea* [Marquardt *et al.*, 2007]. Remarkably, after doing the replacement

$$F_{\omega} \longrightarrow [g_{\omega} + h_{-\omega}] \quad (2.170)$$

in Eq. (2.167), the correlation function Eq. (2.167) *exactly corresponds to the function K* , defined in Eq. (2.142). Moreover, the contribution of the first and second terms of Eq. (2.164) are directly related to the contribution from Σ_{SE} and Σ_{VX} in Eq. (2.141), after lifting the average over diffusive trajectories into the exponent:

$$\langle e^{-t\Gamma[\mathbf{z}(\tau)]} \rangle_{\{\mathbf{z}(\tau)\}} \approx e^{-t\langle \Gamma[\mathbf{z}(\tau)] \rangle_{\{\mathbf{z}(\tau)\}}} = e^{-F(t)}. \quad (2.171)$$

Thus, by comparing both approaches, it is conjectured by Marquardt *et al.* (2007); von Delft *et al.* (2007) that the Fermi sea can be accounted for in the path integral approach via the substitution (2.170). See also Cohen *et al.* (2009) for a detailed discussion of this substitution. As a result, Eq. (2.164) reproduces precisely the three regimes for the dephasing time described in Section 2.2.5. We refer to our detailed discussion of this point in ‘‘VII’’ of Section 2.4.

2.3 To be published: Two-loop calculation of the generalized diffusion propagator

Consider the *generalized diffusion propagator*, which is defined as the disorder averaged correlation function

$$P(\mathbf{x}, \mathbf{y}, \omega) \equiv \frac{1}{2\pi\rho} \overline{G_{\epsilon}^R(\mathbf{x}, \mathbf{y}) G_{\epsilon-\omega}^A(\mathbf{y}, \mathbf{x})}, \quad (2.172)$$

where ρ is the density of states and $G^{R/A}$ are the usual retarded/advanced Green's functions. We are interested in the diffusive regime, $|\mathbf{x} - \mathbf{y}| \gg \ell$, $1/\tau \gg \omega$, where ℓ is the mean free path and τ is the transport time. Following the discussion in Section 2.1.2, we can write P as

$$P(\mathbf{q}, \omega) = P_d(\mathbf{q}, \omega) + \delta P(\mathbf{q}, \omega), \quad P_d(\mathbf{q}, \omega) = \frac{1}{D\mathbf{q}^2 - i\omega}, \quad (2.173)$$

where P_d is the classical diffusion propagator, which we denote by a wavy double-line, see Fig. 2.21(a).

In the following, we will calculate the quantum corrections $\delta P(\mathbf{q}, \omega)$ diagrammatically up to the second loop. We will use two different approaches to deal with the unphysical UV-divergences associated with the ballistic (short-range) parts of the diagrams (also known as Hikami boxes) and which are related to the violation of particle number conservation: (1) Applying the ideas of [Brezin *et al.* \(1980\)](#), who used a *dimensional regularization* scheme, we simply drop all divergent constant terms in the sums [[Ostrovsky and Kravtsov, 2013](#)]. (2) We explicitly construct particle number conserving diagrams by dressing the Hikami boxes of the diagrams not by hand, but by moving the external vertices into adjacent impurity ladders. Since this construction removes the divergences by rearranging the ballistic parts of the diagrams, we call it *ballistic regularization* in the following.

Remarkably, we will see below that after summing the relevant diagrams, both approaches lead to the same particle number conserving expressions in the unitary ($\gamma \rightarrow \infty$) as well as the orthogonal ($\gamma \rightarrow 0$) ensemble, cf. Eqs. (2.210, 2.211).

2.3.1 Dimensional regularization

The one-loop quantum correction is shown in Fig. 2.21(b), which includes a Cooperon propagator C . We find

$$\delta P_{(1)}(\mathbf{q}, \omega) = \frac{1}{2\pi\rho} \frac{1}{(D\mathbf{q}^2 - i\omega)^2} \frac{1}{V} \sum_{\mathbf{Q}} \frac{1}{D\mathbf{Q}^2 - i\omega} \times \frac{1}{2\pi\rho\tau^4} H_4^{(1)}, \quad (2.174)$$

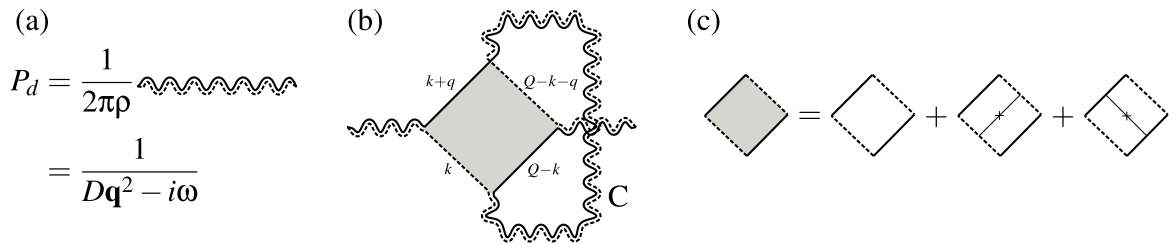


Figure 2.21: (a) Classical diffusion propagator. (b) One-loop quantum correction. (c) Dressing of the 4-point Hikami box.

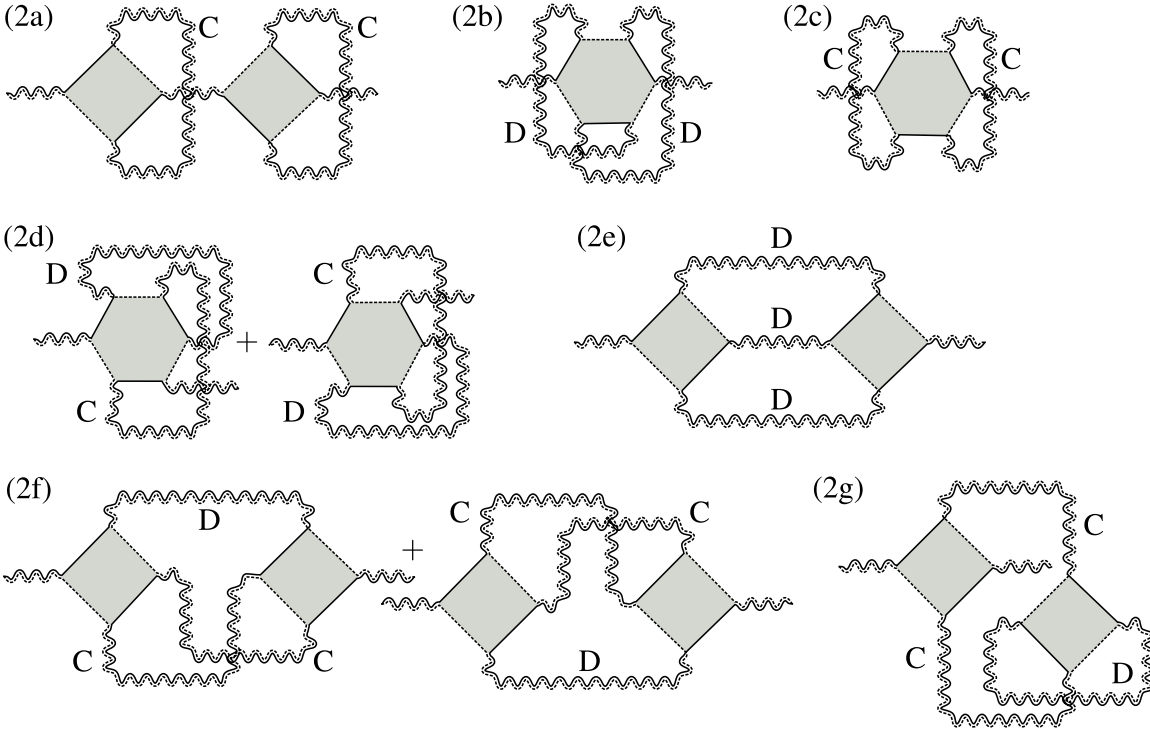


Figure 2.22: Diagrams for the two-loop correction of the generalized diffusion propagator.

where $H_4^{(1)}$ denotes the 4-point Hikami box, which should be dressed according to Fig. 2.21(c). A straightforward calculation by expanding the Green's functions in all transferred energies/momenta yields

$$\frac{1}{2\pi\rho\tau^4}H_4^{(1)} = 2D\mathbf{q}^2 + 2D\mathbf{Q}^2 - 2i\omega. \quad (2.175)$$

Evidently, using Eq. (2.175) in Eq. (2.174) leads to an UV-divergence of the \mathbf{Q} -sum in all dimensions $d > 0$. This divergence is related to the violation of the particle conservation law. To restore the conservation law, one can use a general prescription of the dimensional scheme which allows us to formally drop any divergent momentum sums with constant summands [Ostrovsky and Kravtsov, 2013]:

$$\frac{1}{V} \sum_{\mathbf{Q}} 1 \text{ “=” } 0. \quad (2.176)$$

In particular, in Eqs. (2.174, 2.175) we subtract “-2” in the summand and find

$$\delta P_{(1)}(\mathbf{q}, \omega) = \frac{1}{2\pi\rho} \frac{1}{(D\mathbf{q}^2 - i\omega)^2} \frac{1}{V} \sum_{\mathbf{Q}} \frac{1}{D\mathbf{Q}^2 - i\omega} [2D\mathbf{q}^2]. \quad (2.177)$$

Eq. (2.177) yields $\delta P_{(1)}(\mathbf{q} = 0, \omega) = 0$.

For the two-loop quantum correction, 7 diagrams have to be calculated which are shown in Fig. 2.22. The diagram (2a) can be calculated straightforwardly by using Eq. (2.177):

$$\delta P_{(2a)}(\mathbf{q}, \omega) = \frac{1}{2\pi\rho} \frac{1}{(D\mathbf{q}^2 - i\omega)^3} \frac{1}{V} \sum_{\mathbf{Q}_1, \mathbf{Q}_2} \frac{1}{D\mathbf{Q}_1^2 - i\omega} \frac{1}{D\mathbf{Q}_2^2 - i\omega} [(2D\mathbf{q}^2)^2]. \quad (2.178)$$

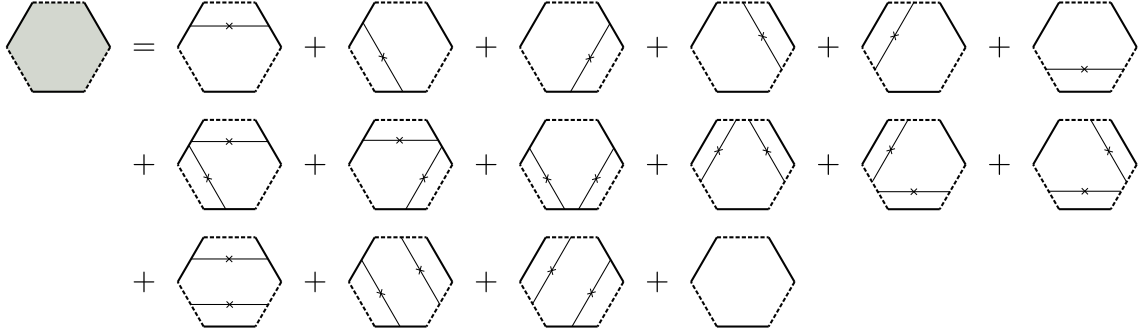


Figure 2.23: Dressing of the 6-point Hikami box.

Diagram (2b) contains a 6-point Hikami box which should be dressed in 16 different ways shown in Fig. 2.23. Expanding the Green's functions in all transferred energies/momenta yields

$$\frac{1}{2\pi\rho\tau^6}H_6^{(2b)} = -4D\mathbf{q}^2 - 4D\mathbf{Q}_1^2 - 4D\mathbf{Q}_2^2 + 6i\omega. \quad (2.179)$$

Omitting all formally divergent sums of constant expressions according to the dimensional scheme prescription, cf. Eq. (2.176), we find

$$\delta P_{(2b)}(\mathbf{q}, \omega) = \frac{1}{2\pi\rho} \frac{1}{(D\mathbf{q}^2 - i\omega)^2} \frac{1}{V} \sum_{\mathbf{Q}_1, \mathbf{Q}_2} \frac{1}{D\mathbf{Q}_1^2 - i\omega} \frac{1}{D\mathbf{Q}_2^2 - i\omega} [-4D\mathbf{q}^2 - 2i\omega]. \quad (2.180)$$

Note that $\delta K_{(2b)}$ does not conserve particle number alone, but we will see below that the term $\sim -2i\omega$ is canceled in the final result.

Diagrams (2c) and (2d) are similar to (2b), their answers read:

$$\delta P_{(2c)}(\mathbf{q}, \omega) = \frac{1}{2\pi\rho} \frac{1}{(D\mathbf{q}^2 - i\omega)^2} \frac{1}{V} \sum_{\mathbf{Q}_1, \mathbf{Q}_2} \frac{1}{D\mathbf{Q}_1^2 - i\omega} \frac{1}{D\mathbf{Q}_2^2 - i\omega} [-4D\mathbf{q}^2 - 2i\omega], \quad (2.181)$$

$$\delta P_{(2d)}(\mathbf{q}, \omega) = \frac{1}{2\pi\rho} \frac{1}{(D\mathbf{q}^2 - i\omega)^2} \frac{1}{V} \sum_{\mathbf{Q}_1, \mathbf{Q}_2} \frac{1}{D\mathbf{Q}_1^2 - i\omega} \frac{1}{D\mathbf{Q}_2^2 - i\omega} [-8D\mathbf{q}^2 - 4i\omega]. \quad (2.182)$$

Diagram (2e) contains two 4-point Hikami boxes giving each

$$\frac{1}{2\pi\rho\tau^4}H_4^{(2e)} = D(\mathbf{q} + \mathbf{Q}_1)^2 + D(\mathbf{q} + \mathbf{Q}_2)^2 - 2i\omega. \quad (2.183)$$

To apply Eq. (2.176), we first re-arrange the terms as follows:

$$\begin{aligned} \delta P_{(2e)}(\mathbf{q}, \omega) &= \frac{1}{2\pi\rho} \frac{1}{(D\mathbf{q}^2 - i\omega)^2} \frac{1}{V} \sum_{\mathbf{Q}_1, \mathbf{Q}_2} \frac{[D(\mathbf{q} + \mathbf{Q}_1)^2 + D(\mathbf{q} + \mathbf{Q}_2)^2 - 2i\omega]^2}{(D\mathbf{Q}_1^2 - i\omega)(D\mathbf{Q}_2^2 - i\omega)(D(\mathbf{q} + \mathbf{Q}_1 + \mathbf{Q}_2)^2 - i\omega)} \end{aligned} \quad (2.184)$$

$$= \frac{1}{2\pi\rho} \frac{1}{(D\mathbf{q}^2 - i\omega)^2} \frac{1}{V} \sum_{\mathbf{Q}_1, \mathbf{Q}_2} \left[\frac{1}{D\mathbf{Q}_1^2 - i\omega} + \frac{1}{D\mathbf{Q}_2^2 - i\omega} + \frac{1}{D(\mathbf{q} + \mathbf{Q}_1 + \mathbf{Q}_2)^2 - i\omega} \times \right. \quad (2.185)$$

$$\times \left\{ 4 + \frac{2D[\mathbf{q}\mathbf{Q}_1 - (\mathbf{Q}_1 - \mathbf{q})(\mathbf{q} + \mathbf{Q}_1 + \mathbf{Q}_2)]}{D\mathbf{Q}_1^2 - i\omega} + \frac{2D[\mathbf{q}\mathbf{Q}_2 - (\mathbf{Q}_2 - \mathbf{q})(\mathbf{q} + \mathbf{Q}_1 + \mathbf{Q}_2)]}{D\mathbf{Q}_2^2 - i\omega} \right. \quad (2.186)$$

$$\left. + \frac{D\mathbf{q}^2 + i\omega}{D\mathbf{Q}_1^2 - i\omega} + \frac{D\mathbf{q}^2 + i\omega}{D\mathbf{Q}_2^2 - i\omega} + \frac{4D^2[\mathbf{q}(\mathbf{q} + \mathbf{Q}_1 + \mathbf{Q}_2)]^2}{(D\mathbf{Q}_1^2 - i\omega)(D\mathbf{Q}_2^2 - i\omega)} \right\}.$$

Evidently, when applying Eq. (2.176), the first two terms in the rectangular brackets of (2.185) are zero. After re-defining $\mathbf{q} + \mathbf{Q}_1 + \mathbf{Q}_2$ as either \mathbf{Q}_1 or \mathbf{Q}_2 , it is evident that the same is true for the first term in curly brackets of line (2.186), while the second and third terms vanish after angular averaging. In total, we find:

$$\begin{aligned} \delta P_{(2e)}(\mathbf{q}, \omega) & \quad (2.187) \\ &= \frac{1}{2\pi\rho} \frac{1}{(D\mathbf{q}^2 - i\omega)^2} \frac{1}{V} \sum_{\mathbf{Q}_1, \mathbf{Q}_2} \frac{1}{D\mathbf{Q}_1^2 - i\omega} \frac{1}{D\mathbf{Q}_2^2 - i\omega} \left[2D\mathbf{q}^2 + 2i\omega + \frac{4D^2[\mathbf{q}(\mathbf{q} + \mathbf{Q}_1 + \mathbf{Q}_2)]^2}{D(\mathbf{q} + \mathbf{Q}_1 + \mathbf{Q}_2)^2 - i\omega} \right]. \end{aligned}$$

Diagram (2f) contains two 4-point Hikami boxes giving

$$\begin{aligned} & \frac{1}{(2\pi\rho\tau^4)^2} \left[H_4^{(2f)} \times H_4^{(2f)} \right] \quad (2.188) \\ &= [D(\mathbf{q} + \mathbf{Q}_1)^2 + D(\mathbf{Q}_1 + \mathbf{Q}_2)^2 - 2i\omega] \times [D(\mathbf{q} + \mathbf{Q}_2)^2 + D(\mathbf{Q}_1 + \mathbf{Q}_2)^2 - 2i\omega]. \end{aligned}$$

Again rearranging the terms similar to Eq. (2.184) and using Eq. (2.176), we find:

$$\begin{aligned} \delta P_{(2f)}(\mathbf{q}, \omega) & \quad (2.189) \\ &= \frac{1}{2\pi\rho} \frac{1}{(D\mathbf{q}^2 - i\omega)^2} \frac{1}{V} \sum_{\mathbf{Q}_1, \mathbf{Q}_2} \frac{1}{D\mathbf{Q}_1^2 - i\omega} \frac{1}{D\mathbf{Q}_2^2 - i\omega} \left[10D\mathbf{q}^2 + 2i\omega + \frac{8D^2(\mathbf{q}\mathbf{Q}_1)(\mathbf{q}\mathbf{Q}_2)}{D(\mathbf{q} + \mathbf{Q}_1 + \mathbf{Q}_2)^2 - i\omega} \right]. \end{aligned}$$

Finally, for diagram (2g), we find

$$\frac{1}{(2\pi\rho\tau^4)^2} \left[H_4^{(2g)} \times H_4^{(2g)} \right] = [2D\mathbf{q}^2 + 2D\mathbf{Q}_1^2 - 2i\omega] \times [2D\mathbf{Q}_1^2 + 2D\mathbf{Q}_2^2 - 2i\omega], \quad (2.190)$$

and

$$\begin{aligned} \delta P_{(2g)}(\mathbf{q}, \omega) & \quad (2.191) \\ &= \frac{1}{2\pi\rho} \frac{1}{(D\mathbf{q}^2 - i\omega)^2} \frac{1}{V} \sum_{\mathbf{Q}_1, \mathbf{Q}_2} \frac{1}{D\mathbf{Q}_1^2 - i\omega} \frac{1}{D\mathbf{Q}_2^2 - i\omega} \left[4D\mathbf{q}^2 + 4i\omega + \frac{4i\omega D\mathbf{q}^2}{D\mathbf{Q}_1^2 - i\omega} \right]. \end{aligned}$$

Collecting all parts together, we find the answers (2.210, 2.211), see Section 2.3.3.

2.3.2 Ballistic regularization

In this section we construct particle number conserving diagrams by moving the external vertices into adjacent impurity ladders [Hastings *et al.*, 1994]. We have already discussed this procedure in Section 2.1.2, cf. Fig. 2.5 and Fig. 2.6.

To illustrate the idea, we have drawn an external vertex close to an impurity ladder in Fig. 2.24(a): By moving the external vertex (on the left) up, into the ladder, we generate a diagram which resembles the dressing of a Hikami box, while keeping the total number of impurities of the diagram fixed. Applying this to the diagram of Fig. 2.21(b), see Fig. 2.24(b), where an impurity ladder with momentum-transfer \mathbf{Q} is attached at the top and bottom of the Hikami box, we can generate both required dressings of the 4 point Hikami box. Note that calculating the diagrams in this way means that the undressed box is effectively multiplied by an extra factor of $[1 + i\tau\omega - \tau D\mathbf{Q}^2]$, since it contains one extra ‘‘step’’ of the ladder, cf. Fig. 2.24(d).

Importantly, all dressings shown in Fig. 2.21(c) and Fig. 2.23 have to be generated in this way, and we will see below that this is not immediately possible for the diagrams involving 6-point Hikami

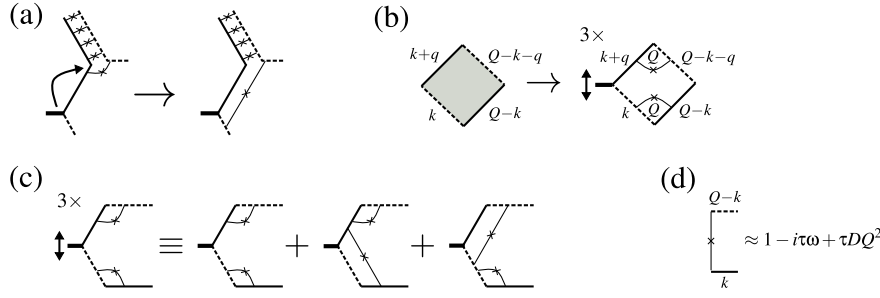


Figure 2.24: (a) Dressing of the Hikami box by moving a vertex. (b) Ballistic regularization of the Hikami box of Fig. 2.21(b). (c) Illustration of our *arrow notation*. (d) One “step” of an impurity ladder.

boxes. In this case, additional impurity lines have to be added, followed by, again, moving the vertices into adjacent ladders, whenever possible.

Note that a large number of diagrams is generated by this procedure, which makes the calculation prone to arithmetic mistakes. To double check the following results, we have written a “Mathematica” script, which is appended in Appendix A.1.

To simplify drawing all necessary diagrams, we have introduced an *arrow notation* in Fig. 2.24(b), defined in Fig. 2.24(c): Arrows at a vertex pointing in the direction of a nearby impurity ladder stand for the sum over the undressed diagram and the diagram where the vertex has moved one impurity into the ladder. The number “3x” above the arrow denotes how many diagrams of the same order in τ are generated by this procedure, i.e. in the example of Fig. 2.24(c) the vertex is moved one impurity into the upper impurity ladder and one impurity into the lower ladder, such that 3 diagrams should be summed up. This notation will be used extensively below.

Let us first calculate the Hikami box of the one-loop diagram accordingly: The undressed diagram which contains one extra “step” gives

$$\frac{1}{2\pi\rho\tau^4}\tilde{H}_4^{(1),(A)} = \tau^{-1} [2 + 6i\tau\omega - 2\tau D(\mathbf{q}^2 + \mathbf{Q}^2)] [1 + i\tau\omega - \tau D\mathbf{Q}^2], \quad (2.192)$$

and by moving the vertex once up and down, we obtain

$$\frac{1}{2\pi\rho\tau^4}\tilde{H}_4^{(1),(B)} = \tau^{-1} [-1 - 4i\tau\omega + 2\tau D(\mathbf{q}^2 + \mathbf{q}\mathbf{Q} + \mathbf{Q}^2)], \quad (2.193)$$

and

$$\frac{1}{2\pi\rho\tau^4}\tilde{H}_4^{(1),(C)} = \tau^{-1} [-1 - 4i\tau\omega + 2\tau D(\mathbf{q}^2 - \mathbf{q}\mathbf{Q} + \mathbf{Q}^2)]. \quad (2.194)$$

Summing all terms in the lowest order in τ yields

$$\frac{1}{2\pi\rho\tau^4}\tilde{H}_4^{(1)} = \frac{1}{2\pi\rho\tau^4} [\tilde{H}_4^{(1),(A)} + \tilde{H}_4^{(1),(B)} + \tilde{H}_4^{(1),(C)}] = 2D\mathbf{q}^2, \quad (2.195)$$

which leads to Eq. (2.177). Note that this result, as well as all further results for Hikami boxes below, is proportional to the external momentum \mathbf{q} and thus guarantees particle conservation for each diagram separately.

Let us now consider the two-loop diagrams: Again, the reducible diagram (2a) is straightforward, see Eq. (2.178). To calculate diagram (2b) using ballistic regularization, we move the vertices of the

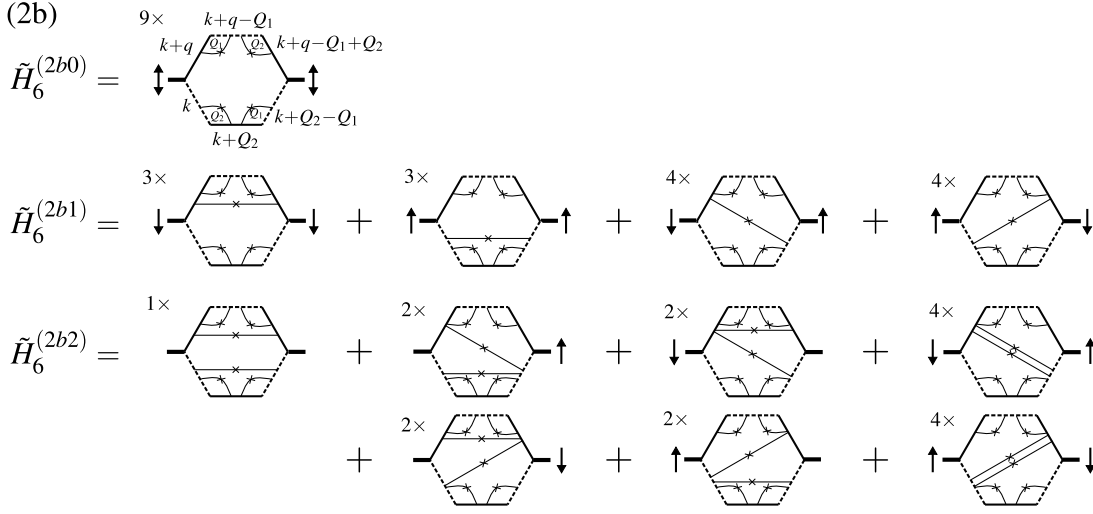


Figure 2.25: Ballistic regularization of the Hikami boxes of diagram (2b).

6-point Hikami box (see the first line of Fig. 2.25) into the adjacent diffusons, which generates 9 of the 16 diagrams. The result is:

$$\frac{1}{2\pi\rho\tau^6}\tilde{H}_6^{(2b0)} = -6D\mathbf{q}^2. \quad (2.196)$$

To generate the missing 7 of the 16 diagrams required to dress a 6-point Hikami box, we have to add the diagrams (2b1), shown in the second line of Fig. 2.25, which contain one extra impurity line. Note that these diagrams also involve products of two 4-point Hikami boxes (the last two diagrams in the second line of Fig. 2.25) of the same order in τ . These diagrams might as well be included in diagram (2e), but we included them in (2b) to restore particle number conservation. Further note that the two 4-point Hikami boxes can be dressed independently, thus, 4 instead of 3 diagrams of the same order are generated by moving the vertices. The result of the corresponding 14 diagrams is

$$\frac{1}{2\pi\rho\tau^6}\tilde{H}_6^{(2b1)} = +6D\mathbf{q}^2. \quad (2.197)$$

We see that the diagrams $\tilde{H}_6^{(2b0)}$ and $\tilde{H}_6^{(2b1)}$ cancel. Still 1 of the 16 dressings of the 6-point Hikami box is missing. Thus, we also have to consider the 17 diagrams (2b2), shown in the last line of Fig. 2.25, which contain two extra impurities:

$$\frac{1}{2\pi\rho\tau^6}\tilde{H}_6^{(2b2)} = -2D\mathbf{q}^2. \quad (2.198)$$

In total we obtain:

$$\delta P_{(2b)}(\mathbf{q}, \omega) = \frac{1}{2\pi\rho} \frac{1}{(D\mathbf{q}^2 - i\omega)^2} \frac{1}{V} \sum_{\mathbf{Q}_1, \mathbf{Q}_2} \frac{1}{D\mathbf{Q}_1^2 - i\omega} \frac{1}{D\mathbf{Q}_2^2 - i\omega} [-2D\mathbf{q}^2]. \quad (2.199)$$

Diagram (2c), see Fig. 2.26, is equivalent to (2b) with the result:

$$\delta P_{(2c)}(\mathbf{q}, \omega) = \frac{1}{2\pi\rho} \frac{1}{(D\mathbf{q}^2 - i\omega)^2} \frac{1}{V} \sum_{\mathbf{Q}_1, \mathbf{Q}_2} \frac{1}{D\mathbf{Q}_1^2 - i\omega} \frac{1}{D\mathbf{Q}_2^2 - i\omega} [-2D\mathbf{q}^2]. \quad (2.200)$$

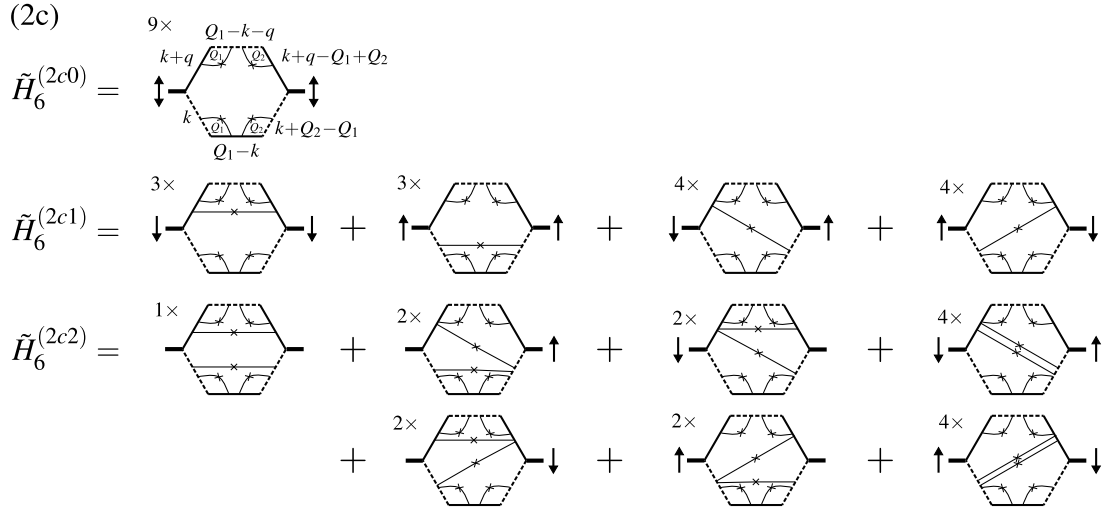


Figure 2.26: Ballistic regularization of the Hikami boxes of diagram (2c).

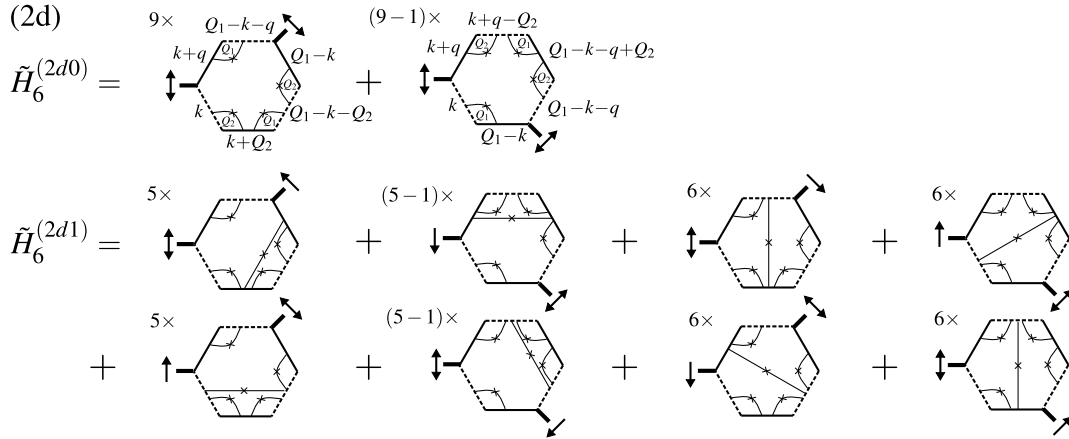


Figure 2.27: Ballistic regularization of the Hikami boxes of diagram (2d).

For the diagrams (2d) on the other hand, see the first line of Fig. 2.27, we find from the corresponding 17 diagrams:

$$\frac{1}{2\pi\rho\tau^6} H_6^{(2d0)} = 16D\mathbf{q}^2. \quad (2.201)$$

Note that the case where both vertices move into the same Cooperon is only counted once, since it is equivalent for both diagrams of (2d0). Thus, only 8 of the 9 possible diagrams are included in one of the two diagrams. To generate all 16 dressings of the Hikami box, we also have to include the 42 diagrams (2d1) in the second line of Fig. 2.27 with the result:

$$\frac{1}{2\pi\rho\tau^6} H_6^{(2d1)} = -16D\mathbf{q}^2. \quad (2.202)$$

We see that the diagrams (2d0) and (2d1) cancel:

$$\delta P_{(2d)}(\mathbf{q}, \omega) = 0. \quad (2.203)$$

$$(2g) \quad H_4^{(2g)} \times H_4^{(2g)} = \begin{array}{c} \text{3} \times \\ \updownarrow \\ \begin{array}{c} k+q \quad Q_1-k-q \\ \swarrow \quad \searrow \\ \text{---} \quad \text{---} \\ \swarrow \quad \searrow \\ k \quad Q_1-k \end{array} \end{array} \times \left(\begin{array}{c} Q_1-k' \quad k' \\ \swarrow \quad \searrow \\ \text{---} \quad \text{---} \\ \swarrow \quad \searrow \\ Q_1-k'-Q_2 \quad k'+Q_2 \end{array} + \begin{array}{c} \text{---} \\ \swarrow \quad \searrow \\ \text{---} \end{array} + \begin{array}{c} \text{---} \\ \swarrow \quad \searrow \\ \text{---} \end{array} \right)$$

Figure 2.30: Ballistic regularization of the Hikami boxes of diagram (2g).

2.3.3 Conclusions

An overview of the results can be found in Fig. 2.31.

Unitary ensemble

The result for the unitary ensemble corresponding to the limit $\gamma \rightarrow \infty$ is obtained by dropping all diagrams containing Cooperon propagators. Note that there is no one-loop quantum correction in the unitary ensemble, since Fig. 2.21(b) contains a Cooperon. From diagrams (2b) and (2e) we find for the unitary ensemble:

$$\begin{aligned} \delta P_{\text{unitary}}(\mathbf{q}, \omega) & \quad (2.210) \\ &= \frac{1}{2\pi\rho} \frac{2D\mathbf{q}^2}{(D\mathbf{q}^2 - i\omega)^2} \frac{1}{V} \sum_{\mathbf{Q}_1, \mathbf{Q}_2} \frac{1}{D\mathbf{Q}_1^2 - i\omega} \frac{1}{D\mathbf{Q}_2^2 - i\omega} \left[\frac{2D[\mathbf{q}(\mathbf{q} + \mathbf{Q}_1 + \mathbf{Q}_2)]^2 / \mathbf{q}^2}{D(\mathbf{q} + \mathbf{Q}_1 + \mathbf{Q}_2)^2 - i\omega} - 1 \right]. \end{aligned}$$

Orthogonal ensemble

In the orthogonal ensemble, corresponding to $\gamma \rightarrow 0$, Cooperons and diffusons are identical. Summing all one- and two-loop diagrams, we find for the orthogonal ensemble:

$$\begin{aligned} \delta P_{\text{orthogonal}}(\mathbf{q}, \omega) &= \frac{1}{2\pi\rho} \frac{2D\mathbf{q}^2}{(D\mathbf{q}^2 - i\omega)^2} \frac{1}{V} \sum_{\mathbf{Q}_1} \frac{1}{D\mathbf{Q}_1^2 - i\omega} \times \quad (2.211) \\ & \left[1 + 2 \sum_{\mathbf{Q}_2} \frac{1}{D\mathbf{Q}_2^2 - i\omega} \left\{ \frac{D\mathbf{q}^2}{D\mathbf{q}^2 - i\omega} + \frac{i\omega}{D\mathbf{Q}_1^2 - i\omega} + \frac{D^2 [\mathbf{q}(\mathbf{q} + \mathbf{Q}_1 + \mathbf{Q}_2)]^2 + 2D^2(\mathbf{q}\mathbf{Q}_1)(\mathbf{q}\mathbf{Q}_2)}{[D\mathbf{q}^2][D(\mathbf{q} + \mathbf{Q}_1 + \mathbf{Q}_2)^2 - i\omega]} \right\} \right]. \end{aligned}$$

Mixed ensemble

In the ballistic regularization scheme, we construct the Hikami boxes by moving vertices into nearby particle-hole (diffuson) or particle-particle (Cooperon) ladders. In this scheme, we can determine the γ -dependence of the diagrams by using the model of magnetic impurities [Hikami *et al.*, 1980]: In contrast to the impurities discussed before, magnetic impurities can break the time-reversal symmetry of the system. They can be described by introducing a slightly reduced scattering rate for collisions in the particle-particle channel, since they depend on incoming and outgoing momenta of the electrons. Thus, we can effectively replace $1/\tau \rightarrow 1/\tau - \gamma_{\text{mi}}$ ($\gamma_{\text{mi}} \ll 1/\tau$ is the effective reduction of the scattering rate) for collisions in the particle-particle channel, and keep $1/\tau$ for collisions in the particle-hole channel. In the ballistic regularization scheme, we observe that the number of scattering events in the particle-particle channel is kept constant after moving the vertex, since we move a *diffuson dressed* external vertex, which keeps the direct of propagation invariant. Only the inner 4-point Hikami box of diagram (2g), cf. the discussion before Eq. (2.208), acquires a dependence on γ_{mi} , since it cannot be generated by moving the external vertex. Of course, γ_{mi} is different from the dephasing rate γ discussed in Section 2.2.5. But we can use γ_{mi} to “mark” all impurity ladders which are sensitive

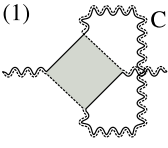
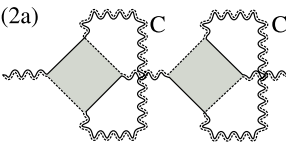
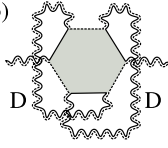
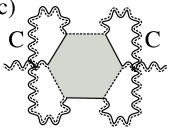
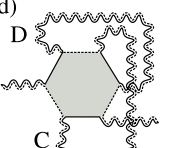
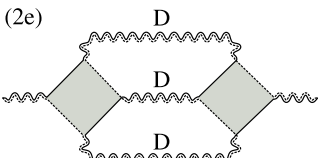
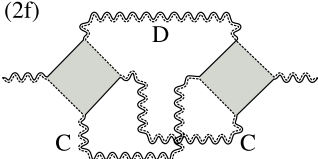
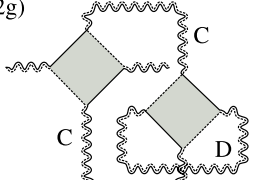
$\frac{1}{2\pi\rho} \frac{1}{(Dq^2 - i\omega)^2} \frac{1}{V} \times$	Dimensional regularization	Ballistic regularization
(1) 	$\sum_{\mathbf{Q}} \frac{1}{DQ^2 - i\omega} [2Dq^2]$	$\sum_{\mathbf{Q}} \frac{1}{DQ^2 - i\omega} [2Dq^2]$
(2a) 	$\frac{1}{Dq^2 - i\omega} \sum_{\mathbf{Q}_1, \mathbf{Q}_2} \frac{1}{DQ_1^2 - i\omega} \frac{1}{DQ_2^2 - i\omega} [(2Dq^2)^2]$	$\frac{1}{Dq^2 - i\omega} \sum_{\mathbf{Q}_1, \mathbf{Q}_2} \frac{1}{DQ_1^2 - i\omega} \frac{1}{DQ_2^2 - i\omega} [(2Dq^2)^2]$
(2b) 	$\sum_{\mathbf{Q}_1, \mathbf{Q}_2} \frac{1}{DQ_1^2 - i\omega} \frac{1}{DQ_2^2 - i\omega} [-4Dq^2 - 2i\omega]$	$\sum_{\mathbf{Q}_1, \mathbf{Q}_2} \frac{1}{DQ_1^2 - i\omega} \frac{1}{DQ_2^2 - i\omega} [-2Dq^2]$
(2c) 	$\sum_{\mathbf{Q}_1, \mathbf{Q}_2} \frac{1}{DQ_1^2 - i\omega} \frac{1}{DQ_2^2 - i\omega} [-4Dq^2 - 2i\omega]$	$\sum_{\mathbf{Q}_1, \mathbf{Q}_2} \frac{1}{DQ_1^2 - i\omega} \frac{1}{DQ_2^2 - i\omega} [-2Dq^2]$
(2d) 	$\sum_{\mathbf{Q}_1, \mathbf{Q}_2} \frac{1}{DQ_1^2 - i\omega} \frac{1}{DQ_2^2 - i\omega} [-8Dq^2 - 4i\omega]$	0
(2e) 	$\sum_{\mathbf{Q}_1, \mathbf{Q}_2} \frac{1}{DQ_1^2 - i\omega} \frac{1}{DQ_2^2 - i\omega} \times \left[2Dq^2 + 2i\omega + \frac{4D^2[\mathbf{q}(\mathbf{q} + \mathbf{Q}_1 + \mathbf{Q}_2)]^2}{D(\mathbf{q} + \mathbf{Q}_1 + \mathbf{Q}_2)^2 - i\omega} \right]$	$\sum_{\mathbf{Q}_1, \mathbf{Q}_2} \frac{1}{DQ_1^2 - i\omega} \frac{1}{DQ_2^2 - i\omega} \frac{1}{D(\mathbf{q} + \mathbf{Q}_1 + \mathbf{Q}_2)^2 - i\omega} \times [4D^2(\mathbf{q}(\mathbf{q} + \mathbf{Q}_1 + \mathbf{Q}_2))^2]$
(2f) 	$\sum_{\mathbf{Q}_1, \mathbf{Q}_2} \frac{1}{DQ_1^2 - i\omega} \frac{1}{DQ_2^2 - i\omega} \times \left[10Dq^2 + 2i\omega + \frac{8D^2(\mathbf{q}\mathbf{Q}_1)(\mathbf{q}\mathbf{Q}_2)}{D(\mathbf{q} + \mathbf{Q}_1 + \mathbf{Q}_2)^2 - i\omega} \right]$	$\sum_{\mathbf{Q}_1, \mathbf{Q}_2} \frac{1}{DQ_1^2 - i\omega} \frac{1}{DQ_2^2 - i\omega} \frac{1}{D(\mathbf{q} + \mathbf{Q}_1 + \mathbf{Q}_2)^2 - i\omega} \times [8D^2(\mathbf{q}\mathbf{Q}_1)(\mathbf{q}\mathbf{Q}_2)]$
(2g) 	$\sum_{\mathbf{Q}_1, \mathbf{Q}_2} \frac{1}{DQ_1^2 - i\omega} \frac{1}{DQ_2^2 - i\omega} \left[4Dq^2 + 4i\omega + \frac{4i\omega Dq^2}{DQ_1^2 - i\omega} \right]$	$\sum_{\mathbf{Q}_1, \mathbf{Q}_2} \frac{1}{(DQ_1^2 - i\omega)^2} \frac{1}{DQ_2^2 - i\omega} [4(Dq^2)(DQ_1^2)]$

Figure 2.31: Overview and comparison of our results.

to time-reversal symmetry. After rearranging the terms, and substituting $D\mathbf{Q}_{1,2}^2 \rightarrow D\mathbf{Q}_{1,2}^2 + \gamma$ in all impurity ladders which contain γ_{mi} , we obtain:

$$\begin{aligned} \delta P(\mathbf{q}, \omega) = \frac{1}{2\pi\rho} \frac{2D\mathbf{q}^2}{(D\mathbf{q}^2 - i\omega)^2} \frac{1}{V} \sum_{\mathbf{Q}_1, \mathbf{Q}_2} & \left(P_d(\mathbf{Q}_1, \omega) P_d(\mathbf{Q}_2, \omega) \left[\frac{2D[\mathbf{q}(\mathbf{q} + \mathbf{Q}_1 + \mathbf{Q}_2)]^2 / \mathbf{q}^2}{D(\mathbf{q} + \mathbf{Q}_1 + \mathbf{Q}_2)^2 - i\omega} - 1 \right] \right. \\ & + P_c(\mathbf{Q}_1, \omega) P_c(\mathbf{Q}_2, \omega) \left[\frac{D\mathbf{q}^2 + i\omega}{D\mathbf{q}^2 - i\omega} + \frac{4D(\mathbf{q}\mathbf{Q}_1)(\mathbf{q}\mathbf{Q}_2) / D\mathbf{q}^2}{D(\mathbf{q} + \mathbf{Q}_1 + \mathbf{Q}_2)^2 - i\omega} \right] \\ & \left. + P_c(\mathbf{Q}_1, \omega) P_d(\mathbf{Q}_2, \omega) [2 + 2i\omega P_c(\mathbf{Q}_1, \omega)] \right). \end{aligned} \quad (2.212)$$

Only the Cooperon propagators, P_c , in Eq. (2.212) acquire a dependence on γ .

2.4 Publication: Thermal noise and dephasing due to electron interactions in nontrivial geometries

The following 8 pages have been published in the journal *Physical Review B*.

PHYSICAL REVIEW B **84**, 054204 (2011)**Thermal noise and dephasing due to electron interactions in nontrivial geometries**M. Treiber,¹ C. Texier,² O. M. Yevtushenko,¹ J. von Delft,¹ and I. V. Lerner³¹*Ludwig Maximilians University, Arnold Sommerfeld Center and Center for Nano-Science, Munich, DE-80333, Germany*²*Univ. Paris Sud, CNRS, LPTMS, UMR 8626 & LPS, UMR 8502, Orsay FR-91405, France*³*School of Physics and Astronomy, University of Birmingham, Birmingham, B15 2TT, United Kingdom*

(Received 5 May 2011; published 5 August 2011)

We study Johnson-Nyquist noise in macroscopically inhomogeneous disordered metals and give a microscopic derivation of the correlation function of the scalar electric potentials in real space. Starting from the interacting Hamiltonian for electrons in a metal and the random phase approximation, we find a relation between the correlation function of the electric potentials and the density fluctuations, which is valid for arbitrary geometry and dimensionality. We show that the potential fluctuations are proportional to the solution of the diffusion equation, taken at zero frequency. As an example, we consider networks of quasi-one-dimensional disordered wires and give an explicit expression for the correlation function in a ring attached via arms to absorbing leads. We use this result in order to develop a theory of dephasing by electronic noise in multiply-connected systems.

DOI: 10.1103/PhysRevB.84.054204

PACS number(s): 07.50.Hp, 42.50.Lc, 73.63.-b

I. INTRODUCTION

Electronic noise generated by the thermal excitation of charge carriers has been observed and explained by Johnson and Nyquist more than 80 years ago¹ and discussed in great detail in the literature since then. More recently, it has been found that this so-called Johnson-Nyquist noise is the main source of dephasing in mesoscopic systems at low temperatures of a few Kelvins where phonons are frozen out. Dephasing puts an IR cut-off for interference phenomena, such as quantum corrections to the classical conductivity.²

The current interest in this topic arises from studies of dephasing in mesoscopic systems which consist of connected quasi-one-dimensional (1D) disordered wires, see Fig. 1, including connected rings and grids.^{3,4} It has been found (both experimentally⁵ and theoretically⁶⁻¹⁰) that dephasing depends not only on the dimensionality, but also on the geometry of the system. The noise correlation function is well-understood for macroscopically homogeneous systems such as infinite wires or isolated rings, but has so far not been studied in multiply-connected networks with leads attached at arbitrary points. The goal of this paper is to give a transparent and systematic description of the thermal noise properties for such systems. In particular, we will derive an expression for the fluctuations of the scalar electric potentials for arbitrary geometries, Eq. (31), and a general expression for the corresponding dephasing rate, Eq. (45). Throughout, we assume that a description of the noise in terms of scalar potentials is sufficient, i.e., we neglect the fluctuations of the transverse component of the electromagnetic field (for a detailed discussion of the latter, see Ref. 2).

Let us start by reviewing simplified arguments to derive the noise correlation function: Johnson and Nyquist concluded that thermal noise in electrical conductors is approximately white, meaning that the power spectral density is nearly constant throughout the whole frequency spectrum. If, in addition, the fluctuations are uncorrelated for different points in space, a correlation function for the random thermal currents in the classical limit is independent of frequency ω and momentum \mathbf{q} . The power spectrum of the current density reads

$$\langle |\mathbf{j}|^2 \rangle(\mathbf{q}, \omega) = 2T\sigma_0. \quad (1)$$

Here, $\sigma_0 = e^2\nu D$ is the Drude conductivity of the disordered system, D and ν are the diffusion constant and the density of states, respectively. Naively applying Ohm's law, $\mathbf{j}(\mathbf{q}) = \sigma_0\mathbf{E}(\mathbf{q})$, to Eq. (1) and using the relation between the electric field and the scalar potential, $e\mathbf{E}(\mathbf{q}) = -i\mathbf{q}V(\mathbf{q})$, we find

$$\langle |V|^2 \rangle(\mathbf{q}, \omega) = \frac{2Te^2}{\sigma_0} \frac{1}{q^2}. \quad (2)$$

The correlation function, Eq. (2), corresponds to the coupling of a given electron to the bath of the surrounding electrons.² Thus $\langle |V|^2 \rangle$ describes the process of successive emission and reabsorption of a photon, which is described effectively by the scalar potential V . The factor $1/q^2$ coincides with the solution of a diffusion equation in an infinite system, which reflects the fact that the currents, Eq. (1), are uncorrelated in space.

These simple arguments are based on the homogeneity of the system and have assumed a local relation between potential and current, whereas transport properties in disordered metals are substantially nonlocal.¹⁰⁻¹³ In this paper, we derive an analogy of Eq. (2) for disordered systems with arbitrary geometry and dimensionality; this will in particular apply to networks of disordered wires. A detailed calculation, which takes into account all properties of the mesoscopic samples, has to be done in the real-space representation. Starting points are the usual linear response formalism and the fluctuation-dissipation theorem (FDT).¹⁴ Although most ingredients of the following discussion will be familiar to experts, we hope that the manner in which they have been assembled here will be found not only to be pedagogically useful, but also helpful for further theoretical studies.

The paper is organized as follows: in Sec. II, we propose a heuristic description of the potential fluctuations. In Sec. III, we review a microscopic approach to the noise correlation function, based on a relation of the fluctuations of the scalar potentials to the fluctuations of the density, using the random phase approximation (RPA). In Sec. IV, we evaluate the density response function χ for disordered systems by using a real-space representation for arbitrary geometries. We apply this result to the noise correlation function in Sec. V. In Sec. VI, we show how the noise correlation function can be calculated for networks of disordered wires. Finally, in Sec. VII, we

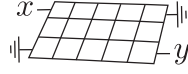
M. TREIBER *et al.*PHYSICAL REVIEW B **84**, 054204 (2011)

FIG. 1. A network of wires. We are interested in the noise correlations between arbitrary points \mathbf{x} and \mathbf{y} of multiply-connected networks attached to leads (denoted by the usual ground symbol) at arbitrary points.

discuss the relation to the fundamental problem of dephasing by electronic interactions.

II. HEURISTIC DESCRIPTION OF POTENTIAL FLUCTUATIONS

A description of fluctuations in metals within the linear response formalism naturally starts with an analysis of the density fluctuations in the model of noninteracting electrons described by the standard free-electron Hamiltonian $\hat{H}^{(0)}$. This system is perturbed by an external scalar potential $V(\mathbf{x}, t)$ coupled to the density operator $\hat{n}(\mathbf{x})$:

$$\hat{H}^{(1)} = \int d\mathbf{x} V(\mathbf{x}, t) \hat{n}(\mathbf{x}). \quad (3)$$

The response of the (induced) charge density,

$$\begin{aligned} n_{\text{ind}}(\mathbf{x}, \omega) &\equiv \int_{-\infty}^{\infty} dt e^{i\omega t} [\langle \hat{n}(\mathbf{x}, t) \rangle_{\text{pert}} - \langle \hat{n}(\mathbf{x}) \rangle] \\ &= - \int d\mathbf{y} \chi(\mathbf{x}, \mathbf{y}, \omega) V(\mathbf{y}, \omega), \end{aligned} \quad (4)$$

is governed by the (retarded) density response function:

$$\chi(\mathbf{x}, \mathbf{y}, \omega) = i \int_0^{\infty} dt e^{i(\omega+i0)t} \langle [\hat{n}(\mathbf{x}, t), \hat{n}(\mathbf{y}, 0)] \rangle. \quad (5)$$

Here, $\langle \dots \rangle_{\text{pert}}$ and $\langle \dots \rangle$ denote quantum/statistical averaging with respect to the perturbed and unperturbed Hamiltonian, respectively. The FDT relates the equilibrium density fluctuations to the imaginary (dissipative) part of the response function,

$$\begin{aligned} \langle |n|^2 \rangle(\mathbf{x}, \mathbf{y}, \omega) &\equiv \int_{-\infty}^{\infty} dt e^{i\omega t} \langle \hat{n}(\mathbf{x}, t) \hat{n}(\mathbf{y}, 0) \rangle \\ &= F(\omega) \text{Im}[\chi(\mathbf{x}, \mathbf{y}, \omega)], \end{aligned} \quad (6)$$

where

$$F(\omega) = \frac{2}{1 - e^{-\omega/T}}. \quad (8)$$

In writing Eqs. (6)–(8), we have exploited detailed balance and time-reversal symmetry. The latter implies $\chi(\mathbf{x}, \mathbf{y}, \omega) = \chi(\mathbf{y}, \mathbf{x}, \omega)$.¹⁴

The question, which we are going to address in this paper, is how to characterize the fluctuations of the electric potential V . For this purpose we consider the “dual” case, where some external density $n_{\text{ext}}(\mathbf{x}, t)$ is the perturbation that couples to the “potential operator” \hat{V} .¹⁵

$$\hat{H}^{(2)} = \int d\mathbf{x} \hat{V}(\mathbf{x}) n_{\text{ext}}(\mathbf{x}, t). \quad (9)$$

The linear response of \hat{V} to the perturbation can be written as

$$\langle \hat{V}(\mathbf{x}, \omega) \rangle_{\text{pert}} = \int d\mathbf{y} \Upsilon(\mathbf{x}, \mathbf{y}, \omega) n_{\text{ext}}(\mathbf{y}, \omega), \quad (10)$$

defining the response function Υ . In analogy to Eq. (7), the response function also characterizes the equilibrium fluctuations of the potential:¹⁶

$$\langle |V|^2 \rangle(\mathbf{x}, \mathbf{y}, \omega) = F(\omega) \text{Im}[-\Upsilon(\mathbf{x}, \mathbf{y}, \omega)]. \quad (11)$$

Calculating the response function $\Upsilon(\mathbf{x}, \mathbf{y}, \omega)$ is a complicated task because it requires precise knowledge of the potential operator $\hat{V}(\mathbf{x})$. Instead, we can identify the potential $V(\mathbf{x}, \omega)$ in Eq. (4) with the response $\langle \hat{V}(\mathbf{x}, \omega) \rangle_{\text{pert}}$ in Eq. (10) to relate Υ to χ : in the limit of strong screening in good conductors (called the unitary limit⁹), electroneutrality is satisfied locally. Therefore, the induced charge exactly compensates the external charge: $n_{\text{ind}}(\mathbf{x}, \omega) = -n_{\text{ext}}(\mathbf{x}, \omega)$. Now inserting Eq. (4) into Eq. (10) (or vice versa), we obtain

$$\int d\mathbf{x}' \Upsilon(\mathbf{x}, \mathbf{x}', \omega) \chi(\mathbf{x}', \mathbf{y}, \omega) = \delta(\mathbf{x} - \mathbf{y}). \quad (12)$$

If χ is known, Eqs. (11) and (12) allow one to calculate the correlation function of the scalar potential.

Let us recall the well-known case of macroscopically homogeneous diffusive systems. The expression for the disordered averaged response function $\bar{\chi}$ reads^{17,18}

$$\bar{\chi}(\mathbf{q}, \omega) = v \frac{Dq^2}{Dq^2 - i\omega} = 1/\Upsilon(\mathbf{q}, \omega), \quad (13)$$

where we used Eq. (12). Inserting Eq. (13) into Eq. (11), we find

$$\langle |V|^2 \rangle(\mathbf{q}, \omega) = \frac{1}{v} \frac{\omega F(\omega)}{Dq^2}, \quad (14)$$

which reduces to Eq. (2) in the limit $\omega \ll T$.

III. NOISE CORRELATION FUNCTION FOR ARBITRARY GEOMETRIES: MICROSCOPIC APPROACH

In Eqs. (3) and (9), we introduced the operators \hat{n} and \hat{V} assuming that either $V(\mathbf{x}, t)$ or $n_{\text{ext}}(\mathbf{x}, t)$ are external perturbations. In fact, the fluctuations originate inside of the system and the starting point of a microscopic description is the part of the Hamiltonian, which describes electron interactions,

$$\hat{H}_{\text{int}} = \int d\mathbf{x} d\mathbf{y} U_0(\mathbf{x}, \mathbf{y}) \hat{\psi}^\dagger(\mathbf{x}) \hat{\psi}^\dagger(\mathbf{y}) \hat{\psi}(\mathbf{y}) \hat{\psi}(\mathbf{x}), \quad (15)$$

where $U_0(\mathbf{x}, \mathbf{y})$ is the bare Coulomb interaction. In the mean-field approximation, Eq. (15) gives rise to a correction, called Hartree contribution, to the electron energy:

$$\Delta E^{(\text{Hartree})} \approx \int d\mathbf{x} d\mathbf{y} U_0(\mathbf{x}, \mathbf{y}) \langle \hat{n}(\mathbf{x}) \rangle \langle \hat{n}(\mathbf{y}) \rangle, \quad (16)$$

where $\hat{n}(\mathbf{x}) = \hat{\psi}^\dagger(\mathbf{x}) \hat{\psi}(\mathbf{x})$.

The Coulomb interactions are dynamically screened, which can be accounted for in the framework of the RPA, provided that the electron density is high,

$$\begin{aligned} U_{\text{RPA}}(\mathbf{x}, \mathbf{y}, \omega) &= U_0(\mathbf{x}, \mathbf{y}) - \int d\mathbf{x}' d\mathbf{y}' U_0(\mathbf{x}, \mathbf{x}') \chi(\mathbf{x}', \mathbf{y}', \omega) \\ &\quad \times U_{\text{RPA}}(\mathbf{y}', \mathbf{y}, \omega), \end{aligned} \quad (17)$$

see Fig. 2. Note that $-\chi$ [see the definition in Eq. (5)] is equal to the bubble diagrams of Fig. 2, see e.g., Ref. 18. In

M. TREIBER *et al.*

PHYSICAL REVIEW B **84**, 054204 (2011)

where $D = v_F \ell / d$ is the diffusion constant for a d dimensional system. Thus, the vertex function is proportional to the diffusion propagator, $\Gamma(\mathbf{x}, \mathbf{y}, \omega) = P(\mathbf{x}, \mathbf{y}, \omega) / \tau$.

Collecting the short- and long-range contributions and taking the limit $T \ll \epsilon_F$, we obtain from Eq. (21)

$$\bar{\chi}(\mathbf{x}, \mathbf{y}, \omega) = v (\delta(\mathbf{x} - \mathbf{y}) + i\omega P(\mathbf{x}, \mathbf{y}, \omega)). \quad (25)$$

Equation (25) is valid for arbitrary geometries since it is based only on the diffusive approximation and does not require macroscopic homogeneity.

V. NOISE CORRELATION FUNCTION IN DISORDERED SYSTEMS

Let us simplify Eq. (17) for a disordered conductor. Using Eq. (25) and

$$-\frac{1}{4\pi e^2} \Delta_{\mathbf{x}} U_0(\mathbf{x}, \mathbf{x}') = \delta(\mathbf{x} - \mathbf{x}'), \quad (26)$$

Eq. (17) can be written as

$$\left(1 - \frac{\Delta_{\mathbf{x}}}{\kappa^2}\right) U_{\text{RPA}}(\mathbf{x}, \mathbf{y}, \omega) + i\omega \int d\mathbf{x}' P(\mathbf{x}, \mathbf{x}', \omega) \times U_{\text{RPA}}(\mathbf{x}', \mathbf{y}, \omega) = \frac{1}{v} \delta(\mathbf{x} - \mathbf{y}), \quad (27)$$

where we introduced the Thomas-Fermi screening wave vector $\kappa = \sqrt{4\pi e^2 v}$, which corresponds to the inverse screening length in three dimensional (3D) bulk systems. The kernel of Eq. (27) is a solution to the diffusion equation (24), which can be expanded in terms of eigenfunctions of the Laplace operator. Consequently, the kernel is always separable and Eq. (27) has a unique solution (see, e.g., Ref. 19 for details on how the solution can be found). Using the semigroup property of the diffusion propagators,

$$\int d\mathbf{x}' P(\mathbf{x}, \mathbf{x}', \omega) P(\mathbf{x}', \mathbf{y}, 0) = \frac{i}{\omega} [P(\mathbf{x}, \mathbf{y}, 0) - P(\mathbf{x}, \mathbf{y}, \omega)],$$

one can check that

$$U_{\text{RPA}}(\mathbf{x}, \mathbf{y}, \omega) = \frac{1}{v} \left(\frac{1}{-D\Delta_{\mathbf{x}} - i\omega} + \frac{1}{D\kappa^2} \right)^{-1} P(\mathbf{x}, \mathbf{y}, 0) \quad (28)$$

satisfies Eq. (27). In practice, the 3D Thomas-Fermi screening length κ^{-1} is a microscopic scale, thus the typical value of the first term of the right-hand side of Eq. (28), $(Dq_{\text{typ}}^2 - i\omega_{\text{typ}})^{-1}$, is larger than $1/D\kappa^2 = 1/4\pi\sigma_0$ for good conductors (this is the so-called unitary limit, for details see Ref. 9):

$$\frac{1}{|Dq_{\text{typ}}^2 - i\omega_{\text{typ}}|} \gg \frac{1}{D\kappa^2}. \quad (29)$$

In this limit, using the diffusion Eq. (24), we obtain from Eq. (28):

$$U_{\text{RPA}}(\mathbf{x}, \mathbf{y}, \omega) = \frac{1}{v} [\delta(\mathbf{x} - \mathbf{y}) - i\omega P(\mathbf{x}, \mathbf{y}, 0)]. \quad (30)$$

We remind that $P(\mathbf{x}, \mathbf{y}, 0)$ is always real. As a result, Eqs. (20) and (30) yield

$$\langle |V|^2 \rangle(\mathbf{x}, \mathbf{y}, \omega) = \frac{1}{v} \omega F(\omega) P(\mathbf{x}, \mathbf{y}, 0), \quad (31)$$

where $F(\omega)$ is given by Eq. (8). The real-space demonstration of Eqs. (30) and (31) for macroscopically inhomogeneous systems, are among the main results of the paper. It is worth emphasizing the frequency-space factorization of the correlator, which plays an important role in the theory of dephasing, cf. Sec. VII. The relation of Eq. (31) to the correlation function of the currents, Eq. (1), is discussed in Appendix B, and allows to put the presentation of the introduction on firm ground.

Note that Eq. (29) allows one to neglect the term $\Delta_{\mathbf{x}}/\kappa^2$ in Eq. (27) and thus reduce Eq. (27) to the form of the phenomenological integral equation (12), with U_{RPA} taking the place of Υ . [The same replacement leads from Eq. (11) to Eq. (20).] In other words, the electric potential of the fluctuating charge densities itself is negligible when screening is strong enough (i.e., good conductors in the unitary limit), justifying *a posteriori* our assumptions in the phenomenological Sec. II.

The fact that the correlation function of the potential is proportional to the solution of the diffusion equation at zero frequency, cf. Eq. (31), may be understood as a nonlocal version of the Johnson-Nyquist theorem, since $P(\mathbf{x}, \mathbf{y}, 0)$ can be related to the classical dc resistance $\mathcal{R}(\mathbf{x}, \mathbf{y})$ between the points \mathbf{x} and \mathbf{y} (see Ref. 20):

$$\mathcal{R}(\mathbf{x}, \mathbf{y}) = \frac{2D}{\sigma_0} \left\{ \frac{1}{2} [P(\mathbf{x}, \mathbf{x}, 0) + P(\mathbf{y}, \mathbf{y}, 0)] - P(\mathbf{x}, \mathbf{y}, 0) \right\}. \quad (32)$$

For example, in an infinitely long quasi-1D wire of cross section s , the solution of the diffusion equation is $P(\mathbf{x}, \mathbf{y}, 0) = -|x - y|/(Ds)$, where x is the component of \mathbf{x} along the wire. Hence, we recover a resistance proportional to the distance between the points, $\mathcal{R}(\mathbf{x}, \mathbf{y}) = |x - y|/(s\sigma_0)$.

VI. NOISE CORRELATION FUNCTION IN NETWORKS OF DISORDERED WIRES

Let us now illustrate the calculation of the noise correlation function, Eq. (31), for a network of disordered wires. The main ingredient to Eq. (31) is the solution of the diffusion equation (24) at zero frequency. Wires allow a quasi-1D description of diffusion, where transverse directions can be integrated out since $P(\mathbf{x}, \mathbf{y}, \omega)$ is assumed to be constant on the scale of the width of the wire. As a result, we replace $P(\mathbf{x}, \mathbf{y}, \omega) \rightarrow P(x, y, \omega)/s$, where s is the cross section of the wires and $P(x, y, \omega)$ solves the 1D diffusion equation in the network, x and y being coordinates along the wires. Recently, effective methods have been developed to solve the resulting diffusion equation for arbitrary networks.^{10,20-22} We

THERMAL NOISE AND DEPHASING DUE TO ELECTRON . . .

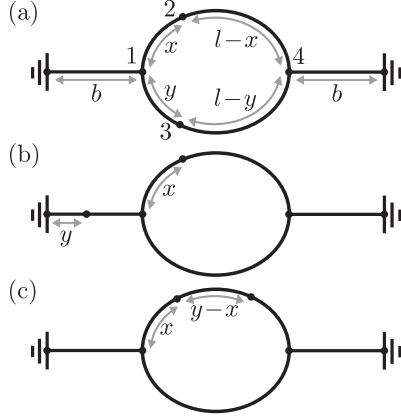
PHYSICAL REVIEW B **84**, 054204 (2011)

FIG. 5. The network corresponding to a symmetric ring made of four wires connected to two absorbing leads. The length of the arcs is l and the length of the connecting arms is b . Vertices are labeled by numbers $\alpha = 1, 2, 3$, and 4. Vertices “1” and “4” denote the points where the ring is connected to the arms. Vertex “2” is always placed in the upper arc, defining the running coordinate x . Vertex “3” determines the y coordinate and is placed either in the adjacent arc (panel a) or in the left arc (panel b) or in the same arc (panel c).

will review these methods in this section and evaluate the noise correlation function for a simple example.

We start by introducing some basic notations: a network is a set of vertices, labeled by an index α , connected via wires of arbitrary length, say $l_{\alpha\beta}$ for the wire connecting vertices α and β . Let us define a vertex matrix \mathcal{M} as

$$\mathcal{M}_{\alpha\beta} = \delta_{\alpha\beta} \sum_{\gamma} \frac{a_{\alpha\gamma}}{l_{\alpha\gamma}} - \frac{a_{\alpha\beta}}{l_{\alpha\beta}}, \quad (33)$$

where $a_{\alpha\beta} = 1$ if the vertices α and β are connected and $a_{\alpha\beta} = 0$ otherwise. The solution of the diffusion equation at zero frequency between arbitrary vertices α and β of the network is given by the entries of the inverse matrix \mathcal{M} divided by the diffusion constant:

$$P(\alpha, \beta, 0) = (\mathcal{M}^{-1})_{\alpha\beta} / D. \quad (34)$$

This allows us to calculate the noise correlation function between arbitrary points of a network by inserting vertices and inverting \mathcal{M} . As an aside, note that arbitrary boundary conditions can be included in this scheme easily (see Refs. 22 and 20 for details).

Let us consider the network shown in Fig. 5, representing a ring connected to absorbing leads. For simplicity, we assumed that the ring is symmetric: the two arcs are of the same length l and the connecting arms of length b . We evaluate the noise correlation function for two points in this network by inserting two vertices, called “2” and “3”. Vertex 2 is always placed in the upper arc, encoding the running coordinate x in the length of the connected wires. Vertex 3 determines the y coordinate and is placed either in the lower arc or in the left connecting

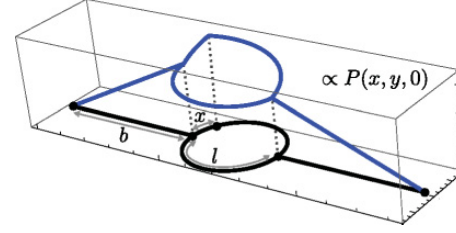


FIG. 6. (Color online) The solution to the diffusion equation at zero frequency, $P(x, y, 0) \propto \langle |V|^2 \rangle(x, y, \omega)$, where $\langle |V|^2 \rangle$ is given by Eqs. (36)–(38), for a fixed coordinate x in the upper arm of the ring (indicated by the dot), as a function of y traversing the network. $\langle |V|^2 \rangle(x, y, \omega)$ is linear in y and its derivative has a discontinuity at $y = x$.

arm or in the upper arc. In the first case, Fig. 5(a), the vertex matrix, Eq. (33), is given by

$$\mathcal{M} = \begin{pmatrix} \frac{1}{b} + \frac{1}{x} + \frac{1}{y} & -\frac{1}{x} & -\frac{1}{y} & 0 \\ -\frac{1}{x} & \frac{1}{x} + \frac{1}{l-x} & 0 & -\frac{1}{l-x} \\ -\frac{1}{y} & 0 & \frac{1}{y} + \frac{1}{l-y} & -\frac{1}{l-y} \\ 0 & -\frac{1}{l-x} & -\frac{1}{l-y} & \frac{1}{b} + \frac{1}{l-x} + \frac{1}{l-y} \end{pmatrix}. \quad (35)$$

The diffusion propagator is then given by $P(x, y, 0) = (\mathcal{M}^{-1})_{23} / D$, and we obtain from Eq. (31) the correlation function as a function of the running coordinates $x, y \in [0, l]$:

$$\langle |V|^2 \rangle(x, y, \omega) = \frac{\omega F(\omega) b(l(2b+l) - (x+y)l + 2xy)}{Dvs l(4b+l)}. \quad (36)$$

When vertex 3 is placed in the connecting arm, $x \in [0, l]$ and $y \in [0, b]$ [Fig. 5(b)], we get

$$\langle |V|^2 \rangle(x, y, \omega) = \frac{\omega F(\omega) y(2b+l-x)}{Dvs 4b+l}. \quad (37)$$

Finally, when vertex 3 is placed in the same arc of the ring as vertex 2 [see Fig. 5(c)], following the same logic we obtain, with $0 < x < y < l$,

$$\langle |V|^2 \rangle(x, y, \omega) = \frac{\omega F(\omega) bl(2b+l) + xl(3b+l) - ybl - xy(2b+l)}{Dvs l(4b+l)}. \quad (38)$$

All other configurations can be found by symmetry arguments. We plot $P(x, y, 0)$ for y traversing the whole network in Fig. 6. Note that the resulting function is linear in y and its derivative has a discontinuity at $y = x$ (cf. Ref. 7).

VII. APPLICATION TO DEPHASING

The precise characterization of potential fluctuations is very important in studying phase coherent properties of disordered metals at low temperatures. To be specific, let us discuss a particular coherent property: the weak localization correction to the conductivity. Let us recall that the weak localization (WL) correction $\Delta\sigma \equiv \bar{\sigma} - \sigma_0$ is a small contribution to the

M. TREIBER *et al.*PHYSICAL REVIEW B **84**, 054204 (2011)

averaged conductivity arising from quantum interference of reversed diffusive electronic trajectories.²³

At low temperatures, dephasing is dominated by electron interactions, that can be accounted for through a contribution to the phase accumulated by two time-reversed interfering trajectories in a fluctuating electric field²:

$$\Phi[\mathbf{x}(\tau)] = \int_0^t dt [V(\mathbf{x}(\tau), \tau) - V(\mathbf{x}(\tau), t - \tau)]. \quad (39)$$

When averaged over the Gaussian fluctuations of the electric field, $\langle e^{i\Phi} \rangle_V = e^{-\frac{1}{2}\langle \Phi^2 \rangle_V}$ yields a phase difference that cuts off the contributions of long electronic trajectories. Introducing the trajectory-dependent dephasing rate $\Gamma[\mathbf{x}(\tau)] = \frac{1}{2T} \langle \Phi[\mathbf{x}(\tau)]^2 \rangle_V$, the weak localization correction takes the form:^{7,20,24,25}

$$\Delta\sigma(\mathbf{x}) = -\frac{2e^2 D}{\pi} \int_0^\infty dt P(\mathbf{x}, \mathbf{x}, t) \langle e^{-t\Gamma[\mathbf{x}(\tau)]} \rangle_{\{\mathbf{x}(\tau)\}}, \quad (40)$$

where $\langle \dots \rangle_{\{\mathbf{x}(\tau)\}}$ is the average with respect to closed diffusive trajectories of duration t starting from \mathbf{x} (not to be confused with the thermal average $\langle \dots \rangle_V$ over the electric potential V). The phase fluctuations can then be related to the potential fluctuations:

$$\frac{1}{2} \langle \Phi[\mathbf{x}]^2 \rangle = \int_0^t d\tau d\tau' \int_{-\infty}^\infty \frac{d\omega}{2\pi} [e^{-i\omega(\tau-\tau')} - e^{-i\omega(\tau+\tau'-t)}] \times \langle |V|^2 \rangle_\varphi(\mathbf{x}(\tau), \mathbf{x}(\tau'), \omega). \quad (41)$$

Here, we have introduced a new noise correlator,

$$\langle |V|^2 \rangle_\varphi(\mathbf{x}, \mathbf{y}, \omega) = \frac{1}{v} \omega F_\varphi(\omega) P(\mathbf{x}, \mathbf{y}, 0), \quad (42)$$

obtained from Eq. (31) by replacing $F(\omega)$ with a modified function $F_\varphi(\omega)$ (given below), on the origin of which we now comment. Equation (20) is well-known in the theory of dephasing: its version symmetrized with respect to frequency arises naturally when comparing the diagrammatic calculation of the dephasing time^{26,27} with the influence functional approach describing electrons moving in a random Gaussian field V .^{24,28,29} Diagrammatically, the symmetrized Eq. (20) represents the Keldysh component of the screened-electron-interaction propagator, the only substantial difference being that the diagrammatically calculated correlation function involved in the dephasing process acquires so-called Pauli factors that account for the fact that the Fermi sea limits the phase space available for inelastic transitions.²⁸ These factors lead to the following replacement of the function $F(\omega)$ in Eq. (20) and also in Eq. (31):

$$F(\omega) \xrightarrow{\text{sym}} \coth(\omega/2T) \xrightarrow{\text{Pauli}} \frac{\omega/2T}{\sinh^2(\omega/2T)} \equiv F_\varphi(\omega). \quad (43)$$

This restricts the energy transfer to $|\omega| < T$,^{24,27} but does not affect the factorization of the correlator. Inserting Eq. (42) into Eq. (41) leads to

$$\frac{1}{2} \langle \Phi[\mathbf{x}]^2 \rangle = \frac{2T}{v} \int_0^t d\tau d\tau' P(\mathbf{x}(\tau), \mathbf{x}(\tau'), 0) \int_{-\infty}^\infty \frac{d\omega}{2\pi} \times [e^{-i\omega(\tau-\tau')} - e^{-i\omega(\tau+\tau'-t)}] \frac{\omega}{2T} F_\varphi(\omega). \quad (44)$$

The fact that the frequency dependent function $\frac{\omega}{2T} F_\varphi(\omega)$ is symmetric allows us to add to $P(\mathbf{x}(\tau), \mathbf{x}(\tau'), 0)$ the term

$-\frac{1}{2}[P(\mathbf{x}(\tau), \mathbf{x}(\tau), 0) + P(\mathbf{x}(\tau'), \mathbf{x}(\tau'), 0)]$, which does not contribute to the integral (44). Therefore, we finally end up with the following expression for the dephasing rate,

$$\Gamma[\mathbf{x}(\tau)] = e^2 T \int_0^t \frac{d\tau}{t} \int_0^t d\tau' [\delta_T(\tau + \tau' - t) - \delta_T(\tau - \tau')] \times \mathcal{R}(\mathbf{x}(\tau), \mathbf{x}(\tau')), \quad (45)$$

written in terms of the resistance \mathcal{R} , defined in Eq. (32). The function $\delta_T(t)$, a broadened delta function of width $1/T$ and height T , is the Fourier transform of $\frac{\omega}{2T} F_\varphi(\omega)$, which is given by

$$\delta_T(\tau) = \pi T w(\pi T \tau), \quad w(y) = \frac{y \coth y - 1}{\sinh^2 y}. \quad (46)$$

Equation (45), which is one of the main results of our paper, generalizes the results obtained in Refs. 8,9,24, and 28 for an infinite wire and an isolated ring to arbitrary geometry. In the classical noise limit $T \rightarrow \infty$, $\delta_T(\tau)$ may be replaced by a $\delta(\tau)$ function: the second term of Eq. (45) vanishes and we recover the results of Refs. 7 and 20.

Let us now illustrate Eq. (45) by calculating the dephasing time for the well-understood case of one and two-dimensional isolated simply-connected samples. The dephasing time can be extracted from the condition

$$1 \equiv \Gamma(\tau_\varphi) \tau_\varphi, \quad (47)$$

where $\Gamma(t)$ is given by the functional Eq. (45), averaged over the typical closed random walks $\mathbf{x}(\tau)$ of duration t in the system. The problem is governed by the interplay of three time scales: the Thouless time $\tau_{\text{Th}} = L^2/D$, depending on the system size L , the thermal time $\tau_T = 1/T$ (related to the thermal length $L_T = \sqrt{D/T}$), and the dephasing time τ_φ .

(i) Diffusive regime, $\tau_T \ll \tau_\varphi \ll \tau_{\text{Th}}$ ($L_T \ll L_\varphi \ll L$): this is the regime considered in Refs. 2 and 25, where the width of the broadened delta functions in Eq. (45), τ_T , is the shortest time scale. Thus, when averaging over paths $\mathbf{x}(\tau)$, the characteristic length scale $|x - y|$ entering the resistance $\mathcal{R}(x, y)$ can be determined as follows: for the first δ_T term, this length is governed by free diffusion, since $|\mathbf{x}(\tau) - \mathbf{x}(t - \tau)| \sim \sqrt{D\tau}$, hence $|x - y| \sim \sqrt{D\tau}$. For the second term, the characteristic length is set by the width of the delta function, $|x - y| \sim \sqrt{D\tau_T}$. In 1D, where $\mathcal{R}(x, y) \sim |x - y|/\sigma_0 s$, the first term dominates and we immediately obtain from Eq. (47) $1/\tau_\varphi \sim (e^2 \sqrt{DT}/\sigma_0 s)^{2/3}$. In 2D, the diffuson at zero frequency is logarithmic as well as the resistance (32), $\mathcal{R}(x, y) \sim \ln(|x - y|/\sigma_0 d)$, where d is the width of the sample, which can be understood from the fact that the resistance of a plane connected at two corners scales logarithmically with the system size. Equation (47) gives $1 \sim e^2 T \tau_\varphi \ln(T \tau_\varphi)/\sigma_0 d$, and for the dephasing time, $1/\tau_\varphi \sim e^2 T \ln(e^2/\sigma_0 d)/\sigma_0 d$.

(ii) Ergodic regime, $\tau_T \ll \tau_{\text{Th}} \ll \tau_\varphi$ ($L_T \ll L \ll L_\varphi$): the width of $\delta_T(\tau)$ in Eq. (45) is still the shortest time scale but, in contrast to (i), the typical trajectories $\mathbf{x}(\tau)$ explore the whole system, setting the length scale of diffusion to the system size L , cf. Refs. 6 and 7. In full analogy to the diffusive regime, but replacing $\sqrt{D\tau}$ by L , we find for 1D, $1/\tau_\varphi \sim e^2 L T/\sigma_0 s$, and for 2D, $1/\tau_\varphi \sim e^2 T \ln(\tau_{\text{Th}}/\tau_T)/\sigma_0 d$.³⁰ These examples show that for nontrivial geometries, dephasing due to electron interactions cannot be accounted for through

a unique dephasing rate depending only on dimensionality, but must be described by a functional of the trajectories $\mathbf{x}(\tau)$ since the qualitative behavior of τ_φ follows from the geometry dependent typical distance $|\mathbf{x}(\tau) - \mathbf{x}(\tau')|$.

For sufficiently low temperatures, on the other hand, Eq. (45) is capable to describe the crossover to a 0D regime, where, apart from a dependence on the total system size, geometry becomes unimportant.

(iii) 0D regime, $\tau_{\text{Th}} \ll \tau_T \ll \tau_\varphi$ ($L \ll L_T \ll L_\varphi$): here, the width of the delta functions in Eq. (45), τ_T , is larger than τ_{Th} . Hence, the trajectories reach the ergodic limit $\mathbf{x}(\tau \geq \tau_{\text{Th}}) \sim L$ before the electric potential has significantly changed: dephasing is strongly reduced. Let us denote the maximal resistance reached at the ergodic limit as \mathcal{R}_{erg} and replace the resistance in Eq. (45) by $\mathcal{R} \rightarrow \mathcal{R} - \mathcal{R}_{\text{erg}}$, without changing the result, since \mathcal{R}_{erg} is constant and its contribution vanishes after integrating over τ and τ' . The difference $\mathcal{R} - \mathcal{R}_{\text{erg}}$ is nonzero only during time differences $\tau - \tau' \lesssim \tau_{\text{Th}}$ before reaching ergodicity. Thus the leading contribution comes from the second δ_T term in Eq. (45), which is constant at its maximum T during such short time scales. We find $1 \sim -e^2 T^2 \tau_\varphi \int_0^{\tau_{\text{Th}}} d\tau [\mathcal{R}(\mathbf{x}(\tau), 0) - \mathcal{R}_{\text{erg}}]$ and since the \mathcal{R}_{erg} term dominates, we obtain a dephasing time $1/\tau_\varphi \sim e^2 T^2 \tau_{\text{Th}} \mathcal{R}_{\text{erg}}$, independent of geometry and with the characteristic $\sim T^2$ behavior.³¹

VIII. CONCLUSIONS

In this paper, we have considered fluctuations of the scalar electric potentials in macroscopically inhomogeneous metals. We have shown how to relate the density fluctuations to the potential fluctuations, emphasizing the role of electronic interactions, provided a real space derivation of the density response function, and illustrated these general ideas for the case of networks of metallic wires. Finally, we have obtained a trajectory-dependent functional, Eq. (45), which describes dephasing by electron interactions for arbitrary geometries and accounts for the quantum noise contribution. When applied to networks, Eq. (45) can describe the full crossover from the 0D to the 1D and the 2D regime.

ACKNOWLEDGMENTS

We acknowledge illuminating discussions with F. Marquardt and support from the DFG through SFB TR-12 (O. Ye.), DE 730/8-1 (M. T.) and the Cluster of Excellence, Nanosystems Initiative, Munich.

APPENDIX A: SELF CONSISTENT ANALYSIS OF SCREENING

We recall here how to obtain Eq. (17) using a self-consistent treatment of screening in real space.³² Starting points are the following three equations: (i) the excess charge density is decomposed into external and induced contributions

$$\delta n(\mathbf{x}, \omega) = n_{\text{ext}}(\mathbf{x}, \omega) + n_{\text{ind}}(\mathbf{x}, \omega). \quad (\text{A1})$$

(ii) The induced charge is related to the potential $V(\mathbf{x}, \omega)$ by the density response function, cf. Eq. (4):

$$n_{\text{ind}}(\mathbf{x}, \omega) = - \int d\mathbf{y} \chi(\mathbf{x}, \mathbf{y}, \omega) V(\mathbf{y}, \omega). \quad (\text{A2})$$

(iii) The Poisson equation

$$\Delta V(\mathbf{x}, \omega) = -4\pi e^2 \delta n(\mathbf{x}, \omega). \quad (\text{A3})$$

Self-consistency lies in the fact that the response involves the screened potential $V(\mathbf{x}, \omega)$ and not the bare ‘‘external’’ potential related to $n_{\text{ext}}(\mathbf{x}, \omega)$. The screened effective interaction between electrons $U_{\text{RPA}}(\mathbf{x}, \mathbf{y}, \omega)$ is obtained by placing an external charge at \mathbf{y} , so that the external density is $n_{\text{ext}}(\mathbf{x}, \omega) = \delta(\mathbf{x} - \mathbf{y})$, and associating the resulting screened potential $V(\mathbf{x}, \omega)$ in Eq. (A3) with $U_{\text{RPA}}(\mathbf{x}, \mathbf{y}, \omega)$. We obtain

$$-\frac{1}{4\pi e^2} \Delta_x U_{\text{RPA}}(\mathbf{x}, \mathbf{y}, \omega) + \int d\mathbf{x}' \chi(\mathbf{x}, \mathbf{x}', \omega) U_{\text{RPA}}(\mathbf{x}', \mathbf{y}, \omega) = \delta(\mathbf{x} - \mathbf{y}). \quad (\text{A4})$$

Convolution with the Coulomb interaction gives Eq. (17).

APPENDIX B: CURRENT DENSITY CORRELATIONS

We discuss here the relation between the density and the current density correlations. The response of the (induced) current density is characterized by the conductivity tensor σ ,

$$\langle \hat{j}_\alpha(\mathbf{x}, \omega) \rangle_{\text{neq}} = \int d\mathbf{y} \sigma_{\alpha\beta}(\mathbf{x}, \mathbf{y}, \omega) E_\beta(\mathbf{y}, \omega), \quad (\text{B1})$$

which is related to Eq. (5) by current conservation:

$$\nabla_\alpha \nabla'_\beta \sigma_{\alpha\beta}(\mathbf{x}, \mathbf{x}', \omega) = -i\omega e^2 \chi(\mathbf{x}, \mathbf{x}', \omega). \quad (\text{B2})$$

The thermal fluctuations of the current density can be obtained from $\langle j_\alpha j_\beta^\dagger \rangle(\mathbf{x}, \mathbf{y}, \omega) = \omega F(\omega) \text{Re}[\sigma_{\alpha\beta}(\mathbf{x}, \mathbf{y}, \omega)]$, in analogy to the discussion in Sec. II, assuming time-reversal symmetry, $\sigma_{\alpha\beta}(\mathbf{x}, \mathbf{y}, \omega) = \sigma_{\beta\alpha}(\mathbf{y}, \mathbf{x}, \omega)$.

Let us now examine the case of disordered metals. The classical contribution to the averaged nonlocal dc conductivity has been derived in Ref. 12. Their result can be generalized straightforwardly to nonzero frequencies,

$$\overline{\sigma}_{\alpha\beta}(\mathbf{x}, \mathbf{x}', \omega) = \sigma_0 [\delta_{\alpha\beta} \delta(\mathbf{x} - \mathbf{x}') - D \nabla_\alpha \nabla'_\beta P(\mathbf{x}, \mathbf{x}', \omega)], \quad (\text{B3})$$

which obeys the condition (B2) with Eq. (25) substituted for χ . For the current correlations, we find³³

$$\overline{\langle j_\alpha j_\beta^\dagger \rangle}(\mathbf{x}, \mathbf{x}', \omega) = \sigma_0 \omega F(\omega) \{ \delta_{\alpha\beta} \delta(\mathbf{x} - \mathbf{x}') - D \nabla_\alpha \nabla'_\beta \text{Re}[P(\mathbf{x}, \mathbf{x}', \omega)] \}. \quad (\text{B4})$$

Since the diffuson $P(\mathbf{x}, \mathbf{x}', \omega)$ decays exponentially on a length scale $L_\omega = \sqrt{D/\omega}$, this expression shows that current correlations can be considered as purely local over the scale $\|\mathbf{x} - \mathbf{x}'\| \gg L_\omega$, i.e., $\overline{\langle |j|^2 \rangle}(\mathbf{x}, \mathbf{x}', \omega) \simeq \sigma_0 \omega F(\omega) \delta(\mathbf{x} - \mathbf{x}')$. In the limit of classical noise, $F(\omega) \omega \simeq 2T$, we recover precisely Eq. (1).

M. TREIBER *et al.*PHYSICAL REVIEW B **84**, 054204 (2011)

- ¹J. B. Johnson, *Phys. Rev.* **32**, 97 (1928); H. Nyquist, *ibid.* **32**, 110 (1928).
- ²B. L. Altshuler, A. G. Aronov, and D. E. Khmel'nitsky, *J. Phys. C* **15**, 7367 (1982).
- ³M. Ferrier, L. Angers, A. C. H. Rowe, S. Guéron, H. Bouchiat, C. Texier, G. Montambaux, and D. Mailly, *Phys. Rev. Lett.* **93**, 246804 (2004).
- ⁴F. Schopfer, F. Mallet, D. Mailly, C. Texier, G. Montambaux, C. Bäuerle, and L. Saminadayar, *Phys. Rev. Lett.* **98**, 026807 (2007).
- ⁵M. Ferrier, A. C. H. Rowe, S. Guéron, H. Bouchiat, C. Texier, and G. Montambaux, *Phys. Rev. Lett.* **100**, 146802 (2008).
- ⁶T. Ludwig and A. D. Mirlin, *Phys. Rev. B* **69**, 193306 (2004).
- ⁷C. Texier and G. Montambaux, *Phys. Rev. B* **72**, 115327 (2005).
- ⁸M. Treiber, O. M. Yevtushenko, F. Marquardt, J. von Delft, and I. V. Lerner, *Phys. Rev. B* **80**, 201305(R) (2009).
- ⁹M. Treiber, O. M. Yevtushenko, F. Marquardt, J. von Delft, and I. V. Lerner, in *Perspectives of Mesoscopic Physics: Dedicated to Yoseph Imry's 70th Birthday*, edited by A. Aharony, O. Entin-Wohlman (World Scientific, Singapore, 2010), Chap. 20.
- ¹⁰C. Texier and G. Montambaux, *Phys. Rev. Lett.* **92**, 186801 (2004).
- ¹¹A. Yu. Zyuzin and B. Z. Spivak, *Sov. Phys. JETP* **66**, 560 (1987); [*Zh. Eksp. Teor. Fiz.* **93**, 994 (1987)].
- ¹²C. L. Kane, R. A. Serota, and P. A. Lee, *Phys. Rev. B* **37**, 6701 (1988).
- ¹³I. V. Lerner, *Sov. Phys. JETP* **68**, 143 (1989) [*Zh. Eksp. Teor. Fiz.* **95**, 253 (1989)].
- ¹⁴L. D. Landau and E. M. Lifshitz, *Statistical Physics*, 3rd ed. (Butterworth-Heinemann, 1980), Vol. 5.
- ¹⁵In general, if the electromagnetic field is not quantized, as is the case here, the potential is not an operator; the assumption of a potential operator arises from electronic interactions that relate the internal electronic density operator to the electric potential.
- ¹⁶The different signs in Eqs. (7) and (11) reflect the different sign conventions in Eqs. (4) and (10).
- ¹⁷D. Vollhardt and P. Wölfle, *Phys. Rev. B* **22**, 4666 (1980).
- ¹⁸E. Akkermans and G. Montambaux, *Mesoscopic Physics of Electrons and Photons* (Cambridge University Press, Cambridge, 2007).
- ¹⁹R. P. Kanwal, *Linear Integral Equations: Theory & Technique* (Birkhäuser, Boston, 1997).
- ²⁰C. Texier, P. Delplace, and G. Montambaux, *Phys. Rev. B* **80**, 205413 (2009).
- ²¹M. Pascaud and G. Montambaux, *Phys. Rev. Lett.* **82**, 4512 (1999).
- ²²E. Akkermans, A. Comtet, J. Desbois, G. Montambaux, and C. Texier, *Ann. Phys. (NY)* **284**, 10 (2000).
- ²³D. E. Khmel'nitskii, *Physica B & C* **126**, 235 (1984).
- ²⁴F. Marquardt, J. von Delft, R. Smith, and V. Ambegaokar, *Phys. Rev. B* **76**, 195331 (2007).
- ²⁵G. Montambaux and E. Akkermans, *Phys. Rev. Lett.* **95**, 016403 (2005).
- ²⁶I. L. Aleiner, B. L. Altshuler, and M. E. Gershenson, *Waves in Random and Complex Media* **9**, 201 (1999).
- ²⁷J. von Delft, F. Marquardt, R. Smith, and V. Ambegaokar, *Phys. Rev. B* **76**, 195332 (2007).
- ²⁸J. von Delft, *Int. J. Mod. Phys. B* **22**, 727 (2008).
- ²⁹S. Chakravarty and A. Schmid, *Phys. Rep.* **140**, 193 (1986).
- ³⁰Compare with Y. Takane, *Anomalous Behavior of the Dephasing Time in Open Diffusive Cavities*, *J. Phys. Soc. Jpn.* **72**, 233 (2003), where vertex diagrams^{27,28} have not been considered.
- ³¹U. Sivan, Y. Imry, and A. G. Aronov, *Europhys. Lett.* **28**, 115 (1994).
- ³²T. Christen and M. Büttiker, *Europhys. Lett.* **35**, 523 (1996).
- ³³Note that the FDT expresses thermal correlations $\langle j^2 \rangle(\mathbf{x}, \mathbf{y}, \omega) \equiv \langle j(\mathbf{x}, \omega) j(\mathbf{y}, -\omega) \rangle \sim \text{Re}[\bar{\sigma}(\mathbf{x}, \mathbf{y}, \omega)]$, dominated by short-range contributions; this should not be confused with the mesoscopic correlations $\langle j(\mathbf{x}, \omega) \rangle \langle j(\mathbf{x}', \omega') \rangle \sim \sigma(\mathbf{x}, \mathbf{y}, \omega) \sigma(\mathbf{x}', \mathbf{y}', \omega')$ studied in Refs. 11–13, dominated by long-range contributions.

Chapter 3

Quantum corrections to the conductance

In Chapter 2, we have discussed the loop-expansion in diffusive propagators of disorder averaged correlation functions. We have argued that, in open systems, the relative magnitude of the quantum corrections is controlled by the inverse dimensionless conductance, which we defined as

$$g \equiv 2\pi \frac{E_{\text{Th}}}{\Delta}, \quad (3.1)$$

cf. Section 2.1.4. The distinction between *open* and *confined* systems will play an important role in the following: In the former, the electrons leave the system as soon as they have traversed it once, i.e. after the Thouless time τ_{Th} . In the latter, they dwell in the system much longer than τ_{Th} . In this chapter, we will show that g actually corresponds to the conductance measured in a transport experiment on an open system. We calculate g from the current response function and derive the so-called weak-localization correction and the universal conductance fluctuations. Their dependence on dephasing due to electron interactions at low T is analyzed in detail. We compare the perturbative calculation with the results from RMT valid for confined system. Finally, we discuss the situation in two particular confined systems, namely an almost isolated quasi-1D ring and a quantum-dot, and show that the elusive 0D regime of dephasing can be observed at the onset of mesoscopic universality in such systems.

3.1 The conductance of disordered metals

3.1.1 The classical conductance

The conductivity of disordered metals at finite temperatures can be calculated using the Keldysh perturbation theory which we have introduced in Section 2.2.1 [Rammer and Smith, 1986]. Starting point is the expectation value of the current density operator in the absence of an external electric field:

$$\mathbf{j}^\alpha(\mathbf{x}, t) = \frac{e}{im} \left\langle \hat{\Psi}^\dagger(\mathbf{x}, t) (\partial_{\mathbf{x}}^\alpha \hat{\Psi}(\mathbf{x}, t+0)) + (\partial_{\mathbf{x}}^\alpha \hat{\Psi}^\dagger(\mathbf{x}, t)) \hat{\Psi}(\mathbf{x}, t+0) \right\rangle, \quad (3.2)$$

where $\partial_{\mathbf{x}}^\alpha$ denotes the directional derivative of \mathbf{x} in the direction $\alpha = x, y, z$ and we assumed spin-degeneracy. The expectation value of the field operators is directly related to the Green's functions, see [Rammer and Smith, 1986]:

$$\langle \hat{\Psi}^\dagger(\mathbf{x}, t) \hat{\Psi}(\mathbf{x}, t) \rangle = -i [G^K(\mathbf{x}, t; \mathbf{x}, t+0) - G^R(\mathbf{x}, t; \mathbf{x}, t+0) + G^A(\mathbf{x}, t; \mathbf{x}, t+0)]. \quad (3.3)$$

Let us now include a weak external electric field $\mathbf{E}_\omega(\mathbf{x})$, which we conveniently express in terms of a vector potential $\mathbf{A}_\omega(\mathbf{x}) = \mathbf{E}_\omega(\mathbf{x})/i\omega$. Expanding Eq. (3.2) to linear order in \mathbf{A} using Eq. (3.3) yields

$$\mathbf{j}_\omega^{\alpha(1)}(\mathbf{x}) = -\frac{e}{m} \int \frac{d\varepsilon}{2\pi} \lim_{\mathbf{x}' \rightarrow \mathbf{x}} (\partial_{\mathbf{x}}^\alpha - \partial_{\mathbf{x}'}^\alpha) \left[G_{\varepsilon-\omega, \varepsilon}^{K(1)}(\mathbf{x}, \mathbf{x}') \right] - \frac{ne^2}{m} \mathbf{A}_\omega^\alpha(\mathbf{x}), \quad (3.4)$$

where the second term is the diamagnetic contribution¹ (n is the average electron density), see e.g. [Bruus and Flensberg \(2004\)](#), and $G_{\varepsilon_1, \varepsilon_2}^{K(1)}(\mathbf{x}, \mathbf{y})$ is the first order term of the expansion of the Fourier transform of $G^K(\mathbf{x}, t_1; \mathbf{y}, t_2)$ in \mathbf{A} :²

$$G_{\varepsilon-\omega, \varepsilon}^{K(1)}(\mathbf{x}, \mathbf{y}) = \frac{ie}{2m} \int d^d \mathbf{z} \sum_{\beta} \mathbf{A}_\omega^\beta(\mathbf{z}) \times \lim_{\mathbf{z}' \rightarrow \mathbf{z}} \left(\partial_{\mathbf{z}}^\beta - \partial_{\mathbf{z}'}^\beta \right) \left[G_{\varepsilon-\omega}^K(\mathbf{x}, \mathbf{z}) G_\varepsilon^R(\mathbf{z}', \mathbf{y}) + G_{\varepsilon-\omega}^A(\mathbf{x}, \mathbf{z}) G_\varepsilon^K(\mathbf{z}', \mathbf{y}) \right]. \quad (3.5)$$

The Green's functions on the r.h.s of Eq. (3.5) are taken at $\mathbf{A} = 0$. Using Eq. (3.5) in Eq. (3.4), we find:

$$\mathbf{j}_\omega^{\alpha(1)}(\mathbf{x}) = \int d^d \mathbf{y} \sum_{\beta} \sigma_\omega^{\alpha\beta}(\mathbf{x}, \mathbf{y}) i\omega \mathbf{A}_\omega^\beta(\mathbf{y}). \quad (3.6)$$

with the non-local conductivity tensor

$$\sigma_\omega^{\alpha\beta}(\mathbf{x}, \mathbf{y}) = -\frac{ne^2}{i\omega m} \delta_{\alpha\beta} \delta(\mathbf{x} - \mathbf{y}) - \frac{2e^2}{\omega m^2} \int \frac{d\varepsilon}{2\pi} \left[G_{\varepsilon-\omega}^K(\mathbf{x}, \mathbf{y}) \overset{\leftrightarrow\alpha}{\partial}_{\mathbf{x}} \overset{\leftrightarrow\beta}{\partial}_{\mathbf{y}} G_\varepsilon^R(\mathbf{y}, \mathbf{x}) + G_{\varepsilon-\omega}^A(\mathbf{x}, \mathbf{y}) \overset{\leftrightarrow\alpha}{\partial}_{\mathbf{x}} \overset{\leftrightarrow\beta}{\partial}_{\mathbf{y}} G_\varepsilon^K(\mathbf{y}, \mathbf{x}) \right], \quad (3.7)$$

where we introduced the symmetrized directional derivative

$$f(\mathbf{x}) \overset{\leftrightarrow\alpha}{\partial}_{\mathbf{x}} g(\mathbf{x}) \equiv \frac{1}{2} \lim_{\mathbf{x}' \rightarrow \mathbf{x}} (\partial_{\mathbf{x}}^\alpha - \partial_{\mathbf{x}'}^\alpha) f(\mathbf{x}) g(\mathbf{x}'). \quad (3.8)$$

In thermal equilibrium, the Keldysh Green's function, G^K , can be related to the retarded/advanced Green's functions via Eq. (2.75). As a result, we obtain products of Green's functions with equal retardation, $G^R G^R$ and $G^A G^A$, and terms with different retardation $G^R G^A$. The former terms have no nontrivial dependence on disorder, cf. the discussion after Eq. (2.32), in the absence of interactions³. It can be shown, similar to Eq. (2.87) (for details see e.g. [Rammer and Smith \(1986\)](#)), that they cancel the diamagnetic term in Eq. (3.7), which restores gauge invariance. As a result Eq. (3.7) simplifies to

$$\sigma_\omega^{\alpha\beta}(\mathbf{x}, \mathbf{y}) = \frac{2e^2}{m^2} \int \frac{d\varepsilon}{2\pi} \frac{h_{\varepsilon-\omega} - h_\varepsilon}{\omega} G_{\varepsilon-\omega}^A(\mathbf{x}, \mathbf{y}) \overset{\leftrightarrow\alpha}{\partial}_{\mathbf{x}} \overset{\leftrightarrow\beta}{\partial}_{\mathbf{y}} G_\varepsilon^R(\mathbf{y}, \mathbf{x}). \quad (3.9)$$

In the following, we are only interested in spatially homogeneous electric fields in Eq. (3.6).⁴ Moreover, we concentrate on the current component in the direction of the field, described by the so-called

-
1. Note that the diamagnetic contribution alone is unphysical since it violates gauge invariance and diverges in the direct current (DC) limit, $\omega \rightarrow 0$. Thus, it should be canceled by a contribution from the first terms in Eq. (3.4).
 2. Note that G^R and G^A in Eq. (3.3) do not depend on \mathbf{A} to linear order due to $G^R(t)G^R(-t) = G^A(t)G^A(-t) = 0$.
 3. In the presence of electron interactions, the terms with equal retardation play an important role in the description of the so-called Altshuler-Aronov interaction corrections. These corrections are temperature dependent, however, they do not depend on magnetic field or the dephasing time discussed in Section 2.2.
 4. The case of arbitrary fields has been studied in detail in [Kane et al. \(1988\)](#).

longitudinal conductivity, and neglect the transverse components. The transverse components are related to the Hall effect, which we do not consider here. Therefore, we can integrate over \mathbf{y} in Eq. (3.6) and obtain after symmetrization:

$$\sigma_\omega = \frac{1}{d} \sum_\alpha \frac{1}{V^2} \int d^d \mathbf{x} \int d^d \mathbf{y} \sigma_\omega^{\alpha\alpha}(\mathbf{x}, \mathbf{y}). \quad (3.10)$$

The quantity measured in a transport experiment is the conductance, which is related to the conductivity by Ohm's law:

$$G_\omega = L^{d-2} \sigma_\omega. \quad (3.11)$$

Eq. (3.11) is a generalization of the usual form $G = \sigma S/L$ for a sample of length L and cross-section S to arbitrary dimensions. We obtain

$$\begin{aligned} G_\omega &= \frac{1}{dL^2} \sum_\alpha \frac{1}{V} \int d^d \mathbf{x} \int d^d \mathbf{y} \sigma_\omega^{\alpha\alpha}(\mathbf{x}, \mathbf{y}) \\ &= \frac{2e^2}{dm^2L^2} \int \frac{d\varepsilon}{2\pi} \frac{h_{\varepsilon-\omega} - h_\varepsilon}{\omega} \frac{1}{V} \int d^d \mathbf{x} \int d^d \mathbf{y} G_\varepsilon^R(\mathbf{y}, \mathbf{x}) \overleftrightarrow{\nabla}_\mathbf{x} \overleftrightarrow{\nabla}_\mathbf{y} G_{\varepsilon-\omega}^A(\mathbf{x}, \mathbf{y}), \end{aligned} \quad (3.12)$$

where $\overleftrightarrow{\nabla}_\mathbf{x}$ is defined in analogy to Eq. (3.8), but with the directional derivative replaced by gradients. At small frequencies $\omega \ll T$, we can use the following approximation

$$\lim_{\omega \ll T} \frac{h_{\varepsilon-\omega} - h_\varepsilon}{\omega} = -\frac{\partial f_\varepsilon}{\partial \varepsilon}, \quad f_\varepsilon = \frac{1}{e^{\varepsilon/T} + 1}, \quad (3.13)$$

where f_ε is the Fermi distribution function. Note that $-\frac{\partial f_\varepsilon}{\partial \varepsilon}$ is a broadened delta function of width $T \ll \varepsilon_F$, centered around ε_F . After impurity averaging, the product of Green's functions depends only weakly on ε in this energy range, see the discussion after Eq. (2.86). Thus, we can integrate over ε and obtain for the disorder averaged conductance:

$$\overline{G}_\omega = \frac{e^2}{\pi d m^2 L^2} \frac{1}{V} \int d^d \mathbf{x} \int d^d \mathbf{y} \overline{G_\varepsilon^R(\mathbf{y}, \mathbf{x}) \overleftrightarrow{\nabla}_\mathbf{x} \overleftrightarrow{\nabla}_\mathbf{y} G_{\varepsilon-\omega}^A(\mathbf{x}, \mathbf{y})}. \quad (3.14)$$

Note that the r.h.s of Eq. (3.14) does not depend on ε , but we keep ε here just as in Section 2.1.2. After a Fourier transform, we finally obtain

$$\overline{G}_\omega = \frac{e^2}{\pi d L^2 m^2} \frac{1}{V} \sum_{\mathbf{k}, \mathbf{k}'} \mathbf{k} \mathbf{k}' \overline{G_\varepsilon^R(\mathbf{k}, \mathbf{k}') G_{\varepsilon-\omega}^A(\mathbf{k}', \mathbf{k})}. \quad (3.15)$$

Let us now evaluate the disorder average of Eq. (3.15) in analogy to our discussion in Section 2.1.2. In the limit $(\varepsilon_F \tau)^{-1} \ll 1$ the disorder average $\overline{G^R G^A}$ is given by the ladder approximation, which is shown in Fig. 3.1. However, in contrast to the generalized diffusion propagator, there are additional factors \mathbf{k} and \mathbf{k}' in Eq. (3.15). These vector-valued factors correspond to the momentum of the Green's functions at the vertices in Fig. 3.1, which are often called *vector vertices* in this context. Due to the symmetry of the disorder averaged Green's functions, $\overline{G^{R/A}(\mathbf{k})} = \overline{G^{R/A}(-\mathbf{k})}$, the following sum vanishes:

$$\sum_{\mathbf{k}} \mathbf{k} \overline{G^R(\mathbf{k})} \overline{G^A(\mathbf{k})} = 0. \quad (3.16)$$

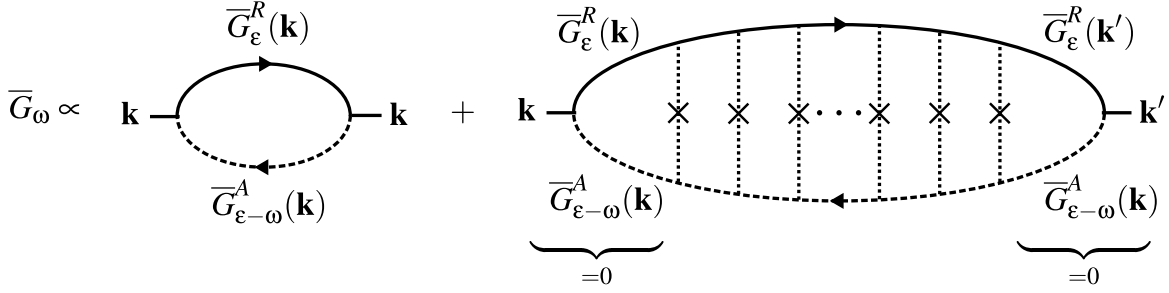


Figure 3.1: The classical disorder averaged conductance \bar{G}_ω . Due to the factors \mathbf{k} (and \mathbf{k}') the particle-hole ladder diagram does not contribute for spatially homogeneous electric fields.

As a result, the ladder diagram in the particle-hole channel does not contribute to the average conductance. However, the case of having no impurity lines between the two Green's functions at all survives and gives the contribution:

$$\bar{G}_\omega = \frac{e^2}{\pi d L^2 m^2 V} \sum_{\mathbf{k}} k^2 \bar{G}_\epsilon^R(\mathbf{k}) \bar{G}_{\epsilon-\omega}^A(\mathbf{k}). \quad (3.17)$$

The Green's functions are strongly peaked around the Fermi momentum, thus we can move $k^2 \simeq (mv_F)^2$ in out of the integral:

$$\bar{G}_\omega \approx \frac{e^2 v_F^2}{\pi d} \frac{1}{L^2 V} \sum_{\mathbf{k}} \bar{G}_\epsilon^R(\mathbf{k}) \bar{G}_{\epsilon-\omega}^A(\mathbf{k}). \quad (3.18)$$

Finally, using Eq. (2.16) to evaluate the sum, we obtain at $\omega\tau \ll 1$:

$$\bar{G}_\omega \approx \frac{e^2 v_F^2}{\pi d} \frac{1}{L^2} 2\pi\rho\tau (1 + i\omega\tau) = 2e^2 \frac{E_{\text{Th}}}{\Delta} (1 + i\omega\tau), \quad (3.19)$$

where we identified the Thouless energy $E_{\text{Th}} = D/L^2$ and the level spacing $\Delta = 1/(\rho V)$. Note that the frequency dependence of the conductance \bar{G}_ω is weak for the experimentally relevant parameter range $\omega \ll 1/\tau^1$, and we will neglect it in the following.

The dimensionless conductance g is defined as the conductance G measured in units of $e^2/(2\pi)$. At zero frequency, we recover Eq. (3.1), up to a factor of 2 due to spin degeneracy:

$$\bar{g} = \frac{\bar{G}_0}{e^2/(2\pi)} = 4\pi \frac{E_{\text{Th}}}{\Delta}. \quad (3.20)$$

In the following, we denote the *disorder averaged* dimensionless conductance by $g = \bar{g}$, and we will omit the symbol for disorder averaging. Using the standard expression for the mean level spacing, see e.g. [Akkermans and Montambaux \(2007\)](#), Eq. (3.20) can be rewritten as follows:

$$g = A_d (k_F L)^{d-2} (k_F \ell) \gg 1, \quad (3.21)$$

where A_d is a system-dependent dimensionless coefficient ~ 1 . Thus, the classical conductance is always large in the limit $(\epsilon_F \tau)^{-1} \ll 1$ in $d = 2, 3$. The same is true for quasi-1D² systems, as long as the transverse system size is larger than λ_F .

1. The regime $1/\tau \ll \omega$ is practically impossible to reach in a normal metal, since $1/\tau$ usually lies in the far infrared. It can only be studied in certain heavy fermion systems [[Dressel and Scheffler, 2006](#)].
 2. We remind the reader that ‘‘quasi-1D’’ denotes a two or three dimensional system, where diffusion is effectively one dimensional: the transverse dimensions are smaller than the mean free path ℓ .

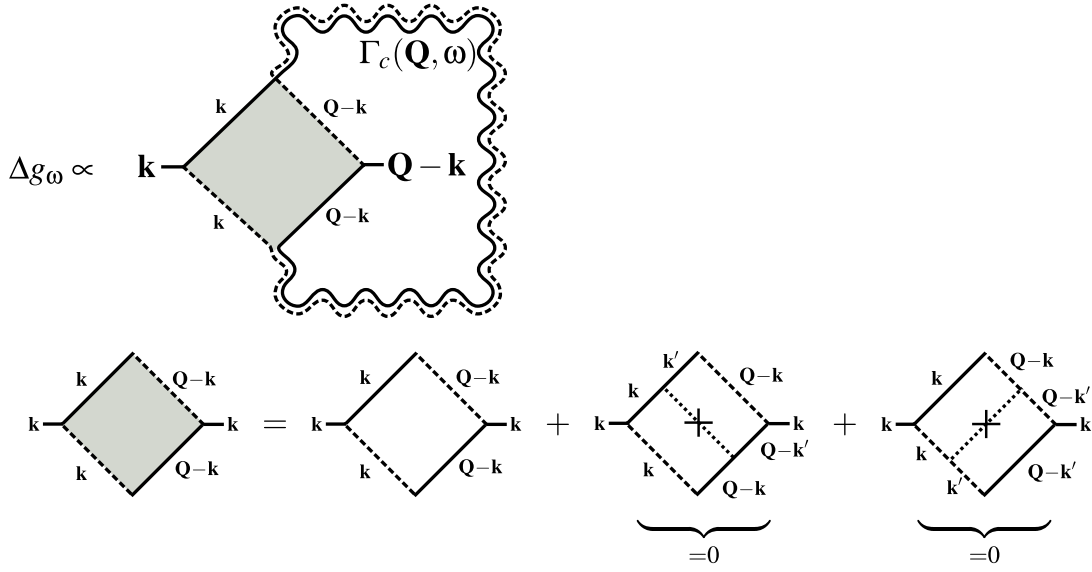


Figure 3.2: The weak localization correction to the disorder averaged dimensionless conductance $g_\omega = 2\pi\bar{G}_\omega/e^2$. The Hikami box cannot be dressed by additional impurity lines due to the identity (3.16).

3.1.2 Quantum corrections to the conductance: weak localization

In full analogy with our discussion in Section 2.1.2, the leading quantum correction to the conductance is obtained in the loop-expansion by inserting a maximally-crossed impurity ladder in the diagram for the conductance, Fig. 3.1. Keeping in mind that due to the identity (3.16) there can be no impurity lines in the particle-hole channel at the vector vertices, we obtain in analogy with Fig. 2.4 the diagram shown in Fig. 3.2. It includes a 4-point Hikami box, which we denote H_4^{WL} in the following. The expression for the one-loop quantum correction reads [Khmel'nitskii, 1984]:

$$\Delta g_\omega = \frac{2}{dL^2 m^2} \sum_{\mathbf{Q}} H_4^{WL}(\mathbf{Q}, \omega) \Gamma_c(\mathbf{Q}, \omega), \quad (3.22)$$

where

$$H_4^{WL}(\mathbf{Q}, \omega) = \frac{1}{V} \sum_{\mathbf{k}} \mathbf{k}(\mathbf{Q} - \mathbf{k}) \bar{G}_\varepsilon^R(\mathbf{k}) \bar{G}_{\varepsilon - \omega}^A(\mathbf{Q} - \mathbf{k}) \bar{G}_\varepsilon^R(\mathbf{Q} - \mathbf{k}) \bar{G}_{\varepsilon - \omega}^A(\mathbf{k}). \quad (3.23)$$

Note that this Hikami box cannot be dressed by additional impurity lines due to Eq. (3.16), see the second line of Fig. 3.2. Taking into account that all odd terms in \mathbf{k} vanish due to symmetry, and using the fact that the Green's functions are strongly peaked around the Fermi momentum k_F , we can calculate the Hikami box by expanding the Green's functions in $D\mathbf{Q}^2\tau$ and $\omega\tau$, and then using Eq. (2.16). We obtain to lowest order in $(\varepsilon_F\tau)^{-1}$:

$$H_4^{WL}(\mathbf{Q}, \omega) = -\frac{1}{V} \sum_{\mathbf{k}} \mathbf{k}^2 \left[\bar{G}_0^R(\mathbf{k}) \right]^2 \left[\bar{G}_0^A(\mathbf{k}) \right]^2 \approx -4\pi\rho\tau^3 k_F^2. \quad (3.24)$$

Inserting Eq. (3.24) in Eq. (3.22) we find:

$$\Delta g_\omega = -4E_{\text{Th}} \sum_{\mathbf{Q}} P_c(\mathbf{Q}, \omega). \quad (3.25)$$

Eq. (3.25) is also often called the *weak-localization* (WL) correction, since it corresponds to the onset of the Anderson localization transition mentioned in Chapter 1, see [Abrahams *et al.* \(1979\)](#). Note that the WL correction is *negative*¹, and leads to a reduction of the classical conductance (3.20). As expected, we see that Eq. (3.25) corresponds to Eq. (3.18), with the renormalized diffusion constant $D^*(\omega)$ introduced in Eq. (2.30) [[Gorkov *et al.*, 1979](#)]:

$$\Delta g_\omega = 4\pi\rho V \frac{D^*(\omega) - D}{L^2}. \quad (3.26)$$

The dependence on a dephasing rate of Eq. (3.25) follows directly from our discussion in Section 2.1.3 and Section 2.2. In the absence of a magnetic field, we obtain

$$\Delta g_\omega = -4E_{\text{Th}} \sum_{\mathbf{Q}} \frac{1}{D\mathbf{Q}^2 - i\omega + 1/\tau_\phi(T)}. \quad (3.27)$$

In an open system, at $\omega = 0$ and for strong dephasing, $1/\tau_\phi(T) \gg E_{\text{Th}}$, the sum can be approximated by an integral, with the result

$$\lim_{1 \gg E_{\text{Th}}\tau_\phi} \Delta g_{\omega=0} = \begin{cases} -2 \frac{\sqrt{D\tau_\phi(T)}}{L} & (\text{quasi-1D}) \\ -\frac{2}{\pi} \ln \frac{\sqrt{D\tau_\phi(T)}}{\ell} & (2\text{D}) \end{cases}. \quad (3.28)$$

Furthermore, the weak-localization correction does not depend on $\tau_\phi(T)$ in 3D, cf. the discussion in Section 2.1.4. Evidently, the dependence of Δg on $\tau_\phi(T)$ is most easily studied in quasi-1D systems, since the logarithmic dependence on $\tau_\phi(T)$ in 2D systems makes it difficult to distinguish between the regimes discussed in Section 2.2.5. In the opposite limit of weak dephasing, $E_{\text{Th}} \gg 1/\tau_\phi(T)$,² the weak-localization correction (3.27) becomes independent of $\tau_\phi(T)$ in open systems for *any* dimension and approaches a “universal” value ~ 1 . Thus, the crossover to 0D dephasing at $T \simeq E_{\text{Th}}$ always happens in the “universal” regime, since $T \gg 1/\tau_\phi(T)$. The question arises whether the observability of 0D dephasing is improved in confined systems, and we will examine this question in more detail in Section 3.3.

To conclude, let us now evaluate the temperature dependence of Eq. (3.27) explicitly for a particular open system: For simplicity we assume a quasi-1D ring with circumference L , which is connected to ideally absorbing leads. In this case, $\mathbf{Q} = \frac{2\pi n}{L}$ with $n \neq 0 \in \mathbb{Z}$, and the sum over \mathbf{Q} in Eq. (3.27) can be evaluated exactly. This yields:

$$\Delta g_\omega^{(\text{ring})} = -\frac{2E_{\text{Th}}}{1/\tau_\phi(T) - i\omega} \left[\pi \sqrt{\frac{1/\tau_\phi(T) - i\omega}{(2\pi)^2 D/L^2}} \coth \left(\pi \sqrt{\frac{1/\tau_\phi(T) - i\omega}{(2\pi)^2 D/L^2}} \right) - 1 \right]. \quad (3.29)$$

In the DC case, ($\omega \rightarrow 0$), we identify two regimes: (a) at $1/\tau_\phi(T) \gg (2\pi)^2 D/L^2$, we can approximate $\coth(\dots) \approx 1$ in Eq. (3.29) and obtain $-\Delta g_{\omega=0}^{(\text{ring})} \propto \sqrt{\tau_\phi(T)}$; (b) at $(2\pi)^2 D/L^2 \gg 1/\tau_\phi(T)$, on the other hand, the two terms in square brackets in Eq. (3.29) cancel to leading order and the subleading order gives a constant which is independent of $\tau_\phi(T)$: The WL correction saturates. The constant is given by

$$\Delta g_{\omega=0, T=0}^{(\text{ring})} = -4E_{\text{Th}} \sum_{n \neq 0} \frac{1}{D(\frac{2\pi n}{L})^2} = -\frac{1}{3}. \quad (3.30)$$

1. For strong spin-orbit coupling, which we do not consider in the following, the sign in Eq. (3.25) can be reversed, leading to so-called *weak-antilocalization* [[Hikami *et al.*, 1980](#)].
2. We remark that the regime $E_{\text{Th}} \gg 1/\tau_\phi$ is also often called *mesoscopic*, since the whole system is phase coherent.

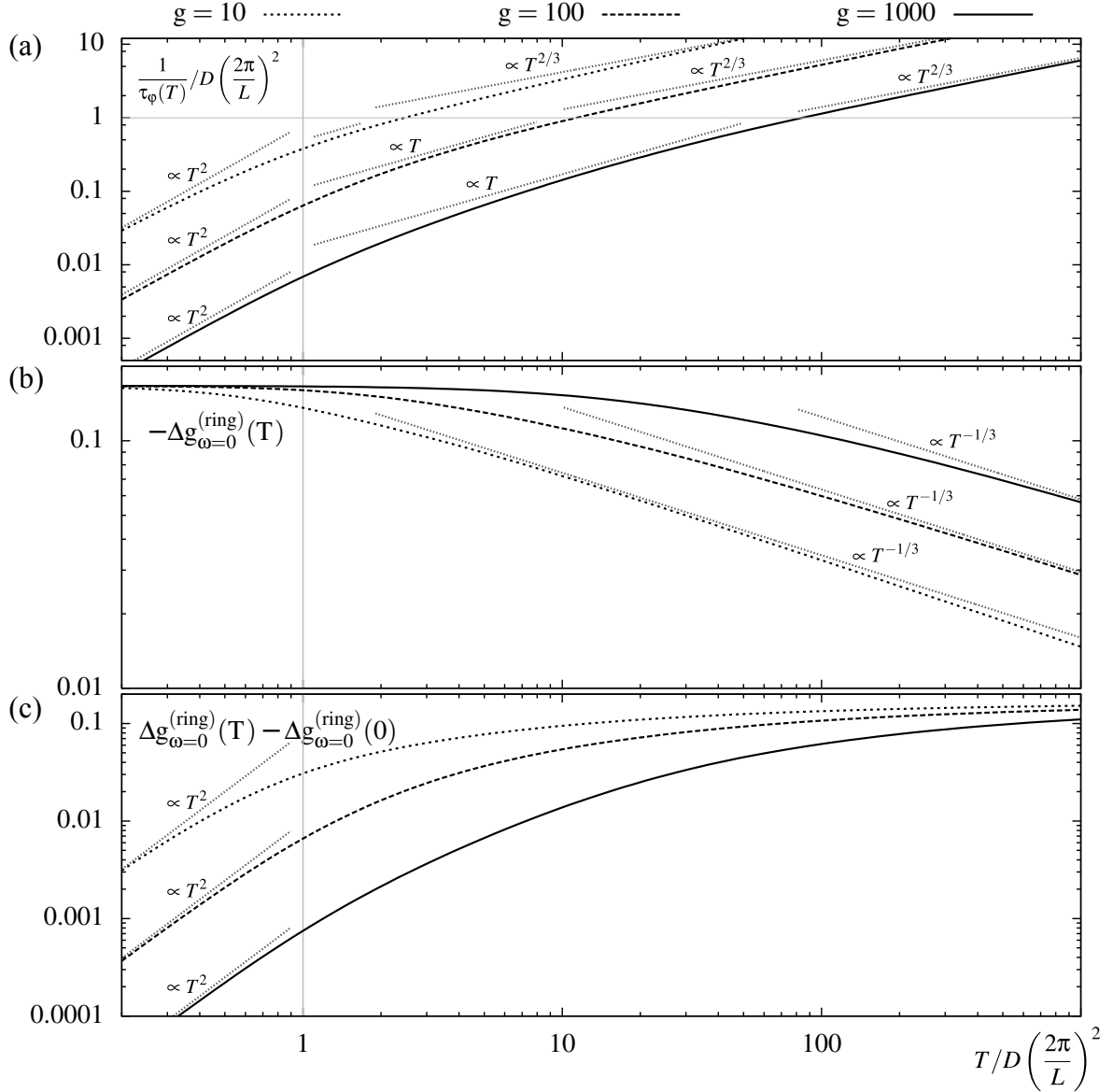


Figure 3.3: Temperature dependence of the WL correction (per spin) of a quasi-1D ring.

We have already evaluated the dephasing time for this case in Section 2.2.5, cf. Fig. 2.19. We remind the reader that dephasing is always diffusive in the regime (a) with $\tau_\phi(T) \propto T^{-2/3}$. In the regime (b) it can be either ergodic with $\tau_\phi(T) \propto T^{-1}$ at $T \gtrsim E_{\text{Th}}$ or OD with $\tau_\phi(T) \propto T^{-2}$ at $E_{\text{Th}} \gtrsim T$. For convenience, we show the dephasing time from Fig. 2.19 again in Fig. 3.3(a) for three different values of g . In Fig. 3.3(b) we show the corresponding WL correction to the conductance as a function of T calculated from Eq. (3.27). Note that temperature of the onset of saturation coincides with the onset of ergodic dephasing. In Fig. 3.3(c) we show the WL correction subtracted from its value at $T \rightarrow 0$. At $T \lesssim (2\pi)^2 D/L^2$ the subtracted curve shows OD dephasing, $\Delta g_{\omega=0}^{(\text{ring})}(T) - \Delta g_{\omega=0}^{(\text{ring})}(0) \propto T^2$. However, a rather large measurement precision is needed to study the temperature dependence on top of the saturated value. Moreover, the saturation depends on the contact between the ring and the leads and is distorted by the temperature dependence of Δg in the leads. Nevertheless, in a high-precision measurement of an open wire with a small conductance connected to large 3D leads, an observation

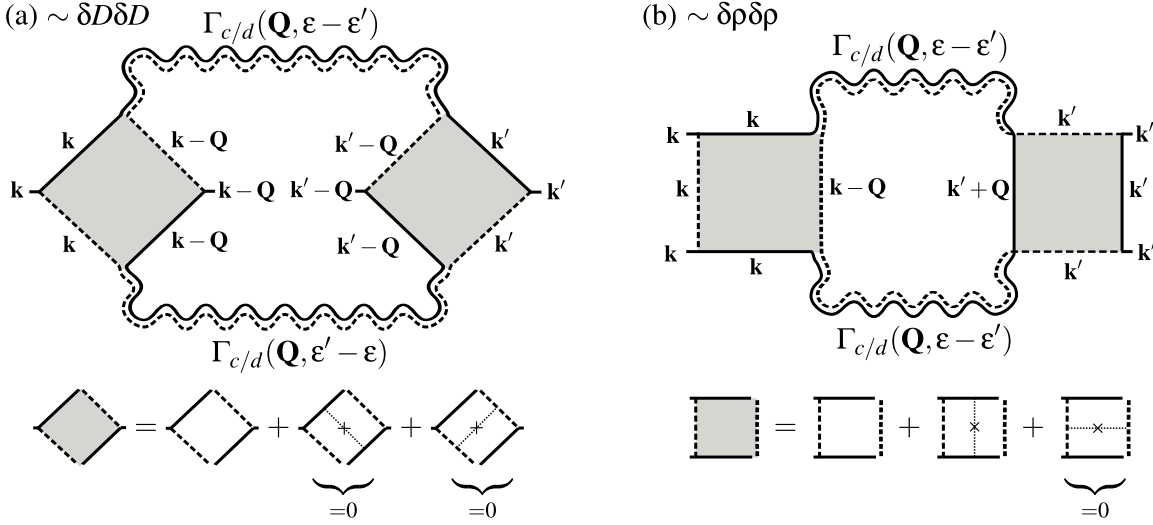


Figure 3.4: Universal conductance fluctuations.

of 0D dephasing might be feasible.

3.1.3 Universal conductance fluctuations

In the previous section, we have seen that the dephasing rate $\gamma = 1/\tau_\phi$ determines the amplitude of the weak-localization correction to the disorder averaged conductance. In this section, we consider the second moment of g_ω w.r.t. the disorder probability density (2.2): the so-called conductance fluctuations $\overline{\delta g^2}$. These fluctuations describe not only the correlations of the conductance between samples with different impurity configurations, but also the fluctuations of the conductance of a single sample as a function of magnetic field or Fermi energy. The latter follows from the fact that already a small change in the magnetic field or the Fermi energy leads to a significant shift of the particle energies and their quantum mechanical phases, such that all interference phenomena are effectively described by a different impurity configuration.

Conductance fluctuations are a relatively broad topic and the full distribution of the conductance is relatively well understood today. Importantly, the distribution of g is not necessarily Gaussian, see [Lerner \(1990\)](#); [McCann and Lerner \(1996, 1998\)](#) for a detailed discussion. The purpose of our brief analysis here is to discuss whether we can extract the dephasing rate γ in different regimes, including the 0D regime, directly from the amplitude of the fluctuations.

In general it is expected that at sufficiently short dephasing times, when the system is non-mesoscopic, $\tau_\phi \ll \tau_{\text{Th}}$, samples are *self-averaging*: The system is effectively composed of a large number of phase-coherent sub-systems, such that the fluctuations average out. Evidently, this is not the case in the 0D regime, which always requires $\tau_\phi \ll \tau_{\text{Th}}$, see the discussion in Section 2.2.5, however, the magnitude of the fluctuations might be parametrically smaller than Δg . Thus, a further purpose of this section is to analyze whether an additional ensemble average is necessary to extract 0D dephasing from a transport experiment.

The conductance fluctuations have been studied first by [Lee and Stone \(1985\)](#) and [Altshuler \(1985\)](#). The corresponding diagrams can be constructed by considering *two* of the “bubble diagrams” for the conductance, i.e. Fig. 3.1 without the impurity lines, and dressing them in all possible ways by impurity ladders. To leading order in $(\varepsilon_F \tau)^{-1}$ the relevant resulting diagrams each have two vertices close to each other [[Akkermans and Montambaux, 2007](#)]. They are shown in Fig. 3.4: The dia-

gram of Fig. 3.4(a) is often interpreted as the correlation function of the diffusion constant ($\overline{\delta D \delta D}$), and Fig. 3.4(b) as the correlation function of the density of states ($\overline{\delta \rho \delta \rho}$) [Altshuler and Shklovskii, 1986]. Both diagrams are structurally similar and consist of two impurity ladders (in the particle-hole or particle-particle channel, corresponding to diffuson, P_d , or Cooperon, P_c , propagators) attached to two 4-point Hikami boxes. Note that due to the factors \mathbf{k} and \mathbf{k}' , the Hikami boxes have “vector vertices”, and can be dressed only partially, cf. the Hikami box for Δg in Fig. 3.2. In Fig. 3.4(a) only the undressed Hikami box contributes, and the impurity ladders are taken at opposite energies $\varepsilon - \varepsilon'$ and $\varepsilon' - \varepsilon$. Thus, they are complex conjugates and their contribution includes a modulus square of the diffusive propagators:

$$\overline{\delta g_\varepsilon \delta g_{\varepsilon'}}^{(\delta D \delta D)} = 8E_{\text{Th}}^2 \sum_{\mathbf{Q}} |P_c(\mathbf{Q}, \varepsilon - \varepsilon')|^2 + |P_d(\mathbf{Q}, \varepsilon - \varepsilon')|^2. \quad (3.31)$$

In Fig. 3.4(b), on the other hand, one of the dressings of the Hikami box is non-zero, since it includes an even number of \mathbf{k} -factors. As a result, the contribution of the Hikami box in Fig. 3.4(a) is twice as large as that of Fig. 3.4(b). The diagram shown in Fig. 3.4(b) and its complex conjugate give twice the real part. In total, one obtains from Fig. 3.4(b):

$$\overline{\delta g_\varepsilon \delta g_{\varepsilon'}}^{(\delta \rho \delta \rho)} = 8E_{\text{Th}}^2 \sum_{\mathbf{Q}} \text{Re} [P_c(\mathbf{Q}, \varepsilon - \varepsilon')^2 + P_d(\mathbf{Q}, \varepsilon - \varepsilon')^2]. \quad (3.32)$$

The Cooperon propagators in Eqs. (3.31, 3.32) depend on τ_ϕ in the same way as the weak-localization correction, Eq. (3.27). In addition, the diffusons can also be sensitive to dephasing since they are not protected by particle conservation, see e.g. the detailed discussion in Akkermans and Montambaux (2007). The relation between the dephasing rates appearing in the Cooperons and in the diffusons is discussed in Blanter (1996) and Aleiner and Blanter (2002).

The dependence of $\overline{\delta g^2}$ on temperature and a magnetic field has been analyzed in Lee *et al.* (1987). At finite temperature we obtain from Eqs. (3.12, 3.13) at $\omega \ll T \ll \varepsilon_F$:

$$\overline{\delta g^2}(T) = \int d\varepsilon d\varepsilon' \frac{\partial f}{\partial \varepsilon} \frac{\partial f}{\partial \varepsilon'} \overline{\delta g_\varepsilon \delta g_{\varepsilon'}}. \quad (3.33)$$

Since the fluctuations depend only on the difference in energies, Eq. (3.33) can be rewritten as follows:

$$\overline{\delta g^2}(T) = \int \frac{d\omega}{2T} F\left(\frac{\omega}{2T}\right) \overline{\delta g^2}(\omega) \quad F(x) = \frac{x \coth x - 1}{\sinh^2 x}, \quad (3.34)$$

where $F(\omega/2T)$ restrict the energy transfer ω to $|\omega| \lesssim T$. Substituting Eq. (3.31) and Eq. (3.32) into Eq. (3.34), we see that the fluctuations reach a “universal” value as soon as $T \ll E_{\text{Th}}$, which also implies $1/\tau_\phi(T) \ll E_{\text{Th}}$:

$$\overline{\delta g^2}(T \ll E_{\text{Th}}) \sim 1. \quad (3.35)$$

For open systems, Eq. (3.35) directly follows from $P_c(\omega = 0) \sim P_d(\omega = 0) \sim 1/E_{\text{Th}}$ at $1/\tau_\phi(T) \ll E_{\text{Th}}$, but Eq. (3.35) also holds for confined geometries, see Serota *et al.* (1987). At higher temperatures, $T \gtrsim E_{\text{Th}}$, on the other hand, Eq. (3.34) predicts that the fluctuations become temperature dependent due to the function F . In fact, it has been shown in Aleiner and Blanter (2002)¹ that the fluctuations can be written directly in terms of the weak-localization correction (3.25):

$$\overline{\delta g^2} = -\frac{2\pi E_{\text{Th}}}{3T} [\Delta g + \Delta g_{P_c \rightarrow P_d}]_{\ell \rightarrow \sqrt{D/T}}, \quad (3.36)$$

1. See also the more general proof in appendix E of Texier and Montambaux (2005).

where the second term in rectangular brackets is obtained by replacing the Cooperon propagator in Eq. (3.25) by a diffuson propagator. Moreover the short distance cutoff ℓ , which is relevant in dimensions $d > 1$ in Eq. (3.25) is replaced by $\sqrt{D/T}$ in both terms. We see from Eq. (3.36) that in the intermediate temperature range $1/\tau_\phi(T) \ll E_{\text{Th}} \ll T$, the fluctuations are smaller than the weak-localization correction by a factor of E_{Th}/T . However, at the crossover to 0D dephasing, $T \lesssim E_{\text{Th}}$, the magnitude of Δg and of $\overline{\delta g \delta g}$ are of the same order, since they are both “universal” and with magnitude ~ 1 . Since the samples cannot be self-averaging in this temperature range either, 0D dephasing can be observed from Δg only by averaging over a large number of samples.

We conclude with the observation that the magnitude of the fluctuations is *not* well suited to study the crossover to 0D : The intrinsic temperature dependence described by Eq. (3.34) and the change of the temperature dependence of $\tau_\phi(T)$, which both occur at $T \simeq E_{\text{Th}}$, interfere with each other and make a clear observation of the crossover more difficult. Thus, in the following, we will not consider the fluctuations in more details, and always assume a suitable ensemble average.

3.2 The random matrix theory of quantum transport

In Section 2.1.6 we have argued that the properties of disordered metals where spatial degrees of freedom can be neglected (such as a disordered quantum dot) show a remarkable universality, such that their properties only depend on the symmetry class described by the parameter β . These systems can be described by assuming that the Hamiltonian is a random matrix from one of the Wigner-Dyson ensembles. As a result, certain quantities, such as the average energy-level correlation functions, can be calculated non-perturbatively. However, our discussion was so-far restricted to isolated systems.

Using RMT in the calculation of the conductance is possible by relating the conductance to a so-called *scattering matrix* S via the celebrated Landauer formula [Landauer, 1957; Imry, 1986; Büttiker, 1986a], as we will see in the following.

3.2.1 Conductance as a scattering problem

In this section we give a brief derivation of the Landauer formula for a quasi-1D system following Fisher and Lee (1981), and then discuss how the formalism can be extended to arbitrary systems. Consider a disordered conductor of Length L and cross-section A connected to ideal reservoirs in a parallel electric field. According to Eq. (3.14), we can write the dimensionless conductance (at $\omega = 0$) as follows:

$$g = -\frac{1}{m^2 L^2} \int d^d \mathbf{x} d^d \mathbf{x}' G_\epsilon^R(\mathbf{x}_\perp, \mathbf{x}'_\perp, x_\parallel, x'_\parallel) \overset{\leftrightarrow}{\partial}_{x_\parallel} \overset{\leftrightarrow}{\partial}_{x'_\parallel} G_\epsilon^A(\mathbf{x}'_\perp, \mathbf{x}_\perp, x'_\parallel, x_\parallel) \quad (3.37)$$

where \mathbf{x}_\perp are the perpendicular components of \mathbf{x} , and x_\parallel is its parallel component. The next step is to Fourier transform the Green's functions with respect to the perpendicular coordinates:

$$G_{ab}^R(x_\parallel, x'_\parallel) = G_\epsilon^R(\mathbf{k}_a, \mathbf{k}_b, x_\parallel, x'_\parallel) = \frac{1}{A} \int d^{d-1} \mathbf{x}_\perp d^{d-1} \mathbf{x}'_\perp G_\epsilon^R(\mathbf{x}_\perp, \mathbf{x}'_\perp, x_\parallel, x'_\parallel) e^{i(\mathbf{k}_a \mathbf{x}_\perp - \mathbf{k}_b \mathbf{x}'_\perp)}, \quad (3.38)$$

where we denote the transverse modes by a and b . Note that in the assumed geometry the number of transverse modes (which are often called *channels* in this context) is finite since they are quantized in units of $2\pi/W$ and restricted by the Fermi momentum k_F . Thus, the number of transverse channels can be estimated by

$$N \approx \frac{\pi k_F^2}{2\pi(2\pi/W)^2} = \frac{k_F^2 S}{4\pi}. \quad (3.39)$$

Recent advances in nanofabrication have made it possible to create samples with $W \simeq \lambda_F$, such that the number of transverse channels can be as low as $N \simeq 1$.

Using Eq. (3.38) in Eq. (3.37) we find:

$$g = -\frac{e^2}{2\pi m^2 L^2} \int dx_{\parallel} dx'_{\parallel} \sum_{a,b} G_{ab}^R(x_{\parallel}, x'_{\parallel}) \overset{\leftrightarrow}{\partial}_{x_{\parallel}} \overset{\leftrightarrow}{\partial}_{x'_{\parallel}} G_{ab}^A(x'_{\parallel}, x_{\parallel}). \quad (3.40)$$

In Eq. (3.40), the integrand cannot depend on x_{\parallel} due to current conservation [Imry, 2002]. Thus, we can equally set $x_{\parallel} = 0$ and $x_{\parallel} = L$ in the contact region. Assuming non-interacting ballistic leads, the x_{\parallel} -dependence of the Green's functions in this region is simply $\exp(ik_a x_{\parallel})$, see Datta (1997) for a detailed discussion. As a result, we obtain the *Landauer formula*:

$$g = -\frac{e^2}{2\pi} \sum_{a,b} T_{ab}, \quad T_{ab} = v_a v_b |G_{ab}^R(0, L)|^2, \quad (3.41)$$

where $v_{a/b} = k_{a/b}/m$ are the longitudinal velocities and T_{ab} are the so-called *transmission coefficients*. We emphasize that the number of transmission coefficients depends only on the transverse size of the wire at the contacts.

Evidently, one can generalize Eq. (3.41) for arbitrary systems which have a left and a right contact: the entire inner structure of the system is then fully included in the transmission coefficients. Thus, Eq. (3.41) constitutes a reformulation of the conductance problem in terms of the modes of the incoming and outgoing electrons. Eq. (3.41) can also be expressed in terms of a *transmission matrix*,

$$\mathbf{T}_{ab} = i\sqrt{v_a v_b} G_{ab}^R(0, L), \quad (3.42)$$

such that

$$g = \frac{e^2}{2\pi} \sum_{ab} |\mathbf{T}_{ab}|^2. \quad (3.43)$$

The transmission matrix describes the amplitude of transmission of a particle entering the left contact in channel a to propagate through the sample and exit through the right contact in channel b . Usually, one also analogously defines a transmission matrix from right to left, \mathbf{T}' , and corresponding reflection matrices \mathbf{R} and \mathbf{R}' . All 4 matrices constitute the so-called *scattering matrix*:

$$\mathbf{S} = \begin{pmatrix} \mathbf{R} & \mathbf{T}' \\ \mathbf{T} & \mathbf{R}' \end{pmatrix} \quad (3.44)$$

Note that *particle conservation* requires *unitarity* of the \mathbf{S} matrix:

$$\mathbf{S}^\dagger \mathbf{S} = \mathbf{S} \mathbf{S}^\dagger = \mathbf{1}. \quad (3.45)$$

3.2.2 Quantum corrections

With Eqs. (3.43, 3.44), we have expressed the conductance in terms of a scattering matrix \mathbf{S} . Although, we have considered an open wire in the derivation, the formalism can be straightforwardly generalized to arbitrary systems. The number of rows and columns of \mathbf{S} depends only on the size of the contacts. In particular, we can consider a confined system with small contacts. In such systems, the electrons spend a much larger time in the system than the Thouless time, τ_{Th} , which is the average time needed to traverse the system once. We denote the time spend in the system in the following as dwelling time τ_{dw} . If

$$\tau_{\text{dw}} \gg \tau_{\text{Th}} = 1/E_{\text{Th}} \quad (3.46)$$

the electrons explore the inner part of the system ergodically before they leave the system. In this limit, it is expected that the scattering matrix becomes *universal*, i.e. independent of the actual size, shape, or impurity concentration of the system. Such a system is usually called a *quantum dot*, since it effectively has no spatial degrees of freedom, and can be described by a universal Hamiltonian [Kurland *et al.*, 2000].

To obtain a random matrix theory of the scattering matrix of such a quantum dot, two approaches can be found in the literature: (1) One applies random directly to the Hamiltonian of the system, and then analyses how the corresponding \mathbf{S} -matrix can be constructed. This approach uses a standard extension to scattering theory, the so-called R -matrix theory [Wigner and Eisenbud, 1947]. A detailed review of this approach can be found in Verbaarschot *et al.* (1985) or Weidenmüller (1990). (2) One applies random matrix theory directly to the scattering matrix \mathbf{S} and ignores the underlying Hamiltonian. In particular, Blümel and Smilansky (1988) proposed to use a constant distribution:

$$P(\mathbf{S}) = \text{const.} \quad (3.47)$$

Eq. (3.47) characterizes a system where all scattering processes are equally probable. Of course, additionally, \mathbf{S} has to be a unitary matrix if a strong magnetic field B is applied ($\beta = 2$, unitary ensemble); and a unitary symmetric matrix if $B = 0$ ($\beta = 1$, orthogonal ensemble)¹. Note that the random matrix ensemble for the unitary matrix \mathbf{S} is called *Dyson's circular ensemble*, which is in contrast to the so-called *Wigner-Dyson ensemble* for the Hamiltonian \mathbf{H} .

The implications of Eq. (3.47) for quantum transport have been discussed in Baranger and Mello (1994); Jalabert *et al.* (1994), see also the extensive review Beenakker (1997) and the introduction in Brouwer (1997). Note that the conductance is related to the transmission matrix \mathbf{T} , (3.42), and not directly to the scattering matrix \mathbf{S} . \mathbf{S} and \mathbf{T} are related by Eq. (3.44) and one can employ the following decomposition,

$$\mathbf{S} = \begin{pmatrix} \mathbf{u} & 0 \\ 0 & \mathbf{v}' \end{pmatrix} \begin{pmatrix} \sqrt{1-\mathcal{T}} & i\sqrt{\mathcal{T}} \\ i\sqrt{\mathcal{T}} & \sqrt{1-\mathcal{T}} \end{pmatrix} \begin{pmatrix} \mathbf{u}' & 0 \\ 0 & \mathbf{v} \end{pmatrix}, \quad (3.48)$$

where $\mathbf{u}, \mathbf{u}', \mathbf{v}, \mathbf{v}'$ are $N \times N$ unitary matrices and $\mathcal{T} = \text{diag}(T_1, T_2, \dots)$ includes the transmission coefficients T_i , cf. Eq. (3.41). The distribution of the T_i can be found from the Jacobian of the transformation (3.48), and is given by:

$$P(\{T_i\}) = \prod_{i < j} |T_i - T_j|^\beta \prod_{j=1}^N T_j^{\beta/2-1}. \quad (3.49)$$

Note the similarity between Eq. (3.49) and the Vandermonde determinant (2.57).

In the RMT for the Hamiltonian we were mainly interested in the limit $N \rightarrow \infty$. The RMT for the scattering matrix, on the other hand, is useful for all values of N . In particular, the case of single-mode leads $N = 1$ is described by the probability distribution

$$P(T) = \frac{\beta}{2} T^{\beta/2-1}. \quad (3.50)$$

Note that this distribution is highly non-Gaussian. The average transmission value can be obtained straightforwardly:

$$g \sim \bar{T} = \int_0^1 dT T P(T) = \frac{\beta}{\beta+2} = \begin{cases} 1/2 - 1/6 & (\text{GOE}, \beta = 1) \\ 1/2 & (\text{GUE}, \beta = 2) \end{cases}. \quad (3.51)$$

1. Note that we assume the absence of spin-orbit scattering for simplicity.

The value $1/2$ in the GUE ($\beta = 2$) reflects the fact that on average only half of the electrons are transmitted through a perfectly symmetric quantum dot, while the other half is reflected. The weak-localization correction is given by the difference of the GOE and the GUE. We see from Eq. (3.51) that it is given by the universal value $-1/6$ for single-mode quantum dots. For spin-degenerate systems, the result (3.51) should be multiplied by an additional factor of 2. Thus, the WL correction of the *confined* quantum dot is (coincidentally¹) identical to that of the open ring calculated in Eq. (3.30).

The situation is more complicated for arbitrary N . In the limiting case of many-mode leads, $N \gg 1$, the distribution becomes Gaussian and one obtains [Brouwer, 1997]:

$$g \sim \overline{\sum_{i=1}^N T_i} = \frac{N}{2} + \frac{\beta - 2}{4\beta} + O(1/N) \approx \begin{cases} N/2 - 1/4 & (\text{GOE}, \beta = 1) \\ N/2 & (\text{GUE}, \beta = 2) \end{cases}. \quad (3.52)$$

We conclude that the RMT predicts a WL correction $\Delta g \sim 1$, and the precise value depends on the contacts, in particular the number of channels.

We note in passing that also the fluctuations of the conductance have been calculated using the RMT for the scattering matrix, however, they are not well suited to study the 0D crossover due to their intrinsic temperature dependence, cf. Section 3.1.3. The latter is discussed in the context of the RMT in Efetov (1995).

3.2.3 Models of dephasing

Two methods have been used in the past to include the loss of phase coherence in the random matrix theory of quantum transport: (1) In the first method the quantum dot is coupled to an additional fictitious lead to a phase-randomizing reservoir [Büttiker, 1986b]. The distribution of the conductance for single- and multi-channel systems has been evaluated for this case by Brouwer and Beenakker (1995). The conductance of the “dephasing lead”, g_ϕ , is assumed to be related to the dephasing rate $\gamma = 1/\tau_\phi$ via:

$$g_\phi = \gamma/\Delta, \quad (3.53)$$

where Δ is the level spacing of the dot defined in Eq. (2.47), see e.g. Brouwer and Beenakker (1997) for a discussion. (2) In the second method, an additional imaginary potential is included to the Hamiltonian of the quantum dot, which is of the form [McCann and Lerner, 1996]:

$$H' = -i\gamma/2, \quad (3.54)$$

and then its effect on the scattering matrix is studied.

At first glance, both approaches seem to describe very different physical situations. In particular, it seems not plausible that the additional localized lead can serve as a model for dephasing by electron interactions, which occur uniformly inside of the quantum dot. However, Brouwer and Beenakker (1997) have proposed a version of the dephasing lead model which is equivalent to the imaginary potential model: After introducing an additional tunnel barrier with transparency Γ_ϕ , and taking the limit of infinitely many “dephasing channels” N_ϕ of the dephasing lead, while simultaneously fixing $g_\phi = N_\phi \Gamma_\phi$, both approaches lead to the same dependence of the conductance on γ .

The result can be summed up in terms of an interpolation formula suggested in Baranger and Mello (1995):

$$g = \frac{N}{2} \left(1 - \frac{1}{(2N+1) + 2\pi\gamma/\Delta} \right). \quad (3.55)$$

1. Since the open ring is equivalent to two open wires connected in parallel, the weak-localization correction of an open wire is twice as large as that of the single lead quantum dot.

Note that Eq. (3.55) is valid for arbitrary N (see also Brouwer and Beenakker (1997) for a detailed derivation of the case $N \gg 1$), and reproduces the $\gamma \rightarrow 0$ results, Eqs. (3.52, 3.51).

Several experiments have tried to extract the dependence of γ on temperature using Eq. (3.55), and to provide evidence for 0D dephasing, see e.g. Clarke *et al.* (1995); Huibers *et al.* (1999). However, we stress that 0D dephasing always requires $\gamma \lesssim \Delta$, cf. Section 2.2.5 and thus cannot dominate the amplitude of g according to Eq. (3.55). The differences between the RMT result, Eq. (3.55), and the perturbative result, Eq. (3.27), are discussed in more details in the following section.

3.3 Dephasing in non-trivial geometries

So far, we have considered only simple geometries. For simplicity, we have assumed in our derivation of the weak-localization correction in Section 3.1 that the system is effectively rectangular, and connected with one surface to ideal absorbing leads (i.e. *open*): This allowed us (a) to use a simple form Ohm's law, $G = \sigma L^{d-2}$, relating conductance and conductivity, Eq. (3.11), and (b) to define a Thouless time of the form $\tau_{\text{Th}} = L^2/D$. To calculate the *classical* conductance for more complicated geometries, this description is usually sufficient: The system can be divided into simple rectangular sub-systems and the conductance of the total system is then obtained using Kirchhoff's circuit laws.

In Section 3.2, on the other hand, we have seen how confined systems (in the limit $\tau_{\text{dw}} \gg \tau_{\text{Th}}$) can be effectively described in terms of a random matrix ensemble for the scattering matrix \mathbf{S} . However, this approach neither tries to give an accurate description of the contacts, nor of the inner geometry. It relies on the assumption that electrons can be described as plane waves before and after they traverse the system; and that the inner spatial structure of the system is irrelevant. The dephasing rate $\gamma = 1/\tau_\phi$ is introduced in this description phenomenologically, cf. Eq. (3.53), and, in contrast to the perturbative treatment of Section 3.1, it is not guaranteed that the γ introduced in Eq. (3.53) corresponds to the same dephasing rate discussed in Section 2.2.5. Importantly, we have found that for few-channel contacts, $N \simeq 1$, the weak-localization correction saturates at $\gamma \lesssim \Delta$, see Eq. (3.55), while in open systems the saturation occurs at $\gamma \lesssim E_{\text{Th}}$. Thus, we expect that confined systems are better suited to study the 0D crossover.

In the following Section 3.3.1 we propose a simplified model to describe dephasing in a confined system. Namely, we study an almost isolated ring with a phenomenologically introduced dwelling time τ_{dw} . We discuss the temperature dependence of the weak-localization correction in all details in Section 3.4 and Section 3.5. We argue that the ring geometry is particularly well suited to study the 0D crossover, since distorting contributions of the leads can be effectively filtered from contributions of the ring by applying an additional magnetic field.

The description of the quantum corrections in more complicated geometries is a difficult task, since the diffusive propagators describe long-range electron trajectories. The typical length of the contributing trajectories is governed by the dephasing length and can exceed all of the characteristic length scales of the system at sufficiently low temperatures. To systematically study non-trivial geometries, several *effective methods* have been developed, which describe the full system in terms of simpler sub-systems. One example is an effective description in terms of a network of quantum dots, see Kupferschmidt and Brouwer (2008). Another method, which we discuss in Section 3.3.2, is an effective description in terms of quasi-1D wires connected at vertices, which constitute a so-called *graph*. We have developed a general procedure to include dephasing in their description with the help of our results in Section 2.4, and we apply this procedure to calculate the weak-localization correction for a disordered quantum dot in Section 3.6.

Note that we do not consider the case of tunneling contacts in our work, which would lead to a further complication of the problem due to electric repulsion of the electrons in the confined part of

the system: the so-called *Coulomb blockade* [Aleiner *et al.*, 2002; Blanter *et al.*, 2006].

3.3.1 Confined geometries

The random matrix theory discussed in Section 3.2 describes a confined quantum dot with N channel contacts. One assumes that the spatial degrees of freedom of the inner part are unimportant and can be neglected. We can picture such a system as being composed of three *open* metals: A left and right contact with conductance $g_c \sim N$ and a central region with a conductance $g_1 \gg g_c$. Note that g_1 determines the average level spacing inside of the dot: $g_1 = 2\pi E_{\text{Th}}/\Delta$. In this language, the weak-localization correction (3.55) of the system assumes the form:

$$\Delta g \sim -E_{\text{Th}} \frac{g_c}{g_1} \frac{1}{E_{\text{Th}} \frac{g_c}{g_1} + \gamma}, \quad (3.56)$$

for spin degenerate systems. The ratio g_c/g_1 determines the effectivity of the confinement. Thus, a “natural” definition of the dwelling time is as follows:

$$\tau_{\text{dw}} \equiv \tau_{\text{Th}} \frac{g_1}{g_c}. \quad (3.57)$$

Using Eq. (3.57) in Eq. (3.56), we obtain:

$$\Delta g \sim -\frac{1}{\tau_{\text{dw}}} \frac{1}{1/\tau_{\text{dw}} + \gamma}. \quad (3.58)$$

We see that the RMT result Eq. (3.58) for confined systems predicts a dependence of Δg on γ as soon as $\gamma \gg 1/\tau_{\text{dw}}$. Note that this is in full agreement with the perturbative result for open systems, Eq. (3.27), where $\tau_{\text{Th}} \simeq \tau_{\text{dw}}$.

This observation allows us to formulate a simple effective perturbative model for dephasing in confined systems: The RMT describes the spatially homogeneous part of the weak-localization correction corresponding to the $\mathbf{Q} = 0$ mode of the Cooperon. Thus, the IR-divergence, present in isolated systems at small γ is regularized by $1/\tau_{\text{dw}}$ according to Eq. (3.58). As a consequence, Eq. (3.27) should be replaced in a confined system, $\tau_{\text{dw}} \gg \tau_{\text{Th}}$, as follows:

$$\Delta g \simeq -E_{\text{Th}} \sum_{\mathbf{Q} \neq 0} \frac{1}{D\mathbf{Q}^2 + \gamma} \xrightarrow{\text{confinement}} \Delta g \simeq -E_{\text{Th}} \frac{g_c}{g_1} \sum_{\text{all } \mathbf{Q}} \frac{1}{D\mathbf{Q}^2 + 1/\tau_{\text{dw}} + \gamma}. \quad (3.59)$$

This model is equivalent to a *closed* system with a homogeneous electron dissipation rate $1/\tau_{\text{dw}}$. The reduction of the overall amplitude due to Eq. (3.56) reflects the fact that contact and dot are connected in series, $g = (2/g_c + 1/g_1)^{-1} \simeq g_c/2$. Note that the dephasing rate γ in Eq. (3.59) is equal to the rate discussed in Section 2.2.5 and *independent* of τ_{dw} . The reason is that the constant mode $1/\tau_{\text{dw}}$ does not contribute in Eq. (2.148), since it cannot lead to a finite phase difference. The dwelling time just provides an *additional* effective source of dephasing,¹ which should be added to the dephasing rate via *Matthiessen’s rule*:

$$\gamma \rightarrow \gamma + 1/\tau_{\text{dw}}. \quad (3.60)$$

We study the consequences of this model applied to a quasi-1D ring in detail in Section 3.4. In particular, we discuss the observability of 0D dephasing and argue that an additional perpendicular

1. The independence of γ on τ_{dw} also follows from the path integral picture discussed in Section 2.2.6: The dephasing rate is obtained by calculating the phase difference acquired by a path of given duration t . Provided that such a path exists, an average over its spatial probability density, cf. Eq. (2.143), is independent of τ_{dw} .

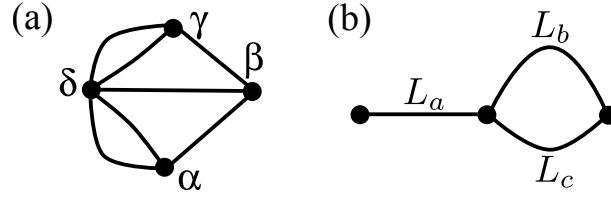


Figure 3.5: (a) A network of quasi-1D wires connected at vertices $\alpha, \beta, \gamma, \delta$. (b) Illustration of the effective length \mathcal{L} of Eq. (3.62).

magnetic field helps to filter distorting contributions from the leads. More details are given in Section 3.5, where we also take into account a finite conductance of the lead g_l , and discuss the optimal ratios of g_c , g_1 , and g_l to study the 0D crossover. We conclude that an almost isolated ring is the ideal system to study 0D dephasing in a transport experiment.

3.3.2 Networks of wires

A network of wires can be described in terms of a so-called *graph*. It is defined as a set of wires, also called bonds, connected to each other at vertices, see the example shown in Fig. 3.5(a), where $N = 7$ bonds are connected at $M = 4$ vertices. The latter are denoted by Greek letters $\alpha, \beta, \gamma, \delta$. The wires are assumed to be identical in material and width, but can differ in length. However, a different width can be realized by assuming several wires in parallel.

In analogy to Kirchhoff's circuit laws for the classical conductance g , the quantum corrections Δg of such a graph have to be weighted depending on the length of the wires. Starting from the Landauer formula (3.41), Texier and Montambaux (2004) have shown that Δg can be obtained from

$$\Delta g = -4D \frac{1}{\mathcal{L}^2} \sum_i \frac{\partial \mathcal{L}}{\partial L_i} \int_{\text{wire } i} dx P_c(x, x, \omega = 0), \quad (3.61)$$

where \mathcal{L} is the effective total length of the system obtained similar to calculating the total resistance, cf. Eq. (3.25). For example,

$$\mathcal{L} = L_a + (1/L_b + 1/L_c)^{-1}, \quad (3.62)$$

corresponds to the effective length for a wire of length L_a connected in series to two wires of length L_b and L_c which are connected in parallel, see Fig. 3.5(b).

However, the Cooperon P_c in Eq. (3.61), corresponding to the return probability of a diffusive trajectory, still depends on the whole network for sufficiently weak dephasing rates γ . Thus, the solution of the diffusion equation which governs P_c has to be calculated for the entire graph. In this context one usually studies the Laplace transform (w.r.t. time) of the diffusion equation instead, which is defined as

$$[\gamma - D\Delta_x] P(x, y, \gamma) = \delta(x - y). \quad (3.63)$$

Evidently, $P(x, y, \gamma)$ describes the diffusion probability with a *constant* dephasing rate γ . Using the formalism developed by Doucot and Rammal (1985), $P(x, y, \gamma)$ can be evaluated for an arbitrary point in a network of wires. Starting point is a suitable $M \times M$ matrix \mathcal{M} (M is the number of vertices), which encodes the lengths and connection of the wires, and is defined as follows:¹

$$\mathcal{M}_{\alpha\beta}^\gamma \equiv \sum_{(\alpha\delta)} \sqrt{\gamma/D} \coth\left(\sqrt{\gamma/D} L_{\alpha\delta}\right) - \delta_{\alpha\beta} \sqrt{\gamma/D} \sinh\left(\sqrt{\gamma/D} L_{\alpha\delta}\right)^{-1}, \quad (3.64)$$

1. Note that Eq. (3.64) simplifies to ‘‘Eq.(33)’’ of Section 2.4 in the limit $\gamma \rightarrow 0$.

where the sum $\overline{\sum_{(\alpha\delta)}}$ runs over all bonds $(\alpha\delta)$, which are connected to α in the network, and $L_{\alpha\beta}$ is the length of the bond between vertices α and β . Imposing current conservation at each vertex of the graph, it can be shown (see our brief discussion in “Section 3” of Section 3.6 or the detailed derivation in Akkermans and Montambaux (2007)) that the diffusion probability between two vertices α and β is given by the inverse of \mathcal{M} :

$$P(\alpha, \beta, \gamma) = \frac{1}{D} [\mathcal{M}^{-1}]_{\alpha\beta}. \quad (3.65)$$

Since additional vertices can be inserted anywhere in the network, Eq. (3.65) can be used to calculate the (Laplace transformed) diffusion probability between arbitrary positions on the graph. We emphasize that this formalism is very efficient, since the probabilities are obtained by a simple matrix inversion, albeit it only describes a system with a constant dephasing rate γ .

For the case of a perfectly regular network, i.e. a network where the electric current through each bond is approximately identical, Eq. (3.61) simplifies to

$$\Delta g \propto - \int_{\substack{\text{whole} \\ \text{network}}} dx P_c(x, x). \quad (3.66)$$

In this case, the quantum correction can be written in a remarkably simple form using the so-called *spectral determinant* $S(\gamma)$:

$$\Delta g \propto - \frac{\partial}{\partial \gamma} S(\gamma), \quad S(\gamma) \equiv \det[\gamma - D\Delta_x]. \quad (3.67)$$

$S(\gamma)$ can be expressed in terms of the matrix \mathcal{M} as follows [Akkermans *et al.*, 2000; Comtet *et al.*, 2005; Texier, 2008]:

$$S(\gamma) = \gamma^{\frac{M-N}{2}} \overline{\prod_{(\alpha\beta)}} \sinh\left(\sqrt{\gamma/D} L_{\alpha\beta}\right) \det \mathcal{M}, \quad (3.68)$$

where the product $\overline{\prod_{(\alpha\beta)}}$ runs over all bonds of the network. Equations similar to Eq. (3.67) for the weak-localization correction can be derived for the conductance fluctuations [Akkermans and Montambaux, 2007], the Altshuler-Aronov correction [Texier and Montambaux, 2007] or the persistent currents [Pascaud and Montambaux, 1999].

Using these methods, several non-trivial geometries have been studied in the past: Doucot and Rammal (1985, 1986) considered different types of regular lattices, such as ladders, and infinite square and honeycomb lattices; Santhanam (1989) included different boundary conditions to model the connection of the system to various types of leads; Texier and Montambaux (2005); Texier (2007) considered rings attached to wires of various length connected to different types of leads; and Texier *et al.* (2009) analyzed regular networks, chains of rings and hollow cylinders.

In all of these works, the dephasing rate γ was either assumed to be constant throughout the whole system, or some simplifying assumptions were employed to relate γ to its value in simpler geometries. We emphasize that, to the best of our knowledge, no dephasing rate has been obtained that differs substantially from our discussion in Section 2.2.5. In particular, the UV-cutoff due to Pauli blocking plays an important role in networks of wires only if the relevant trajectories are confined to a region where $L \ll \sqrt{D/T}$, and L is the size of the region. Since dephasing is weak in such a situation, $\tau_\phi \sim gE_{\text{Th}}/T^2$, the electrons have to remain confined at least during a time span $g\tau_{\text{Th}}$, where g is the conductance of the confined region. Otherwise, the trajectories can leave the confined region and large parts of the phase difference are acquired in “non-0D” parts of the system, where dephasing is substantially stronger (see also our discussion in “Section 20.8” of Section 3.5).

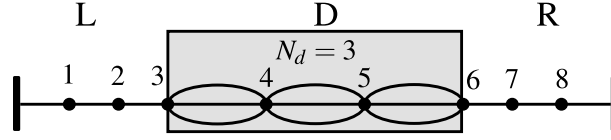


Figure 3.6: A quantum dot model based on a graph with 8 vertices.

As an aside, we note that Pauli blocking can become important in regular grid networks, too: For sufficiently low temperatures, a regular grid behaves similar to an infinite 2D plane, and 2D dephasing requires an UV-cutoff to regularize a logarithmic divergence, cf. Section 2.2.5. In the grid, this cutoff is given by $\min(T, D/a^2)$, where a is the size of one cell of the grid [Texier *et al.* \(2009\)](#). Thus, at $T \ll D/a^2$, Pauli blocking plays a role, albeit it only leads to a temperature dependent logarithm, which is difficult to detect experimentally, in particular, because the weak-localization correction depends logarithmically on γ in this regime, cf. Section 3.1.2.

In Section 3.6 we propose a procedure to take into account dephasing in networks more carefully, which we outline briefly in the following: The dephasing rate can be calculated from the functional discussed in Section 2.2.6. Using Eq. (2.164) and Eq. (2.167), we obtain after a Fourier transform:

$$\Gamma[\mathbf{z}(\tau)] = \frac{T}{\rho t} \int_0^t d\tau \int_0^t d\tau' [\delta_T(\tau - \tau') - \delta_T(\tau + \tau' - t)] P_d(\mathbf{z}(\tau), \mathbf{z}(\tau'), \omega = 0), \quad (3.69)$$

where δ_T is a broadened delta function of width $1/T$ and height T , see also “Eq. (45)” of Section 2.4. Evidently, $P_d(\omega = 0)$ in Eq. (3.69) can be directly obtained for any network from Eq. (3.65), after taking the limit $\gamma \rightarrow 0$. The next step is to average Eq. (3.69) over diffusive trajectories, cf. Eq. (2.162), to obtain the dephasing rate. Thus, the time-dependent probability is needed, which can be obtained from Eq. (3.65), too, via an inverse Laplace transform:

$$P(x, y, t) = \frac{1}{2\pi i} \int_{-i\infty}^{i\infty} d\gamma e^{\gamma t} P(x, y, \gamma). \quad (3.70)$$

Eq. (3.70) can be evaluated by converting the integral into a pole integral. The poles γ_n coincide with the zeros of the spectral determinant $S(\gamma_n) = 0$, since the probability is obtained by inversion of \mathcal{M} and $S(\gamma) \sim \det \mathcal{M}$. Note that the γ_n can be found analytically for any given network. Moreover, since the Laplace transformed probabilities $P(x, y, \gamma)$ are sums of simple hyperbolic functions, the average over the diffusive trajectories can also be done analytically. As a result, the dephasing rate becomes a function of position on the network, which should then be included in the Cooperon obtained from Eq. (3.65). Only the sum over poles γ_n and the integrals over time in Eq. (3.69) remain, and can be calculated numerically.

In principle, this procedure can be applied to arbitrary (finite) networks of wires, and it describes the quantum corrections in the whole temperature range. As an example, we study a quantum dot model in Section 3.6 and evaluate the weak-localization correction at finite temperatures accounting for interaction induced dephasing. It consists of three regions, see Fig. 3.6: a central region “C” describing the dot where N_d wires are connected in parallel, and two identical left- and right- wires, “L” and “R”, connected to leads, which mimic contacts of a real system. We find that the model is similar to the simple “dwelling time”-model, which we introduced in Section 3.3.1 and discuss in Section 3.4 and Section 3.5. Remarkably, we find that the strength of the confinement, measured by N_d , has no significant influence on the temperature dependence at low temperatures, since the conductance of each wire was assumed to be rather small ($g \simeq 5$), in correspondence with present experiments, see “Fig. 4(b)” of Section 3.6. At small g , the crossover to 0D dephasing occurs close to the universal

regime of the weak-localization correction even in completely open systems, cf. Section 3.1.2. However, we stress that this observation is based on the assumption of strongly absorbing leads. This assumption is in particular questionable in unconfined system, since the electron trajectories might be able to return into the system if it is not sufficiently confined. A better model of the leads is highly desirable, albeit difficult to achieve.

In any case, 0D dephasing can be observed only after subtracting the quantum corrections from their universal value at low temperature. Unfortunately, the conductance is very sensitive to the type of contacts and leads in the particular experiment in this temperature range, which makes the observation of the crossover very difficult in a transport experiment. However, we show in the following Chapter 4 that 0D dephasing is also accessible in isolated systems, where these problems do not appear.

3.4 Publication: Dimensional crossover of the dephasing time in disordered mesoscopic rings

The following 4 pages have been published in the journal *Physical Review B*.

PHYSICAL REVIEW B **80**, 201305(R) (2009)**Dimensional crossover of the dephasing time in disordered mesoscopic rings**M. Treiber,¹ O. M. Yevtushenko,¹ F. Marquardt,¹ J. von Delft,¹ and I. V. Lerner²¹*Arnold Sommerfeld Center and Center for Nano-Science, Ludwig-Maximilians-University, Munich D-80333, Germany*²*School of Physics and Astronomy, University of Birmingham, Birmingham B15 2TT, United Kingdom*

(Received 13 October 2009; published 10 November 2009)

We study dephasing by electron interactions in a small disordered quasi-one-dimensional (1D) ring weakly coupled to leads. We use an influence functional for quantum Nyquist noise to describe the crossover for the dephasing time $\tau_\varphi(T)$ from diffusive or ergodic 1D ($\tau_\varphi^{-1} \propto T^{2/3}, T^1$) to zero-dimensional (0D) behavior ($\tau_\varphi^{-1} \propto T^2$) as T drops below the Thouless energy. The crossover to 0D, predicted earlier for two-dimensional and three-dimensional systems, has so far eluded experimental observation. The ring geometry holds promise of meeting this long-standing challenge, since the crossover manifests itself not only in the smooth part of the magnetoconductivity but also in the amplitude of Altshuler-Aronov-Spivak oscillations. This allows signatures of dephasing in the ring to be cleanly extracted by filtering out those of the leads.

DOI: 10.1103/PhysRevB.80.201305

PACS number(s): 73.63.-b, 72.10.-d, 72.15.Rn

I. INTRODUCTION

Over the last 20 years numerous theoretical¹⁻⁸ and experimental¹⁰⁻¹⁵ works have studied the mechanism of dephasing in electronic transport and its dependence on temperature T and dimensionality in disordered condensed-matter systems. At low temperatures dephasing is mainly due to electron interactions, with the dephasing time $\tau_\varphi(T)$ increasing as T^{-a} when $T \rightarrow 0$.

The dephasing time controls the scale of a negative weak localization (WL) correction to the magnetoconductivity and (under certain conditions) the magnitude of universal conductance fluctuations (UCFs). If T is so low that τ_φ exceeds $\tau_{\text{Th}} = \hbar/E_{\text{Th}}$, the time required for an electron to cross (diffusively or ballistically) a mesoscopic sample (E_{Th} is the Thouless energy), UCFs become T independent. This leaves WL as the only tool to measure the T dependence of dephasing in mesoscopic wires or quantum dots at very low T . For quantum dots, a dimensional crossover was predicted⁴ from $\tau_\varphi \propto T^{-1}$, typical for a two-dimensional (2D) electron gas,¹ to $\tau_\varphi \propto T^{-2}$ when the temperature is lowered into the zero-dimensional (0D) regime,

$$\hbar/\tau_\varphi \ll T \ll E_{\text{Th}}, \quad (1)$$

where the coherence length and the thermal length are both larger than the system size independent of geometry and real dimensionality of the sample. Although the $\tau_\varphi \propto T^{-2}$ behavior is quite generic, arising from the fermionic statistics of conduction electrons, experimental efforts¹³ to observe it have so far been unsuccessful. The reasons for this are unclear. Conceivably dephasing mechanisms other than electron interactions were dominant, or the regime of validity of the 0D description had not been reached. In any case, other ways of testing the dimensional crossover for τ_φ are desirable.

Here we study dephasing in a quasi-1D mesoscopic ring weakly coupled to two well-conducting leads through narrow point contacts. We find a dimensional crossover for $\tau_\varphi(T)$ from diffusive or ergodic 1D ($\propto T^{-2/3}, T^{-1}$) to 0D ($\propto T^{-2}$) behavior as T is decreased below E_{Th} and propose a detailed experimental scenario for observing this behavior. It reveals itself not only via the WL corrections to the smooth part of magnetoconductivity but also via the amplitude of the

Altshuler-Aronov-Spivak (AAS) oscillations¹⁶ that result from closed trajectories with a nonzero winding number acquiring the Aharonov-Bohm phase. For sufficiently weak lead-ring coupling (specified below), the magnitude of AAS oscillations will be independent of dephasing in the leads. Thus, the ring geometry provides a more promising setup for the observation of the dimensional crossover than 2D or 3D settings.

II. DEPHASING IN WEAK LOCALIZATION

The WL correction to the conductivity is governed by coherent backscattering of the electrons from static disorder and, to the lowest order, is due to the enhancement of the return probability caused by constructive interference of two time reversed trajectories described by the so-called Cooperon \mathcal{C} .^{17,18} In this order, the WL correction to the conductivity, in units of the Drude conductivity σ_0 , is given by¹⁹

$$\Delta g = \frac{\Delta\sigma}{\sigma_0} = -\frac{1}{\pi\nu} \int_0^\infty dt' \mathcal{C}(t'). \quad (2)$$

Here ν is the electron density of states per spin at the Fermi surface and $\hbar = 1$ henceforward. Dephasing limits the scale of this contribution and effectively results in the suppression of the Cooperon at long times:

$$\mathcal{C}(t) \equiv C_0(t) \exp[-t/\tau_H - t/\tau_{\text{dw}} - \mathcal{F}(t)]. \quad (3)$$

We consider here low temperatures where the phonon contribution to dephasing is negligible and three main sources contribute to the Cooperon decay with time: an applied magnetic field H characterized by the time scale τ_H (Ref. 20); the leakage of particles from the ring characterized by the dwell time τ_{dw} (Ref. 21); and electron interactions, whose effects can be described in terms of the decay function $\mathcal{F}(t)$,^{1,3} which grows with time and may be used to define a dephasing time via $\mathcal{F}(\tau_\varphi) = 1$.

$\mathcal{F}(t)$ can be obtained using the influence functional approach,^{6,7} which gives results for the magnetoconductivity that are practically equivalent to those originally obtained in Ref. 1. Roughly speaking, an electron traversing a random walk trajectory $x(t_1)$ of duration t acquires a random phase

TREIBER *et al.*PHYSICAL REVIEW B **80**, 201305(R) (2009)

$\varphi_T = \int_0^t dt_1 V(x(t_1), t_1)$ due to the random potential V describing the Nyquist noise originating from electron interactions; the variance of this phase, averaged over all closed random walks (crw), gives the decay function, $\mathcal{F}(t) = \frac{1}{2} \langle \delta\varphi_t^2 \rangle_{\text{crw}}$. A careful treatment^{6,7} gives

$$\mathcal{F}(t) = \int_0^t d^2 t_{1,2} \langle \overline{VV}(x_{12}, t_{12}) - \overline{VV}(x_{12}, \bar{t}_{12}) \rangle_{\text{crw}}, \quad (4)$$

where $x_{12} \equiv x(t_1) - x(t_2)$; $t_{12} \equiv t_1 - t_2$; $\bar{t}_{12} \equiv t_1 + t_2 - t$. The noise is assumed Gaussian, with correlation function

$$\overline{VV}(x, t) = (2e^2 T / \sigma_0 A) Q(x) \delta_T(t). \quad (5)$$

Here A is the wire's cross-sectional area, the diffuson $Q(x)$ is the time-averaged solution of the diffusion equation, and $\delta_T(t)$ is a broadened δ function of width $T \approx 1/T$ and height $\approx T$ given by^{7,8}

$$\delta_T(t) = \pi T w(\pi T t), \quad w(y) = \frac{y \coth(y) - 1}{\sinh^2(y)}. \quad (6)$$

This form takes into account the Pauli principle in a quantum description of Nyquist noise and reproduces the results⁵ of leading order perturbation theory in the interaction for Δg . The broadening of $\delta_T(t)$ is the central difference between quantum noise and the classical noise considered in previous treatments,^{1,6} which used a sharp $\delta(t)$ function instead. Note that Eq. (4) is free from IR singularities, because the x -independent part of \overline{VV} (the diffuson “zero mode”) does not contribute to \mathcal{F} .

III. QUALITATIVE PICTURE

We begin with a qualitative discussion of dephasing in an isolated quasi-1D system of size L . Since Nyquist electric field fluctuations are white noise in space, the x dependence of V behaves like a random walk in space ($\sim \sqrt{|x|}$), so that $Q(x) \sim |x|$. For $\tau_T \ll \tau_{\text{Th}}$, the potential seen during one traversal of the system is also white noise in time, i.e., $\delta_T(t) \rightarrow \delta(t)$.

In the *diffusive regime* ($\tau_T \ll t \ll \tau_{\text{Th}}$), a random walk $x(t_1)$ of duration t does not feel the boundaries, hence, $|x(t_1)| \sim \sqrt{t}$. Thus, $\mathcal{F}(t) \propto T \int_0^t \sqrt{t_1} dt_1 \propto T t^{3/2}$, reproducing the well-known result $\tau_\varphi \propto T^{-2/3}$.¹

In the *ergodic regime* ($\tau_T \ll \tau_{\text{Th}} \ll t$), the trajectory fully explores the whole system, thus, $|x(t_1)| \sim L$ instead, which reproduces $\mathcal{F}(t) \propto TLt$ and $\tau_\varphi \propto T^{-1}$.⁶

We are primarily interested in the *0D regime* reached at $T \ll E_{\text{Th}} (\tau_{\text{Th}} \ll \tau_T \ll t)$. In contrast to the previous two regimes, a typical trajectory visits the vicinity of any point x in the interval $[0, L]$ several times during the time τ_T (see Fig. 1). On time scales shorter than this time τ_T the potential is effectively frozen, so that the broadened δ function in Eq. (5) saturates at its maximum, $\delta_T(t) \rightarrow T$, and the variance of V is of order $T^2|x|$. The phase picked up during τ_T becomes $\varphi_{\tau_T} = \tau_T \int_0^{\tau_T} dx p(x) V(x, t_1)$, where $p(x) dx$ is the fraction of time the trajectory spends near x . Then only small statistical deviations from the completely homogeneous limit, $p(x) = 1/L$ (reached for $\tau_T \rightarrow \infty$), yield a phase difference between the two time-reversed trajectories. These deviations scale like

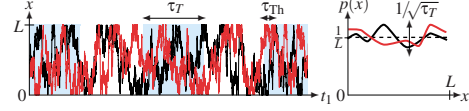


FIG. 1. (Color online) Left: a pair of time-reversed diffusive trajectories exploring ergodically a region of size L . The fluctuating noise potential is frozen during time intervals (indicated by shading) of duration $\tau_T = 1/T$ sketched here to be $\gg \tau_{\text{Th}}$. Right: the density $p(x)$ of points x visited by a particular trajectory during the time interval τ_T fluctuates around $1/L$ with fluctuations $\delta p \sim 1/\sqrt{\tau_T}$.

$\delta p \sim 1/\sqrt{\tau_T}$, since the number of “samples” (i.e., of traversals of the system during time τ_T) effectively grows with τ_T . Thus, setting $V \sim T\sqrt{|x|}$, we estimate $\varphi_{\tau_T} \sim \tau_T L^{3/2} T / \sqrt{\tau_T}$, so that $\langle \delta\varphi_{\tau_T}^2 \rangle \sim L^3 T^2 \tau_T$. Adding up the contributions from t/τ_T independent time intervals ($t \gg \tau_T$), we find $\mathcal{F}(t) \propto L^3 T^2 t$, implying $\tau_\varphi \sim T^{-2}$, characteristic of 0D systems.⁴ Thus, when τ_{Th} becomes the smallest time scale, a *dimensional crossover* occurs and the system becomes effectively 0D.

The qualitative behavior of τ_φ in all three regimes also follows upon extracting τ_φ self-consistently from the standard perturbative expression for the Cooperon self-energy.^{2,7,8} Inserting the usual cutoffs T and $1/\tau_\varphi$ for the frequency transferred between the diffusive electrons and their Nyquist noise environment and excluding the diffuson zeroth mode via a cutoff at $1/L$ of the transferred momentum, we have (omitting numerical prefactors)

$$\frac{1}{\tau_\varphi} \propto \frac{T}{g_1 L} \int_{1/\tau_\varphi}^T d\omega \int_{1/L}^{\infty} \frac{D dq}{(Dq^2)^2 + \omega^2}, \quad g_1 = \frac{\hbar \sigma_0 A}{e^2 L}, \quad (7)$$

where g_1 is the 1D dimensionless conductance, $D = v_F \ell$ the 1D diffusion constant, v_F the Fermi velocity, and ℓ the mean free path. Writing $E_{\text{Th}} = D/L^2$ this yields $\tau_\varphi \propto (g_1 / \sqrt{E_{\text{Th}} T})^{2/3}$, g_1/T , or $E_{\text{Th}} g_1 / T^2$ for the diffusive ($\tau_T \ll \tau_\varphi \ll \tau_{\text{Th}}$), ergodic ($\tau_T \ll \tau_{\text{Th}} \ll \tau_\varphi$), or 0D ($\tau_{\text{Th}} \ll \tau_T \ll \tau_\varphi$) regimes, respectively, as above (with dimensionful parameters reinstated). Equation (7) illustrates succinctly that the modes dominating dephasing lie near the infrared cutoff ($\omega \approx \tau_\varphi^{-1}$ or E_{Th}) for the diffusive or ergodic regimes but near the ultraviolet cutoff $\omega \approx T$ for the 0D regime [which is why, in the latter, the broadening of $\delta_T(t)$ becomes important].

IV. ANALYTICAL RESULTS

We now turn to a quantitative analysis.²² The diffuson in the ring geometry is¹⁸

$$Q(x) = \frac{L_{\text{dw}} \cosh([L - 2|x|]/2L_{\text{dw}})}{2 \sinh(L/2L_{\text{dw}})}, \quad (8)$$

where $L_{\text{dw}} = \sqrt{D\tau_{\text{dw}}}$ and x is the cyclic coordinate along the ring. Terms of order $\tau_{\text{Th}}/\tau_{\text{dw}}$ (small for an almost isolated ring) do not change the parametric dependence of \mathcal{F} on T, t , and L so that we neglect them below, setting $\tau_{\text{dw}} = \infty$ in Eq. (4). Inserting Eqs. (5), (6), and (8) into Eq. (4), the decay function $\mathcal{F}_n(t)$ for a given winding number n can be calculated as in Ref. 6 but replacing $\delta(t)$ by $\delta_T(t)$:

DIMENSIONAL CROSSOVER OF THE DEPHASING TIME...

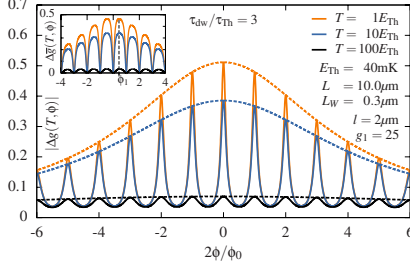
PHYSICAL REVIEW B **80**, 201305(R) (2009)

FIG. 2. (Color online) The WL correction $|\Delta g(T, \phi)|$ (solid lines), its envelope $|\Delta g_{\text{en}}(T, \phi)|$ (dashed lines), and their difference $\Delta \bar{g} = |\Delta g_{\text{en}}| - |\Delta g|$ (inset), plotted as function of magnetic flux $2\phi/\phi_0$, for three different temperatures.

$$\mathcal{F}_n(t) = -\frac{4\pi T t}{g_1 L} \int_0^1 du z(u) \langle Q \rangle_{\text{crw}}(u),$$

$$\langle Q \rangle_{\text{crw}}(u) = \frac{L}{2} \sum_{k=1}^{\infty} \frac{\cos(2\pi k n u)}{(\pi k)^2} e^{-(2\pi k)^2 E_{\text{Th}} t u(1-u)},$$

$$z(u) = -2\pi T t(1-u)w(\pi T t u) + \int_{-\pi T t u}^{\pi T t u} dv w(v). \quad (9)$$

Equation (9) yields the following results for the diffusive,^{1,23} ergodic,⁶ and 0D regimes at $|n| \ll E_{\text{Th}} t$:

$$\mathcal{F}_n(t) \approx \begin{cases} \frac{\delta_{n,0} \pi^{3/2}}{2g_1} \sqrt{E_{\text{Th}} T} t^{3/2}, & \tau_T \ll t \ll \tau_{\text{Th}} & (10a) \\ \frac{\pi T t}{3g_1}, & \tau_T \ll \tau_{\text{Th}} \ll t & (10b) \\ \frac{\pi^2}{270g_1} \frac{T^2 t}{E_{\text{Th}}}, & \tau_{\text{Th}} \ll \tau_T \ll t. & (10c) \end{cases}$$

Subleading terms in the three limiting cases (10a)–(10c) are of order $\mathcal{O}[(\tau_T/t)^{1/2}, (t/\tau_{\text{Th}})^{1/2}]$, $\mathcal{O}[(\tau_T/\tau_{\text{Th}})^{1/2}, \tau_{\text{Th}}/t]$, and $\mathcal{O}[(\tau_{\text{Th}}/\tau_T)^2, (\tau_T/t)]$, respectively. Note that the crossover temperatures where $\tau_{\text{diff}}^{\text{diff}} \approx \tau_{\text{diff}}^{\text{erg}}$ or $\tau_{\text{diff}}^{\text{erg}} \approx \tau_{\text{diff}}^{\text{0D}}$, namely, $c_1 g_1 E_{\text{Th}}$ or $c_2 E_{\text{Th}}$, respectively, involve large prefactors, $c_1 = 27/4 \approx 7$ and $c_2 = 90/\pi \approx 30$, which should aid experimental efforts to reach the 0D regime.

For a ring of rectangular cross section $A = L_w L_H$ and circumference L , the Cooperon can then be written as

$$\mathcal{C}(t) \approx \sum_{n=-\infty}^{+\infty} \frac{e^{-(nL)^2/4Dt}}{\sqrt{4\pi Dt}} e^{-t/\tau_H - \mathcal{F}_n(t) - t/\tau_{\text{dw}}} e^{in\theta}, \quad (11)$$

with (restoring \hbar) $\tau_H = 9.5(\hbar c/eH)^2 \times (l/DL^3)$ and $\theta = 4\pi\phi/\phi_0$, where $\phi = \pi(L/2\pi)^2 H$ is the flux through the ring and $\phi_0 = hc/e$.^{15,16,24} Inserting Eqs. (9) and (11) into Eq. (2) gives the desired WL correction for the ring weakly coupled to leads. The resulting value of $|\Delta g(T, \phi)|$ increases with decreasing T , Fig. 2, in a manner governed by τ_{diff} : since only trajectories with $|n| \lesssim 2\sqrt{t/\tau_{\text{Th}}}$ contribute, the diffusive regime (n restricted to 0) gives $|\Delta g| \propto \sqrt{\tau_{\text{diff}}/\tau_{\text{Th}}}/g_1 \propto (E_{\text{Th}}/g_1^2 T)^{1/3}$, whereas the ergodic regime (sum on n is $\propto t^{1/2}$) gives $|\Delta g| \propto (\tau_{\text{diff}}/\tau_{\text{Th}})/g_1 \propto E_{\text{Th}}/T$, as long as $\tau_{\text{diff}} < \tau_H, \tau_{\text{dw}}$. With decreasing T , the growth of $|\Delta g(T, \phi)|$

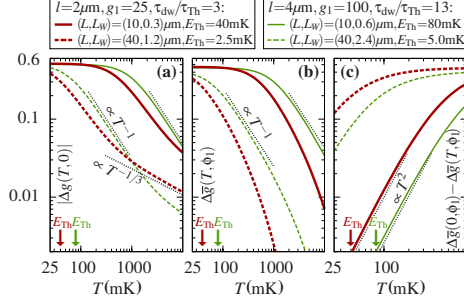


FIG. 3. (Color online) T dependence of (a) the WL correction at zero field, $|\Delta g(T, 0)|$ and (b) at finite field with envelope subtracted, $|\Delta g(T, \phi_1)|$; (c) the difference $\Delta \bar{g}(0, \phi_1) - \Delta \bar{g}(T, \phi_1)$, which reveals a crossover to T^2 behavior for $T \ll 30E_{\text{Th}}$. The flux ϕ_1 , which weakly depends on T , marks the first maximum of $\Delta \bar{g}(T, \phi)$; see inset of Fig. 2.

saturates toward $|\Delta g(0, \phi)|$ once τ_{diff} increases past $\min(\tau_H, \tau_{\text{dw}})$, with $|\Delta g(0, \phi)| - |\Delta g(T, \phi)| \propto \tau_{\text{diff}}^{-1}$ vanishing as T or T^2 in the ergodic or 0D regimes, respectively.

V. FILTERING OUT LEADS

For simplicity, above we did not model the leads explicitly. In real experiments, however, Δg is affected by dephasing in the leads, which might mask the signatures of dephasing in the ring. Similar concerns apply to quantum dots connected to leads (cf. the $\tau_{\text{diff}} \propto T^{-1}$ behavior observed in Ref. 13), or finite-size effects in a network of disordered wires,¹⁵ where paths encircling a given unit cell might spend significant time in neighboring unit cells as well (cf. $T^{-1/3}$ behavior observed in Refs. 15 and 25 at $\tau_{\text{diff}}/\tau_{\text{Th}} \geq 1$). To filter out the effect of leads, we construct¹⁵ from $|\Delta g(T, \phi)|$ its nonoscillatory envelope $|\Delta g_{\text{en}}(T, \phi)|$, obtained by setting $\theta=0$ in Eq. (11) while retaining $\tau_H \neq 0$, and study the difference

$$\Delta \bar{g}(T, \phi) = |\Delta g_{\text{en}}(T, \phi)| - |\Delta g(T, \phi)|. \quad (12)$$

This procedure is illustrated in Fig. 2. $\Delta \bar{g}$ is dominated by paths with winding numbers $n \geq 1$ which belong to the ring. Contributions to $\Delta \bar{g}$ from Cooperons extending over both the ring and a lead will be subleading for well-conducting leads with a small contact-lead-contact return probability. Concretely, for N -channel point contacts with conductance $g_{\text{cont}} = NT_{\text{cont}}$, this requires leads with dimensionless conductance $g_{\text{lead}} \gg N$.²⁶

VI. SUGGESTED EXPERIMENTS

To observe the predicted 1D-to-0D crossover experimentally, several conditions need to be satisfied. Our theory assumes (i) $L \gg \ell \gg L_w \gg \lambda_F$ (λ_F is the Fermi wavelength). Ensuring that we stay in the WL regime requires (ii) a large dimensionless conductance, $g_1 \propto (\ell/L)(L_w L_H/\lambda_F^2) \gg 1$, and (iii) a finite τ_{dw} to limit the growth of Δg with decreasing T ; choosing the limit, somewhat arbitrarily, as $\Delta g \approx \frac{1}{2}$ at $T, H=0$ implies $\tau_{\text{dw}}/\tau_{\text{Th}} \approx g_1/8$. Estimating $\tau_{\text{dw}}/\tau_{\text{Th}} \approx g_1/g_{\text{cont}}$, this implies $8 \lesssim g_{\text{cont}}$ and thus the absence of Coulomb block-

TREIBER *et al.*PHYSICAL REVIEW B **80**, 201305(R) (2009)

ade. (iv) We also need $\tau_{\text{Th}} \ll \tau_{\text{dw}}$, or $g_{\text{cont}} \ll g_1$, to ensure that trajectories with $|n| \geq 1$, responsible for AAS oscillations, remain relevant. (v) To maximize the WL signal, the transmission per channel should be maximal, thus, we suggest $T_{\text{cont}} \approx 1$ and $N \approx 10$. (vi) The relevant temperature range, $[T_{\text{dil}}, T_{\text{ph}}]$, is limited from below by dilution refrigeration ($T_{\text{dil}} \approx 10$ mK) and from above by our neglect of phonons ($T_{\text{ph}} \approx 5$ K). (vii) The ring should be small enough that $c_2 E_{\text{Th}} \gtrsim T_{\text{dil}}$. (viii) The interaction-induced dephasing rate τ_{φ}^{-1} , though decreasing with decreasing T , should for $T \approx T_{\text{dil}}$ not yet be negligible compared to the T -independent rates τ_H^{-1} and τ_{dw}^{-1} . These constraints can be met, e.g., with rings prepared from a 2D GaAs/AlGaAs heterostructure with $\lambda_F \approx 30$ nm, $v_F \approx 2.5 \times 10^5$ m/s, and $g_1 = 4\pi L_W / \lambda_F L$, by adjusting g_1 and E_{Th} by suitably choosing L and L_W .

To illustrate this, numerical results for $|\Delta g|$ and $\Delta \bar{g}$, obtained from Eq. (2) using experimentally realizable parameters,^{9,10,15,27} are shown in Figs. 2 and 3 for several combinations of ℓ , L , and L_W . The regime where Δg exhibits diffusive $T^{-1/3}$ behavior ($7g_1 E_{\text{Th}} \ll T \ll T_{\text{ph}}$) is visible only for our smallest choices of both g_1 and E_{Th} [Fig. 3(a); heavy dashed line]. AAS oscillations in $|\Delta g|$ and $\Delta \bar{g}$ (Fig. 2), which require $\tau_{\text{Th}} \ll \tau_{\varphi}$, first emerge at the crossover from the diffusive to the ergodic regime. They increase in magnitude with

decreasing T , showing ergodic T^{-1} behavior for $30E_{\text{Th}} \ll T \ll 7g_1 E_{\text{Th}}$ [Figs. 3(a) and 3(b)], and eventually saturate toward their $T=0$ values, with $\Delta \bar{g}(0, \phi) - \Delta \bar{g}(T, \phi)$ showing the predicted 0D behavior, $\propto T^2$, for $T \lesssim 5E_{\text{Th}}$, see Fig. 3(c) (there $\tau_{\varphi} \gg \tau_{\text{dw}}$, i.e., dephasing is weak).

VII. CONCLUSIONS

The AAS oscillations of a quasi-1D ring weakly coupled to leads can be exploited to filter out the effects of dephasing in the leads, thus, offering a way to finally observe, for $T \lesssim 5E_{\text{Th}}$, the elusive but fundamental 0D behavior $\tau_{\varphi} \sim T^{-2}$. This would allow *quantitative* experimental tests of the role of temperature as ultraviolet frequency cutoff in the theory of dephasing.

ACKNOWLEDGMENTS

We acknowledge helpful discussions with B. Altshuler, C. Bäuerle, N. Birge, Y. Blanter, P. Brouwer, L. Glazman, Y. Imry, V. Kravtsov, J. Kupferschmidt, A. Mirlin, Y. Nazarov, A. Rosch, D. Weiss, and V. Yudson and support from the DFG through Grant No. SFB TR-12, the Emmy-Noether program, and the Nanosystems Initiative Munich Cluster of Excellence. We also acknowledge support from the NSF under Grant No. PHY05-51164 and from the EPSRC-GB under Grant No. T23725/01.

- ¹B. L. Altshuler, A. G. Aronov, and D. E. Khmel'nitsky, *J. Phys. C* **15**, 7367 (1982).
- ²H. Fukuyama and E. Abrahams, *Phys. Rev. B* **27**, 5976 (1983).
- ³B. L. Altshuler and A. G. Aronov, in *Electron-Electron Interactions in Disordered Systems*, edited by A. L. Efros and M. Pollak (North-Holland, Amsterdam, 1985), Vol. 1.
- ⁴U. Sivan, Y. Imry, and A. G. Aronov, *Europhys. Lett.* **28**, 115 (1994).
- ⁵I. L. Aleiner, B. L. Altshuler, and M. E. Gershenson, *Waves Random Media* **9**, 201 (1999); I. L. Aleiner, B. L. Altshuler, and Y. M. Galperin, *Phys. Rev. B* **63**, 201401(R) (2001); I. L. Aleiner and Y. M. Blanter, *ibid.* **65**, 115317 (2002).
- ⁶T. Ludwig and A. D. Mirlin, *Phys. Rev. B* **69**, 193306 (2004); C. Texier and G. Montambaux, *ibid.* **72**, 115327 (2005).
- ⁷F. Marquardt, J. von Delft, R. A. Smith, and V. Ambegaokar, *Phys. Rev. B* **76**, 195331 (2007).
- ⁸J. von Delft, F. Marquardt, R. A. Smith, and V. Ambegaokar, *Phys. Rev. B* **76**, 195332 (2007).
- ⁹Y. Niimi, Y. Baines, T. Capron, D. Mailly, F. Y. Lo, A. D. Wieck, T. Meunier, L. Saminadayar, and C. Bäuerle, *Phys. Rev. Lett.* **102**, 226801 (2009).
- ¹⁰C. M. Marcus, R. M. Westervelt, P. F. Hopkins, and A. C. Gos-sard, *Phys. Rev. B* **48**, 2460 (1993).
- ¹¹A. Yacoby, M. Heiblum, H. Shtrikman, V. Umansky, and D. Mahalu, *Semicond. Sci. Technol.* **9**, 907 (1994).
- ¹²B. Reulet, H. Bouchiat, and D. Mailly, *Europhys. Lett.* **31**, 305 (1995).
- ¹³A. G. Huibers, M. Switkes, C. M. Marcus, K. Campman, and A. C. Gossard, *Phys. Rev. Lett.* **81**, 200 (1998); A. G. Huibers, S. R. Patel, C. M. Marcus, P. W. Brouwer, C. I. Duruo, and J. S. Harris, *ibid.* **81**, 1917 (1998); A. G. Huibers, J. A. Folk, S. R. Patel, C. M. Marcus, C. I. Duruo, and J. S. Harris, *ibid.* **83**,

5090 (1999).

- ¹⁴A. B. Gougam, F. Pierre, H. Pothier, D. Esteve, and N. O. Birge, *J. Low Temp. Phys.* **118**, 447 (2000).
- ¹⁵M. Ferrier, A. C. H. Rowe, S. Gueron, H. Bouchiat, C. Texier, and G. Montambaux, *Phys. Rev. Lett.* **100**, 146802 (2008).
- ¹⁶B. L. Altshuler, A. G. Aronov, and B. Z. Spivak, *JETP Lett.* **33**, 94 (1981).
- ¹⁷L. P. Gor'kov, A. I. Larkin, and D. E. Khmel'nitskii, *JETP Lett.* **30**, 228 (1979).
- ¹⁸E. Akkermans and G. Montambaux, *Mesoscopic Physics of Electrons and Photons* (Cambridge University Press, Cambridge, 2007).
- ¹⁹D. E. Khmel'nitskii, *Physica B+C* **126**, 235 (1984).
- ²⁰B. L. Altshuler and A. G. Aronov, *JETP Lett.* **33**, 499 (1981).
- ²¹P. W. Brouwer and C. W. J. Beenakker, *Phys. Rev. B* **55**, 4695 (1997); E. McCann and I. V. Lerner, *ibid.* **57**, 7219 (1998).
- ²²Quantitative details and an alternative approach based on the kinetic equation will be presented elsewhere.
- ²³Closed trajectories with $n \neq 0$ contribute only weakly to $\Delta \sigma$ at $t \ll \tau_{\text{Th}}$; see Eq. (11). That is why we do not include the case $n \neq 0$ in Eq. (10a) (Ref. 6).
- ²⁴For specular boundary scattering in a channel geometry, see C. W. J. Beenakker and H. van Houten, *Phys. Rev. B* **38**, 3232 (1988).
- ²⁵Note that 0D dephasing can not be observed in a network of well-connected unit cells, since trajectories are effectively not confined at $\tau_{\varphi} / \tau_{\text{Th}} \gg 1$.
- ²⁶J. N. Kupferschmidt and P. W. Brouwer (private communication).
- ²⁷O. Yevtushenko, G. Lutjering, D. Weiss, and K. Richter, *Phys. Rev. Lett.* **84**, 542 (2000).

3.5 Publication: Dimensional Crossover of the Dephasing Time in Disordered Mesoscopic Rings: From Diffusive through Ergodic to 0D Behavior

The following 26 pages have been published as *Chapter 20* in the book *Perspectives of Mesoscopic Physics: Dedicated to Yoseph Imry's 70th Birthday*, edited by A. Aharony and O. Entin-Wohlman (World Scientific, Singapore, 2010).

Chapter 20

Dimensional Crossover of the Dephasing Time in Disordered Mesoscopic Rings: From Diffusive through Ergodic to 0D Behavior

M. Treiber, O.M. Yevtushenko, F. Marquardt and J. von Delft
Arnold Sommerfeld Center and Center for Nano-Science, Ludwig Maximilians University, Munich, D-80333, Germany

I.V. Lerner

School of Physics and Astronomy, University of Birmingham, Birmingham, B15 2TT, UK

We analyze dephasing by electron interactions in a small disordered quasi-one dimensional (1D) ring weakly coupled to leads, where we recently predicted a crossover for the dephasing time $\tau_\varphi(T)$ from diffusive or ergodic 1D ($\tau_\varphi^{-1} \propto T^{2/3}, T^1$) to 0D behavior ($\tau_\varphi^{-1} \propto T^2$) as T drops below the Thouless energy E_{Th} .¹ We provide a detailed derivation of our results, based on an influence functional for quantum Nyquist noise, and calculate all leading and subleading terms of the dephasing time in the three regimes. Explicitly taking into account the Pauli blocking of the Fermi sea in the metal allows us to describe the 0D regime on equal footing as the others. The crossover to 0D, predicted by Sivan, Imry and Aronov for 3D systems,² has so far eluded experimental observation. We will show that for $T \ll E_{\text{Th}}$, 0D dephasing governs not only the T -dependence for the smooth part of the magnetoconductivity but also for the amplitude of the Altshuler-Aronov-Spivak oscillations, which result only from electron paths winding around the ring. This observation can be exploited to filter out and eliminate contributions to dephasing from trajectories which do not wind around the ring, which may tend to mask the T^2 behavior. Thus, the ring geometry holds promise of finally observing the crossover to 0D experimentally.

20.1. Introduction

Over the last twenty-five years many theoretical and experimental works addressed quantum phenomena in mesoscopic disordered metallic rings.³

This subject was launched in part by several seminal papers by Joe Imry and his collaborators^{4–11}, and continues to be of great current interest. One intensively-studied topic involves persistent currents, which can flow without dissipation due to quantum interference in rings prepared from normal metals.^{4,12–15} Attention was also paid to Aharonov-Bohm oscillations in the conductance through a mesoscopic ring attached to two leads,^{5–7,10,16} and the closely related oscillations of the negative weak localization (WL) correction to the magnetoconductivity.^{17,18} These oscillations result from the interference of closed trajectories which have a non-zero winding number acquiring the Aharonov-Bohm phase. Both persistent currents and magnetooscillations require the ring to be phase coherent, since any uncertainty of the quantum phase due to the environment or interactions immediately suppresses all interference phenomena.¹⁹

The mechanism of dephasing in electronic transport and its dependence on temperature T in disordered conductors was studied in numerous theoretical^{2,19–27} and experimental^{28–35} works. The characteristic time scale of dephasing is called the dephasing time τ_φ . At low temperatures phonons are frozen out and dephasing is mainly due to electron interactions, with the dephasing time $\tau_\varphi(T)$ increasing as T^{-a} when $T \rightarrow 0$, $a > 0$.

The scaling of the dephasing time with temperature depends on the dimensionality of the sample.²⁰ It was predicted in a pioneering paper by Sivan, Imry and Aronov² that the dephasing time in a disordered quantum dot shows a dimensional crossover from $\tau_\varphi \propto T^{-1}$, typical for a $2D$ electron gas,²⁰ to $\tau_\varphi \propto T^{-2}$ when the temperature is lowered into the $0D$ regime:

$$\hbar/\tau_\varphi \ll T \ll \hbar/\tau_{\text{Th}}, \quad (20.1)$$

where $\tau_{\text{Th}} = \hbar/E_{\text{Th}}$ is the Thouless time, i.e. the time required for an electron to cross (diffusively or ballistically) the mesoscopic sample; E_{Th} is the Thouless energy. In this low- T , $0D$ regime, the coherence length and the thermal length are both larger than the system size, independent of geometry and real dimensionality of the sample. In this regime WL is practically the only tool to measure the T -dependence of dephasing in mesoscopic wires or quantum dots (the mesoscopic conductance fluctuations go over to a universal value of order e^2/h for $T \ll E_{\text{Th}}$ ³).

Although the $\tau_\varphi \propto T^{-2}$ behavior is quite generic, arising from the fermionic statistics of conduction electrons, experimental efforts^{31–33} to observe it have so far been unsuccessful. The reasons for this are today still unclear. Conceivably dephasing mechanisms other than electron interactions were dominant, or the regime of validity of the $0D$ description

had not been reached. In any case, other ways of testing the dimensional crossover for τ_φ are desirable.

In a recent paper,¹ we described the crossover of the dephasing time to the $0D$ regime in a mesoscopic ring weakly coupled to leads. We considered a ring of the type shown in Fig. 20.1 with dimensionless $1D$ conductance

$$g_1 = \frac{h\sigma_0 A}{e^2 L}, \quad (20.2)$$

where A and L are the ring's cross section and circumference and σ_0 is its classical Drude conductivity. In the present paper we give a detailed derivation of our results based on an influence functional approach for *quantum noise*. This approach explicitly takes into account the Pauli blocking of the electrons in the metal, which will allow us to describe quantitatively all regimes of the dephasing time in a quasi- $1D$ ring on an equal footing and to calculate first order correction terms to the dephasing time. In particular, we will see that Pauli blocking dominates the regime of $0D$ dephasing. We find that in the $0D$ regime, T^{-2} behavior also emerges for the amplitude of the Altshuler-Aronov-Spivak (AAS) oscillations of the conductivity¹⁷ in a magnetic field, which arise from pairs of time-reversed paths encircling the ring at least once. A necessary requirement to reach this regime is that electron trajectories are effectively confined in the system. Thus the conductance through the contact, g_{cont} , is assumed to be much smaller than g_1 , such that the time an electron spends inside the ring, the dwelling time τ_{dw} , is much larger than the time an electron needs to explore the whole ring, i.e. the Thouless time τ_{Th} .

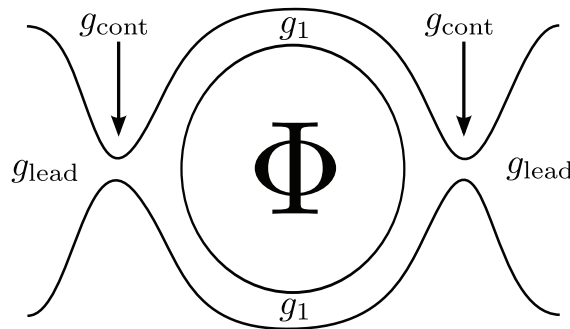


Fig. 20.1. A ring weakly coupled to leads: We assume a metallic system, where the conductance at the contacts g_{cont} is much smaller than the conductance of the ring g_1 and of the lead g_{lead} , i.e. $(g_{\text{lead}}, g_1) \gg g_{\text{cont}} \gg 1$. This assures (a) that the average time electrons spend in the ring (τ_{dw}) is much larger than the average time they need to explore the whole ring (τ_{Th}) and (b) that the probability for electrons which escaped from the ring to return back to it is small.

We will show below that after subtracting from the amplitude of the AAS-oscillations the non-oscillating background, only contributions to dephasing from paths encircling the ring will contribute. However, some of these paths may involve loops which not only encircle the ring, but along the way also enter the lead and reenter the ring (see Fig. 20.6(b) below). Such lead-ring cross-contributions to dephasing will contribute a non- $0D$ T -dependence to the conductance and hence tend to mask the $0D$ behavior. We shall argue that by additionally choosing the conductance of the connected leads, g_{lead} , to be larger than g_{cont} , dephasing due to lead-ring cross-contributions, can be neglected, and the remaining contributions will be characterized by $0D$ dephasing.

20.2. Dephasing and Weak Localization

In a disordered metal, the conductivity is reduced by coherent backscattering of the electrons from impurities, an effect known as weak localization (WL). In a semi-classical picture it can be understood as the constructive interference of closed, time-reversed random-walks through the metal's impurity landscape. It is most pronounced in systems of low dimensionality d where the integrated return probability becomes large for long times. For an infinite system characterized by the diffusion constant $D = v_F l / d$ (v_F is the Fermi velocity and l is the mean free path), the probability of a random walk of duration t to return back to its origin is given by

$$\mathcal{C}_0(t) = (4\pi Dt)^{-d/2}. \quad (20.3)$$

To leading order in $1/g_1$, the relative correction to the conductance (20.2) can be written as

$$\Delta g = \frac{\Delta \sigma}{\sigma_0} = -\frac{1}{\pi \nu} \int_0^\infty dt \mathcal{C}(t), \quad (20.4)$$

where ν is the density of states per volume in the ring and we have set $\hbar = 1$ henceforth. The function $\mathcal{C}(t)$ is the so called Cooperon propagator corresponding to the interference amplitude of the time-reversed random walks. $\mathcal{C}(t)$ reduces to Eq. (20.3) if time-reversal symmetry is fully preserved. Processes which destroy this symmetry lead to a suppression of this contribution at long times, since the random walks and their time-reversed counterparts acquire a different phase. The model we are considering assumes a suppression of the Cooperon of the following form

$$\mathcal{C}(t) \equiv \mathcal{C}_0(t) \exp[-t/\tau_H - t/\tau_{\text{dw}} - \mathcal{F}(t)]. \quad (20.5)$$

In Eq. (20.5), we consider dephasing due to the effect of an external magnetic field leading to the cutoff $\tau_H \sim 1/H$ of the integral in Eq. (20.4).⁴³ Furthermore, our model of an almost isolated ring assumes an average dwelling time, τ_{dw} , of the electrons in the ring.⁴⁵

Our primary interest is the effect of electron interactions, which we describe in terms of the *Cooperon decay function* $\mathcal{F}(t)$, which grows with time and may be used to define a dephasing time via

$$\mathcal{F}(\tau_\varphi) = 1. \quad (20.6)$$

Dephasing due to electron interactions can be understood roughly as follows: At finite temperatures the interactions lead to thermal fluctuations (noise) of the electron's potential energy $V(\mathbf{x}, t)$. Then the closed paths contributing to WL and their time-reversed counterparts effectively "see" a different local potential, leading to a phase difference. This is most clearly seen in a path integral representation of the Cooperon in a time-dependent potential,²⁰ which is given by

$$\mathcal{C}(t) \propto \int_{\mathbf{x}(0)=\mathbf{x}_0}^{\mathbf{x}(t)=\mathbf{x}_0} \mathcal{D}\mathbf{x} e^{i\varphi(t)} e^{-\int_0^t dt_1 \mathcal{L}(t_1)}. \quad (20.7)$$

Here the Lagrangian $\mathcal{L}(t_1) = \dot{\mathbf{x}}^2(t_1)/4D$ describes diffusive propagation, and $\varphi(t)$ is a phase corresponding to the time-reversed structure of the Cooperon:

$$\varphi(t) = \int_0^t dt_1 [V(\mathbf{x}(t_1), t_1) - V(\mathbf{x}(t_1), t - t_1)]. \quad (20.8)$$

Assuming that the noise induced by electron interactions is Gaussian, the decay function $\mathcal{F}(t)$ in Eq. (20.5) can be estimated from $\mathcal{F}(t) = \frac{1}{2} \overline{\langle \varphi^2 \rangle}_{\text{crw}}$, where $\overline{\dots}$ denotes averaging over realizations of the noise and $\langle \dots \rangle_{\text{crw}}$ over closed random walks of duration t from \mathbf{x}_0 back to \mathbf{x}_0 . $\mathcal{F}(t)$ is then given in terms of a difference of the noise correlation functions, taken at reversed instances of time:

$$\mathcal{F}(t) = \int_0^t d^2 t_{1,2} \left\langle \overline{V V}(\mathbf{x}_{12}, t_{12}) - \overline{V V}(\mathbf{x}_{12}, \bar{t}_{12}) \right\rangle_{\text{crw}}. \quad (20.9)$$

Here $t_{12} = t_1 - t_2$ and $\bar{t}_{12} = t_1 + t_2 - t$, while $\mathbf{x}_{12} = \mathbf{x}(t_1) - \mathbf{x}(t_2)$ is the distance of two points of the closed random walk taken at times t_1 and t_2 . For an infinite wire and the case of classical Nyquist noise (defined in Eq. (20.11) below), Eq. (20.9) has been shown^{26,27} to give results practically equivalent to the exact results obtained in Ref. [20].

20.3. Thermal Noise due to Electron Interactions

Electron interactions in the metal lead to thermal fluctuations of the electric field \mathbf{E} , producing so-called Nyquist noise. In the high temperature limit, it can be obtained from the classical Fluctuation-Dissipation Theorem leading to a field-field correlation function in 3D of the form

$$\overline{\mathbf{E}\mathbf{E}}(\mathbf{q}, \omega) \xrightarrow{|\omega| \ll T} \frac{2T}{\sigma_0}. \quad (20.10)$$

Note that the fluctuations of the fields do not depend on \mathbf{q} or ω , i.e. they correspond to white noise in space and time. To describe dephasing in a quasi-1D wire, we need the correlation function of the corresponding scalar potentials V in a quasi-1D wire. Since $E = \frac{1}{e}\nabla V$, the noise correlator that corresponds to the classical limit (20.10) has the form

$$\overline{VV}_{\text{class}}(\mathbf{q}, \omega) = \frac{2Te^2}{\sigma_0} \frac{1}{\mathbf{q}^2}. \quad (20.11)$$

This so-called classical Nyquist noise is frequency independent, i.e. corresponds to “white noise”. For present purposes, however, we need its generalization to the case of quantum noise, valid for arbitrary ratios of $|\omega|/T$. In particular, \overline{VV} is expected to become frequency-dependent: it should go to zero for $|\omega| \gg T$, since the Pauli principle prevents scattering processes into final states occupied by other electrons in the Fermi sea.³⁸ A careful analysis of quantum noise has been given recently in Ref. [26] and Ref. [27]. The authors derived an effective correlation function for the quantum noise potentials that properly accounts for the Pauli principle. It is given by

$$\overline{VV}(\mathbf{q}, \omega) = \text{Im}\mathcal{L}^R(\mathbf{q}, \omega) \frac{\omega/2T}{\sinh(\omega/2T)^2} \quad (20.12)$$

with

$$\mathcal{L}^R(\mathbf{q}, \omega) = -\frac{D\mathbf{q}^2 - i\omega}{2\nu D\mathbf{q}^2 + (D\mathbf{q}^2 - i\omega)/V(\mathbf{q})}; \quad (20.13)$$

$V(q)$ is the Fourier-transformed bare Coulomb potential (not renormalized due to diffusion) in the given effective dimensionality.

If the momentum and energy transfer which dominates dephasing is small then the second term of the denominator of Eq. (20.13) can be neglected so that Eq. (20.13) reduces to

$$\text{Im}\mathcal{L}^R(\mathbf{q}, \omega) \simeq \frac{\omega}{2\nu D\mathbf{q}^2}. \quad (20.14)$$

This simplification holds true, in particular, in the high temperature (diffusive) regime where $\omega \ll T$.²⁰ We will argue below (see Eqs. (20.54) to (20.57)) that the same simplification can be used in the low temperature regime where $|\omega| \sim T \lesssim E_{\text{Th}}$.¹

Inserting Eq. (20.14) in Eq. (20.12) with $\sigma_0 = 2e^2\nu D/A$, where A is the cross-section perpendicular to the current direction, we obtain

$$\overline{VV}(\mathbf{q}, \omega) = \frac{2e^2 T}{\sigma_0 A} \frac{1}{\mathbf{q}^2} \left(\frac{\omega/2T}{\sinh(\omega/2T)} \right)^2. \quad (20.15)$$

In the time and space domain, this correlator factorizes into a product of time- and space-dependent parts:

$$\overline{VV}(\mathbf{x}, t) = \frac{2e^2 T}{\sigma_0 A} Q(\mathbf{x}) \delta_T(t), \quad (20.16)$$

where $\delta_T(t)$ is a broadened delta function of width $1/T$ and height T :

$$\delta_T(t) = \pi T w(\pi T t), \quad w(y) = \frac{y \coth(y) - 1}{\sinh^2(y)}. \quad (20.17)$$

The fact that the noise correlator (20.16) is proportional to a *broadened* peak $\delta_T(t)$ is a direct consequence of the effects of Pauli blocking. Previous approaches often used a sharp Dirac-delta peak instead. In the frequency domain this corresponds to white noise and leads to (20.11), instead of our frequency-dependent form (20.12). Such a ‘‘classical’’ treatment reproduces correct results for the dephasing time when processes with small energy transfers $|\omega| \ll T$ dominate. However, it has been shown in Ref. [2] that this is in fact not the case in the $0D$ limit $T \ll E_{\text{Th}}$, where the main contribution to dephasing is due to processes with $|\omega| \simeq T$. Thus, the results become dependent on the form of the cutoff that eliminates modes with $|\omega| > T$ to account for the Pauli principle. For such purposes, previous treatments typically introduced a sharp cutoff, $\theta(T - |\omega|)$, by hand. However, the precise form of the cutoff becomes important in an analysis interested not only in qualitative features, but quantitative details. The virtue of (20.11) is that it encodes the cutoff in a quantitatively reliable fashion. (For example, it was shown²⁶ to reproduce a result first obtained in Ref. [23], namely the subleading term in an expansion of the large-field magnetoconductance (for quasi-1D wires) in powers of the small parameter $1/\sqrt{T\tau_H}$.)

The position-dependent part of Eq. (20.16), the so-called diffuson at zero frequency $Q(\mathbf{x})$, is the time-integrated solution of the diffusion equation. In the isolated system, it satisfies

$$-\Delta Q(\mathbf{x}) = \delta(\mathbf{x}), \quad (20.18)$$

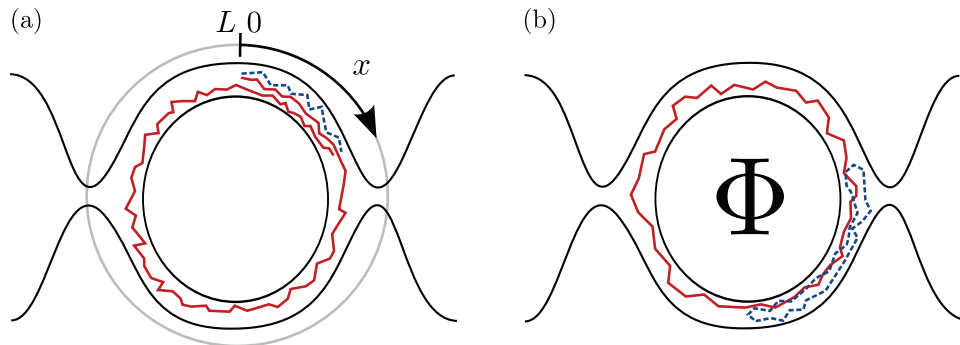


Fig. 20.2. (a) Illustration of our choice of the coordinate system: Both paths have the same start and end point ($0 \mapsto x$), but the dashed path has winding number $n = 0$ and the solid path $n = 1$. (b) Two *closed* paths in the ring contributing to the Cooperon. The contribution of the solid path (with winding number $n = 1$) is affected by the flux Φ , since the path (and its time-reversed counterpart) acquire an Aharonov-Bohm phase when interfering with itself at their origin. This gives rise to the Altshuler-Aharonov-Spivak oscillations. The dashed path with $n = 0$ is unaffected by the flux, since the acquired phase at the origin is zero.

with given boundary conditions, which govern the distribution of the eigenmodes of Q . In an isolated system, where a $\mathbf{q} = 0$ mode is present, $Q(\mathbf{x})$ diverges. However, the decay function is still regular, since terms in Q which do not depend on \mathbf{x} simply cancel out in Eq. (20.9) and cannot contribute to dephasing.

To evaluate the decay function Eq. (20.9), we note that only the factor $Q(\mathbf{x})$ in Eq. (20.16) depends on \mathbf{x} , thus, the average $\langle Q(\mathbf{x}) \rangle_{\text{crw}}$ has to be calculated. This will be done in the next section for an almost isolated ring. Then, after a qualitative discussion in 20.5, we proceed by evaluating $\mathcal{F}(t)$ in section 20.6.

20.4. Diffusion in the almost Isolated Ring

The probability density of a random walk in a $1D$, infinite, isotropic medium to travel the distance x in time t is given by

$$P_0(x, t) = \frac{1}{\sqrt{4\pi Dt}} e^{-x^2/4Dt}. \quad (20.19)$$

In an isolated ring, electrons can reach each point without or after winding around the ring n times, where n is called *winding number*. Denoting the probability density for the latter type of path by $P_n(x, t)$, the diffusion

probability density can be expanded in n as

$$P(x, t) = \sum_{n=-\infty}^{+\infty} P_n(x, t), \quad P_n(x, t) = \frac{1}{\sqrt{4\pi Dt}} e^{-(x+nL)^2/4Dt}, \quad (20.20)$$

where L is the circumference of the ring and $x \in [0, L]$ is the cyclic coordinate along the ring, see Fig. 20.2(a). To model the effect of the two contacts of the ring, we assume that an electron, on average, stays inside the ring only for the duration of the dwelling time τ_{dw} , introduced in Eq. (20.5), and then escapes with a vanishing return probability. This simplified model of homogeneous dissipation, strictly applicable only in the limit $\tau_{\text{Th}} \ll \tau_{\text{dw}}$ and for a very large lead conductance, captures all the essential physics of the $0D$ crossover we are interested in. Our present assumptions lead to the following replacement of the diffusion probability density:

$$P(x, t) \rightarrow P(x, t) e^{-t/\tau_{\text{dw}}}. \quad (20.21)$$

Furthermore, the spatial dependence of the noise correlation function (20.13) acquires an additional dissipation term in the denominator. Thus, in contrast to the isolated case, $Q(x)$ now satisfies the Laplace transform of the diffusion equation, given by

$$\left[\frac{1}{L_{\text{dw}}^2} - \Delta \right] Q(x) = \delta(x), \quad (20.22)$$

where $L_{\text{dw}} = \sqrt{\tau_{\text{dw}} D}$. For a ring with circumference L we obtain

$$Q(x) = \frac{L_{\text{dw}}}{2} \frac{\cosh\left([L - 2|x|]/2L_{\text{dw}}\right)}{\sinh(L/2L_{\text{dw}})}. \quad (20.23)$$

We can expand Eq. (20.23) for the almost isolated ring in powers of $\tau_{\text{Th}}/\tau_{\text{dw}} \ll 1$:

$$Q(x) \approx C - \frac{|x|}{2} \left(1 - \frac{|x|}{L} \right) + \mathcal{O}\left(\frac{\tau_{\text{Th}}}{\tau_{\text{dw}}}\right), \quad (20.24)$$

where the x -independent first term, $C = L\tau_{\text{dw}}/\tau_{\text{Th}}$, describes the contribution of the zero mode. As expected, see the discussion after Eq. (20.18), it diverges in the limit $\tau_{\text{Th}}/\tau_{\text{dw}} \rightarrow 0$.

Having described the diffuson in our model of the almost isolated ring, we can proceed by calculating the closed random walk average (crw) of Eq. (20.24). We will see below that we need to consider the random walk

average with respect to closed paths with a specific winding number n only. For an isolated ring, using Eq. (20.20), it can be written as

$$\langle Q \rangle_{\text{crw}}(t_{12}, n) = \int_0^L d^2 x_{1,2} Q(x_{12}) P_{\text{crw}}(x_{12}, t_{12}, n), \quad (20.25)$$

with

$$P_{\text{crw}}(x_{12}, t_{12}, n) = \sum_{i+j+k=n} \frac{P_i(x_{01}, t_1) P_j(x_{12}, t_{21}) P_k(x_{20}, t - t_2)}{P_n(0, t)}, \quad (20.26)$$

where we used the notation $x_{\alpha\beta} = x_\alpha - x_\beta$ and $t_{\alpha\beta} = t_\alpha - t_\beta$. Obviously, the replacement (20.21) does not affect this averaging procedure, so that it remains valid in our model of homogeneous dissipation. Note that the expression (20.26) depends in fact only on x_{12} and not on x_0 , as can be verified by integrating both sides of the equation over x_0 using the following semi-group property in the ring:

$$\int_0^L dx_2 P_l(x_{12}, t_1) P_m(x_{23}, t_2) = P_{l+m}(x_{13}, t_1 + t_2). \quad (20.27)$$

Doing the average of Eq. (20.23) according to Eq. (20.25), we finally obtain

$$\langle Q \rangle_{\text{crw}}(t_{12}, n) = C - \frac{L}{2} \sum_{k=1}^{\infty} \frac{\cos(2\pi knu)}{(\pi k)^2} e^{-(2\pi k)^2 E_{\text{Th}} t_{12}(1-t_{12}/t)}. \quad (20.28)$$

It follows that a finite dissipation rate does not affect the decay function to leading order in $\tau_{\text{Th}}/\tau_{\text{dw}}$.

For the Cooperon, an expansion similar to Eq. (20.20) can be done. In addition to that, the dependence of the Cooperon on an external magnetic field changes due to the ring geometry. It not only leads to the suppression of the Cooperon at long times, but also, due to the Aharonov-Bohm effect, to Altshuler-Aronov-Spivak oscillations¹⁷ of the WL-correction, see Fig. 20.2(b). Combining these remarks with Eq. (20.5) and inserting Eq. (20.3) with $d = 1$, we write the Cooperon in our model as

$$\mathcal{C}(t) = \sum_{n=-\infty}^{+\infty} \frac{e^{-(nL)^2/4Dt}}{\sqrt{4\pi Dt}} e^{-t/\tau_H - t/\tau_{\text{dw}} - \mathcal{F}_n(t)} e^{in\theta}, \quad (20.29)$$

where $\theta = 4\pi\phi/\phi_0$ and $\phi = \pi(L/2\pi)^2 H$ is the flux through the ring ($\phi_0 = 2\pi c/e$ is the flux quantum). Note that the decay function \mathcal{F} is now a function of n : Since we used an expansion in winding numbers n , we should consider the phase (20.8) acquired by paths with the winding number n only. Thus, the crw-average in Eq. (20.9) has to be performed with respect to paths with given winding number n only, as anticipated in Eq. (20.25).

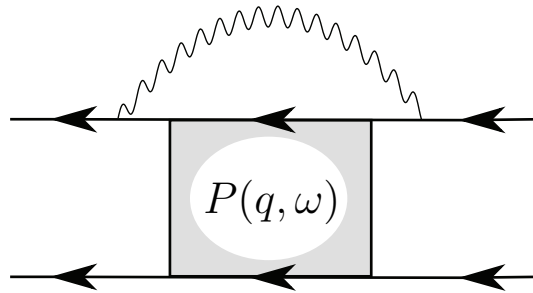


Fig. 20.3. Typical diagram from the expansion of the Cooperon self energy. The shaded area denotes impurity lines, described by the diffusion propagator Eq. (20.31). The upper solid lines correspond to a retarded electron Green's function and the lower to an advanced (or vice versa). Wiggly lines denote electron interactions, described by Eq. (20.16).

20.5. Qualitative Picture from the Perturbative Expansion of the Cooperon

In our previous paper¹ we showed how all the regimes of the dephasing time in an isolated ring can be understood qualitatively from the influence functional picture. In particular, we demonstrated how $0D$ dephasing emerges from the assumption of a noise field that is effectively “frozen” on the time scale τ_{Th} (since $|\omega| \simeq T \ll E_{\text{Th}}$), leading to a drastically reduced dephasing rate. The qualitative behavior of τ_φ also follows from the standard perturbative expression for the Cooperon self-energy. Such self-energy diagrams are of the type shown in Fig. 20.3 and were first evaluated in Ref. [21]. This diagram and its complex conjugate give contributions to the dephasing time of the form

$$\frac{1}{\tau_\varphi} \propto \int d\omega \int dq \overline{V}V(q, \omega) \text{Re}[P(q, \omega)] , \quad (20.30)$$

where the diffuson $P(q, \omega)$ is given by the Fourier transform of Eq. (20.19):

$$P(q, \omega) = \frac{1}{Dq^2 - i\omega} . \quad (20.31)$$

We have already mentioned that large energy transfers are suppressed according to Eq. (20.15) leading to an upper cutoff at T of the frequency integration. Furthermore, it was shown in Refs. [26,27] that vertex contributions to these self-energy diagrams cure the infrared divergences in the frequency integration, leading to a cutoff at $1/\tau_\varphi$. Such fluctuations are simply too slow to influence the relevant paths. Note that in contrast to the perturbative treatment presented in this section, the path integral calculation leading to the expression Eq. (20.9) for the decay function is free of

these IR divergences. In fact, it was shown that the first term of Eq. (20.9) corresponds, when compared to a diagrammatic evaluation of the Cooperon self-energy, to the so-called self-energy contributions (shown in Fig. 20.3), while the second term corresponds to the so-called vertex contributions.

In the ring geometry, the diffuson has quantized momenta and the $q = 0$ mode can not contribute. For a qualitative discussion we may take this into account by inserting a lower cutoff $1/L$ of the momentum integration.

Taking into account the above remarks, we can estimate the dephasing time as

$$\frac{1}{\tau_\varphi} \propto \frac{T}{g_1 L} \int_{1/\tau_\varphi}^T d\omega \int_{1/L}^\infty dq \frac{D}{(Dq^2)^2 + \omega^2}. \quad (20.32)$$

Eq. (20.32) illustrates succinctly that the modes dominating dephasing lie near the infrared cutoff ($\omega \simeq \tau_\varphi^{-1}$ or E_{Th}) for the diffusive or ergodic regimes, but near the ultraviolet cutoff $\omega \simeq T$ for the 0D regime, which is why, in the latter, the broadening of $\delta_T(t)$ becomes important. Performing the integrals in Eq. (1.28) and solving for τ_φ self-consistently, we find three regimes:

(1) The *diffusive regime*, for $\tau_T \ll \tau_\varphi \ll \tau_{\text{Th}}$, with

$$\tau_\varphi \propto (g_1/\sqrt{E_{\text{Th}}T})^{2/3}; \quad (20.33)$$

(2) the *ergodic regime*, for $\tau_T \ll \tau_{\text{Th}} \ll \tau_\varphi$, with

$$\tau_\varphi \propto g_1/T; \quad (20.34)$$

(3) and the *0D regime*, reached at $\tau_{\text{Th}} \ll \tau_T \ll \tau_\varphi$, with

$$\tau_\varphi \propto g_1 E_{\text{Th}}/T^2. \quad (20.35)$$

Here, $\tau_T = \sqrt{D/T}$ is the thermal time. Expressing (20.35) in terms of the level spacing $\delta = E_{\text{Th}}/g_1$ we find $\tau_\varphi \delta \propto E_{\text{Th}}^2/T^2$. This ratio is $\gg 1$ in the 0D regime, implying that dephasing is so weak that the dephasing rate $1/\tau_\varphi$ is smaller than the level spacing.

20.6. Results for the Cooperon Decay Function

For a systematic analysis of the Cooperon decay function, we rewrite Eq. (20.9) in terms of an integral over the dimensionless variable $u = t_{12}/t$:

$$\mathcal{F}_n(t) = \frac{4\pi T t}{g_1} \int_0^1 du z(u) q_n(u), \quad (20.36)$$

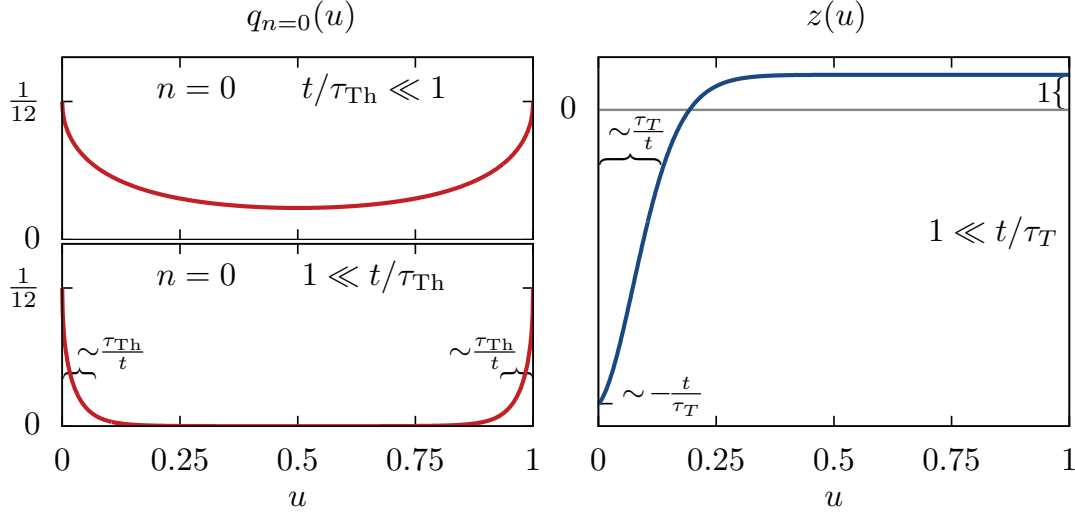


Fig. 20.4. Functions $q_{n=0}(u)$ (left panel) defined in Eq. (20.38) and $z(u)$ (right panel) defined in Eq. (20.37).

where the kernel

$$z(u) = -2\pi T t (1-u) w(\pi T t u) + \int_{-\pi T t u}^{\pi T t u} dv w(v) \quad (20.37)$$

depends on the parameter $tT = t/\tau_T$, and the dimensionless crw-averaged diffuson

$$q_n(u) = \frac{\langle Q \rangle_{\text{crw}}(ut) - C}{L} = -\frac{1}{2} \sum_{k=1}^{\infty} \frac{\cos(2\pi k n u)}{(\pi k)^2} e^{-(2\pi k)^2 (t/\tau_{\text{Th}}) u(1-u)}, \quad (20.38)$$

depends on t/τ_{Th} , see Eq. (20.28). Note that we can add or subtract an arbitrary number from $q_n(u)$ without changing the result, since constant terms in $q_n(u)$, describing the zero mode, do not contribute to dephasing, because of the following property of $z(u)$:

$$\int_0^1 du z(u) = 0. \quad (20.39)$$

Both functions, Eq. (20.37) and Eq. (20.38), are illustrated in Fig 20.4 in all relevant limiting cases. Note that in the regime of WL we always have $\tau_T \ll t$. In the opposite regime the interaction correction to the conductivity (Altshuler-Aronov correction) originating from the Friedel oscillations dominate,⁴⁸ which we do not consider here.

We proceed with an asymptotic evaluation of Eq. (20.36). For large t/τ_{Th} , $q_n(u)$ is non-zero ($\simeq \frac{1}{12}$) only in the intervals $0 < u < \tau_{\text{Th}}/t$ and

$1 - \tau_{\text{Th}}/t < u < 1$, see Fig. 20.4. For small t/τ_{Th} and $n = 0$ we can use the expansion

$$q_{n=0}(u) \approx \frac{1}{12} - \frac{1}{\sqrt{\pi}} \sqrt{\frac{t}{\tau_{\text{Th}}}} (u(1-u)) + \frac{t}{\tau_{\text{Th}}} (u(1-u)). \quad (20.40)$$

For larger n the exponential function in Eq. (20.38) can be expanded since the sum converges at $k \simeq 1$.

For $\tau_T \ll t$, $z(u)$ is large ($\sim -t/\tau_T$) in the interval $0 < u < \tau_T/t$ and $z(u) \approx 1$ otherwise. Thus, it will be convenient to decompose $z(u) = \bar{z} + \tilde{z}(u)$ into a constant part $\bar{z} = +1$ and a peaked part $\tilde{z}(u) = z(u) - 1$. For contributions of the peaked type one observes that

$$\int_0^1 du \tilde{z}(u) u^s = \begin{cases} -1, & s = 0; \\ -\sqrt{\frac{\tau_T}{t}} \frac{\sqrt{2\pi}}{4} |\zeta(\frac{1}{2})|, & s = 1/2; \\ -\frac{\tau_T}{t}, & s = 1. \end{cases} \quad (20.41)$$

We identify the following 3 regimes:

Diffusive regime $\tau_T \ll t \ll \tau_{\text{Th}}$ and $n = 0$: Here we can use the expansion Eq. (20.40). The constant term does not contribute, due to Eq. (20.39). The main contribution to the integral comes from values of u where $z(u) \approx 1$. Thus, we decompose $z(u) = \bar{z} + \tilde{z}(u)$ as suggested above. The leading result and corrections $\propto \sqrt{t/\tau_{\text{Th}}}$ due to the second and third term in Eq. (20.40) stem from \bar{z} . Corrections $\propto \sqrt{t/\tau_T}$ can be calculated with the help of Eq. (20.41) with $s = 1/2$ from the $\tilde{z}(u)$ part. In total we obtain for $n = 0$:

$$\mathcal{F}_{n=0}(t) = \frac{\pi^{3/2} \sqrt{E_{\text{Th}}}}{2g_1} T t^{3/2} \left(1 + \frac{2^{3/2} \zeta(\frac{1}{2})}{\pi} \frac{1}{\sqrt{tT}} - \frac{4}{3\sqrt{\pi}} \sqrt{\frac{t}{\tau_{\text{Th}}}} \right). \quad (20.42)$$

Diffusive regime $\tau_T \ll t \ll \tau_{\text{Th}}$ and $|n| > 0$: For winding numbers larger than zero, we expand the exponential function in (20.38). In contrast to the case of $n = 0$, the leading result comes here from the peaked part $\tilde{z}(u)$. After expanding the exponential function and doing the sum over k , we can apply Eq. (20.41) with $s = 0$ and $s = 1$ to find the leading result and a correction $\sim \tau_T/t$. For \bar{z} , we observe that the first term vanishes since the integral is over n full periods of \cos . The second term of the expansion gives a correction $\sim t/\tau_{\text{Th}}$ and in total for $0 < |n| \ll t/\tau_T$:

$$\mathcal{F}_n(t) = \frac{\pi}{3g_1} T t \left(1 - \frac{2}{n^2} \frac{t}{\tau_{\text{Th}}} - \frac{6}{\pi n} \frac{\tau_T}{t} \right). \quad (20.43)$$

Note that in the diffusive regime, winding numbers $|n| > 0$ only contribute weakly to the conductivity, see Eq. (20.29).

Ergodic regime $\tau_T \ll \tau_{Th} \ll t$: In this regime, the main contribution to the conductivity will not depend on n , since we may neglect the cos-term of $q_n(u)$ as long as $|n| \ll t/\tau_{Th}$. This restriction on n is justified by the fact that large values of $|n|$ give contributions smaller by a factor of $\sim \exp(-n^2 t/\tau_{Th})$, see Eq. (20.29).

Again, we decompose $z(u) = \bar{z} + \tilde{z}(u)$. For the $\tilde{z}(u)$ part, we use the expansion of $q_{n=0}(u)$, Eq. (20.40), where the constant term $1/12$ will yield the main result. Corrections due to the second term of Eq. (20.40) are $\sim \sqrt{\tau_T/\tau_{Th}}$, because of Eq. (20.41) with $s = 1/2$. For \bar{z} , we do the integral over u directly using $\int_0^1 du \exp(-xu(1-u)) \xrightarrow{x \rightarrow \infty} 2/x$. From this we obtain a correction $\sim \tau_{Th}/t$ and in total

$$\mathcal{F}_n(t) = \frac{\pi}{3g_1} Tt \left(1 - \frac{6}{\sqrt{2\pi}} \sqrt{\frac{\tau_T}{\tau_{Th}}} - \frac{1}{30} \frac{\tau_{Th}}{t} \right). \quad (20.44)$$

It is not surprising that the case $|n| > 0$ in the diffusive regime gives, to leading order, the same results as all n of the ergodic regime (compare Eq. (20.44) to (20.43)), since higher winding numbers are by definition always ergodic: The electron paths explore the system completely.

0D regime $\tau_{Th} \ll \tau_T \ll t$: In this regime, $q_n(u)$ is more sharply peaked than $z(u)$, since $\tau_T/t \gg \tau_{Th}/t$. This means that the electron reaches the fully ergodic limit (where $q(u) = \text{const}$ and no dephasing can occur) before the fluctuating potential changes significantly. Thus, the potential is effectively frozen and only small statistical deviations from the completely ergodic limit yield a phase difference between the two time-reversed trajectories. The width of the peak of $z(u)$ becomes unimportant, instead, we can expand $z(u)$ around $u = 0$ and $u = 1$. Furthermore, we can expand the argument of the exponential function in $q_n(u)$ and then extend the integral to $+\infty$ and scale u by $k\pi$:

$$\mathcal{F}_n(t) = \frac{4\pi Tt}{g_1} \int_0^\infty du \left[\frac{2\pi Tt}{3} - 1 - \frac{4\pi^3}{15} (tT)^3 u^2 \right] \sum_{k=1}^\infty \frac{\cos(2nu)}{(k\pi)^3} e^{-4k\pi E_{Th} tu} \quad (20.45)$$

(the -1 in the integrand stems from the region $u \approx 1$). Now, assuming $|n| \ll t/\tau_{Th}$, the integral over u can be done and then the sum over k

386

M. Treiber et al.

evaluated. The result is

$$\mathcal{F}_n(t) = \frac{\pi^2 \tau_{\text{Th}}}{270 g_1} T^2 t \left(1 - \frac{3}{2\pi} \frac{1}{Tt} - \frac{\pi^2}{210} \frac{T^2}{E_{\text{Th}}^2} \right). \quad (20.46)$$

Note that, as mentioned before, the precise form of the shape of $\tilde{z}(u)$, corresponding to the broadened delta function Eq. (20.17), matters only in $0D$ regime.

To summarize, we found the following regimes:

$$\mathcal{F}_n(t) \simeq \begin{cases} \frac{\pi^{3/2}}{2g_1} \sqrt{E_{\text{Th}} T} t^{3/2}, & \tau_T \ll t \ll \tau_{\text{Th}}, n = 0; & (20.47a) \\ \frac{\pi T t}{3g_1}, & \tau_T \ll t \ll \tau_{\text{Th}}, |n| > 0; & (20.47b) \\ \frac{\pi T t}{3g_1}, & \tau_T \ll \tau_{\text{Th}} \ll t, \text{ all } n; & (20.47c) \\ \frac{\pi^2}{270 g_1} \frac{T^2 t}{E_{\text{Th}}}, & \tau_{\text{Th}} \ll \tau_T \ll t, \text{ all } n. & (20.47d) \end{cases}$$

Note that the crossover temperatures where $\tau_\varphi^{\text{diff}} \simeq \tau_\varphi^{\text{erg}}$ or $\tau_\varphi^{\text{erg}} \simeq \tau_\varphi^{0D}$, namely $c_1 g_1 E_{\text{Th}}$ or $c_2 E_{\text{Th}}$, respectively, involve large prefactors, $c_1 = 27/4 \simeq 7$ and $c_2 = 90/\pi \simeq 30$. This can be seen in a numerical evaluation of Eq. (20.36), which is presented in Fig. 20.6. In particular, one observes that the onset of the $0D$ regime is already at temperatures smaller than $30E_{\text{Th}}$, i.e. well above E_{Th} . This should significantly simplify experimental efforts to reach this regime.

20.7. Correction to the Conductance

Inserting Eq. (20.29) into Eq. (20.4), we obtain the temperature dependent correction to the conductance

$$\Delta g(T, \phi) = - \frac{4L}{g_1 \tau_{\text{Th}}} \int_0^\infty dt \sum_{n=-\infty}^{+\infty} \frac{e^{-(n/2)^2 \tau_{\text{Th}}/t}}{\sqrt{4\pi D t}} e^{-t/\tau_H - t/\tau_{\text{dw}} - \mathcal{F}_n(t)} \cos(4\pi n \phi / \phi_0). \quad (20.48)$$

The resulting value of $|\Delta g(T, \phi)|$ increases with decreasing T in a manner governed by τ_φ . We recall that in the high temperature regime dephasing can be relatively strong, so that one can neglect effects of dissipation (i.e.

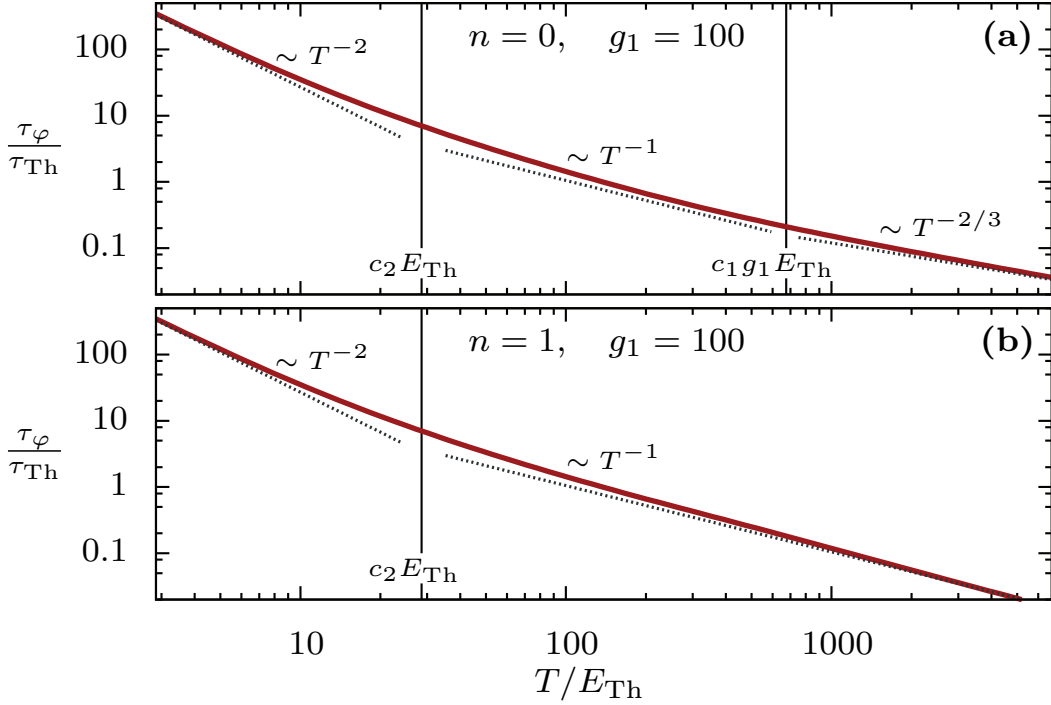


Fig. 20.5. Dephasing time τ_ϕ extracted from Eq. (20.36) and $\mathcal{F}_n(\tau_\phi) = 1$ for $g_1 = 100$. (a) Shows the result for zero winding number $n = 0$ and (b) for $n = 1$. For winding numbers $|n| > 0$ the diffusive regime, $\tau_\phi \sim T^{-2/3}$, is absent.

particle escape out of the ring) and of the external magnetic field on the Cooperon if $\tau_\phi(T) \ll \min[\tau_H, \tau_{dw}]$. In the diffusive regime, $\tau_\phi \ll \tau_{Th}$, $\Delta g(T, \phi)$ is dominated by the trajectories with $n = 0$ since the contribution of the trajectories with $|n| \geq 2\sqrt{t/\tau_{Th}} \sim \sqrt{\tau_\phi/\tau_{Th}}$ is exponentially small. Thus we arrive at:²⁰

$$|\Delta g| \simeq \frac{2}{g_1} \sqrt{\frac{\tau_\phi}{\tau_{Th}}} \propto \left(\frac{E_{Th}}{g_1^2 T} \right)^{1/3}. \quad (20.49)$$

In contrast, the trajectories with large winding number contribute in the ergodic regime, $\tau_T \ll \tau_{Th} \ll \tau_\phi$, therefore, converting the sum to the integral $\sum_n \exp(-(n/2)^2 \tau_{Th}/t) \simeq \int dn \exp(-(n/2)^2 \tau_{Th}/t) \sim \sqrt{t/\tau_{Th}}$, Eq. (20.48) yields^{24,25}

$$|\Delta g| \simeq \frac{4}{g_1} \frac{\tau_\phi}{\tau_{Th}} \propto \frac{E_{Th}}{T}. \quad (20.50)$$

Dephasing due to electron interactions becomes *weak* in the 0D regime and, therefore, the situation drastically changes at the crossover from the ergodic regime to the 0D one. In particular, we find $\tau_\phi \gg g_1 \tau_{Th}$, see Eq. (20.47c) and as far as g_1 is large, one may enter a low temperature

regime where $\tau_\varphi \geq \tau_{\text{dw}}$. In this case, the temperature independent parts of the Cooperon decay must be taken into account. In our model, with decreasing T , the growth of $|\Delta g(T, \phi)|$ saturates towards $|\Delta g(0, \phi)|$ once τ_φ increases past $\min[\tau_H, \tau_{\text{dw}}]$ (a more quantitative consideration is given in the next section). Nevertheless, the temperature dependence of Δg is still governed by $\tau_\varphi(T)$ and we can single it out by subtracting the conductance from its limiting value at $T = 0$. Then the difference

$$|\Delta g(0, \phi)| - |\Delta g(T, \phi)| \simeq \frac{4}{g_1} \frac{\tau_{\text{dw}}^2}{\tau_{\text{Th}} \tau_\varphi} \propto \left(\frac{\tau_{\text{dw}} T}{g_1} \right)^2 \quad (20.51)$$

shows T^2 -behavior in the $0D$ regime.

20.8. Suggested Experiments

Our theoretical predictions should be observable in real experiments, provided that several requirements are met. We list these conditions in accordance with their physical causes, focusing below on the example of a ring prepared from a quasi- $1D$ wire of width L_W on a $2D$ surface.

20.8.1. Validity of theoretical predictions

1D diffusion: We have used the theory of $1D$ diffusion which calls for the following inequalities

$$L \gg (\ell, L_W) \gg \lambda_F; \quad (20.52)$$

λ_F is the Fermi wavelength.

Weak localization regime: Eq. (20.48) describes the leading weak localization correction to the conductance. Subleading corrections can be neglected if (a) the classical conductance of the ring is large

$$g_1 \propto (\ell/L)(L_W/\lambda_F) \gg 1; \quad (20.53)$$

and (b) the leading correction to the conductivity is smaller than its classical value, $|\Delta g| < 1$. The former condition can be assured by a proper choice of the ring geometry and of the material while, in the low temperature regime, the latter is provided by finite dissipation.

Time-/spatial-dependence of the noise correlation function: We have used the noise correlation function (20.16) where dependencies on time- and space-coordinates are factorized. This simplified form requires the following condition (see Section 20.3):

$$2\nu D\mathbf{q}^2 \gg (D\mathbf{q}^2 - i\omega)/V(\mathbf{q}). \quad (20.54)$$

In the $0D$ regime we can roughly estimate typical values, $D\mathbf{q}^2 \sim \omega \sim E_{\text{Th}}$, arriving at the inequality

$$\nu V(\mathbf{q}) \gg 1. \quad (20.55)$$

For a quasi- $1D$ wire on a $2D$ structure, ν and V can be written as (restoring \hbar)

$$\nu_{2D} = \frac{m_e}{2\pi\hbar^2}, \quad (20.56)$$

where m_e is the electron mass, and

$$V_{1D}(q) = \frac{e^2 L_W}{4\pi\epsilon_0} |\ln(L_W^2 q^2)| \quad (20.57)$$

(in SI units). Thus, (20.55) implies that L_W cannot be taken to be overly small. Inserting material parameters, however, this condition turns out not to be very restrictive, as long as ν_{2D} is reasonably large.

Contacts (dissipation and absence of the Coulomb blockade):

The presence of contacts, through which electrons can escape into leads, is mimicked in our model through the homogeneous dissipation rate $1/\tau_{\text{dw}}$. We have assumed weak dissipation:

$$\tau_{\text{Th}} \lesssim \tau_{\text{dw}}. \quad (20.58)$$

This ensures that the winding trajectories with $|n| \geq 1$, responsible for AAS oscillations, are relevant. On the other hand, τ_{dw} cannot be taken to be arbitrarily large, since the growth of the WL correction to the conductance with decreasing temperature is cut off mainly due to this temperature independent dissipation, and this cutoff has to occur sufficiently soon that the relative correction remains small, else we would leave the WL regime. Choosing the zero temperature limit, somewhat arbitrary, as $|\Delta g(0, \phi)| = 1/2$, we find from Eq. (20.50)

$$\tau_{\text{dw}}/\tau_{\text{Th}} \lesssim g_1/8. \quad (20.59)$$

We note that our assumptions imply $\tau_\varphi \gg g_1\tau_{\text{Th}} > \tau_{\text{dw}}$ in the $0D$ regime, i.e., dephasing due to electron interactions is weak (each electron contributing to transport through the ring is dephased only a little bit during the course of its stay in the ring). Nevertheless, we demonstrate below (see Fig. 20.8) that the T^2 -dependence of the conductance should be visible in real experiments.

To choose a suitable value for the conductance at the contacts, we estimate $\tau_{\text{dw}}/\tau_{\text{Th}} \simeq g_1/g_{\text{cont}}$, which results in

$$8 \lesssim g_{\text{cont}}. \quad (20.60)$$

We suppose that the contacts are open and have a maximal transmission per channel at the contact

$$T_{\text{cont}} = 1 \Rightarrow g_{\text{cont}} = T_{\text{cont}}N = N, \quad (20.61)$$

(N is the number of transmitting reflectionless channels at the contact). This choice allows one to maximize the WL effect and, simultaneously, to minimize any Coulomb blockade effects, which we have neglected.

20.8.2. Possible experimental setup

Temperature range: The relevant temperature range, $[T_{\text{dil}}, T_{\text{ph}}]$, is limited from below by dilution refrigeration ($T_{\text{dil}} \simeq 10\text{mK}$) and from above by our neglect of phonons ($T_{\text{ph}} \simeq 5\text{K}$). Furthermore, the ring should be small enough that $c_2E_{\text{Th}} \gtrsim T_{\text{dil}}$; c_2E_{Th} is the upper estimate for the temperature of the crossover to the $0D$ regime, see the discussion after Eq. (20.47).

Contributions from the leads: We have considered an ideal situation and calculated the Cooperon decay function for the isolated ring, where the finite dissipation rate $1/\tau_{\text{dw}}$ does not affect the decay function up to leading order in $\tau_{\text{Th}}/\tau_{\text{dw}}$. This means that the Cooperons are assumed to live completely inside the ring and not influenced by dephasing in the leads, i.e. it corresponds to the situation shown in Fig. 20.6(a).

In real experiments, the correction to the conductance, Δg , is sensitive to dephasing in the leads because Cooperons exist which either belong to the lead (e.g. the situation shown in Fig. 20.6(c)) or extend over both the ring and the lead (Fig. 20.6(b))⁴⁹. (Note that in contrast to Ref. [51] or Ref. [49], we do not consider Cooperons with a Hikami-box directly at the contact, since we chose $T_{\text{cont}} = 1$.)

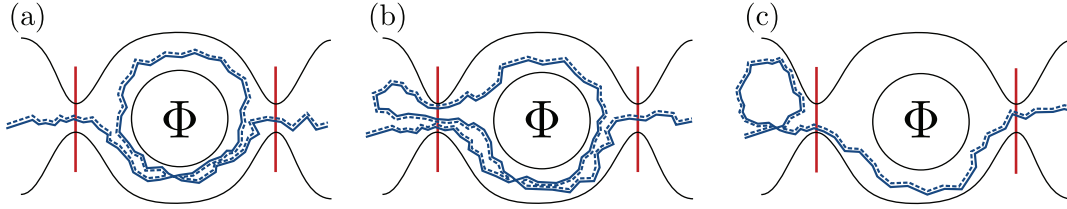


Fig. 20.6. (a) a “ring”-Cooperon, confined entirely to the ring; (b) a “cross”-Cooperon, extending from the ring to the lead and back; (c) a “lead”-Cooperon, confined entirely to the leads.

Contributions of such trajectories might mask the signatures of dephasing in the confined region (the ring). This concern also applies to quantum dots connected to leads (cf. the $\tau_\varphi \propto T^{-1}$ -behavior observed in Refs. [31–33]), or finite-size effects in a network of disordered wires,³⁵ where paths encircling a given unit cell might spend significant time in neighboring unit cells as well (cf. $T^{-1/3}$ -behavior observed in Ref. [35] at $\tau_\varphi/\tau_{\text{Th}} \geq 1$).

We will now argue that if the lead dimensionless conductance is larger than the contact conductance⁵⁰

$$g_{\text{lead}} \gg g_{\text{cont}} = N, \quad (20.62)$$

then the ring-Cooperon yields the dominating contribution to the WL corrections. Let us focus on the ergodic and 0D regimes, for which $\tau_\varphi \gg \tau_{\text{Th}}$, so that that the Cooperon ergodically explores the entire ring. Then the probability to find a closed loop in the ring is proportional to the dwell time, $p_{\text{ring}} \propto \tau_{\text{dw}}/\nu$, which is $\propto 1/g_{\text{cont}}$. Thus we can estimate:

- the probability to enter the ring as $p_{\text{in}} \sim g_{\text{cont}}/g_{\text{lead}}$;
- the probability to find a closed loop in the ring as $p_{\text{ring}} \sim (\tau_{\text{dw}}/\nu) \sim 1/g_{\text{cont}}$;
- the probability to exit the ring as $p_{\text{out}} \sim (\tau_{\text{dw}}/\nu)g_{\text{cont}} \sim 1$;
- the probability to find a closed loop in the diffusive lead as $p_{\text{lead}} \sim 1/g_{\text{lead}}$

Using these estimates, the probabilities to find a ring-, cross-, or lead-Cooperon are

$$P_{\text{C-ring}} \sim p_{\text{in}} \times p_{\text{ring}} \times p_{\text{out}} \sim 1/g_{\text{lead}}; \quad (20.63)$$

$$P_{\text{C-cross}} \sim p_{\text{in}} \times p_{\text{ring}} \times p_{\text{out}} \times p_{\text{in}} \times p_{\text{out}} \sim g_{\text{cont}}/g_{\text{lead}}^2; \quad (20.64)$$

$$P_{\text{C-lead}} \sim p_{\text{lead}} \times p_{\text{in}} \times p_{\text{out}} \sim g_{\text{cont}}/g_{\text{lead}}^2, \quad (20.65)$$

respectively. Thus we arrive at:

$$P_{C\text{-lead}} \sim P_{C\text{-cont}} \sim P_{C\text{-ring}} \times g_{\text{cont}}/g_{\text{lead}} \ll P_{C\text{-ring}}, \quad (20.66)$$

which proves that the ring-Cooperon dominates the WL correction for our choice of parameters if $g_{\text{lead}} \gg g_{\text{cont}}$.

Since the $0D$ regime implies weak dephasing it is highly desirable to improve the “signal-to-noise” ratio by filtering out contributions which do not show $0D$ dephasing. This can be done³⁵ by constructing from $|\Delta g(T, \phi)|$ its non-oscillatory envelope $|\Delta g_{\text{en}}(T, \phi)|$, obtained by setting $\theta = 0$ in Eq. (20.29) while retaining $\tau_H \neq 0$, and studying the difference

$$\Delta \bar{g}(T, \phi) = |\Delta g_{\text{en}}(T, \phi)| - |\Delta g(T, \phi)|. \quad (20.67)$$

This procedure is illustrated in Fig. 20.7. The lead-Cooperons do not have the Aharonov-Bohm phase and are eliminated by this filtering procedure. Unfortunately, cross-Cooperons cannot be filtered in this manner, since they do experience the Aharonov-Bohm phase. Nevertheless, if the condition $g_{\text{cont}} \ll g_{\text{lead}}$ holds, $\Delta \bar{g}$ is completely dominated by paths residing only in the ring in accordance with the estimate Eq. (20.66).

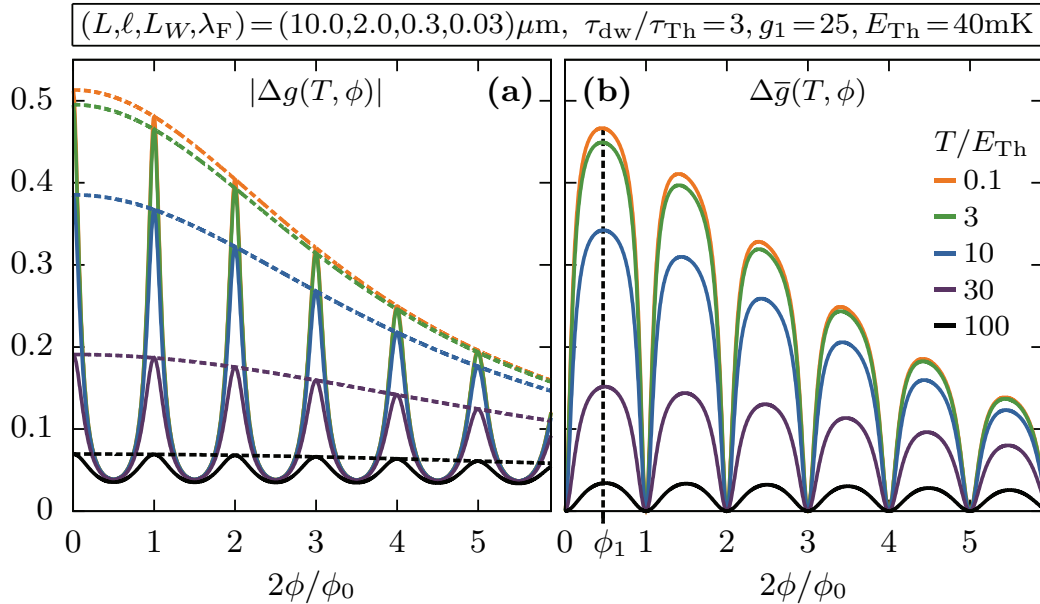


Fig. 20.7. (a) The WL correction $|\Delta g(T, \phi)|$ (solid lines), its envelope $|\Delta g_{\text{en}}(T, \phi)|$ (dashed lines) and (b) their difference $\Delta \bar{g} = |\Delta g_{\text{en}}| - |\Delta g|$, plotted as function of magnetic flux $2\phi/\phi_0$, for five different temperatures between $0.1E_{\text{Th}}$ and $100E_{\text{Th}}$ (increasing from top to bottom).

20.8.3. Numerical results for 2D GaAs/AlGaAs heterostructures

All above-mentioned constraints can be met, e.g., with rings prepared from a 2D GaAs/AlGaAs heterostructure. In such systems, diffusive behavior emerges from specular boundary scattering of the electrons, see Ref. [46], leading to the following dephasing time due to the external magnetic field:

$$\tau_H = 9.5(c/eH)^2 \times (l/DL_W^3). \quad (20.68)$$

Furthermore, inserting Eq. (20.56) into the 2D conductivity $\sigma_{2D} = 2e^2\nu_{2D}D$ with $D = v_F\ell$, we obtain the corresponding dimensionless conductance:

$$g_1 = \frac{h}{e^2} \frac{\sigma_{2D}L_W}{L} = 4\pi \frac{L_W\ell}{\lambda_FL}. \quad (20.69)$$

A typical Fermi wavelength in a GaAs/AlGaAs heterostructure is $\lambda_F \approx 30\text{nm}$ ($v_F \approx 2.5 \cdot 10^5\text{m/s}$).^{28,35,39,47} Thus, by suitably choosing L , L_W and ℓ we can adjust g_1 and E_{Th} to make all regimes of the dephasing time accessible.

Numerical results for $|\Delta g|$ and $\Delta\bar{g}$, obtained from Eq. (20.4) using experimentally realizable parameters, are shown in Figs. 20.7 and 20.8 for several combinations of these parameters. The regime where Δg exhibits

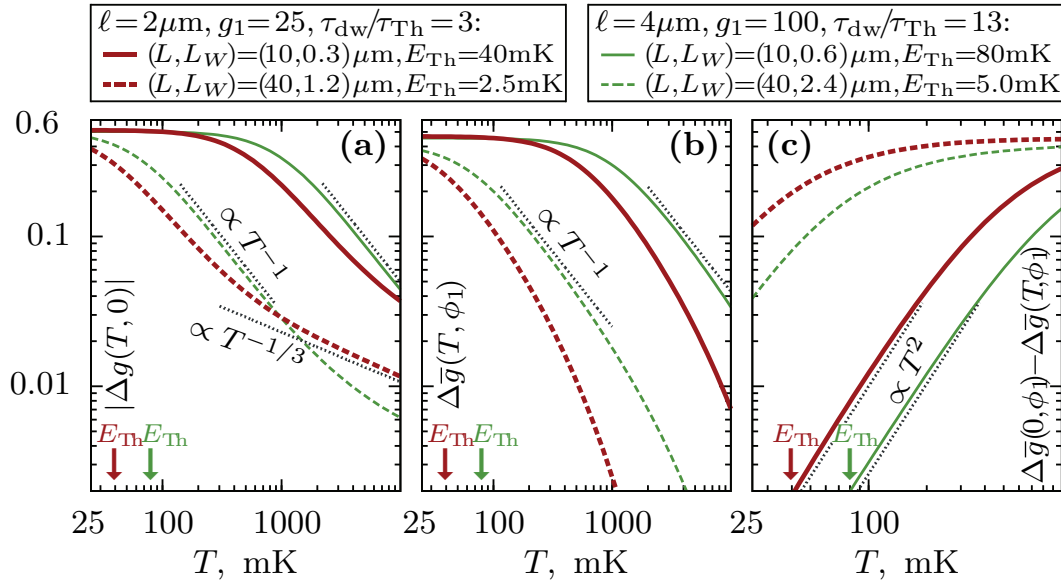


Fig. 20.8. T -dependence of (a) the WL correction at zero field, $|\Delta g(T, 0)|$ and (b) at finite field with envelope subtracted, $\Delta\bar{g}(T, \phi_1)$; (c) the difference $\Delta\bar{g}(0, \phi_1) - \Delta\bar{g}(T, \phi_1)$, which reveals a crossover to T^2 -behavior for $T \ll 30E_{Th}$. The flux ϕ_1 , which weakly depends on T , marks the first maximum of $\Delta\bar{g}(T, \phi)$, see Fig. 20.7(b). [This figure is reproduced from Ref. [1]]

diffusive $T^{-1/3}$ behavior ($7g_1E_{\text{Th}} \ll T \ll T_{\text{ph}}$) is visible only for our smallest choices of both g_1 and E_{Th} (Fig. 20.8(a), heavy dashed line). AAS oscillations in $|\Delta g|$ and $\Delta\bar{g}$ (Fig. 20.7), which require $\tau_{\text{Th}} \ll \tau_\varphi$, first emerge at the crossover from the diffusive to the ergodic regime. They increase in magnitude with decreasing T , showing ergodic T^{-1} behavior for $30E_{\text{Th}} \ll T \ll 7g_1E_{\text{Th}}$ (Figs. 20.8(a),(b)), and eventually saturate towards their $T = 0$ values, with $\Delta\bar{g}(0, \phi) - \Delta\bar{g}(T, \phi)$ showing the predicted $0D$ behavior, $\propto T^2$, for $T \lesssim 5E_{\text{Th}}$, see Fig. 20.8(c).

20.9. Conclusions

For an almost isolated disordered quasi-1D ring with $T \gg E_{\text{Th}}$, the T -dependence of the dephasing time has been known to behave as $\tau_\varphi \propto T^{-2/3}$ (Ref. [20]) or $\propto T^{-1}$ (Refs. [24,25]) in the diffusive or ergodic regimes, respectively. Here we showed how it crosses over, for $T \ll 30E_{\text{Th}}$, to $\tau_\varphi \propto T^{-2}$, in agreement with the theory of dephasing in $0D$ systems (Ref. [2]). This crossover manifests itself in both the smooth part of the magnetoconductivity and the amplitude of the AAS oscillations. Importantly, the latter fact can be exploited to decrease the effects of dephasing in the leads, by subtracting from the magnetoconductivity its smooth envelope. While we did not give an exhaustive study of all contributions to dephasing in the connected ring, we were able to show that the leading contribution results only from trajectories confined to the ring. Thus, an analysis of the T -dependence of the AAS oscillation amplitude may offer a way to finally observe, for $T \lesssim 5E_{\text{Th}}$, the elusive but fundamental $0D$ behavior $\tau_\varphi \sim T^{-2}$. Its observation, moreover, would allow *quantitative* experimental tests of the role of temperature as ultraviolet frequency cut-off in the theory of dephasing. An interesting challenge for future works consists in a more realistic model of the connection to the leads. Work on the model of an N -channel ring attached via two arms with fewer channels to absorbing boundaries is currently in progress.⁵²

Acknowledgments

We acknowledge illuminating discussions with B. L. Altshuler, C. Bäuerle, N. O. Birge, Ya. M. Blanter, P. W. Brouwer, L. I. Glazman, Y. Imry, V. E. Kravtsov, J. Kupferschmidt, A. D. Mirlin, Y. V. Nazarov, A. Rosch, D. Weiss and V. I. Yudson. We acknowledge support from the DFG through SFB TR-12, the Emmy-Noether program and the Nanosystems Initiative

Munich Cluster of Excellence; from the NSF, Grant No. PHY05-51164; and from the EPSRC, Grant No. T23725/01.

References

1. M. Treiber, O. M. Yevtushenko, F. Marquardt, J. von Delft, and I. V. Lerner, *Phys. Rev. B* **80**, 201305(R) (2009).
2. U. Sivan, Y. Imry, and A. G. Aronov, *Europhys. Lett.* **28**, 115 (1994).
3. Y. Imry, in *Introduction to Mesoscopic Physics*, Oxford University Press (1997)
4. M. Büttiker, Y. Imry, and R. Landauer, *Phys. Rev. A* **96**, 365 (1983).
5. M. Büttiker, Y. Imry, and M. Ya. Azbel, *Phys. Rev. A* **30**, 1982 (1984).
6. Y. Gefen, Y. Imry, and M. Ya. Azbel, *Phys. Rev. Lett.* **52**, 129 (1984).
7. M. Büttiker, Y. Imry, R. Landauer, and S. Pinhas, *Phys. Rev. B* **31**, 6207 (1984).
8. M. Murat, Y. Gefen, and Y. Imry, *Phys. Rev. B* **34**, 659 (1985).
9. Y. Imry, and N. S. Shiren, *Phys. Rev. B* **33**, 7992 (1986).
10. A. D. Stone, and Y. Imry, *Phys. Ref. Lett.* **56**, 189 (1986).
11. B. L. Altshuler, Y. Gefen, and Y. Imry, *Phys. Rev. Lett.* **66**, 88 (1990).
12. L. P. Levy, G. Dolan, J. Dunsmuir, and H. Bouchiat, *Phys. Rev. Lett.* **64**, 2074 (1990).
13. H. Bluhm, N. C. Koshnick, J. A. Bert, M. E. Huber, and K. A. Moler, *Phys. Rev. Lett.* **102**, 136802 (2009).
14. A. C. Bleszynski-Jayich, W. E. Shanks, B. Peaudecerf, E. Ginossar, F. von Oppen, L. I. Glazman, and J. G. E. Harris, arXiv:0906.4780 (2009).
15. Y. Imry, *Physics* **2**, 24 (2009).
16. R. A. Webb, S. Washburn, C. P. Umbach, and R. B. Laibowitz, *Phys. Rev. Lett.* **54**, 2696 (1985).
17. B. L. Altshuler, A. G. Aronov, and B. Z. Spivak, *JETP Lett.* **33**, 94 (1981).
18. D. Y. Sharvin, and Y. V. Sharvin, *Pis'ma Zh. Teor. Eksp. Fiz.* **34**, 285 (1981).
19. A. Stern, Y. Aharonov, and Y. Imry, *Phys. Rev. A* **41**, 3436 (1990).
20. B. L. Altshuler, A. G. Aronov, and D. E. Khmel'nitsky, *J. Phys. C* **15**, 7367 (1982).
21. H. Fukuyama and E. Abrahams, *Phys. Rev. B*, **27**, 5976 (1983).
22. B. L. Altshuler and A. G. Aronov, in *Electron-Electron Interactions in Disordered Systems*, edited by A. L. Efros and M. Pollak, North-Holland, Amsterdam, 1 (1985).
23. I. L. Aleiner, , B. L. Altshuler, and M. E. Gershenson, *Waves in Random Media* **9**, 201 (1999).
24. T. Ludwig and A. D. Mirlin, *Phys. Rev. B* **69**, 193306 (2004).
25. C. Texier and G. Montambaux, *Phys. Rev. B* **72**, 115327 (2005).
26. F. Marquardt, J. von Delft, R. A. Smith, and V. Ambegaokar, *Phys. Rev. B* **76**, 195331 (2007).
27. J. von Delft, F. Marquardt, R. A. Smith, and V. Ambegaokar, *Phys. Rev. B* **76**, 195332 (2007).

28. C. M. Marcus, R. M. Westervelt, P. F. Hopkins, and A. C. Gossard, *Phys. Rev. B* **48**, 2460 (1993).
29. A. Yacoby, M. Heiblum, H. Shtrikman, V. Umansky, and D. Mahalu, *Semicond. Sci. Tech.* **9**, 907 (1994).
30. B. Reulet, H. Bouchiat, and D. Mailly, *Europhys. Lett.* **31**, 305 (1995).
31. A. G. Huibers, M. Switkes, C. M. Marcus, K. Campman, and A. C. Gossard, *Phys. Rev. Lett.* **81**, 200 (1998);
32. A. G. Huibers, S. R. Patel, C. M. Marcus, P. W. Brouwer, C. I. Duruöz, and J. S. Harris, Jr., *Phys. Rev. Lett.* **81**, 1917 (1998);
33. A. G. Huibers, J. A. Folk, S. R. Patel, C. M. Marcus, C. I. Duruöz and J. S. Harris, Jr., *Phys. Rev. Lett.* **83**, 5090 (1999).
34. A. B. Gougam, F. Pierre, H. Pothier, D. Esteve, and N. O. Birge, *J. Low Temp. Phys.* **118**, 447 (2000).
35. M. Ferrier, A. C. H. Rowe, S. Gueron, H. Bouchiat, C. Texier, and G. Montambaux, *Phys. Rev. Lett.* **100**, 146802 (2008).
36. I. L. Aleiner, B. L. Altshuler, and Y. M. Galperin, *Phys. Rev. B* **63**, 201401 (2001).
37. I. L. Aleiner and Y. M. Blanter, *Phys. Rev. B* **65**, 115317 (2002).
38. Y. Imry, arXiv: cond-mat/0202044 (2002)
39. Y. Niimi, Y. Baines, T. Capron, D. Mailly, F.-Y. Lo, A. D. Wieck, T. Meunier, L. Saminadayar, and C. Bäuerle, *Phys. Rev. Lett.* **102**, 226801 (2009).
40. L. P. Gor'kov, A. I. Larkin, and D. E. Khmel'nitskii, *JETP Lett.* **30**, 228 (1979).
41. E. Akkermans and G. Montambaux, *Mesoscopic physics of electrons and photons* (Cambridge University Press, Cambridge, 2007).
42. D. E. Khmel'nitskii, *Physica B&C* **126**, 235 (1984).
43. B. L. Altshuler and A. G. Aronov, *JETP Lett.* **33**, 499 (1981).
44. P. W. Brouwer and C. W. J. Beenakker, *Phys. Rev. B* **55**, 4695 (1997);
45. E. McCann and I. V. Lerner, *Phys. Rev. B* **57**, 7219 (1998).
46. C. W. J. Beenakker and H. van Houten, *Phys. Rev. B* **38**, 3232 (1988).
47. O. Yevtushenko, G. Lütjering, D. Weiss, and K. Richter, *Phys. Rev. Lett.* **84**, 542 (2000).
48. B. L. Altshuler, A. G. Aronov, and P. A. Lee, *Phys. Rev. Lett.* **44**, 1288 (1980).
49. Ya. M. Blanter, V. M. Vinokur, and L. I. Glazman, *Phys. Rev. B* **73**, 165322 (2006).
50. J. N. Kupferschmidt, and P. W. Brouwer, (private communication).
51. R. S. Whitney, *Phys. Rev. B* **75**, 235404 (2007).
52. M. Treiber, O. M. Yevtushenko, F. Marquardt, J. von Delft, and I. V. Lerner, to be published.

3.6 Publication: Transport and dephasing in a quantum dot: Multiply connected graph model

The following 11 pages have been published in the journal *Annalen der Physik (Berlin)*.

Transport and dephasing in a quantum dot: Multiply connected graph model

Maximilian Treiber*, Oleg Yevtushenko, and Jan von Delft

Received 15 November 2011, revised 6 December 2011, accepted 2 December 2011

Published online 2 February 2012

Dedicated to Ulrich Eckern on the occasion of his 60th birthday.

Using the theory of diffusion in graphs, we propose a model to study mesoscopic transport through a diffusive quantum dot. The graph consists of three quasi-1D regions: a central region describing the dot, and two identical left- and right- wires connected to leads, which mimic contacts of a real system. We find the exact solution of the diffusion equation for this graph and evaluate the conductance including quantum corrections. Our model is complementary to the RMT models describing quantum dots. Firstly, it reproduces the universal limit at zero temperature. But the main advantage compared to RMT models is that it allows one to take into account interaction-induced dephasing at finite temperatures. Besides, the crossovers from open to almost closed quantum dots and between different regimes of dephasing can be described within a single framework. We present results for the temperature dependence of the weak localization correction to the conductance for the experimentally relevant parameter range and discuss the possibility to observe the elusive 0D-regime of dephasing in different mesoscopic systems.

1 Introduction

In the last decades, dephasing in quantum dots has been studied experimentally and theoretically in great detail. The theoretical description is largely based on results from random matrix theory (RMT), emphasizing the universality in the description of a dot, when spatial degrees of freedom become negligible. While the universal limits are well understood and reproduced in many experiments, a prediction of the full temperature dependence of quantities which are sensitive to dephasing, such as quantum corrections to the classical conductance, Δg , are challenging existing theories. Since RMT is not able

to describe the T dependence on its own, several extensions were introduced in the past to describe their dependence on a dephasing time τ_ϕ , which has to be included phenomenologically, see Sect. 2 for details.

One of the well-known problems in the theory of dephasing in quantum dots originated from the predictions of a seminal paper by Sivan, Imry and Aronov, who showed that dephasing in the so-called 0D regime ($T \ll E_{\text{Th}}$, where E_{Th} is the Thouless energy), behaves as $\tau_\phi \sim T^{-2}$, which results from Pauli blocking of the Fermi sea [1]. However fundamental the origin of 0D dephasing is, it has so far not been observed experimentally. One possible reason for this might be the fact that dephasing is very weak in this regime, such that quantum corrections may reach their universal limit $\Delta g \sim 1$. In general, if the dephasing time is much larger than the time the electron spends in the dot, Δg is governed by a dwelling time τ_{dw} and becomes almost T independent. The remaining small T -dependent part of Δg can be masked, for example, by other T -dependent effects coming from contacts or leads. Thus, to facilitate an experimental observation of 0D dephasing, a comprehensive theory of transport in the quantum dot connected to leads via some contacts is needed, which goes beyond the simple picture provided by RMT.

In this paper we propose an alternative to the RMT description of the quantum dots. Namely, we follow the ideas of [2,3] and model the quantum dot as a network of 1D wires and use the theory of diffusion in graphs to calculate τ_ϕ and Δg . Earlier papers either focused only on small graphs, such as 1D rings [4–6], or the authors intro-

* Corresponding author

E-mail: Maximilian.Treiber@physik.lmu.de,

Phone: +49 (0)89 2180 4533

Ludwig Maximilians University, Arnold Sommerfeld Center and Center for Nano-Science, Munich, 80333, Germany

duced τ_φ only phenomenologically [2, 3, 7]. We generalize the theory of τ_φ for arbitrary graphs and include the regime $T < E_{\text{Th}}$ by taking into account the Pauli principle. Using this theory, we calculate τ_φ for a network describing a quantum dot, taking into account effects of the contacts and the leads. This allows us to demonstrate that the T^2 -dependence of the dephasing rate in 0D regime is substantially distorted in usual transport measurements in quantum dots.

The rest of the paper is organized as follows: In Sect. 2 we give a brief review of known results for dephasing in quantum dots. In Sect. 3, basic results from the theory of diffusion in graphs are presented, and in Sect. 4 we will apply this theory to construct a solvable quantum dot model as an alternative to the well-known RMT models. Results for the quantum corrections to the conductance and the dephasing time are presented in the following Sections. In the conclusions we compare different experimental setups where 0D dephasing could be observed.

2 Dephasing in quantum dots: Brief review of known results

It is well-known that the conductance g of a disordered normal metal is reduced due to quantum mechanical interference of the electron wave functions scattered at static impurities. It has been found that the reduction of g can be expressed via the return probability of coherent electron paths, $P(\mathbf{x}, \mathbf{x}, t)$, (the so-called *Cooperon*) integrated over time and space [8]:

$$\Delta g \equiv g - g_0 = -4E_{\text{Th}} \int_0^\infty dt \int d^d \mathbf{x} P(\mathbf{x}, \mathbf{x}, t). \quad (1)$$

Here g_0 is the classical conductance measured in units of e^2/h , $E_{\text{Th}} = D/\Omega^2$ is the Thouless energy of the system, D is the diffusion constant and Ω is the largest size of the system. Δg is usually referred to as the *weak localization correction*.

Quantum coherence is suppressed by a constant magnetic field and by time-dependent (noisy) fields, or when closed electron paths contributing to $P(\mathbf{x}, \mathbf{x}, t)$ in Eq. (1) are dephased due to inelastic scattering events. The time-scale associated with the latter is called *dephasing time* τ_φ . In the absence of other sources of dephasing, τ_φ yields an infrared cutoff for the time-integral, Eq. (1), and governs the temperature dependence of Δg [9]. At low temperatures, $T \lesssim 1K$, where phonons are frozen, τ_φ is dominated by electron interactions and depends on the dimensionality d and the geometry of the system. The T -dependence of τ_φ in different regimes is governed by an

interplay of τ_φ with the thermal time $\tau_T = 1/T$ and the Thouless time $\tau_{\text{Th}} = 1/E_{\text{Th}}$, see Table 1 for a summary of known regimes in 1D and 2D [10]. For low temperatures and small system sizes, when E_{Th} is the largest energy scale, dephasing becomes effectively zero-dimensional (0D). Therefore, it must be relevant for transport in metallic (diffusive or chaotic) quantum dots [1].

Table 1 Dephasing rate $1/\tau_\varphi$ as a function of temperature T .

	$\tau_T \ll \tau_\varphi \ll \tau_{\text{Th}}$	$\tau_T \ll \tau_{\text{Th}} \ll \tau_\varphi$	$\tau_{\text{Th}} \ll \tau_T \ll \tau_\varphi$
1D	$\propto T^{2/3}$	$\propto T$	$\propto T^2$
2D	$\propto T$	$\propto T \ln(T)$	$\propto T^2$

Note that 0D dephasing requires confinement of the electron paths during times larger than τ_{Th} , since quantum corrections become T independent for $\tau_\varphi \gg \tau_{\text{Th}}$ in fully open systems. As an example, consider the case of a quasi-1D wire of length L connected to absorbing leads, where Δg reads [11]:

$$\Delta g = -4 \sum_{n=1}^{\infty} \frac{1}{(\pi n)^2 + \tau_{\text{Th}}/\tau_\varphi} \Big|_{\tau_\varphi \gg \tau_{\text{Th}}} \approx -\frac{2}{3}. \quad (2)$$

Thus, a detailed calculation of Δg including τ_φ requires solving the full diffusion equation of the connected quantum dot, which is hard to achieve analytically for confined systems.

One way to circumvent this problem is to apply random-matrix theory (RMT) to the scattering matrix S , describing transmission and reflection in the sample. In such an RMT model one assumes that the elements of the Hamiltonian H describing the systems are either real (Gaussian orthogonal ensemble, $\beta_{\text{GOE}} = 1$) or complex (Gaussian unitary ensemble, $\beta_{\text{GUE}} = 2$) random numbers corresponding to a system with time-reversal symmetry or broken time-reversal symmetry.¹ Imposing a Gaussian probability distribution $P(H)$, the scattering matrix S can be constructed using so-called R-matrix theory. Alternatively, a simpler approach starts from a probability distribution of the scattering matrix directly, which is of the form $P(S) = \text{const}$, and S is again only restricted by symmetry arguments. From the scattering matrix, the full non-perturbative distribution of the transmission matrix

¹ Note that in this paper, we consider only the spinless cases.

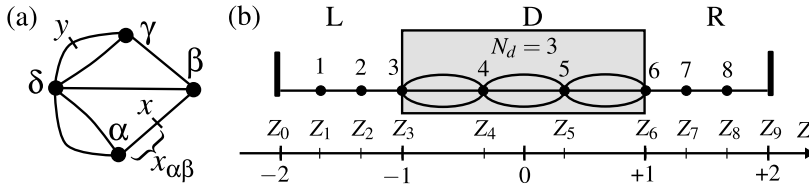


Figure 1 (a) A graph consisting of 9 wires and 6 vertices, denoted by Greek letters. (b) A quantum dot realized as a graph with dimensionless coordinate $Z = x/L$. The labels Z_i denote the position of

the leads ($i = 0, 9$) and the vertices ($i = 1 \dots 8$) on the scale Z . Furthermore, the numbers $i = 1 \dots 8$ correspond to the i th row or column of the vertex matrix \mathcal{M}^Y , Eq. (10)

and the conductance can be obtained. While RMT is unable to predict the temperature dependence of Δg on its own, the difference in g of the cases β_{GOE} and β_{GUE} is equivalent to Δg in the universal limit of $T \rightarrow 0$. The universal values for Δg calculated by RMT are ~ 1 , in particular $\Delta g = 1/3$ for a quantum dot with spinfull single-channel ($N = 1$) contacts and $\Delta g = 1/4$ for many-channel ($N \rightarrow \infty$) contacts [12, 13], but we would like to stress that taking into account dimensionality and geometry of the contacts may lead to different values. Extensions to RMT have been introduced in the past to describe the dependence of Δg on a dephasing time [14], e.g. by including a fictitious voltage probe into the scattering matrix which removes electrons from the phase-coherent motion of the electrons in the quantum dot [15], or by including an imaginary potential equal to $-i/2\tau_\varphi$ in the Hamiltonian from which the scattering matrix is derived [16]. It is expected that τ_φ included in such an approach has the same form as stated in Table 1 for $T \ll E_{\text{Th}}$, i.e. $\tau_\varphi \propto T^{-2}$, but a proof of this expectation and a theory of a crossover between different regimes is still missing.

3 Diffusion in graphs

In this section, we present basic results from the theory of diffusion in graphs, following [11]. A graph is defined as a set of quasi-1D wires connected to each other at vertices, see the example shown in Fig. 1(a). In this section we will show how the solution to the Laplace transformed diffusion equation,

$$(\gamma - D\Delta) P_\gamma(x, y) = \delta(x - y), \quad (3)$$

between arbitrary vertices (with coordinates x and y) of such a graph can be obtained. The time-dependent probability, required to calculate Δg and τ_φ , can be obtained via an inverse Laplace transform:

$$P(x, y, t) = \frac{1}{2\pi i} \int_{-i\infty}^{+i\infty} d\gamma e^{\gamma t} P_\gamma(x, y). \quad (4)$$

It is convenient to introduce the following quantities: We denote the wire between arbitrary vertices α and β as $(\alpha\beta)$ and its length as $L_{\alpha\beta}$. Furthermore, the *running coordinate* along this wire (measured from α) is denoted $x_{\alpha\beta}$, and in the following, we will not distinguish a vertex from the coordinate of the vertex on the graph: For example, $P(\alpha, y)$ is equivalent to $\lim_{x_{\alpha\beta} \rightarrow 0} P(x_{\alpha\beta}, y)$, for any neighboring vertex β of α . The current conservation at some vertex α can be written as follows:

$$-\sum_{(\alpha\beta)} \left[\partial_{x_{\alpha\beta}} P_\gamma(\mu, x_{\alpha\beta}) \right]_{x_{\alpha\beta}=0} = \delta_{\alpha,\mu}, \quad (5)$$

where the symbol $\overline{\sum_{(\alpha\beta)}}$ means summation over all wires $(\alpha\beta)$ which are connected to α .

Consider the point x lying at the coordinate $x_{\alpha\beta}$ of wire $(\alpha\beta)$ in Fig. 1(a). The probability to reach x from some arbitrary other point y of the graph can be expressed in terms of the probabilities from the neighboring vertices of x , i.e. α and β :

$$P_\gamma(y, x) = \quad (6)$$

$$\frac{P_\gamma(y, \alpha) \sinh(\sqrt{\gamma/D}(L_{\alpha\beta} - x_{\alpha\beta})) + P_\gamma(y, \beta) \sinh(\sqrt{\gamma/D}x_{\alpha\beta})}{\sinh(\sqrt{\gamma/D}L_{\alpha\beta})}.$$

Validity of the solution (6) can be checked directly by substituting Eq. (6) into Eq. (3).

Inserting (6) into (5) yields the following equations for vertex α :

$$P_\gamma(\mu, \alpha) \overline{\sum_{(\alpha\beta)}} \sqrt{\gamma/D} \coth(\sqrt{\gamma/D}L_{\alpha\beta}) - \sum_{(\alpha\beta)} P_\gamma(\mu, \beta) \frac{\sqrt{\gamma/D}}{\sinh(\sqrt{\gamma/D}L_{\alpha\beta})} = D\delta_{\alpha,\mu}. \quad (7)$$

Writing down Eq. (7), for every vertex of the graph, we obtain a set of linear equations which can be solved for ar-

bitrary vertices. Let us define a matrix \mathcal{M}^Y as follows:

$$\mathcal{M}_{\alpha\beta}^Y \equiv \sum_{(\alpha\delta)} \left(\delta_{\alpha\beta} \sqrt{\gamma/D} \coth(\sqrt{\gamma/D} L_{\alpha\delta}) - \delta_{\delta\beta} \sqrt{\gamma/D} \sinh(\sqrt{\gamma/D} L_{\alpha\delta})^{-1} \right). \quad (8)$$

It is easy to check that the diffusion probability between arbitrary vertices of the graph is given by the entries of the inverse matrix divided by the diffusion constant [7, 11]:

$$P_\gamma(\alpha, \beta) = \frac{1}{D} (\mathcal{M}^Y)^{-1}_{\alpha\beta}. \quad (9)$$

4 A graph model for a connected quantum dot

In this section we explain how to describe a connected quantum dot by a network of 1D wires. The main advantage of this model is that an exact solution to the diffusion equation can be found.

Consider the network shown in Fig. 1(b). It includes 8 vertices and describes a quantum dot of total length $2L$ attached via two contacts of length L to absorbing leads.² Multiple wires connecting the same vertices (e.g. the three wires connecting vertex 4 with vertex 5) mimic a larger number of channels. Below, we use a dimensionless coordinate $Z = x/L$; the position of the leads is fixed at $Z_0 = -2$, $Z_9 = +2$ and the position of the 3rd and

$$\mathcal{M}_{ijkl}^Y = \begin{pmatrix} \coth(\sqrt{\tilde{\gamma}}|Z_j - Z_i|) + \coth(\sqrt{\tilde{\gamma}}|Z_k - Z_j|) & -1/\sinh(\sqrt{\tilde{\gamma}}|Z_k - Z_j|) \\ -1/\sinh(\sqrt{\tilde{\gamma}}|Z_k - Z_j|) & \coth(\sqrt{\tilde{\gamma}}|Z_k - Z_j|) + \coth(\sqrt{\tilde{\gamma}}|Z_l - Z_k|) \end{pmatrix}. \quad (12)$$

6th vertex, describing the connection of the dot to the contacts, is fixed at $Z_3 = -1$, $Z_6 = +1$. The remaining 6 vertices are auxiliary: There are 3 regions in the system marked by “L” (left contact), “D” (dot) and “R” (right contact). We would like to describe diffusion from an arbitrary point in the system to another. Therefore, we have to place two additional vertices in each region L, D, R. Positions of these vertices define running coordinates. They are arbitrary within the corresponding region, thus each region is subdivided into 3 wires of varying length. The

running coordinates can be expressed via the length of the connecting wires, e.g. the length of the wire connecting vertices 1 and 2 is given by $(Z_2 - Z_1)$.

To describe confinement of the electrons, we assume that all vertices in the regions L and R (including boundaries) are connected by single wires while the vertices in the dot (including its boundaries) are connected via N_d wires. This allows us to tune the system from a simple wire at $N_d = 1$ to an almost closed quantum dot for $N_d \rightarrow \infty$. The corresponding vertex matrix \mathcal{M}^Y , defined in Eqs. (8), is given by

$$\mathcal{M}^Y = \begin{pmatrix} [\mathcal{M}_L^Y] & 0 & 0 & 0 & 0 & 0 & 0 \\ S_L & 0 & 0 & 0 & 0 & 0 & 0 \\ 0 & S_L & C_{LD} & S_{LD} & 0 & 0 & 0 \\ 0 & 0 & S_{LD} & [\mathcal{M}_D^Y] & 0 & 0 & 0 \\ 0 & 0 & 0 & 0 & S_{DR} & 0 & 0 \\ 0 & 0 & 0 & 0 & S_{DR} & C_{DR} & S_R \\ 0 & 0 & 0 & 0 & 0 & S_R & [\mathcal{M}_R^Y] \\ 0 & 0 & 0 & 0 & 0 & 0 & 0 \end{pmatrix}. \quad (10)$$

We have introduced 2×2 blocks,

$$\mathcal{M}_L^Y = \mathcal{M}_{0123}^Y, \quad \mathcal{M}_D^Y = N_d \mathcal{M}_{3456}^Y, \quad \text{and} \quad (11)$$

$$\mathcal{M}_R^Y = \mathcal{M}_{6789}^Y,$$

which are given by:

Expressions for the entries “S” and “C”, which correspond to connected vertices, read

$$S_{L,R} = -1/\sinh(\sqrt{\tilde{\gamma}}(-1 \mp Z_{2,7})),$$

$$S_{LD,DR} = -N_d/\sinh(\sqrt{\tilde{\gamma}}(1 \pm Z_{4,5})),$$

$$C_{LD,DR} = N_d \coth(\sqrt{\tilde{\gamma}}(1 \pm Z_{4,5})) + \coth(\sqrt{\tilde{\gamma}}(-1 \mp Z_{2,7})),$$

where we have defined the dimensionless parameter $\tilde{\gamma} = \gamma/E_{\text{Th}}$, where $E_{\text{Th}} = D/L^2$ is the Thouless energy on the scale L . Note that the total length of the wires which form the graph is $L_{\text{total}} = 2L(N_d + 1)$. Thus, the probabilities obtained via inversion of the matrix (10), cf. Eq. (9), are normalized on L_{total} . For further calculations, it is more convenient to change this normalization from L_{total} to the actual length of the system, $4L$: Firstly, we recall that all N_d wires in the dot connecting the same two vertices have the same length, i.e. these wires are identical. Consider a

² We have chosen this particular ratio of wire lengths to simplify the calculations in the remainder of this section. Note that neither very short nor very long connecting wires are experimentally relevant for quantum dots, since either the confinement to the central region would be lost or the contacts would be unrealistically large.

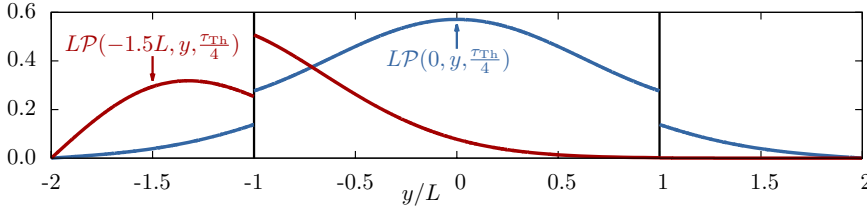


Figure 2 (online color at: www.ann-phys.org) Probability as a function of space for fixed $t = \tau_{\text{Th}}/4$, $N_d = 2$ and initial position $x = -1.5L$ (red curve) or $x = 0$ (blue curve). The initial positions are marked by arrows.

point \mathcal{X} inside the dot which belongs a given wire (out of N_d) and is infinitesimally close to one of the vertices $\alpha = 4$ or 5. The probability to reach \mathcal{X} from any other point is equal to the probability to reach α itself. Let us now introduce a probability \mathcal{P} to reach \mathcal{X} belonging to any of the N_d wires:

$$\mathcal{P}_\gamma(\alpha, \beta) = N^{(\beta)} P_\gamma(\alpha, \beta) \equiv N^{(\beta)} \frac{1}{D} (\mathcal{M}^\gamma)_{\alpha\beta}^{-1}; \quad (13)$$

here $N^{(\beta)} = N_d$ if β is a vertex lying in the dot and $N^{(\beta)} = 1$ otherwise. \mathcal{P} is normalized on $4L$ and it reflects an enhancement of the probability for an electron to stay in the dot by the factor N_d .

Furthermore, we define the *piecewise continuous* function $\mathcal{P}_\gamma(x, y)$ of *continuous* variables $x, y \in [-2L, 2L]$ by selecting two appropriate vertices and replacing the wire-length parameters, Z_α , by x/L or y/L . For example, the probability to reach any point $y \in [-L, L]$ in the dot from a point $x \in [-2L, -L]$ in the left contact, is given by $\mathcal{P}_\gamma(x, y) = N_d \frac{1}{D} (\mathcal{M}^\gamma)_{14}^{-1}$ after replacing Z_1 by x/L and Z_4 by y/L .

An analytic expression for $\mathcal{P}_\gamma(x, y)$ can be evaluated efficiently, but it is lengthy and will be published elsewhere. Besides, the inverse Laplace transform of $\mathcal{P}_\gamma(x, y)$, cf. Eq. (4), can be calculated by exploiting the fact that all poles of $\mathcal{P}_\gamma(x, y)$ are simple and coincide with the zeros of the determinant of \mathcal{M}^γ . Direct calculation yields³

$$\begin{aligned} \det \mathcal{M}^\gamma &\propto S(\tilde{\gamma}) \\ &\equiv \sinh\left(2\sqrt{\tilde{\gamma}}\right) \left((N_d - 1) + (N_d + 1) \cosh\left(2\sqrt{\tilde{\gamma}}\right) \right). \end{aligned} \quad (14)$$

³ We note in passing that $S(\tilde{\gamma})$ is proportional to the so-called spectral determinant, $\det(-D\Delta + \gamma)$, of the graph [1], implying that it does not depend on any of the auxiliary coordinates Z_i .

Solving equation $S(\tilde{\gamma}) = 0$ yields the following poles for the graph under consideration:

$$\begin{aligned} \tilde{\gamma}_k &= -\left(\frac{k\pi}{2}\right)^2, \quad k \in \mathbb{N}^+, \quad \text{or} \\ \tilde{\gamma}_k &= -\left(k\pi + \arccos\sqrt{\frac{N_d}{N_d+1}}\right)^2, \quad k \in \mathbb{Z}. \end{aligned} \quad (15)$$

Note that there is no pole at $\tilde{\gamma} = 0$ since the system is open. Defining the dimensionless function

$$\mathcal{R}(x, y, \tilde{\gamma}) = \frac{D}{L} \frac{\mathcal{P}_{\tilde{\gamma}E_{\text{Th}}}(x, y) S(\tilde{\gamma})}{S'(\tilde{\gamma})}, \quad (16)$$

where $S'(x) = \partial_x S(x)$, we can evaluate the time-dependent probability using the residue theorem by closing the integral contour in Eq. (4) on the left half-plane:

$$\mathcal{P}(x, y, t) = \frac{1}{L} \sum_k \mathcal{R}(x, y, \tilde{\gamma}_k) \exp(\tilde{\gamma}_k E_{\text{Th}} t). \quad (17)$$

$\mathcal{P}(x, y, t)$ is plotted in Fig. 2 for fixed $t = \tau_{\text{Th}}/4$, $N_d = 2$ and x either in the left contact or in the dot. We emphasize that for $N_d > 1$, $\mathcal{P}(x, y, t)$ is discontinuous at $y = \pm L$, describing confinement in the dot. In particular, $\mathcal{P}(x, y, t) = N_d \mathcal{P}(y, x, t)$ for x in a contact and y in the dot. Normalization is reflected by the fact that $\mathcal{P}(x, y, t)$ satisfies a semi-group relation

$$\int_{-2L}^{2L} dy \mathcal{P}(x, y, t_1) \mathcal{P}(y, z, t_2) = \mathcal{P}(x, z, t_1 + t_2). \quad (18)$$

In the next sections we will evaluate the correction to the conductance and the dephasing time using the probability \mathcal{P} .

5 Quantum corrections to the conductance for the quantum dot model

The classical conductance of the system described by Eq. (10) is obtained via Kirchhoff's circuit laws, since the contacts of length L and the central region of length $2L$

(with N_d wires in parallel) are connected in series. Denoting the contact conductance (i.e. the conductance of the left or right wire) as g_c , we obtain

$$g_0 = \frac{g_c}{2}(1 + 1/N_d)^{-1}. \quad (19)$$

Note that the value of g_c cannot be chosen arbitrarily: Assuming that the substrate, from which the wire (length L and width W) is constructed, is 2D or 3D with mean free path ℓ and Fermi wavelength λ_F , the conductance is given by $g_c^{2D} = \ell W / \lambda_F L$ or $g_c^{3D} = 2\ell W^2 / 3\pi\lambda_F^2 L$. Our theory requires $g_c > 4/3$ in order to obtain $g > \Delta g$, and quasi-1D diffusion requires $\lambda_F \ll \ell, W \ll L$. For a quantum-dot of the size of several μm , etched on a GaAs/AlGaAs heterostructure ($\lambda_F \approx 0.05 \mu\text{m}$), we can estimate a typical value of $g_c \sim 5$.

To evaluate the quantum corrections Δg , Eq. (1), we need the return probability defined via Eq. (13) at coinciding α and β . In this section, we consider the case $T = 0$ (i.e., $\tau_\varphi \rightarrow \infty$) and study Δg as a function of the dissipation parameter γ . We calculate matrix elements $[(\mathcal{M}^\gamma)^{-1}]_{11}, [(\mathcal{M}^\gamma)^{-1}]_{44}$ which yield the return probability for the dot:

$$\begin{aligned} \mathcal{P}_\gamma(x, x) \Big|_{x \in [-L, L]} &= \frac{1}{2\sqrt{\gamma D}(N_d + 1)S(\tilde{\gamma})} \\ &\times \left[(N_d - 1)\sinh\left(\sqrt{\tilde{\gamma}}\frac{x}{L}\right) - (N_d + 1)\sinh\left(\sqrt{\tilde{\gamma}}\left(\frac{x}{L} - 2\right)\right) \right] \\ &\times \left[(N_d + 1)\sinh\left(\sqrt{\tilde{\gamma}}\left(\frac{x}{L} + 2\right)\right) - (N_d - 1)\sinh\left(\sqrt{\tilde{\gamma}}\frac{x}{L}\right) \right]; \quad (20) \end{aligned}$$

and for the left wire:

$$\begin{aligned} \mathcal{P}_\gamma(x, x) \Big|_{x \in [-2L, -L]} &= \frac{\sinh\left(\sqrt{\tilde{\gamma}}\left(\frac{x}{L} + 2\right)\right)}{2\sqrt{\gamma D}(N_d + 1)S(\tilde{\gamma})} \quad (21) \\ &\times \left[(N_d - 1)\left((N_d + 1)\sinh\left(\sqrt{\tilde{\gamma}}\frac{x}{L}\right) + (N_d - 1)\sinh\left(\sqrt{\tilde{\gamma}}\left(\frac{x}{L} + 2\right)\right) \right) \right. \\ &\left. - (N_d + 1)\sinh\left(\sqrt{\tilde{\gamma}}\left(\frac{x}{L} + 4\right)\right) - (N_d + 1)^2\sinh\left(\sqrt{\tilde{\gamma}}\left(\frac{x}{L} - 2\right)\right) \right]; \end{aligned}$$

respectively. $\mathcal{P}_\gamma(x, x)$ for the right wire, $x \in [L, 2L]$, can be obtained from the symmetry property $\mathcal{P}_\gamma(x, x) = \mathcal{P}_\gamma(-x, -x)$. In the limit $\gamma \rightarrow 0$, Eqs. (20) and (21) reduce to

$$\mathcal{P}_0(x, x) \Big|_{x \in [-L, L]} = \frac{L((N_d + 1)^2 - (\frac{x}{L})^2)}{2D(N_d + 1)}, \quad (22)$$

$$\mathcal{P}_0(x, x) \Big|_{x \in [-2L, -L]} = \frac{L(2 + \frac{x}{L})(2 - N_d \frac{x}{L})}{2D(N_d + 1)}.$$

Note that the return probability diverges for $x \in [-L, L]$ in the limit $N_d \rightarrow \infty$, since the central region is effectively closed in this limit.

Similarly to Eq. (19), the total quantum corrections have to be properly weighted by using the circuit laws. The total correction can be written as a sum over all wires i of the network [17]:

$$\Delta g = -4D \frac{1}{\mathcal{L}^2} \sum_i \frac{\partial \mathcal{L}}{\partial L_i} \int_{\text{Wire No. } i} dx \mathcal{P}_\gamma(x, x), \quad (23)$$

where \mathcal{L} is the effective total length of the system obtained similar to the total resistance. In the case under consideration, we have

$$\mathcal{L} = L_0 + \frac{1}{1/L_1 + \dots + 1/L_{N_d}} + L_{N_d+1} = 2L(1 + 1/N_d), \quad (24)$$

where $L_0 = L$ corresponds to the left wire, $L_{N_d+1} = L$ to the right wire and $L_1 \dots L_{N_d} = 2L$ to the N_d wires of the dot. We obtain the following expression for the total quantum correction:

$$\begin{aligned} \Delta g &= -E_{\text{Th}} \frac{1}{(1 + 1/N_d)^2} \left[\int_{-2L}^{-L} dx \mathcal{P}_\gamma(x, x) \right. \\ &\left. + \frac{1}{N_d^2} \int_{-L}^L dx \mathcal{P}_\gamma(x, x) + \int_L^{2L} dx \mathcal{P}_\gamma(x, x) \right]. \quad (25) \end{aligned}$$

In Fig. 3, we show the total correction to the conductance according to Eq. (25) as a function of the dissipation parameter γ for different values of N_d . Note that for

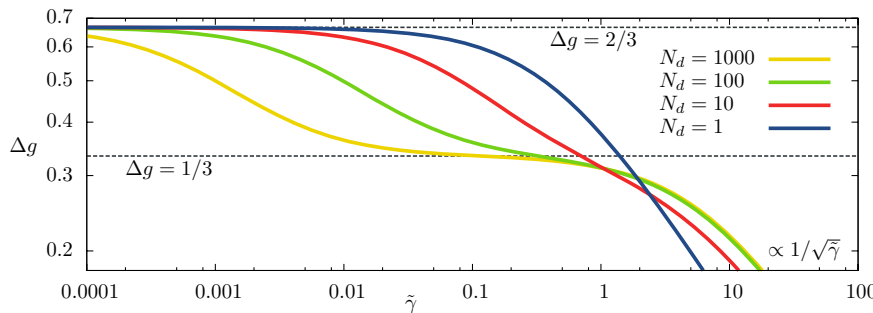


Figure 3 (online color at: www.ann-phys.org) Dependence of the total quantum correction to the conductance of the quantum dot model, Eq. (25), on the dimensionless dissipation parameter $\tilde{\gamma} = \gamma/E_{\text{Th}}$.

$\gamma \gg 1$ all curves are $\propto 1/\sqrt{\gamma}$, similar to an infinite wire with different prefactors corresponding to different effective wire width. We are mainly interested in the regime $\gamma \ll 1$, where the main result originates from the left and right wire and all curves approach the ergodic limit $\lim_{\gamma \rightarrow 0}(\Delta g) = 2/3$, cf. Eq. (2). This limit can be checked in this model by substituting Eqs. (22) into Eq. (25). Thus, in the absence of dissipation, our model has qualitatively the same behavior as RMT theory, albeit the precise universal value differs by a factor ~ 1 , cf. Sect. 2. This difference is due to the fact that RMT assumes structureless contacts and is a 0D model, whereas the validity of the graph model requires $L \gg (W, \ell)$ for the connecting quasi-1D wires. Since the time to reach one contact from the other increases linearly with N_d , there is an intermediate regime at $1/N_d < \tilde{\gamma} < 1$ for large N_d , where the system is described effectively as two wires connected in series via the dot, which just plays the role of an additional lead, such that $\Delta g = 1/3$.

6 Evaluation of the dephasing time for the quantum dot model

The dephasing time, τ_φ , can be calculated from the phase difference acquired by an electron in a time-dependent (fluctuating) potential $V(x, t)$ during a time-reversed traversal of its trajectory $x(t)$ [9]:

$$\Phi[x(\tau)] = \int_0^t d\tau [V(x(\tau), \tau) - V(x(\tau), t - \tau)]. \quad (26)$$

When averaged over the Gaussian fluctuations of the potential $\langle e^{i\Phi} \rangle_V = e^{-\frac{1}{2}\langle \Phi^2 \rangle_V}$, Eq. (26) leads to an exponential cutoff of the return probability⁴

$$\mathcal{P}(x, x, t) \rightarrow \mathcal{P}(x, x, t) \cdot \langle e^{i\Phi[x(\tau)]} \rangle_{\{x(\tau)\}} \approx \mathcal{P}(x, x, t) \cdot e^{-\mathcal{F}(x, t)} \quad (27)$$

where $\langle \dots \rangle_{\{x(\tau)\}}$ means the average is over closed trajectories $x(\tau)$ of duration t , starting and ending at x , and we defined the decay function \mathcal{F} [18, 19]:

$$\mathcal{F}(x, t) = \int_0^t dt_{1,2} \langle \langle (VV)(x(t_1), x(t_2), t_1 - t_2) - \langle (VV)(x(t_1), x(t_2), t - t_1 - t_2) \rangle_{\{x(\tau)\}} \rangle. \quad (28)$$

⁴ Note that in the second equality of Eq. (27), we exponentiate the average over closed path, see [18] for details.

In the case of the graph model for the quantum dot, the usual operational definition of τ_φ reads

$$\mathcal{F}(x, \tau_\varphi(x)) = 1, \quad (29)$$

such that the correction to the conductance is given by Eq. (25) with a position dependent $\gamma(x) = 1/\tau_\varphi(x)$. The correlation function $\langle (VV) \rangle$ entering Eq. (28) is well known for the case of electron interactions in macroscopically homogeneous disordered systems [9]. Recently, we have generalized this theory for inhomogeneous, multiply-connected systems [10]. It has been shown that $\langle (VV) \rangle$ generically is given by

$$\langle (VV) \rangle(x, y, t) = \frac{4\pi T}{g_c L} P_0(x, y) \delta_T(t), \quad (30)$$

where $P_0(x, x) = \lim_{\gamma \rightarrow 0} P_\gamma(x, x)$ and

$$\delta_T(t) = \pi T w(\pi T t) \quad \text{with} \quad w(x) = \frac{x \coth(x) - 1}{\sinh^2 x} \quad (31)$$

is a broadened δ -function which allows us to take into account the Pauli principle [18].

Inserting Eq. (30) into Eq. (28), we find

$$\mathcal{F}(x, t) = \frac{4\pi T}{g_c} \int_0^t dt_{1,2} Q(x, t_m, t_M - t_m, t - t_M) \times [\delta_T(t_1 - t_2) - \delta_T(t_1 + t_2 - t)], \quad (32)$$

where $t_m = \min[t_1, t_2]$ and $t_M = \max[t_1, t_2]$. The function Q is given by the dimensionless quantity DP_0/L , averaged over closed random walks:

$$Q(x_0, t_1, t_2, t_3) = \int_{-2L}^{2L} dx_{1,2} \times \frac{\mathcal{P}(x_0, x_1, t_1) \mathcal{P}(x_1, x_2, t_2) \mathcal{P}(x_2, x_0, t_3) DP_0(x_1, x_2)}{\mathcal{P}(x_0, x_0, t_1 + t_2 + t_3) L}. \quad (33)$$

All probabilities in Eq. (33) can be evaluated analytically from Eq. (17), Eq. (13) and Eq. (10), by deriving the corresponding entries in the inverted vertex matrix $[\mathcal{M}^Y]^{-1}$. The integrand is lengthy and we have chosen the following strategy for calculating the integrals:

1) We use Eq. (17) to rewrite Eq. (33) as:

$$Q(x_0, t_1, t_2, t_3) = \sum_{n,k,l} \frac{\mathcal{Q}(x_0, \tilde{\gamma}_n, \tilde{\gamma}_k, \tilde{\gamma}_l)}{\mathcal{P}(x_0, x_0, t_1 + t_2 + t_3)} e^{\tilde{\gamma}_n t_1 + \tilde{\gamma}_k t_2 + \tilde{\gamma}_l t_3}, \quad \text{with} \quad (34)$$

$$\mathcal{Q}(x_0, \tilde{\gamma}_1, \tilde{\gamma}_2, \tilde{\gamma}_3) = D \int \frac{dx_{1,2}}{L^3} \times \mathcal{R}(x_0, x_1, \tilde{\gamma}_1) \mathcal{R}(x_1, x_2, \tilde{\gamma}_2) \mathcal{R}(x_2, x_0, \tilde{\gamma}_3) P_0(x_1, x_2). \quad (35)$$

The integrals in Eq. (35) over space are evaluated symbolically with the help of a computer algebra program.

2) Since the time dependence of Q in Eq. (34) is simply exponential, one of the time-integrals in Eq. (28) is calculated analytically. As a result, $F(x_0, t)$ simplifies to a single time integral and multiple sums:

$$F(x_0, t) = \frac{(4\pi)^2}{g_c} \frac{\sum_{n,k,l} \mathcal{Q}(x_0, \tilde{\gamma}_n, \tilde{\gamma}_k, \tilde{\gamma}_l) \int_0^{tT} d\tau \mathcal{E}(\tau, \tilde{\gamma}_n, \tilde{\gamma}_k, \tilde{\gamma}_l)}{\sum_m \mathcal{R}(x_0, x_0, \tilde{\gamma}_m) e^{\tilde{\gamma}_m E_{\text{Th}} t}}. \quad (36)$$

Here, the remaining time dependence of the kernel is incorporated in the function \mathcal{E} :

$$\mathcal{E}(\tau, \tilde{\gamma}_1, \tilde{\gamma}_2, \tilde{\gamma}_3) = w(\pi\tau) e^{c_1 t T} \times \left[\frac{\sinh(c_2(tT - \tau)) e^{c_3 \tau}}{2c_2} - \frac{\sinh\left(\frac{c_3}{2}(tT - \tau)\right) \cosh(c_2 \tau) e^{c_3(tT - \tau)/2}}{c_3} \right], \quad (37)$$

with

$$c_1 = (\tilde{\gamma}_1 + \tilde{\gamma}_3) \frac{E_{\text{Th}}}{2T}, \quad c_2 = (\tilde{\gamma}_1 - \tilde{\gamma}_3) \frac{E_{\text{Th}}}{2T}, \quad c_3 = \tilde{\gamma}_2 \frac{E_{\text{Th}}}{T} - c_1. \quad (38)$$

3) The sums and the integral over τ are calculated numerically.

This strategy allows us to calculate τ_φ and to describe the T -dependence of Δg in the quantum dot model, including the full crossover between different regimes of dephasing.

7 Examples of application

In this section, we use the graph model of the quantum dot to calculate $\tau_\varphi(x_0, T)$ and $\Delta g(T)$ in the case $g_c = 5$ for the parameter N_d ranging from $N_d = 1$ (no confinement in the central region) to $N_d = 100$ (almost closed quantum dot connected to ideal leads via two contacts). Our model is valid for this choice of g_c , see the discussion in Sect. 5, and the total conductance of the system $1.25 < g_0 < 2.5$ is close to experimental setups [20, 21]. The results are shown in Fig. 4.

The *dephasing time* is shown in Fig. 4(a) for several values of the origin of the Cooperon, x_0 , which can belong either to the central region (solid blue lines) or the contact (dashed red lines). To check the validity of the

results, we compare τ_φ at high and small temperatures with earlier results for an almost isolated quasi-1D ring of total length $4L$ and total conductance g_1 [22].

If $\tau_T \ll \tau_\varphi \ll \tau_{\text{Th}} \equiv 1/E_{\text{Th}}$, dephasing is not sensitive to the boundary conditions and it is described by the theory of infinite systems [9]. In the ring, the high- T regime appears at $T \gg g_1 E_{\text{Th}}$. The formula for τ_φ in this regime, including sub-leading terms, reads [22]:

$$\frac{\tau_\varphi}{\tau_{\text{Th}}} = \left(\frac{2g_1 E_{\text{Th}}}{\pi^{3/2} T} \right)^{2/3} \left(1 + \frac{2^{5/2}}{3\pi} |\zeta(1/2)| \left(\frac{\pi^{3/2}}{2g_1} \right)^{1/3} \left(\frac{E_{\text{Th}}}{T} \right)^{1/6} + \frac{2}{9\sqrt{\pi}} \left(\frac{2g_1}{\pi^{3/2}} \right)^{1/3} \left(\frac{E_{\text{Th}}}{T} \right)^{1/3} \right). \quad (39)$$

We have reproduced this high- T behavior in the quantum dot model, see Fig. 4(a): Numerically obtained curves coincide with Eq. (39), after substituting $N_d g_c$ for g_1 , when $T \gg (g_c N_d) E_{\text{Th}}$. We note that dephasing in the high- T regime is substantially inhomogeneous in space, since the relevant trajectories are restricted to a small region around x_0 . In particular, for sufficiently high T , all curves for dephasing in the contact ($N_d = 1, 10, 100$) coincide with the curve for $N_d = 1$ in the central region, since the number of channels in the central region is irrelevant for dephasing in the contact. On the other hand, dephasing in the central region itself becomes weaker with increasing N_d , since N_d increases the effective conductance in this region.

In the low- T regime,⁵ $\tau_{\text{Th}} \ll \tau_T \ll \tau_\varphi$, typical electron trajectories explore the whole system many times before dephasing becomes effective [1]. The geometry of the system is not important in this case and, therefore, the low- T regime is usually referred to as *the regime of 0D dephasing*. In the ring, it occurs at $T \ll E_{\text{Th}}$ with τ_φ given by [22]

$$\frac{\tau_\varphi}{\tau_{\text{Th}}} = \frac{135g_1}{32\pi^2} \left(\frac{E_{\text{Th}}}{T} \right)^2 \left(1 + \frac{16\pi}{45g_1} \frac{T}{E_{\text{Th}}} + \frac{128\pi^2}{105} \left(\frac{T}{E_{\text{Th}}} \right)^2 \right). \quad (40)$$

The quantum dot model shows similar behavior at $T \ll E_{\text{Th}}$, after substituting $g_c N_d$ for the ring conductance.

⁵ The intermediate regime, $\tau_T \ll \tau_{\text{Th}} \ll \tau_\varphi$, characterized by $\tau_\varphi \propto T^{-1}$ is strongly distorted in the quantum dot, since: (a) the conductance g_c is relatively small, reducing the range of validity of this regime, and (b) it occurs when typical electron trajectories are of the order of the system size making τ_φ sensitive to the inhomogeneities of the graph.

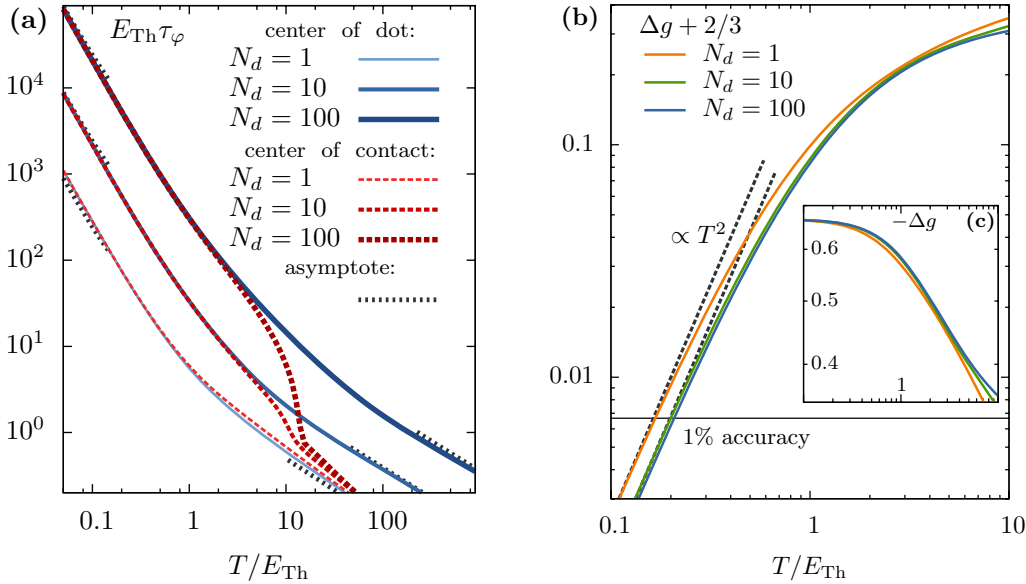


Figure 4 (online color at: www.ann-phys.org) (a) The dephasing time in units of the Thouless time, $1/E_{Th}$, plotted for several values of N_d and x_0 . Solid blue lines, correspond to $x_0 = -0.05L$ close to the center of the dot, while dashed red lines correspond to $x_0 = -1.55L$ close to the center of the left contact. The thickness (and brightness) of the curve determines the number of channels in the dot, $N_d = 1, 10, 100$ from thin to thick (and bright to dark). The black dotted lines correspond to the asymptotic results, Eqs. (39) and (40), derived from an isolated ring geom-

etry, see main text for details. (b) The difference $\Delta g + 2/3$ between the correction to the conductance, Δg , and its universal zero-temperature value, $\Delta g(T=0) = -2/3$, plotted as function of temperature. 0D behavior of the dephasing time, characterized by $\Delta g \propto T^2$, appears at very low temperatures, requiring a precision much larger than 1% on the conductance measurement. Inset: (c) Total correction to the conductance $-\Delta g$ (without subtracting $\Delta g(T=0)$), plotted as function of temperature.

We emphasize that 0D dephasing in our model is governed by atypical trajectories, which explore the dot and the contacts many times during the time scale $t \gg \tau_{dw}$. Therefore, the dephasing time is nearly coordinate independent: Dephasing in the central region and in the contacts is essentially the same.

The correction to the conductance is shown in the inset, Fig. 4(c), for $N_d = 1, 10, 100$. We calculated Δg from the integral in Eq. (25) with a position dependent $\gamma(x) = 1/\tau_{\varphi}(x, T)$. As expected from the discussion in Sect. 5, the curves saturate to the universal value $\Delta g = -2/3$, when $\tilde{\gamma} \equiv \gamma/E_{Th} \ll 1/N_d$. Since $1/\tilde{\gamma} = \tau_{\varphi}/\tau_{Th} \sim (g_c N_d)(E_{Th}/T)^2$ in this regime and g_c is small and fixed, saturation occurs when $T \lesssim E_{Th}$. The intermediate regime for $1/N_d \ll \tilde{\gamma} \ll 1$, where $\Delta g = -1/3$, cf. Fig. 3, is strongly distorted since it lies in the crossover region between high- T and low- T regime. We note that at $T < 10E_{Th}$, curves for different N_d look very similar. Moreover, dephasing is very weak

at $T \ll E_{Th}$ where Δg is governed by a dwell time, τ_{dw} , of the entire system and is practically T -independent. After subtracting the curve from its universal value, see Fig. 4(b), 0D dephasing reveals itself as $\Delta g \propto T^2$ for very low temperatures $T \lesssim 0.2E_{Th}$. At $0.2E_{Th} < T < E_{Th}$ one can observe only a transient, since (i) dephasing is not yet sufficiently weak to justify $\Delta g \propto T^2$ and (ii) the 0D regime of dephasing is not fully reached, cf. Fig. 4(a). Moreover, if the leads are not perfectly absorbing, the transient can be extended even to lower temperatures due to additional dephasing in the leads. All this clearly shows that 0D dephasing cannot be discovered directly in transport measurements through the quantum dot. Even at $T \lesssim 0.2E_{Th}$, a fitting of the experimental data would require g to be measured with a precision of much better than 1%. Alternative possibilities for the experimental observation of 0D dephasing are discussed in the Conclusions.

8 Conclusions

We have suggested a graph model, which allows one to describe transport through mesoscopic quantum dots. The graph includes three quasi-1D regions: identical left- and right- wires and a central region. The identical wires are connected to ideally absorbing leads and mimic the contacts of a real system. The number of conducting channels in the central region can be of the order of- or substantially larger than the number of channels in the contacts. The latter case corresponds to a strong confinement of electrons in the central region. Thus the graph model is able to describe a crossover from opened to closed quantum dots.

The model which we suggest can be viewed as complementary to the seminal RMT model. Firstly, the exact solution to the diffusion equation can be found for the graph model. Secondly, we have shown that our model correctly reproduces the universal regime of transport in full analogy with the RMT solution. Even more importantly, the graph model allows us to take into account interaction induced dephasing in a broad temperature range, i.e., we can describe the full crossover from 1D to 0D regimes.

Using the solution to the diffusion equation on the graph, we have described in detail how to calculate the dephasing time and the weak localization correction to the conductance. Though the intermediate equations are rather lengthy, we have suggested an efficient combination of analytical steps (involving computer algebra) and numerical integration, which helped us to overcome technical difficulties.

The general approach has been illustrated for the system with $g_c = 5$. We have demonstrated that 0D dephasing ($\sim T^2$), which is governed by the Pauli principle and is very generic, occurs in the system at $T \ll E_{\text{Th}}$ at *arbitrary* ratio of the channel numbers in the dots and leads. In this regime, dephasing is governed by atypical trajectories which explore the dot and the contacts many times during the time scale $t \gg \tau_{\text{dw}}$ where the conductance is governed mainly by the dwell time and is almost T -independent. Our results confirm that weak 0D dephasing is substantially distorted by the influence of the contacts and the leads. Therefore, its direct experimental observation in transport through the quantum dot would require not only very low temperatures but also unrealistically precise measurements. We conclude that alternative experimental approaches are needed, where either the effects from the environment are reduced or the system is closed. One possibility to improve the effective precision of the measurements is related to extracting τ_φ from the T -dependence of the Aronov-Altshuler-Spivak

oscillations of the magnetoconductivity in almost closed mesoscopic rings. This option was discussed in recent papers [6, 22] where all effects of the environment were taken into account via a constant dwelling time. We plan to study in more detail the sensitivity of the AAS oscillations on the distortions from the environment using a ring model similar to the model of the dot presented here [23]. The other option is to extract τ_φ from experimental measurements of the electric or magnetic susceptibility of *closed* mesoscopic systems, e.g. by measuring the properties of resonators in which mesoscopic samples are deposited [24]. In closed systems, there is no universal limit of the quantum corrections at $\tau_\varphi \gg \tau_{\text{dw}}$, typical for transport through opened systems. Therefore, the saturation in the closed system can occur at much lower T , making them more suitable for an experimental observation of 0D dephasing. A theoretical description of such experiments will be published elsewhere.

Acknowledgements. We acknowledge illuminating discussions with C. Texier, and support from the DFG through SFB TR-12 (O. Ye.), DE 730/8-1 (M. T.) and the Cluster of Excellence, Nanosystems Initiative Munich.

Key words. Dephasing, quantum dot, weak localization, diffusion in graphs.

References

- [1] U. Sivan, Y. Imry, and A. G. Aronov, *Europhys. Lett.* **28**, 115 (1994).
- [2] B. Doucot and R. Rammal, *Phys. Rev. Lett.* **55**, 1148 (1985).
- [3] B. Doucot and R. Rammal, *J. Phys. (Paris)* **47**, 973 (1986).
- [4] T. Ludwig and A. D. Mirlin, *Phys. Rev. B* **69**, 193306 (2004).
- [5] C. Texier and G. Montambaux, *Phys. Rev. B* **72**, 115327 (2005).
- [6] M. Treiber et al., *Phys. Rev. B* **80**, 201305 (2009).
- [7] C. Texier, P. Delplace, and G. Montambaux, *Phys. Rev. B* **80**, 205413 (2009).
- [8] D. E. Khmel'nitskii, *Physica B + C* **126**, 235 (1984)
- [9] B. L. Altshuler, A. G. Aronov, and D. E. Khmel'nitsky, *J. Phys. C* **15**, 7367 (1982).
- [10] M. Treiber et al., *Phys. Rev. B* **84**, 054204 (2011).
- [11] E. Akkermans and G. Montambaux, in: *Mesoscopic Physics of Electrons and Photons* (Cambridge University Press, Cambridge, 2007).
- [12] H. U. Baranger and P. A. Mello, *Phys. Rev. Lett.* **73**, 142 (1994).
- [13] R. A. Jalabert, J.-L. Pichard, and C. W. J. Beenakker, *Europhys. Lett.* **27**, 255 (1994).

- [14] P. W. Brouwer and C. W. J. Beenakker, *Phys. Rev. B* **55**, 4695 (1997).
- [15] M. Büttiker, *Phys. Rev. B* **33**, 3020 (1986).
- [16] E. McCann and I. V. Lerner, *J. Phys. Condens. Matter* **8**, 6719 (1996).
- [17] C. Texier and G. Montambaux, *Phys. Rev. Lett.* **92**, 186801 (2004).
- [18] F. Marquardt, J. von Delft, R. Smith, and V. Ambegaokar, *Phys. Rev. B* **76**, 195331 (2007).
- [19] J. von Delft, F. Marquardt, R. Smith, and V. Ambegaokar, *Phys. Rev. B* **76**, 195332 (2007).
- [20] A. G. Huibers et al., *Phys. Rev. Lett.* **81**, 200 (1998).
- [21] S. Amasha et al., arXiv:1009.5348 (unpublished).
- [22] M. Treiber et al., Dimensional Crossover of the Dephasing Time in Disordered Mesoscopic Rings: From Diffusive Through Ergodic to 0D Behavior, in: *Perspectives of Mesoscopic Physics – Dedicated to Yoseph Imry's 70th Birthday*, Chap. 20, edited by A. Aharony and O. Entin-Wohlman (World Scientific, Singapore, 2010); arXiv:1001.0479.
- [23] M. Treiber, O. M. Yevtushenko, and J. von Delft, to be published.
- [24] R. Deblock et al., *Phys. Rev. B* **65**, 075301 (2002).

Chapter 4

Quantum corrections to the polarizability

In Chapter 3, we have discussed dephasing at low temperatures in the context of the weak-localization correction to the conductance. We found that the elusive 0D regime of dephasing can be observed only in the universal regime, where the weak-localization correction is dominated by a dwelling time τ_{dw} and the system's real dimensionality is not important. Thus, the characteristic $1/\tau_{\phi} \propto T^2$ behavior of the dephasing time is difficult to observe and heavily depends on the contacts controlling the confinement. In isolated systems, on the other hand, we have effectively $\tau_{\text{dw}} \rightarrow \infty$, making them an ideal candidate to study 0D dephasing.

Furthermore, we have discussed in Section 2.2.5 that in the isolated systems, and in the absence of other sources of dephasing, the 0D regime is characterized by a discreteness of the energy levels. In contrast to the conductivity of a good metal, which is well described by the loop-expansion, discrete level systems are rather described by the non-perturbative random matrix theory (RMT). Thus, an analysis of quantum corrections in isolated systems also provides the unique opportunity to study the crossover from perturbative to non-perturbative regimes.

4.1 Isolated systems: Realizing the canonical ensemble

One of the recent and important results of mesoscopic physics was the realization that the employed statistical ensemble plays an important role in the description of observables [Kamenev and Gefen, 1993; Kamenev *et al.*, 1994; Kamenev and Gefen, 1997b]. Usually the grand-canonical ensemble (GCE), where the chemical potential μ is fixed, is used to describe quantum corrections, cf. Section 2. On the other hand, isolated systems are characterized by a fixed number of particles N and are rather described by the canonical ensemble (CE). Remarkably, a qualitative difference between the CE and the GCE can persist up to energy scales much larger than the level spacing Δ [Kamenev and Gefen, 1997a].

Initiated by the seminal work of Büttiker *et al.* (1983), who predicted a so-called *persistent current* in disordered *phase-coherent* metallic rings, a large effort has been made to describe the magnetic response of isolated samples, see e.g. Cheung *et al.* (1988); Schmid (1991). However, the experimental observation of the persistent current is difficult due to its weakness. In fact, experimental results often differed in sign and magnitude with theoretical predictions [Reulet *et al.*, 1995; Deblock *et al.*, 2002a]. In spite of recent advances in measurement techniques, see Bluhm *et al.* (2009); Bleszynski-Jayich *et al.* (2009), persistent currents remain a rather controversial subject in mesoscopic physics. Thus, in the following, we will solely concentrate on the *electric* response of mesoscopic samples, namely, we will investigate the electrical polarizability of isolated samples in the CE.

To realize the CE, we employ the ideas of Altland *et al.* (1992a,b); Lehle and Schmid (1995):

When the number of particles N in the system is fixed, the chemical potential μ fluctuates. However, the precise value of $\mu \sim \epsilon_F$ is not relevant in the quantum corrections, e.g. the correlation functions such as P and K , defined in Eqs. (2.10, 2.11), do not depend on energy ϵ . In fact, this is a rather general observation for disorder averaged correlation functions, since we have seen in Eq. (2.12) that each “step” of any impurity ladder $d_{\mathbf{q},\omega}$ is independent of the common energy of particle and hole in the limit $(\epsilon_F\tau)^{-1} \ll 1$. From a semi-classical picture, the independence of $d_{\mathbf{q},\omega}$ on ϵ is intuitively clear, since it corresponds to the requirement that the propagation time of particle and hole between two scattering events has to be identical to guarantee constructive interference. However, we stress that the independence on ϵ does not mean that the statistical ensemble is irrelevant. Instead, the fluctuations of the chemical potential induce correlations of the density of states with the correlation functions, i.e. *three-level correlations* become important, as we will see in the following.

For a fixed number of electrons and low temperatures $T \ll \epsilon_F$, all of the lowest electron states of the Fermi sea up to the N 'th state $\epsilon_{\mathbf{k}}$ are occupied. Following [Lehle and Schmid \(1995\)](#), we can thus “pin” the chemical potential to this particular level by setting $\mu = \epsilon_{\mathbf{k}} + 0$. However the level $\epsilon_{\mathbf{k}}$ is not fixed and we should describe its distribution by a normalized weight function $P(\epsilon_{\mathbf{k}})$ centered around ϵ_F and with a support much smaller than ϵ_F but much larger than the level spacing Δ .¹

To give a concrete example, let us consider the correlation function K introduced in Eq. (2.11). Before impurity averaging and for a fixed chemical potential is given by:

$$K^{GCE} = \frac{1}{2\pi\rho} G_{\mu+\epsilon}^R(\mathbf{x}, \mathbf{x}) G_{\mu+\epsilon-\omega}^A(\mathbf{y}, \mathbf{y}). \quad (4.1)$$

Pinning the chemical potential to $\epsilon_{\mathbf{k}}$ to describe the canonical ensemble, we instead have

$$K^{CE} = \frac{1}{2\pi\rho} \frac{\sum_{\mathbf{k}} P(\epsilon_{\mathbf{k}}) G_{\epsilon_{\mathbf{k}}+\epsilon}^R(\mathbf{x}, \mathbf{x}) G_{\epsilon_{\mathbf{k}}+\epsilon-\omega}^A(\mathbf{y}, \mathbf{y})}{\sum_{\mathbf{k}} P(\epsilon_{\mathbf{k}})}. \quad (4.2)$$

Using the definition of the density of states, Eq. (2.8), the normalization constant in Eq. (4.2) can be written as

$$\sum_{\mathbf{k}} P(\epsilon_{\mathbf{k}}) = V \int_{-\infty}^{\infty} d\epsilon P(\epsilon) \rho_{\epsilon} \approx \rho V, \quad (4.3)$$

since the ρ_{ϵ} depends only weakly on ϵ at $\epsilon \ll \epsilon_F$. Therefore, Eq. (4.2) can be written as

$$\begin{aligned} K^{CE} &= \frac{1}{2\pi\rho^2} \int_{-\infty}^{\infty} dE P(E) \rho_E G_{E+\epsilon}^R(\mathbf{x}, \mathbf{x}) G_{E+\epsilon-\omega}^A(\mathbf{y}, \mathbf{y}) \\ &= \frac{i}{(2\pi\rho)^2} \int_{-\infty}^{\infty} dE P(E) [G_E^R(\mathbf{z}, \mathbf{z}) - G_E^A(\mathbf{z}, \mathbf{z})] G_{E+\epsilon}^R(\mathbf{x}, \mathbf{x}) G_{E+\epsilon-\omega}^A(\mathbf{y}, \mathbf{y}). \end{aligned} \quad (4.4)$$

Since the disorder average of the product of Green's functions does not depend on their common energy, we can integrate over E using the normalization $\int_{-\infty}^{\infty} dE P(E) = 1$. As a result, we find for K in the canonical ensemble:

$$\overline{K^{CE}}(\mathbf{x}, \mathbf{y}, \omega) = \frac{i}{(2\pi\rho)^2 V} \int d^d \mathbf{z} \overline{[G_E^R(\mathbf{z}, \mathbf{z}) - G_E^A(\mathbf{z}, \mathbf{z})] G_{E+\epsilon}^R(\mathbf{x}, \mathbf{x}) G_{E+\epsilon-\omega}^A(\mathbf{y}, \mathbf{y})}. \quad (4.5)$$

1. After disorder averaging, this “Fermi-level pinning ensemble” describes an ensemble average of a large number of isolated samples where the number of particles is fixed per sample. However, the particle number is not necessarily the same in different samples of the ensemble, see the discussion in [Altland et al. \(1992a,b\)](#) and [Kamenev and Gefen \(1993\)](#).

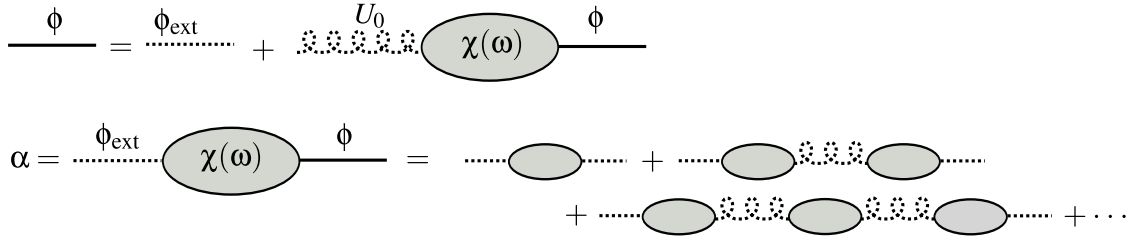


Figure 4.1: Expression for electric potential and the polarizability in the RPA according to Eq. (4.12) and Eq. (4.14).

Note that K^{CE} also includes the Altshuler-Shklovski diagrams shown in Fig. 2.8. However, additional diagrams stemming from correlations between $G_E^{R/A}$ to the other Green's functions have to be taken into account.

As an aside, we note that the \mathbf{z} dependence of the integrand in Eq. (4.5) means that an additional *vertex* has to be taken into account when calculating the corresponding diagrams. However, due to the integral over \mathbf{z} , there is no momentum or energy transferred at this vertex. After impurity averaging, the vertex is merely a product of two disorder averaged Green's functions with the same energy and momentum label. Using the identity

$$\left[\overline{G_\varepsilon^{R/A}(\mathbf{k})} \right]^2 = -\frac{\partial}{\partial \varepsilon} \overline{G_\varepsilon^{R/A}(\mathbf{k})}, \quad (4.6)$$

it can be shown, see [Smith *et al.* \(1998\)](#), that the vertex can be replaced by an additional energy derivative. This replacement greatly reduces the number of possible diagrams, and we use it in Section 4.5 to evaluate the corresponding diagrams for the polarizability.

4.2 The polarizability in the random phase approximation

The electrical polarizability α is defined as the linear response of the dipole moment $\mathbf{d}(\omega)$ to a spatially homogeneous electric field $E(\omega)$:

$$\mathbf{d}(\omega) = \alpha(\omega) \mathbf{E}(\omega), \quad \text{or} \quad \alpha(\omega) = \mathbf{d}(\omega) \cdot \mathbf{E}(\omega) / E(\omega)^2. \quad (4.7)$$

The dipole moment of a metal is defined via

$$\mathbf{d}(\omega) = \int d^d \mathbf{x} (\mathbf{x} \cdot n_{\text{in}}(\mathbf{x}, \omega)), \quad (4.8)$$

where $n_{\text{in}}(\mathbf{x}, \omega)$ is the excess charge density induced by the electric field. n_{in} can be calculated similar to the current density in Section 3.1.1. After expanding

$$n(\mathbf{x}, \omega) = -i [G^K(\mathbf{x}, t; \mathbf{x}, t) - G^R(\mathbf{x}, t; \mathbf{x}, t) + G^A(\mathbf{x}, t; \mathbf{x}, t)] \quad (4.9)$$

to linear order in a potential $\phi(\mathbf{y}, \omega)$, we find

$$n_{\text{in}}(\mathbf{x}, \omega) = -2e^2 \int d^d \mathbf{y} \chi(\mathbf{x}, \mathbf{y}, \omega) \phi(\mathbf{y}, \omega), \quad (4.10)$$

where the so-called *density response function* χ is given by the retarded polarization function $\Pi^R(\mathbf{x}, \mathbf{y}, \omega)$ obtained in Section 2.2.2 (compare Eq. (3.9) with Eq. (2.84)). Following the discussion after Eq. (2.84), we find

$$\chi(\mathbf{x}, \mathbf{y}, \omega) = \Pi^R(\mathbf{x}, \mathbf{y}, \omega) = \rho [\delta(\mathbf{x} - \mathbf{y}) + i\omega P(\mathbf{x}, \mathbf{y}, \omega)], \quad (4.11)$$

where P is the generalized diffusion propagator defined in Eq. (2.10) at given chemical potential, which we have calculated to two-loop order in Section 2.3. However, the potential $\phi(\mathbf{y}, \omega)$ in Eq. (4.10) is not the external potential of the electric field, but the total potential in the presence of the Fermi sea. Following our discussion in Section 2.2.2, screening should be taken into account using the RPA. In this approximation, the total potential ϕ is given by the Dyson equation shown in the first line of Fig. 4.1(a):

$$\phi(\mathbf{x}, \omega) = \phi_{\text{ext}}(\mathbf{x}, \omega) - \int d^d \mathbf{y} d^d \mathbf{z} U_0(\mathbf{x}, \mathbf{y}) \chi(\mathbf{y}, \mathbf{z}, \omega) \phi(\mathbf{z}, \omega), \quad (4.12)$$

with

$$\phi_{\text{ext}}(\mathbf{x}, \omega) = -\mathbf{E}(\omega) \cdot \mathbf{x}. \quad (4.13)$$

Using Eq. (4.7) with Eq. (4.8), we find the following expression for the polarizability, see also Fig. 4.1(a):

$$\alpha(\omega) = \frac{2e^2}{E(\omega)^2} \int d^d \mathbf{x} d^d \mathbf{y} \phi_{\text{ext}}(\mathbf{x}, \omega) \chi(\mathbf{x}, \mathbf{y}, \omega) \phi(\mathbf{y}, \omega). \quad (4.14)$$

Eq. (4.14) is the starting point of our calculation of the polarizability in Section 4.5. Using Eq. (4.10) in Eq. (4.14) and Eq. (4.12), we calculate the quantum corrections in two-loop order and take into account the difference between GCE and CE as discussed in Section 4.1.

To calculate the quantum corrections to Eq. (4.14), a further simplification is often useful [Efetov, 1996]: At small frequencies $\omega \ll E_{\text{Th}}$, the classical contribution to the polarizability (i.e. Eq. (4.11) with P_d substituted for P) is independent of frequency. In this limit, the following strategy can be pursued: (i) We decompose the density response function into a frequency dependent and independent part, $\chi(\omega) = \chi(0) + \delta_\omega \chi(\omega)$ with $\delta_\omega \chi(\omega) \equiv \chi(\omega) - \chi(0)$, see Fig. 4.2. (ii) In the RPA series for α , see Fig. 4.1, we keep only terms to first order in $\delta_\omega \chi(\omega)$. (iii) We re-sum the series left and right of the $\delta_\omega \chi(\omega)$ -term such that:

$$\delta_\omega \alpha(\omega) \equiv \alpha(\omega) - \alpha_0 \approx \frac{2e^2}{E(\omega)^2} \int d^d \mathbf{x} d^d \mathbf{y} \phi_0(\mathbf{x}, \omega) \delta_\omega \chi(\mathbf{x}, \mathbf{y}, \omega) \phi_0(\mathbf{y}, \omega), \quad (4.15)$$

where $\phi_0(\omega)$ solves Eq. (4.12) with $\chi(\omega)$ replaced by $\chi(0)$, see Fig. 4.2, and α_0 is the classical polarizability. Using $\chi(\mathbf{x}, \mathbf{y}, \omega \rightarrow 0) = \rho \delta(\mathbf{x} - \mathbf{y})$ in Eq. (4.12) and applying $\Delta_{\mathbf{x}} |\mathbf{x} - \mathbf{y}|^{-1} = -4\pi \delta(\mathbf{x} - \mathbf{y})$, one obtains the so-called Thomas-Fermi approximation, relating ϕ_0 to the induced charge $n_{\text{in},0}$:

$$\phi_0(\mathbf{x}, \omega) = -\frac{4\pi}{\kappa^2} n_{\text{in},0}(\mathbf{x}, \omega) \quad \text{with} \quad n_{\text{in},0}(\mathbf{x}, \omega) \equiv -\frac{1}{4\pi} \Delta_{\mathbf{x}} \phi_0(\mathbf{x}, \omega), \quad (4.16)$$

where κ is the Thomas-Fermi screening wave vector defined in Eq. (2.80). The induced charge $n_{\text{in},0}(\mathbf{x}, \omega)$ can be determined by classical electrostatics since the response function appearing in ϕ_0 is local and instantaneous. (The frequency dependence of $n_{\text{in},0}$ is simply proportional to the frequency dependence of the external electric field.) Thus, Eqs. (4.15, 4.16) express the quantum corrections to the polarizability purely in terms of the quantum corrections to χ and well-known classical quantities.

4.3 Results from RMT and the sigma-model

Since we are mainly interested to study the onset of 0D dephasing (at $T \lesssim E_{\text{Th}}$), where dephasing is weak, it is instructive to compare our results with the expectations at $\gamma = 0$ from RMT. In a seminal

$$\chi(\omega) = \chi(0) + \delta_\omega \chi(\omega)$$

$$\delta_\omega \alpha(\omega) \approx \text{---} \phi_0 \text{---} \text{---} \delta_\omega \chi(\omega) \text{---} \text{---} \phi_0 \text{---}, \quad \text{---} \phi_0 \text{---} = \text{---} \phi_{\text{ext}} \text{---} + \text{---} U_0 \text{---} \text{---} \chi(0) \text{---} \text{---} \phi_0 \text{---}$$

Figure 4.2: The polarizability to first order in the frequency dependent part of the density response function.

work, [Gorkov and Eliashberg \(1965\)](#) studied the polarizability using results from RMT and found very large quantum corrections. However, [Rice *et al.* \(1973\)](#) have shown that the corrections are significantly reduced if screening is taken into account correctly. (A detailed analysis can be found in [Blanter and Mirlin \(1996\)](#).) More recently, [Blanter and Mirlin \(2001\)](#) calculated the frequency dependence of the quantum corrections to α in the CE.¹ Their derivation is based on the previous works (mainly concerning the GCE) by [Efetov \(1996\)](#)² and [Blanter and Mirlin \(1998\)](#)³. In the following, we will give a brief but exhaustive derivation of their final results in the GCE and the CE.

Starting point of the RMT calculation is an expression of the density response function χ at given chemical potential $\mu \ll T$ in terms of the eigen-functions ϕ_n and -energies ε_n of the Hamiltonian:

$$\chi_\mu(\mathbf{x}, \mathbf{y}, \omega) = \sum_{n,m} \phi_n^*(\mathbf{x}) \phi_n(\mathbf{y}) \phi_m^*(\mathbf{y}) \phi_m(\mathbf{x}) \frac{\theta(\mu - \varepsilon_n) - \theta(\mu - \varepsilon_m)}{\omega + \varepsilon_m - \varepsilon_n + i0}. \quad (4.17)$$

Eq. (4.17) directly follows from Eq. (2.84) after substituting the Lehmann representation of the Green's functions:

$$G_\varepsilon^{R/A}(\mathbf{x}, \mathbf{y}) = \sum_n \frac{\phi_n^*(\mathbf{x}) \phi_n(\mathbf{y})}{\varepsilon - \varepsilon_n \pm i0}, \quad (4.18)$$

and taking the limit $T \rightarrow 0$. When the RMT is used, the quantum corrections are expressed via the difference of unitary and orthogonal ensemble, cf. Section 2.1.6, which we denote by $\delta\bar{\chi} \equiv \bar{\chi}_{GUE} - \bar{\chi}_{GOE}$ in the following.

Importantly, we see from Eq. (4.15), that the spatial dependence of $\delta\bar{\chi}$ cannot be totally neglected. Thus, a description purely in terms of RMT, which neglects all spatial degrees of freedom, cannot be sufficient. Remarkably, it has been shown, [Kravtsov and Mirlin \(1994\)](#); [Blanter and Mirlin \(1997, 1996\)](#), that the correlations of the wave-functions can be calculated even in the non-perturbative regime $\omega \ll \Delta$ using the non-linear sigma model as long as the conductance is sufficiently large. The idea of this method is to decompose the matrix $Q(\mathbf{x})$ (see Section 2.1.5) into a constant part Q_0 describing the zero mode and a spatially dependent part describing nonzero modes. Then the latter can be integrated out perturbatively, with the small parameter being $1/g$. Finally, the integral over the matrix Q_0 is calculated non-perturbatively. As a result, the correlations of the wave-functions are expressed in terms of a (dimensionless) diffusion propagator without zero mode:

$$\mathcal{P}(\mathbf{x}, \mathbf{y}) \equiv \frac{1}{2\pi\rho V} \sum_{\mathbf{q} \neq 0} e^{i\mathbf{q}(\mathbf{x}-\mathbf{y})} P(\mathbf{q}, \omega = 0), \quad (4.19)$$

1. See also [Noat *et al.* \(1996, 2002\)](#) who have obtained similar results and compare them with numerical simulations.
2. We note that [Efetov \(1996\)](#) “incorrectly estimates the contribution of a short-range term” [[Blanter and Mirlin, 1998](#)], and neglects the dominating long-range term.
3. We note that [Blanter and Mirlin \(1998\)](#) contains “an unfortunate arithmetic error” [[Blanter and Mirlin, 2001](#)], leading to the incorrect result $\alpha(\omega = 0) \neq 0$ in the CE.

which we will use below.

We rewrite Eq. (4.17) as

$$\chi_\mu(\mathbf{x}, \mathbf{y}, \omega) = \sum_{\varepsilon_n < \mu < \varepsilon_m} |\Phi_{m,n}(\mathbf{x}, \mathbf{y})|^2 \left(\frac{1}{\varepsilon_m - \varepsilon_n - \omega_+} + \frac{1}{\varepsilon_m - \varepsilon_n + \omega_+} \right), \quad (4.20)$$

where we introduced $\omega_+ = \omega + i0$ and defined

$$|\Phi_{m,n}(\mathbf{x}, \mathbf{y})|^2 \equiv \Phi_m^*(\mathbf{x})\Phi_m(\mathbf{y})\Phi_n^*(\mathbf{y})\Phi_n(\mathbf{x}) = \Phi_n^*(\mathbf{x})\Phi_n(\mathbf{y})\Phi_m^*(\mathbf{y})\Phi_m(\mathbf{x}). \quad (4.21)$$

In the GCE, we set $\mu \rightarrow 0$ and write the sums in Eq. (4.20) in terms of integrals and δ -functions:

$$\begin{aligned} \chi_{GC}(\mathbf{x}, \mathbf{y}, \omega) & \quad (4.22) \\ &= \int_{-\infty}^{-0} d\varepsilon \int_{+0}^{\infty} d\varepsilon_1 \sum_{n,m} \delta(\varepsilon - \varepsilon_n) \delta(\varepsilon_1 - \varepsilon_m) |\Phi_{m,n}(\mathbf{x}, \mathbf{y})|^2 \left(\frac{1}{\varepsilon_1 - \varepsilon - \omega_+} + \frac{1}{\varepsilon_1 - \varepsilon + \omega_+} \right). \end{aligned}$$

To realize the CE, on the other hand, we set the chemical potential to

$$\mu = \varepsilon_k + 0, \quad (4.23)$$

and introduce a weight function $P(\varepsilon_k)$, as discussed in Section 4.1. Separating the sum in two parts: $n = k$ (CE1) and $n < k$ (CE2), we find $\chi_{CE} = \chi_{CE1} + \chi_{CE2}$ with

$$\chi_{CE1}(\mathbf{x}, \mathbf{y}, \omega) = \Delta \sum_{\varepsilon_k} P(\varepsilon_k) \sum_{\varepsilon_n = \varepsilon_k < \varepsilon_m} |\Phi_{m,k}(\mathbf{x}, \mathbf{y})|^2 \left(\frac{1}{\varepsilon_m - \varepsilon_k - \omega_+} + \frac{1}{\varepsilon_m - \varepsilon_k + \omega_+} \right) \quad (4.24)$$

$$= \Delta \int_{-\infty}^{+\infty} dE P(E) \int_{+0}^{+\infty} d\varepsilon \sum_{k,m} \delta(E - \varepsilon_k) \delta(E + \varepsilon - \varepsilon_m) |\Phi_{m,k}(\mathbf{x}, \mathbf{y})|^2 \left(\frac{1}{\varepsilon - \omega_+} + \frac{1}{\varepsilon + \omega_+} \right), \quad (4.25)$$

and

$$\chi_{CE2}(\mathbf{x}, \mathbf{y}, \omega) = \Delta \sum_{\varepsilon_k} P(\varepsilon_k) \sum_{\varepsilon_n < \varepsilon_k < \varepsilon_m} |\Phi_{m,n}(\mathbf{x}, \mathbf{y})|^2 \left(\frac{1}{\varepsilon_m - \varepsilon_n - \omega_+} + \frac{1}{\varepsilon_m - \varepsilon_n + \omega_+} \right) \quad (4.26)$$

$$\begin{aligned} &= \Delta \int_{-\infty}^{+\infty} dE P(E) \int_{-\infty}^{-0} d\varepsilon \int_{+0}^{+\infty} d\varepsilon_1 \sum_{k,m,n} \delta(E - \varepsilon_k) \delta(E + \varepsilon_1 - \varepsilon_m) \delta(E + \varepsilon - \varepsilon_n) |\Phi_{m,n}(\mathbf{x}, \mathbf{y})|^2 \\ & \quad \times \left(\frac{1}{\varepsilon_1 - \varepsilon - \omega_+} + \frac{1}{\varepsilon_1 - \varepsilon + \omega_+} \right). \end{aligned} \quad (4.27)$$

As expected from the discussion in Section 4.1, we see that Eq. (4.27) includes correlations between three energy levels: E , $E + \varepsilon_1$ and $E + \varepsilon$. To calculate the disorder average, we introduce the function

$$\overline{|\Phi(\mathbf{x}, \mathbf{y})|_\varepsilon^2} \equiv \frac{\Delta^2 \overline{\sum_{i,j} |\Phi_{i,j}(\mathbf{x}, \mathbf{y})|^2 \delta(E - \varepsilon_i) \delta(E + \varepsilon - \varepsilon_j)}}{R_2(\varepsilon)}, \quad (4.28)$$

where R_2 is the two-level correlation function defined in Eq. (2.32). Blanter and Mirlin (1997, 1998) have evaluated Eq. (4.28) in the unitary and orthogonal ensemble using the nonlinear sigma model with the result

$$\overline{|\Phi(\mathbf{x}, \mathbf{y})|_\varepsilon^2}_{\varepsilon \ll E_{\text{Th}}} = \frac{1}{V^2} \begin{cases} k_d(\mathbf{x} - \mathbf{y}) + \mathcal{P}(\mathbf{x}, \mathbf{y}) & \text{(GUE)} \\ k_d(\mathbf{x} - \mathbf{y}) + \mathcal{P}(\mathbf{x}, \mathbf{y}) + k_d(\mathbf{x} - \mathbf{y})\mathcal{P}(\mathbf{x}, \mathbf{y}) & \text{(GOE)} \end{cases}, \quad (4.29)$$

where \mathcal{P} is defined in Eq. (4.19) and k_d is a short-range function on the scale ℓ . Since the polarizability is governed by the long-range behavior of χ , see Eq. (4.14), we can neglect the contribution $\sim k_d$ and use the approximation

$$\overline{|\Phi(\mathbf{x}, \mathbf{y})|^2}_{\varepsilon \ll E_{\text{Th}}} \approx \frac{1}{V^2} \mathcal{P}(\mathbf{x}, \mathbf{y}) \quad (\text{GUE}) \text{ and } (\text{GOE}) \quad (4.30)$$

in the following. Importantly, the matrix element (4.30) is independent of ε at $\varepsilon \ll E_{\text{Th}}$. Moreover, we define the matrix element with two energy indices as follows:

$$\overline{|\Phi(\mathbf{x}, \mathbf{y})|^2}_{\varepsilon_1, \varepsilon} \equiv \frac{\Delta^3 \overline{\sum_{i,j,k} |\Phi_{i,j}(\mathbf{x}, \mathbf{y})|^2 \delta(E - \varepsilon_i) \delta(E + \varepsilon_1 - \varepsilon_j) \delta(E + \varepsilon - \varepsilon_k)}}{R_3(\varepsilon_1, \varepsilon)}. \quad (4.31)$$

where the three-level correlation function is defined as

$$R_3(\varepsilon_1, \varepsilon) \equiv \Delta^3 \sum_{i,j,k} \delta(E - \varepsilon_i) \delta(E + \varepsilon_1 - \varepsilon_j) \delta(E + \varepsilon - \varepsilon_k). \quad (4.32)$$

Blanter and Mirlin (2001) have argued that the same long-range behavior as described by Eq. (4.30) can be expected for this quantity at $\varepsilon, \varepsilon_1 \ll E_{\text{Th}}$.

Using the definition (4.28), and integrating out E , by using $\int dE P(E) = 1$, one obtains from Eq. (4.22) for the GCE:

$$\overline{\chi_{\text{GCE}}}(\mathbf{x}, \mathbf{y}, \omega) = \frac{1}{\Delta^2} \int_{+0}^{\infty} d\varepsilon \varepsilon R_2(\varepsilon) \overline{|\Phi(\mathbf{x}, \mathbf{y})|^2}_{\varepsilon} \left(\frac{1}{\varepsilon - \omega_+} + \frac{1}{\varepsilon + \omega_+} \right), \quad (4.33)$$

and from Eqs. (4.25, 4.27) for the CE:

$$\begin{aligned} \overline{\chi_{\text{CE}}}(\mathbf{x}, \mathbf{y}, \omega) & \quad (4.34) \\ &= \frac{1}{\Delta^2} \int_{+0}^{\infty} d\varepsilon \left(\Delta R_2(\varepsilon) \overline{|\Phi(\mathbf{x}, \mathbf{y})|^2}_{\varepsilon} + \int_{+0}^{\varepsilon-0} d\varepsilon_1 R_3(\varepsilon, \varepsilon_1) \overline{|\Phi(\mathbf{x}, \mathbf{y})|^2}_{\varepsilon, \varepsilon_1} \right) \left(\frac{1}{\varepsilon - \omega_+} + \frac{1}{\varepsilon + \omega_+} \right). \end{aligned}$$

It is instructive to split the quantum corrections, $\delta\chi = \chi_{\text{GUE}} - \chi_{\text{GOE}}$, to Eqs. (4.33, 4.34) into 4 parts:

$$\begin{aligned} \delta\overline{\chi_{\text{GCE1}}}(\mathbf{x}, \mathbf{y}, \omega) &= \delta\overline{\chi_{\text{GCE1}}}(\mathbf{x}, \mathbf{y}, \omega) + \delta\overline{\chi_{\text{GCE2}}}(\mathbf{x}, \mathbf{y}, \omega) \\ \delta\overline{\chi_{\text{CE}}}(\mathbf{x}, \mathbf{y}, \omega) &= \delta\overline{\chi_{\text{GCE}}}(\mathbf{x}, \mathbf{y}, \omega) + \delta\overline{\chi_{\text{CE1}}}(\mathbf{x}, \mathbf{y}, \omega) + \delta\overline{\chi_{\text{CE2}}}(\mathbf{x}, \mathbf{y}, \omega), \end{aligned} \quad (4.35)$$

with

$$\delta\overline{\chi_{\text{GCE1}}}(\mathbf{x}, \mathbf{y}, \omega) = \frac{1}{\Delta^2} \int_{+0}^{\infty} d\varepsilon 2\delta \left[R_2(\varepsilon) \overline{|\Phi(\mathbf{x}, \mathbf{y})|^2}_{\varepsilon} \right] \quad (4.36)$$

$$\delta\overline{\chi_{\text{GCE2}}}(\mathbf{x}, \mathbf{y}, \omega) = \frac{1}{\Delta^2} \int_{+0}^{\infty} d\varepsilon \frac{2\omega_+^2}{\varepsilon^2 - \omega_+^2} \delta \left[R_2(\varepsilon) \overline{|\Phi(\mathbf{x}, \mathbf{y})|^2}_{\varepsilon} \right] \quad (4.37)$$

$$\delta\overline{\chi_{\text{CE1}}}(\mathbf{x}, \mathbf{y}, \omega) = \frac{1}{\Delta^2} \int_{+0}^{\infty} d\varepsilon \frac{2\varepsilon}{\varepsilon^2 - \omega_+^2} \Delta \delta \left[R_2(\varepsilon) \overline{|\Phi(\mathbf{x}, \mathbf{y})|^2}_{\varepsilon} \right] \quad (4.38)$$

$$\delta\overline{\chi_{\text{CE2}}}(\mathbf{x}, \mathbf{y}, \omega) = \frac{1}{\Delta^2} \int_{+0}^{\infty} d\varepsilon \frac{2\varepsilon}{\varepsilon^2 - \omega_+^2} \int_{+0}^{\varepsilon-0} d\varepsilon_1 \delta \left[\tilde{R}_3(\varepsilon, \varepsilon_1) \overline{|\Phi(\mathbf{x}, \mathbf{y})|^2}_{\varepsilon, \varepsilon_1} \right], \quad (4.39)$$

where $\tilde{R}_3(\varepsilon, \varepsilon_1) = R_3(\varepsilon, \varepsilon_1) - R_2(\varepsilon)$.

Let us first consider the contribution $\delta\overline{\chi_{GCE1}}$. Using the definition of the matrix element (4.28) in Eq. (4.36), and symmetrizing the ε -integral, we obtain:

$$\begin{aligned}\delta\overline{\chi_{GCE1}}(\mathbf{x}, \mathbf{y}, \omega) &= \int_{-\infty}^{\infty} d\varepsilon \delta \left[\overline{\sum_{i \neq j} |\Phi_{i,j}(\mathbf{x}, \mathbf{y})|^2 \delta(E - \varepsilon_i) \delta(E + \varepsilon - \varepsilon_j)} \right] \\ &= \delta \left[\overline{\sum_{i \neq j} |\Phi_{i,j}(\mathbf{x}, \mathbf{y})|^2 \delta(E - \varepsilon_i)} \right] \\ &= \delta \left[\overline{\sum_{ij} |\Phi_{i,j}(\mathbf{x}, \mathbf{y})|^2 \delta(E - \varepsilon_i)} - \overline{\sum_i |\Phi_{i,i}(\mathbf{x}, \mathbf{y})|^2 \delta(E - \varepsilon_i)} \right].\end{aligned}$$

After summing over j , the first term is just a density of states and does not depend on the ensemble, cf. Eq. (2.66). The second term has been evaluated in [Blanter and Mirlin \(1997, 1998\)](#) using the non-linear sigma model:

$$\overline{|\Phi_{i,i}(\mathbf{x}, \mathbf{y})|^2}_{\varepsilon} \equiv \Delta \overline{\sum_i |\Phi_{i,i}(\mathbf{x}, \mathbf{y})|^2 \delta(\varepsilon - \varepsilon_i)} \approx \frac{1}{V^2} \begin{cases} [1 + \mathcal{P}(\mathbf{x}, \mathbf{y})][1 + k_d(\mathbf{x}, \mathbf{y})] & \text{(GUE)} \\ [1 + 2\mathcal{P}(\mathbf{x}, \mathbf{y})][1 + 2k_d(\mathbf{x}, \mathbf{y})] & \text{(GOE)} \end{cases}. \quad (4.40)$$

Neglecting the short-range contribution, we find

$$\delta\overline{\chi_{GCE1}}(\mathbf{x}, \mathbf{y}, \omega) = \frac{1}{\Delta V^2} \mathcal{P}(\mathbf{x}, \mathbf{y}). \quad (4.41)$$

We will see below that the contribution (4.41) dominates the polarizability in the range $\Delta \ll \omega \ll E_{\text{Th}}$ for both statistical ensembles, the GCE *and* the CE. In the second contribution, $\delta\overline{\chi_{GCE2}}$, the integral is dominated by small $\varepsilon \sim \omega \ll E_{\text{Th}}$. At these values of ε , the matrix element $\delta|\overline{\Phi}_{\varepsilon}^2$ is constant, and we can write:

$$\delta\overline{\chi_{GCE2}}(\mathbf{x}, \mathbf{y}, \omega) = \frac{1}{\Delta^2} \overline{|\Phi(\mathbf{x}, \mathbf{y})|^2}_0 \int_{+0}^{\infty} d\varepsilon \left[\frac{2\omega^2}{\varepsilon^2 - \omega_+^2} \right] \delta[R_2(\varepsilon)]. \quad (4.42)$$

Moreover, since

$$\int_{+0}^{\infty} d\varepsilon \delta R_2(\varepsilon) = 0, \quad (4.43)$$

one can add any constant term in the square brackets of Eq. (4.42). In particular, we can write:

$$\delta\overline{\chi_{GCE2}}(\mathbf{x}, \mathbf{y}, \omega) = \frac{1}{\Delta^2} \overline{|\Phi(\mathbf{x}, \mathbf{y})|^2}_0 \int_{+0}^{\infty} d\varepsilon \left(\frac{1}{\varepsilon - \omega_+} + \frac{1}{\varepsilon + \omega_+} \right) \varepsilon \delta[R_2(\varepsilon)] \quad (4.44)$$

$$= \frac{1}{\Delta^2 V^2} \mathcal{P}(\mathbf{x}, \mathbf{y}) \int_{+0}^{\infty} d\varepsilon \left(\frac{1}{\varepsilon - \omega_+} + \frac{1}{\varepsilon + \omega_+} \right) \varepsilon \delta[R_2(\varepsilon)], \quad (4.45)$$

where we used Eq. (4.30). Similarly, we can neglect the ε dependence of $\overline{|\Phi(\mathbf{x}, \mathbf{y})|^2}_{\varepsilon}$ and $\overline{|\Phi(\mathbf{x}, \mathbf{y})|^2}_{\varepsilon, \varepsilon_1}$ in the terms $\overline{\chi_{CE1}}$ and $\overline{\chi_{CE2}}$ and find

$$\delta\overline{\chi_{CE1}}(\mathbf{x}, \mathbf{y}, \omega) = \frac{1}{\Delta^2 V^2} \mathcal{P}(\mathbf{x}, \mathbf{y}) \int_{+0}^{\infty} d\varepsilon \left(\frac{1}{\varepsilon - \omega_+} + \frac{1}{\varepsilon + \omega_+} \right) \Delta \delta[R_2(\varepsilon)] \quad (4.46)$$

$$\delta\overline{\chi_{CE2}}(\mathbf{x}, \mathbf{y}, \omega) = \frac{1}{\Delta^2 V^2} \mathcal{P}(\mathbf{x}, \mathbf{y}) \int_{+0}^{\infty} d\varepsilon \left(\frac{1}{\varepsilon - \omega_+} + \frac{1}{\varepsilon + \omega_+} \right) \int_{+0}^{\varepsilon-0} d\varepsilon_1 \delta[\tilde{R}_3(\varepsilon, \varepsilon_1)].$$

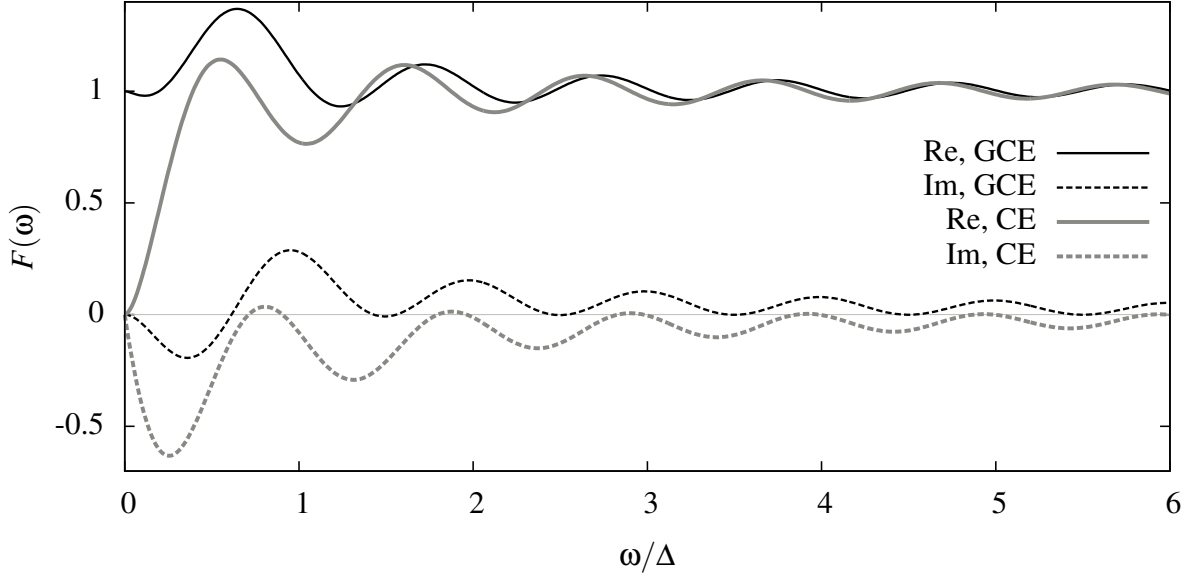


Figure 4.3: Plot of the function $F_{GCE/CE}(\omega)$ defined in Eqs. (4.48, 4.49).

In total, the density response function in the GCE and CE in the limit $\omega \ll E_{Th}$ is given by

$$\overline{\delta\chi_{GCE/CE}(\mathbf{x}, \mathbf{y}, \omega)} = \frac{1}{\Delta V^2} \mathcal{P}(\mathbf{x}, \mathbf{y}) F_{GCE/CE}(\omega), \quad (4.47)$$

where we have introduced the dimensionless functions

$$F_{GCE}(\omega) = 1 + \int_0^\infty \frac{d\varepsilon}{\Delta} \left(\frac{1}{\varepsilon - \omega_+} + \frac{1}{\varepsilon + \omega_+} \right) \varepsilon \delta R_2(0, \varepsilon), \quad (4.48)$$

and

$$F_{CE}(\omega) = 1 + \int_0^\infty \frac{d\varepsilon}{\Delta} \left(\frac{1}{\varepsilon - \omega_+} + \frac{1}{\varepsilon + \omega_+} \right) \left(\varepsilon \delta R_2(0, \varepsilon) + \Delta \delta R_2(0, \varepsilon) + \int_{+0}^{\varepsilon-0} d\varepsilon_1 \delta \tilde{R}_3(\varepsilon, \varepsilon_1) \right). \quad (4.49)$$

The quantum corrections to the polarizability can be obtained from Eq. (4.47) via Eq. (4.15) and Eq. (4.16):

$$\delta\alpha(\omega)_{GCE/CE} \approx \frac{2(4\pi e)^2}{\kappa^4 \Delta V^2} \left[\frac{1}{E(\omega)^2} \int d^d \mathbf{x} d^d \mathbf{y} n_{in,0}(\mathbf{x}, \omega) \mathcal{P}(\mathbf{x}, \mathbf{y}) n_{in,0}(\mathbf{x}, \omega) \right] F_{GCE/CE}(\omega). \quad (4.50)$$

Note that the term in square brackets does not depend on ω and can be determined from classical electrostatics, cf. the discussion after Eq. (4.16). Thus, the frequency dependence of the polarizability is governed entirely by $F_{GCE/CE}(\omega)$.

To evaluate Eq. (4.48) and Eq. (4.49), we can use the expressions for R_2 given in Eqs. (2.70, 2.71) for the unitary and orthogonal ensembles. R_3 can be obtained from the determinant formula (2.69), using the following matrix representation of the biquaternion kernel for the orthogonal ensemble [Mehta, 2004]:

$$K_{N \rightarrow \infty}^{GOE}(s) = \begin{pmatrix} \frac{\sin(\pi s)}{\pi s} & \frac{d}{ds} \frac{\sin(\pi s)}{\pi s} \\ \int_s^\infty du \frac{\sin(\pi u)}{\pi u} & \frac{\sin(\pi s)}{\pi s} \end{pmatrix}, \quad (4.51)$$

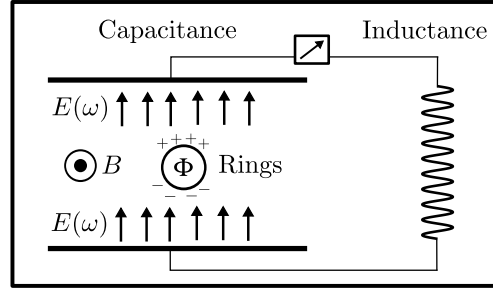


Figure 4.4: Superconducting resonator with polarized rings.

cf. Eq. (2.65) for the unitary case. The resulting expression is very lengthy but can be evaluated straightforwardly. Finally, the principle value integral in Eqs. (4.48, 4.49) has to be carried out numerically to obtain the real part. The result is shown in Fig. 4.3: we note that the real part of the quantum corrections to the polarizability vanishes at $\omega \rightarrow 0$ in the CE, which is due to an identity relating the two-level and the three-level correlation functions entering Eq. (4.49) [Blanter and Mirlin, 2001]. Remarkably, we recover this behavior in the perturbative two-loop calculation in Section 4.5. At larger frequencies $\omega \gg \Delta$, on the other hand, the differences between CE and GCE are small.

4.4 Overview of recent experiments

Recently, the electrical polarizability α of a large number ($N \approx 10^5$) of isolated disordered rings has been measured [Deblock *et al.*, 2000, 2002b]. Due to the large number of rings, it is expected that mesoscopic fluctuations are averaged out and that quantum corrections are present at finite frequency ω_0 of the electric field. The rings were chosen such that

$$E_{\text{Th}} \equiv D/L^2 \approx 71.6\text{mK} \quad \simeq \quad \Delta \approx 80\text{mK} \quad \gg \quad \omega_0 \approx 17\text{mK}, \quad (4.52)$$

corresponding to the conductance $g = 2\pi E_{\text{Th}}/\Delta \approx 5.63$. The temperature dependence of α has been studied in the range $T \approx 20..300\text{mK}$. Thus, at the lowest temperatures, where $T \lesssim E_{\text{Th}}$, 0D dephasing should become relevant.

To extract the polarizability, the rings were placed on top of the capacitive part of a superconducting resonator, see Fig. 4.4. The presence of the rings changed the effective dielectric constant of the capacitance, leading to an observable shift of the resonance frequency ω_0 of the resonator. To see this, we remind the reader that a superconducting resonator can be modeled as a parallel $\mathcal{L}\mathcal{C}$ circuit with the total impedance:

$$Z(\omega) = \left(\frac{1}{Z_C(\omega)} + \frac{1}{Z_L(\omega)} \right)^{-1}, \quad \text{where} \quad Z_C(\omega) = \frac{1}{i\omega C}, \quad Z_L(\omega) = i\omega L, \quad (4.53)$$

and C is the capacitance and L is the inductance of the resonator. Note that at $\omega = \omega_0$, with

$$\omega_0 = \frac{1}{\sqrt{LC}}, \quad (4.54)$$

the circuit is in resonance, meaning that $Z(\omega \rightarrow \omega_0)^{-1} \rightarrow 0$. When the rings are placed on top of the capacitance, the permittivity ϵ changes, and since $C \propto \epsilon$, also the capacitance is modified. The change in permittivity, on the other hand, is governed by the polarizability α of the rings, since $\alpha \propto \epsilon - 1$. It

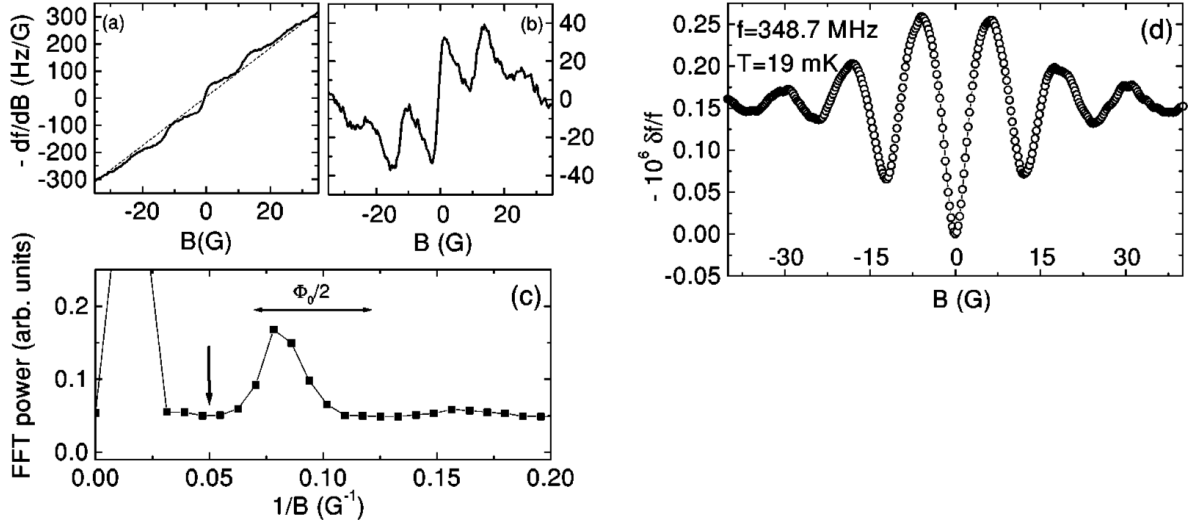


Figure 4.5: (a) Derivative of the resonance frequency of the resonator versus magnetic field. The straight dashed line is due to the field dependence of the penetration length in the resonator, which is made from Niobium. (b) Signal obtained by subtracting the dashed line of (a). (c) Fourier transform of the signal. The arrow indicates the cutoff frequency of the high-pass filter. (d) Frequency shift due to the rings obtained after integration of the high-pass filtered signal of (b). Note that $\delta\alpha \propto -\delta f$ is minimal for $B = 0$. (Pictures taken from [Deblock *et al.* \(2002b\)](#) Fig.7.)

follows that the total impedance in the presence of the rings becomes

$$Z_C(\omega) = \frac{1}{i\omega C(1 + Nk_e\alpha(\omega))} \approx \frac{1}{i\omega C(1 + Nk_e\text{Re}\alpha(\omega))} + \frac{Nk_e\text{Im}\alpha(\omega)}{\omega C}, \quad (4.55)$$

where N is the number of rings and k_e is a coupling constant. (See [Deblock *et al.* \(2002b\)](#) for an estimate of k_e in the experiment.) Thus, the relative change in the capacitance leads to a shift of the resonance frequency due to relation (4.54):

$$\frac{\delta C}{C} = Nk_e\text{Re}\alpha(\omega) \quad \Rightarrow \quad \frac{\delta\omega_0}{\omega_0} = -\frac{1}{2}Nk_e\text{Re}\alpha(\omega). \quad (4.56)$$

We would like to emphasize that this technique allows for a precise determination of the change in polarizability as a function of temperature. However, measuring the frequency dependence of α is impossible, since the resonance frequency (4.54) is fixed by the properties of the resonator. Thus, the RMT-predictions for the frequency dependence, discussed in Section 4.3, remain untested.

As an aside, we see from Eq. (4.55) that the imaginary part of the polarizability can be described as an additional resistance in the circuit. Thus, it can be observed as a shift of the Q-factor of the resonator. However, no temperature dependence of the Q-factor has been measured yet [[Deblock *et al.*, 2000, 2002b](#)] and we concentrate on the real part of α in the following.

In the experiment, an additional weak magnetic field B was applied perpendicular to the rings, see Fig. 4.4, creating a flux Φ through a ring. The resulting oscillations of the signal (as a function of B) had a period consistent with half a flux quantum $\Phi_0/2$, as expected for the ensemble-averaged Aharonov-Bohm effect, see Section 2.1.3. This oscillating part of the magneto-polarizability was extracted using a numerical high-pass filter with a cutoff frequency chosen to be slightly below the first $\Phi_0/2$ mode on the FT-signal to filter the contributions from the ring from those of the resonator, see Fig. 4.5. Even at the lowest temperatures, peaks in the FT-signal of higher $\Phi_0/2$ modes were at

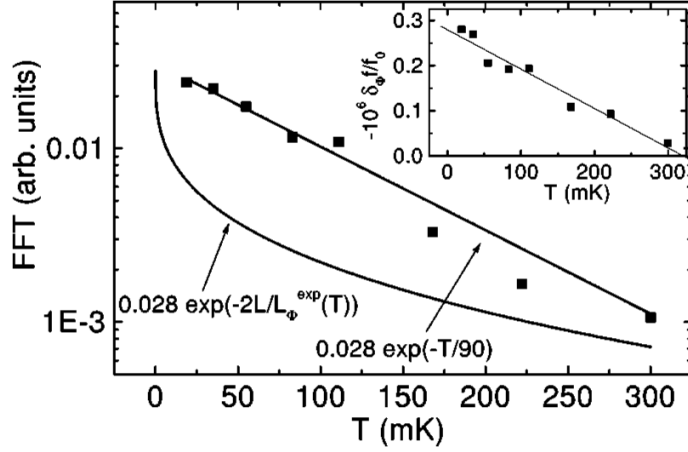


Figure 4.6: T dependence of the $\Phi_0/2$ component of the FT of the signal. The fitting function used is given by Eq. (4.57): The best agreement is found with an exponential decay with a temperature scale of 90mK. Inset: Temperature dependence of the total frequency shift, after applying the high-pass filter. (Pictures taken from [Deblock *et al.* \(2002b\)](#) Fig.9.)

least a factor $1/10$ smaller than that of the first mode, which suggests that the rings were only barely phase coherent, $\gamma \simeq E_{\text{Th}}$. The observed magneto-polarizability, $\delta\alpha = \alpha(B) - \alpha(0)$, is *positive*: α is minimal for zero B . In full agreement with the RMT results, and similar to the weak-localization correction to the conductance. The magnitude of this magneto-polarizability was estimated to be $\approx 5 \cdot 10^{-4} \alpha_0$, where α_0 is the classical polarizability of the rings.

In analogy with results from persistent currents, [Deblock *et al.* \(2000\)](#) suggested to fit the temperature dependence of the $\Phi_0/2$ -component of the signal to

$$\delta_{\Phi_0/2} \alpha(\omega_0, T) \propto \exp(-L/L_\phi(T)), \quad (4.57)$$

see Fig. 4.6. The resulting dephasing length $L_\phi(T) = \sqrt{D\tau_\phi(T)}$ has been found to be $L_\phi(T) \sim 1/T$ in agreement with the result for 0D dephasing, Eq. (2.153). However, we note that this finding is actually contradicting with the observation that only the first mode of the AB-oscillations was visible, since ergodicity $\gamma \ll E_{\text{Th}}$ is required for 0D dephasing, which would imply higher modes of the signal to be large. This contradiction can only be resolved when actual numbers and numerical coefficients are taken into account. We emphasize that Eq. (4.57) is only a phenomenological guess, suggested without backup from theory. In fact, we show in Section 4.5, that a different fitting function should be used.

4.5 Preprint: Quantum Corrections to the Polarizability of Isolated Disordered Metals

The following 12 pages have been made available as a preprint at [arXiv:1304.4342](https://arxiv.org/abs/1304.4342).

Quantum Corrections to the Polarizability and Dephasing in Isolated Disordered Metals

M. Treiber,¹ P. M. Ostrovsky,^{2,3} O. M. Yevtushenko,¹ J. von Delft,¹ and I. V. Lerner⁴

¹Ludwig Maximilians University, Arnold Sommerfeld Center and Center for Nano-Science, Munich, D-80333, Germany

²Max Planck Institute for Solid State Research, Heisenbergstr. 1, 70569 Stuttgart, Germany

³L. D. Landau Institute for Theoretical Physics, 142432 Chernogolovka, Russia

⁴School of Physics and Astronomy, University of Birmingham, Birmingham, B15 2TT, UK

(Dated: April 17, 2013)

We study the quantum corrections to the polarizability of isolated metallic mesoscopic systems using the loop-expansion in diffusive propagators. We show that the difference between connected (grand-canonical ensemble) and isolated (canonical ensemble) systems appears only in subleading terms of the expansion, and can be neglected if the frequency of the external field, ω , is of the order of (or even slightly smaller than) the mean level spacing, Δ . If $\omega \ll \Delta$, the two-loop correction becomes important. We calculate it by systematically evaluating the ballistic parts (the Hikami boxes) of the corresponding diagrams and exploiting electroneutrality. Our theory allows one to take into account a finite dephasing rate, γ , generated by electron interactions, and it is complementary to the non-perturbative results obtained from a combination of Random Matrix Theory (RMT) and the σ -model, valid at $\gamma \rightarrow 0$. Remarkably, we find that the two-loop result for isolated systems with moderately weak dephasing, $\gamma \sim \Delta$, is similar to the result of the RMT+ σ -model even in the limit $\omega \rightarrow 0$. For smaller γ , we discuss the possibility to interpolate between the perturbative and the non-perturbative results. We compare our results for the temperature dependence of the polarizability of isolated rings to the experimental data of Deblock *et al* [Phys. Rev. Lett. **84**, 5379 (2000); Phys. Rev. B **65**, 075301 (2002)], and we argue that the elusive 0D regime of dephasing might have manifested itself in the observed magneto-oscillations. Besides, we thoroughly discuss possible future measurements of the polarizability, which could aim to reveal the existence of 0D dephasing and the role of the Pauli blocking at small temperatures.

I. INTRODUCTION

Interference phenomena in mesoscopic electronic systems require phase coherence, which is cut beyond the so-called dephasing time τ_ϕ . At low temperatures $T \lesssim 1K$, where phonons are frozen out, dephasing is caused mainly by electron interactions, which lead to a finite dephasing rate¹ $\gamma \equiv 1/\tau_\phi$. In large systems with a small Thouless energy, $E_{Th} \ll T$, dephasing crucially depends on dimensionality and geometry². However, if the system is finite and $T \lesssim E_{Th}$, spatial coordinates become unimportant and a 0D regime of rather weak dephasing is expected to occur³. This regime is characterized by a universal temperature dependence of the dephasing rate, $\gamma_{0D} \sim \Delta T^2/E_{Th}^2$, where Δ is the mean-level spacing. This T -dependence of γ can be explained by simple power counting: Pauli blocking restricts the number of available final scattering states of the electrons, therefore both the energy transfer and the available phase-space are $\propto T$, similar to the standard result for a clean Fermi-liquid. However, despite of the fundamental nature and the physical importance of 0D dephasing, attempts to observe it experimentally in mesoscopic systems have been unsuccessful so far.

In transport experiments, the 0D regime is generally difficult to observe, since quantum transport is almost insensitive to γ at $T \ll E_{Th}$. For example, the weak localization correction to the classical dc conductivity is cut mainly by the dwell time, $\tau_{dw} \ll 1/\gamma_{0D}$, see Ref. [4] for a detailed discussion. This is an unavoidable problem which occurs in any open system even if the coupling to leads is weak.

In this work, we concentrate on interference phenomena in isolated systems, where $\tau_{dw} \rightarrow \infty$ and where 0D dephasing is not masked by the coupling to the environment. Deeply in the 0D regime at $\gamma \ll \Delta$, the spectrum of the isolated system is

discrete^{5,6} and, in the absence of other mechanisms of dephasing, random matrix theory (RMT) can be used as a starting point for an effective low-energy theory at $E \ll E_{Th}$ ^{7,8}. Unfortunately, RMT is not appropriate for a systematic account of dephasing.

If one is interested in the (almost 0D) regime $\gamma \leq \Delta$, where the spectrum is not yet discrete, the usual mesoscopic perturbation theory⁹ can be used, which is able to take into account dephasing in all regimes. However, the description of quantum effects in isolated systems provides a further technical challenge. Namely: the usual perturbation theory is well developed for a fixed chemical potential μ , i.e. it describes systems in the grand-canonical ensemble (GCE). Realizing the canonical ensemble (CE), where the number of particles is fixed instead, can be rather tricky, see, e.g., Ref. [10]. In the following, we assume that a description in terms of the so-called Fermi-level pinning ensemble introduced in Ref. [11] and [12] is applicable¹³.

The dephasing rate of an isolated mesoscopic system can be explored, for instance, by measuring quantum components of the electrical polarizability α at a given frequency ω :

$$\alpha(\omega) = \mathbf{d}(\omega) \cdot \mathbf{E}(\omega) / |\mathbf{E}(\omega)|^2. \quad (1)$$

Here \mathbf{E} is a spatially homogeneous electric field and \mathbf{d} is the total induced dipole moment in the sample.

Gorkov and Eliashberg studied the polarizability in the seminal work Ref. [14] by using results from RMT and found very large quantum corrections. Later, it was shown in Ref. [15] that the corrections are significantly reduced if screening is taken into account correctly¹⁶. Efetov reconsidered Gorkov and Eliashberg's calculation in Ref. [17] and derived a formula which accounts for screening in the random phase approximation (RPA) and expresses the quantum cor-

rections to α in terms of correlation functions of the wavefunctions and energy levels of the system. Subsequently, Mirlin and Blanter⁸ studied the polarizability using a combination of RMT and the diffusive σ -model. In particular, they have calculated ω -dependence of α at $\omega \ll E_{\text{Th}}$ for the case of the CE at $\gamma = 0$. Thus, neither the temperature nor the magnetic field dependence of α has been described until now.

Besides the progress made in theory, experimental measurements of the quantum corrections have been reported in Ref. [18] and [19]. The authors measured the T -dependence of the polarizability of small metallic rings placed in a superconducting resonator (with a fixed frequency ω) in a perpendicular magnetic field and tried to extract the T -dependence of τ_ϕ by using an empirical fitting equation. A fingerprint of 0D dephasing was found at low temperatures, though a reliable identification of the temperature dependence of τ_ϕ calls for a more rigorous theory.

Motivated by the experimental results, we develop a perturbative theory for the quantum corrections $\Delta\alpha$ to the polarizability by using the mesoscopic “loop-expansion” in diffusons and Cooperons, where γ plays the role of a Cooperon mass. We have chosen the experimentally relevant parameter range $\max(\omega, \gamma) \gtrsim \Delta$. Generically, the difference between the GCE and the CE can be important up to energies substantially exceeding Δ , see the discussions in Ref. [10]. To check whether this statement also applies for $\Delta\alpha$, we calculate leading and subleading corrections in the Fermi-level pinning ensemble. The former corresponds solely to the one-loop answer of the GCE while the latter includes the two-loop answer of the GCE and additional terms generated by fixing the number of particles in the CE. We show that, within our approach, the leading term of the perturbative expansion for $\Delta\alpha$ suffices for its theoretical description in the experimentally relevant parameter range of Ref. [18] and [19]. This important result of the present paper allows us to find the dependence of $\Delta\alpha$ on temperature and on magnetic field. Our theoretical results are in good qualitative agreement with the experiments, though we show that the present experimental data is not sufficient for a reliable identification of 0D dephasing. We suggest repeating the experimental measurements with higher precision and lower frequencies and using the fitting procedures which we propose in the present paper. We have good hopes that the elusive 0D regime of dephasing may be detectable in this manner in the near future.

The rest of this paper is organized as follows:

Section II: we derive a general expression for the polarizability as a functional of the density response function in the RPA.

Section III: we calculate the leading quantum corrections of the density response function for connected as well as isolated disordered metals. This part of the paper is rather formal and technical. Readers who are not interested in details of the calculations can safely skip it, paying attention only to our key results, which we list here. Firstly, we derive the one- and two-loop quantum corrections for the GCE which are presented in Eqs. (17,18) of Subsection III A. A “naive” loop-expansion for the GCE suffers from a double-counting

problem of some diagrams which leads to a violation of the particle conservation law (electroneutrality) accompanied by artificial UV divergences. We suggest an algorithm of constructing the diagrams which allows one to avoid all these problems. Our method can be straightforwardly checked for the one-loop calculations, see Fig. 2, and we extend it to the much more cumbersome two-loop diagrams shown in Fig. 3. Secondly, we calculate the leading diagrams which appear due to fixing the Fermi level in the CE. Their contribution is given by Eq. (24) of Subsection III B.

Section IV: we use the results from Section III to derive a general equation for the quantum corrections $\Delta\alpha$.

Section V: we compare our findings to the results obtained from a combination of the RMT and the σ -model. We show that the diagrammatic result in the limit of a large conductance, Eq. (30), qualitatively reproduces all features of the non-perturbative answers for almost 0D systems at $0 \leq \omega < E_{\text{Th}}$, see Fig. 7.

Section VI: we apply our results for $\Delta\alpha$ to the ring geometry, present a comparison with previous experiments and discuss possible future measurements which can reliably confirm the existence of 0D dephasing.

II. POLARIZABILITY

The polarizability (1) is governed by the induced dipole moment in the sample,

$$\mathbf{d}(\omega) = \int_V d^3\mathbf{x} [\mathbf{x} \cdot n_{\text{ind}}(\mathbf{x}, \omega)], \quad (2)$$

where n_{ind} is the induced charge density. In the case of a good metal, screening should be taken into account in the random phase approximation (RPA), which results in the following expressions for the Fourier transform of n_{ind} :²⁰

$$n_{\text{ind}}(\mathbf{q}, \omega) = -2e^2 \frac{\chi(\mathbf{q}, \omega)}{\varepsilon(\mathbf{q}, \omega)} \phi_{\text{ext}}(\mathbf{q}, \omega). \quad (3)$$

Here $\phi_{\text{ext}}(\mathbf{x}, \omega) = -\mathbf{E}(\omega) \cdot \mathbf{x}$ is the external electric potential, $\varepsilon(\mathbf{q}, \omega) = 1 - 2U(\mathbf{q})\chi(\mathbf{q}, \omega)$ is the dielectric function, U is the bare Coulomb potential, and χ is the density response function per spin. By using the Kubo formula, χ can be expressed in terms of the commutator of the density operators \hat{n} :

$$\chi(\mathbf{q}, \omega) = i \int_V d^3\mathbf{x} \int_0^\infty dt \langle [\hat{n}(\mathbf{x}, t), \hat{n}(\mathbf{0}, 0)] \rangle e^{-i(\mathbf{q}\mathbf{x} - \omega t)}. \quad (4)$$

We assume spatial homogeneity of the system, which is restored after disorder averaging.

Inserting Eqs. (2,3) in Eq. (1), we find the following expression for the polarizability:

$$\alpha(\omega) = \frac{2e^2}{|\mathbf{E}(\omega)|^2} \frac{1}{V} \sum_{\mathbf{q} \neq \mathbf{0}} \phi_{\text{ext}}(\mathbf{q}, \omega) \frac{\chi(\mathbf{q}, \omega)}{\varepsilon(\mathbf{q}, \omega)} \phi_{\text{ext}}(-\mathbf{q}, \omega). \quad (5)$$

Note that the zero-mode does not contribute to α because of *electroneutrality of the sample*:

$$\chi(\mathbf{q} \equiv \mathbf{0}, \omega) = 0. \quad (6)$$

For a clean metal at $\omega \ll v_F \mathbf{q}$ (v_F is the Fermi velocity), χ is local and is given by the density of states at the Fermi level:

$$\chi(\mathbf{q}, \omega \rightarrow 0) = \rho_0. \quad (7)$$

The same equation holds true for a disordered (classical) metal at $\omega \ll D \mathbf{q}^2$ (D is the diffusion constant), see Section III. Eqs.(5,7) yield the "classical" polarizability α_0 of the disordered sample.

III. DENSITY RESPONSE FUNCTION

In this section, we consider the density response function of the disordered metal which is needed to calculate the polarizability, Eq. (5). We will start with the loop-expansion of the disorder-averaged χ in the GCE: $\bar{\chi}|_{\mu=\text{const}} \equiv \bar{\chi}_\mu$. It is relevant for the polarizability of the connected system. Besides, the two-loop contribution to $\bar{\chi}_\mu$ is needed to study the difference between the answers in the GCE and the CE. The latter is described in the second part of the present section.

We consider only weakly-interacting disordered systems at small temperatures. The main role of the electron interaction is to generate a finite T -dependent dephasing rate for Cooperons. Therefore, we derive the density response function for the non-interacting system at $T = 0$ and take into account $\gamma(T)$ at the end of the calculations.

A. Grand canonical ensemble

Simplifying Eq. (4) for the non-interacting system at $T = 0$ and fixed μ , χ_μ can be presented in terms of retarded/advanced ($G^{R/A}$) Green's functions (GFs)⁹:

$$\chi_\mu(\mathbf{x}, \mathbf{y}, \omega) = - \int_{-\infty}^0 d\varepsilon \quad (8)$$

$$\times \left(\rho_{\mu+\varepsilon}(\mathbf{x}, \mathbf{y}) G_{\mu+\varepsilon-\omega}^A(\mathbf{y}, \mathbf{x}) + G_{\mu+\varepsilon+\omega}^R(\mathbf{x}, \mathbf{y}) \rho_{\mu+\varepsilon}(\mathbf{y}, \mathbf{x}) \right).$$

Here we have introduced the spectral function (or the non-local density of states):

$$\rho_\varepsilon(\mathbf{x}, \mathbf{y}) \equiv \frac{i}{2\pi} [G_\varepsilon^R(\mathbf{x}, \mathbf{y}) - G_\varepsilon^A(\mathbf{x}, \mathbf{y})]. \quad (9)$$

In the presence of a random Gaussian white-noise disorder potential $V(\mathbf{x})$ with correlation function

$$\overline{V(\mathbf{x})V(\mathbf{y})} = \frac{1}{2\pi\rho_0\tau} \delta(\mathbf{x} - \mathbf{y}), \quad (10)$$

the disorder-averaged GFs are given by

$$\overline{G_\varepsilon^{R/A}}(\mathbf{k}) = \frac{1}{\varepsilon - \varepsilon_{\mathbf{k}} \pm i/2\tau}, \quad (11)$$

where τ is the impurity scattering time and $\varepsilon_{\mathbf{k}}$ is the particle dispersion relation.

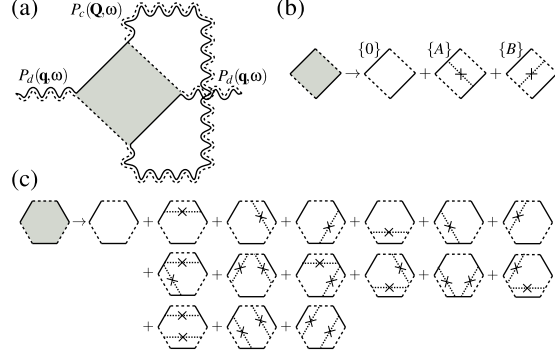


FIG. 1. (a): One-loop correction to the density response function in the GCE. Retarded (advanced) GFs are denoted by solid (dashed) lines. Impurity lines, corresponding to the correlation function (10), are denoted by dotted crossed lines. Diffusive propagators are represented by wavy double lines. They denote impurity ladders between the corresponding GFs of opposite retardation either in the particle-particle (Cooperon, P_c) or in the particle-hole (diffuson, P_d) channel. (b) and (c): Dressed 4- and 6-point Hikami boxes which include diagrams with one or two additional impurity lines connecting GFs of the same retardation.

The disorder average of Eq. (8) can be calculated with the help of the usual diagrammatic methods,¹ which yield the loop-expansion:

$$\bar{\chi}_\mu(\mathbf{q}, \omega) = \chi_0(\mathbf{q}, \omega) + \sum_j \delta\chi_{\text{GCE}}^{(j)}. \quad (12)$$

Here j is the number of loops built from impurity ladder diagrams which include ladders in the particle-hole channel (diffuson propagators) or in the particle-particle channel (Cooperon propagators). The leading (classical) term is well-known¹:

$$\chi_0(\mathbf{q}, \omega) = \rho_0 \frac{D\mathbf{q}^2}{D\mathbf{q}^2 - i\omega}. \quad (13)$$

It obeys the fundamental requirement of electroneutrality, Eq. (6), and reduces to Eq. (7) at $\omega \ll D\mathbf{q}^2$.

The leading quantum correction $\delta\chi_{\text{GCE}}^{(1)}$ describes the weak-localization correction to the diffusion constant²¹ and, therefore, is also well-known. Nevertheless, we would like to recall the basic steps of its derivation, which will be important to find the more complicated subleading term $\delta\chi_{\text{GCE}}^{(2)}$.

The one-loop diagram, which yields $\delta\chi_{\text{GCE}}^{(1)}$, is shown in Fig. 1(a). It includes two diffuson propagators P_d and one Cooperon propagator P_c , which are given by

$$P_d(\mathbf{q}, \omega) = \frac{1}{D\mathbf{q}^2 - i\omega}, \quad P_c(\mathbf{Q}, \omega) = \frac{1}{D\mathbf{Q}^2 - i\omega + \gamma}. \quad (14)$$

The (ballistic) part of the diagram which connects the diffusive propagators is known as a 4-point Hikami box²². It consists of three diagrams of the same order in $(\varepsilon_F\tau)^{-1}$ shown

in Fig. 1(b) and labeled by $\{0\}$, $\{A\}$, and $\{B\}$, which are obtained by inserting additional impurity lines between GFs of the same retardation (“dressing” the Hikami box). The Hikami box should be calculated by expanding the GFs in each of the three diagrams in the transferred momenta and energies. A direct summation of the three diagrams gives

$$H_4^{(\text{direct sum})} = 4\pi\rho_0\tau^4 [D\mathbf{q}^2 + D\mathbf{Q}^2 - i\omega]. \quad (15)$$

The second and third terms in parentheses are manifestly incorrect as they violate electroneutrality, Eq. (6), and lead to an unphysical UV divergence in $\delta\chi_{\text{GCE}}^{(1)}$. The incorrect terms originate from a double-counting problem: the diagram with a single impurity line, which contributes (via the diffusion) to the classical result of Eq. (13), is also included in the quantum correction $\delta\chi_{\text{GCE}}^{(1)}$ via the Cooperon attached to the “undressed” part of the Hikami box – the empty square $\{0\}$. One can eliminate unphysical UV divergent diagrams in the framework of the nonlinear σ -model by choosing an appropriate parameterization of the matrix field^{23,25}. However, to the best of our knowledge a consistent procedure of their elimination in the framework of straightforward diagram techniques was not described in literature. As this is rather important for any calculation beyond the one-loop order, we give a detailed description of such a procedure below.

To avoid the double-counting, the Cooperon ladder of Fig. 1(a) should start with *two* impurity lines when attached to the undressed box, while it should still start with one impurity line when attached to the dressed box. Thus, there is an ambiguity in the independent definition of the Hikami boxes and the ladder diagrams. We suggest a general algorithm which allows us to overcome this ambiguity and generate all properly dressed Hikami boxes obeying electroneutrality^{24,25}.

Let us consider the 4-point Hikami box shown in Fig. 2(a) to illustrate the method. Fig. 2(a) is obtained from Fig. 1(a) by “borrowing” two impurity lines to the undressed Hikami box from the attached Cooperon. We use this undressed box in Fig. 2(a) as a “skeleton diagram” which generates the dressings $\{A\}$ and $\{B\}$ of Fig. 1(b) by moving one of the external vertices (with diffuson attached) past one of the borrowed impurity lines. Two possible movements of the left external vertex are indicated by arrows with labels $\{A\}$ and $\{B\}$ in Fig. 2(a). Fig. 2(b) shows all three components of the fully dressed Hikami box: two generated boxes, $\{A\}$ and $\{B\}$, and the undressed box, $\{0\}$, where the external vertex is not moved. Dressing the Hikami box in this way removes the ambiguity, since all the Cooperon ladders attached to each of the boxes start with two impurity lines, thus avoiding the double-counting. Furthermore, using the identity²⁴

$$\overline{G}_{\varepsilon+\omega}^R(\mathbf{k}+\mathbf{q})\overline{G}_{\varepsilon}^A(\mathbf{k}) \xrightarrow{\mathbf{q}\rightarrow 0} \frac{i\tau}{1-i\tau\omega} \left[\overline{G}_{\varepsilon+\omega}^R(\mathbf{k}) - \overline{G}_{\varepsilon}^A(\mathbf{k}) \right], \quad (16)$$

we illustrate in Fig. 2(c) that in the limit $\mathbf{q} \rightarrow 0$ the generated diagrams automatically cancel each other (to leading order in $(\varepsilon_F\tau)^{-1} \ll 1$) at any \mathbf{Q} and ω , thus ensuring electroneutrality and the absence of the UV divergence.

Summing up the 3 diagrams drawn in Fig. 2(b) and using the resulting expression to calculate the diagram shown

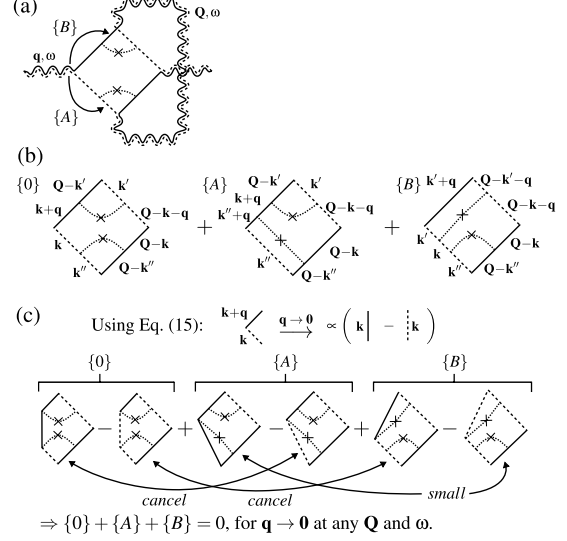


FIG. 2. (a) The “skeleton diagram”, which we use to generate the dressings $\{A\}$ and $\{B\}$ of the Hikami box shown in Fig. 1(b). The arrows with labels $\{A\}$ and $\{B\}$ indicate how the (diffuson attached) external vertex has to be moved to generate the corresponding dressed boxes. (b) The resulting diagrams with the undressed, $\{0\}$, and two dressed boxes can be summed up directly, since no double-counting problem appears. To leading order in the transferred momenta and energies, $(D\mathbf{q}^2\tau, D\mathbf{Q}^2\tau, \omega\tau) \ll 1$, the sum of the three diagrams in (b) is $4\pi\rho_0\tau^4 D\mathbf{q}^2$. (c) Dressing the Hikami box by moving the external vertex guarantees that the answer vanishes at $\mathbf{q} \rightarrow 0$, since the 3 diagrams either cancel each other exactly (at any \mathbf{Q} and ω), or are small in this limit. This can be seen immediately after using the identity (16) and redrawing the boxes $\{0\}$, $\{A\}$ and $\{B\}$ as the 6 diagrams shown in the last line.

in Fig. 1(a), we obtain the well-known result²¹

$$\delta\chi_{\text{GCE}}^{(1)}(\mathbf{q}, \omega) = \frac{1}{\pi V} \frac{D\mathbf{q}^2 i\omega}{(D\mathbf{q}^2 - i\omega)^2} \sum_{\mathbf{Q}} P_c(\mathbf{Q}, \omega). \quad (17)$$

Note that $\delta\chi_{\text{GCE}}^{(1)}/\chi_0 \sim O(\Delta/\max(\omega, \gamma))$, where $\Delta \equiv 1/(\rho_0 V)$. Thus, Eq. (17) describes the dominating quantum correction to $\overline{\chi}_\mu$ if $\max(\omega, \gamma) \gg \Delta$.

To calculate the subleading quantum corrections, one has to consider the two-loop diagrams shown in Fig. 3, which contain momentum sums over diffuson or Cooperon propagators, or both. Thus, their contribution is subleading in either $(\Delta/\max(\omega, \gamma))$, (Δ/ω) , or $(\Delta/D\mathbf{q}^2)$. Note that the diagrams containing only diffusons are not relevant for the experiments, since they are magnetic field independent. We have used the algorithm described above to calculate the 4-point Hikami-boxes $H_4^{(a)-(g1)}$ of Fig. 3 avoiding double-counting and maintaining electroneutrality, Eq. (6). The “inner” Hikami box of Fig. 3(g), $H_4^{(g2)}$, is of different nature because it is connected to two internal Cooperons. Nevertheless, the same double

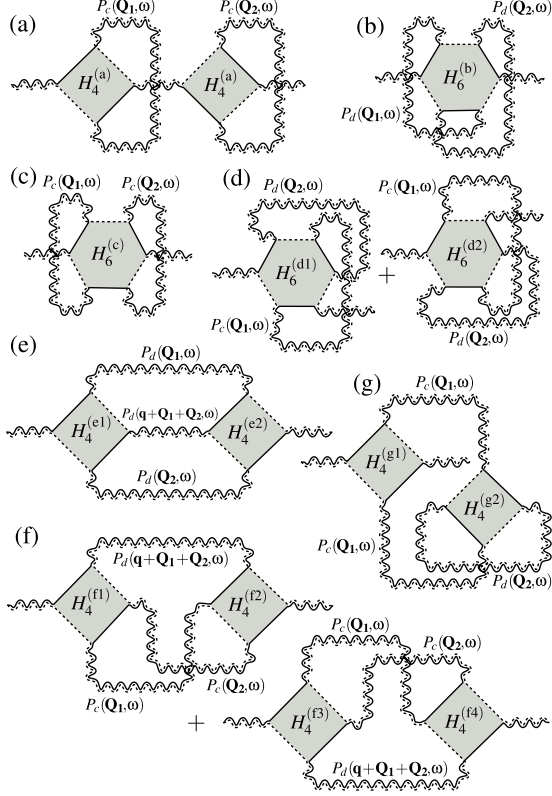


FIG. 3. Diagrams contributing to the two-loop correction $\chi_{\text{GCE}}^{(2)}$. Answers for the Hikami boxes read: $H_4^{(a,g1)} = \mathcal{D}q^2$, $H_6^{(b,c)} = -\tau^2 \mathcal{D}q^2$, $H_6^{(d1,d2)} = 0$, $H_4^{(e1)} \times H_4^{(e2)} = (\mathcal{D}(q(\mathbf{q} + \mathbf{Q}_1 + \mathbf{Q}_2)))^2$, $H_4^{(f1)} \times H_4^{(f2)} = H_4^{(f3)} \times H_4^{(f4)} = 2\mathcal{D}^2(q\mathbf{Q}_1)(q\mathbf{Q}_2)$, and $H_4^{(g2)} = \mathcal{D}(\mathbf{Q}_1^2 + \gamma/D)$, see the main text for details; here $\mathcal{D} = 4\pi\tau^4 D$.

counting problem appears and can be overcome with the help of dressing this box by moving the vertices with the attached Cooperons. As a result, electroneutrality does not necessarily apply for $H_4^{(g2)}$, which is reflected by its γ -dependence, see the next paragraph. Besides, the diagrams shown in Fig. 3(b-d) contain 6-point Hikami boxes. Their dressing is more subtle because of two issues, see the example shown in Fig. 4, which corresponds to the Hikami box $H_6^{(b)}$ of Fig. 3(b): Firstly, starting with the undressed diagram and moving vertices into the attached diffusons, one cannot generate all required 15 dressings shown in Fig. 4(a). Instead, only 8 dressings can be obtained for the 6-point Hikami box, cf. Fig. 4(a). That problem can be solved by considering two more “skeleton diagrams” with one-, Fig. 4(b), and two-, Fig. 4(c), additional impurity lines between GFs of the same retardation. All of the missing dressings can be obtained by applying the above described algorithm similar to Fig. 4(a). Secondly, by moving

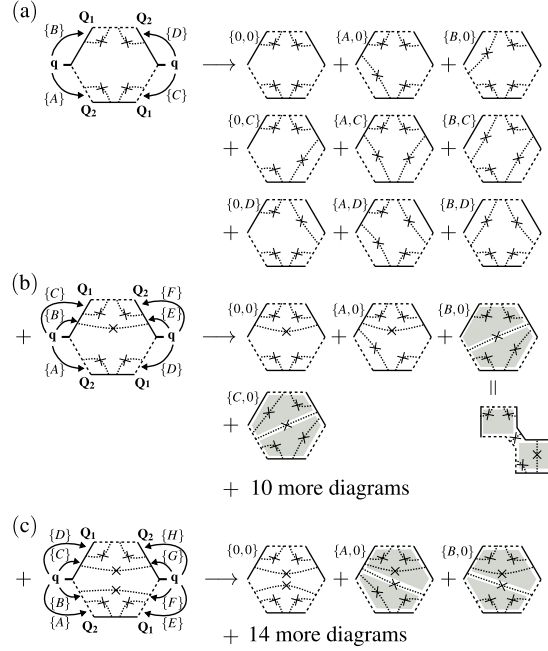


FIG. 4. Dressing of the 6-point Hikami box of Fig. 3(b) using the algorithm introduced in Fig. 2. (a) Only 8 of the 15 dressings are generated by moving the vertices. The other dressings are generated by adding one (b) or two (c) impurity lines, followed by repeating the procedure. This algorithm also generates products of 4-point Hikami boxes, indicated by a grey box. Summing up all 40 diagrams yields $-12\pi\tau^6 Dq^2$.

the vertices of the diagrams in Figs. 4(b,c) new diagrams of the same order in $(\epsilon_F \tau)^{-1} \ll 1$ are generated, which look like products of two dressed or undressed 4-point Hikami boxes with a few-impurity ladder in-between. Several examples are highlighted by grey boxes in Figs. 4(b,c). It is not a priori clear whether such diagrams belong to the diagram shown in Fig. 3(b) or Fig. 3(e). However, keeping them only in the diagram Fig. 3(b) allows us to maintain the electroneutrality in all two-loop diagrams. The total result for $H_6^{(b)}$ is obtained by summing 40 generated diagrams. The 6-point Hikami boxes of Figs. 3(c,d) can be calculated analogously.

Before presenting the final answer, we would like to discuss the way of how to reinstate the finite dephasing rate in the equations. Firstly, γ must be included as a mass term in all Cooperon propagators. Secondly, when calculating the Hikami box $H_4^{(g2)}$ of Fig. 3(g), only the number of coherent modes has to be conserved. The latter is in contrast to all other Hikami boxes, which obey the usual electroneutrality condition, i.e., the conservation of the *total* number of particles. Hence, $H_4^{(g2)}$ is the only Hikami box of the two-loop calculations which is sensitive to dephasing of the Cooperons. This statement can be checked directly with the help of the

model of magnetic impurities. Introducing a slightly reduced scattering rate for all elastic collisions in the particle-particle channel, $1/\tau \rightarrow 1/\tau - \gamma_{\text{mi}}$, where $\gamma_{\text{mi}} \ll 1/\tau$, and keeping $1/\tau$ for collisions in the particle-hole channel, we observe that the Cooperon acquires the mass γ_{mi} since magnetic scattering breaks time-reversal symmetry. Hence, magnetic scattering rate is similar to the dephasing rate; they both provide consistent infrared cut-offs for Cooperons. Applying the algorithm described above, we find that, among all the two-loop diagrams in Fig. 3, the rate γ_{mi} appears only in the expressions for Cooperons and in the Hikami box $H_4^{(g^2)}$. In the latter case, it leads to changing $D\mathbf{Q}_1^2$ to $D\mathbf{Q}_1^2 + \gamma_{\text{mi}}$. Using the analogy between magnetic scattering and dephasing, we conclude that γ enters $H_4^{(g^2)}$ in the same way.

Omitting lengthy and tedious algebra which will be published elsewhere, together with a detailed proof of the validity of our method and an analysis of the IR cut-off in systems with magnetic impurities, the answer for $\delta\chi_{\text{GCE}}^{(2)}$ reads:

$$\delta\chi_{\text{GCE}}^{(2)}(\mathbf{q}, \omega) = \frac{1}{(2\pi)^2 \rho_0 V^2} \frac{2i\omega D \mathbf{q}^2}{(D\mathbf{q}^2 - i\omega)^2} \sum_{\mathbf{Q}_1, \mathbf{Q}_2} \left[\quad (18) \right. \\ P_c(\mathbf{Q}_1, \omega) P_c(\mathbf{Q}_2, \omega) \left(\frac{D\mathbf{q}^2 + i\omega}{D\mathbf{q}^2 - i\omega} + \frac{4D(\mathbf{q}\mathbf{Q}_1)(\mathbf{q}\mathbf{Q}_2)/\mathbf{q}^2}{D(\mathbf{q} + \mathbf{Q}_1 + \mathbf{Q}_2)^2 - i\omega} \right) \\ + P_d(\mathbf{Q}_1, \omega) P_d(\mathbf{Q}_2, \omega) \left(\frac{2D[\mathbf{q}(\mathbf{q} + \mathbf{Q}_1 + \mathbf{Q}_2)]^2/\mathbf{q}^2}{D(\mathbf{q} + \mathbf{Q}_1 + \mathbf{Q}_2)^2 - i\omega} - 1 \right) \\ \left. + P_c(\mathbf{Q}_1, \omega) P_d(\mathbf{Q}_2, \omega) (2 + 2i\omega P_c(\mathbf{Q}_1, \omega)) \right].$$

To conclude this section, we would like to note that our method of dressing the Hikami boxes goes far beyond the initial ideas of Ref. [24]. It is a very powerful and generic working tool which can be extended to even more complicated diagrams, including higher loop corrections, and non-trivial physical problems. For example, our method can be straightforwardly used to describe mesoscopic systems in the ballistic regime, cf. Ref. [26]. Therefore, the diagrammatic approach presented above is complementary to the diffusive nonlinear σ -model which fails to yield ballistic results. One can invent alternative diagrammatic tricks which help to avoid the complexity of the Hikami boxes with scalar vertices. For instance, the density response function can be obtained by calculating the current response function (averaged conductivity) first and then using the continuity equation. In the latter approach, the dressed scalar vertices are replaced by undressed vector ones, which greatly simplifies the calculation²⁷. However, this method cannot describe the full \mathbf{q} -dependence of χ , which is crucial for the polarizability. We have checked that both approaches give the same results in the small- \mathbf{q} limit.

B. Canonical ensemble

In this section, we study the disorder average of the density response function χ in the CE, where the number of particles N is fixed in each sample. Let us first discuss the properties of the statistical ensemble which corresponds to the experimental measurements of the polarizability, such as the experiment

discussed in Section VI. We are mainly interested in the behavior close to the 0D regime, where due to $\tau_\phi \geq 1/E_{\text{Th}}$, there is no self-averaging. Instead, the disorder average is usually realized by an ensemble average. The samples from the ensemble differ in impurity configuration *and* can have slightly different particle number. At $T = 0$ (in the ground state) all single-particle levels below the Fermi level ϵ_F are occupied. However, one cannot fix ϵ_F for the whole ensemble due to randomness of the energy levels *and* due to the fluctuations of N from sample to sample. This can be taken into account by introducing an ϵ_F which fluctuates around the typical value μ^0 ,¹¹ μ^0 fixes the mean value of N in the entire ensemble. It has been shown that such ensembles of isolated disordered samples with fluctuating ϵ_F can be described by the so-called Fermi-level pinning ensemble,^{11,12} which is realized as follows: (i) the Fermi-energy is pinned to an energy level ϵ_k , such that $\epsilon_F = \epsilon_k + 0$. (ii) the level ϵ_k is sampled from a weight function $P(\epsilon_k)$, which is centered at μ^0 and is normalized: $\int P(\epsilon) d\epsilon = 1$. The support of $P(\epsilon_k)$ should be much smaller than μ^0 but much larger than Δ . The correlations resulting from fixing N in the given sample are subsequently reduced to the additional correlations induced by disorder with the help of the following procedure: The expression for the density response function averaged over the fluctuating Fermi energies and over disorder reads:

$$\bar{\chi}(\mathbf{q}, \omega) = \frac{1}{\sum_{\mathbf{k}} P(\epsilon_{\mathbf{k}})} \sum_{\mathbf{k}} \overline{P(\epsilon_{\mathbf{k}}) \chi_{\epsilon_{\mathbf{k}}}(\mathbf{q}, \omega)}. \quad (19)$$

In Eq. (19) we have assumed that the numerator and denominator can be averaged over disorder independently, see the discussion in Ref. [11]. Since the averaged density of states depends only weakly on disorder⁹ and is almost constant on the support of P , the denominator of Eq. (19) can be simplified

$$\sum_{\mathbf{k}} \overline{P(\epsilon_{\mathbf{k}})} = V \int_{-\infty}^{+\infty} dE P(E) \overline{\rho_E} \approx \rho_0 V. \quad (20)$$

Inserting Eq. (8) and Eq. (20) into Eq. (19), we find the disorder averaged density response function in the CE:

$$\bar{\chi}(\mathbf{q}, \omega) = \frac{1}{\rho_0} \int_{-\infty}^{+\infty} dE P(E) \overline{\rho_E \chi_E(\mathbf{q}, \omega)} = \bar{\chi}_\mu + \delta\chi_{\text{CE}}. \quad (21)$$

The loop-expansion of $\bar{\chi}_\mu$ was calculated in the previous section. The quantity $\delta\chi_{\text{CE}}$ describes additional contributions resulting from fluctuations of ϵ_F . It is governed by the irreducible part of the integrand:

$$\delta\chi_{\text{CE}} \equiv \frac{1}{\rho_0} \int_{-\infty}^{+\infty} dE P(E) \left(\overline{\rho_E \chi_E(\mathbf{q}, \omega)} - \overline{\rho_E} \overline{\chi_E(\mathbf{q}, \omega)} \right) \\ \simeq \frac{1}{\rho_0} \left(\overline{\rho_E \chi_E(\mathbf{q}, \omega)} - \rho_0 \overline{\chi_E(\mathbf{q}, \omega)} \right). \quad (22)$$

In Eq. (22), we have assumed that the disorder-averaged quantities are (almost) independent of the absolute values of the particle energies. As a result, the exact form of the weight function $P(\epsilon_k)$ is not important. Let us now derive the leading contribution to $\delta\chi_{\text{CE}}$.

which describes classical diffusive screening, and

$$F(\mathbf{q}, \omega) \equiv \frac{(D\mathbf{q}^2 - i\omega)^2}{D\mathbf{q}^2} \pi V \delta\chi(\mathbf{q}, \omega), \quad (28)$$

which describes the quantum corrections to χ . $g(L)$ denotes the dimensionless conductance of a diffusive system of size L :

$$g(L) \equiv 2\pi E_{\text{Th}}(L)/\Delta, \quad E_{\text{Th}}(L) = D/L^2. \quad (29)$$

Eqs. (26)-(28) together with Eqs. (17), (18) and (24) are the first major results of this paper. The quantum corrections $\Delta\alpha$ are obtained by substituting the terms $\sim F$ and $\sim F^2$ of Eq. (26) into Eq. (5) and summing over \mathbf{q} . We remind the reader that the zero mode does not contribute to the polarizability due to electroneutrality $\chi(\mathbf{0}, \omega) = 0$ and, therefore, we can assume $|\mathbf{q}| \neq 0$ in Eq. (26). The typical momenta which govern the sum in Eq. (5) are $|\mathbf{q}| \sim 1/L$ since the external potential ϕ_{ext} varies on the scale of the sample size L . But we will keep \mathbf{q} below for generality.

V. COMPARISON TO RMT+ σ -MODEL

Let us now compare the results of our perturbative calculations with those of Ref.[8] which are obtained from a combination of the RMT approach and the nonlinear σ -model. The latter will be referred to as ‘‘RMT+ σ -model’’. This comparison requires an assumption $E_{\text{Th}}(L) \gg \max(\Delta, \omega, \gamma)$ which in particular means $g(L) \rightarrow \infty$. In this limit, the term $\sim F^2$ in Eq. (26) acquires an additional smallness (which can be estimated as $O(1/g(L))$) and can be neglected while the term $\sim F^1$ becomes independent of \mathbf{q} . Next, we keep only the zero mode contributions in all sums over internal momenta in the expressions for $\chi_{\text{GCE}}^{(1,2)}$ and $\delta\chi_{\text{CE}}^{(1)}$ and consider the difference of F calculated for unitary and orthogonal ensembles: $\delta_B F(\omega) = F(\omega, B \rightarrow \infty) - F(\omega, 0)$, where B is the strength of an external magnetic field. The terms which contain only diffusons are cancelled in $\delta_B F$.

Using Eqs. (17), (18) and (24), we obtain

$$\delta_B F(\omega, g \rightarrow \infty) = \underbrace{-\frac{i\omega}{\gamma - i\omega}}_{\delta\chi_{\text{GCE}}^{(1)}} - \frac{\Delta}{2\pi} \left[\underbrace{\frac{i\omega - 2\gamma}{(\gamma - i\omega)^2}}_{\delta\chi_{\text{GCE}}^{(2)}} + \underbrace{\frac{2\gamma}{\gamma(\gamma - i\omega)}}_{\delta\chi_{\text{CE}}^{(1)}} \right]. \quad (30)$$

Subscripts under the braces explain the origin of the corresponding terms. The last term must be taken into account only in the CE. The counterpart of Eq. (30) obtained from RMT+ σ -model in Ref.[8] reads:

$$\text{RMT} + \sigma: \quad \delta_B F(\omega) = 1 + \int_{+0}^{\infty} \frac{d\varepsilon}{\Delta} \left(\frac{1}{\varepsilon - \omega} + \frac{1}{\varepsilon + \omega} \right) \times \left[\underbrace{\varepsilon \delta_B R_2(\varepsilon)}_{\text{GCE}} + \Delta \delta_B R_2(\varepsilon) + \int_{+0}^{\varepsilon-0} d\varepsilon_1 \delta_B \tilde{R}_3(\varepsilon, \varepsilon_1) \right]. \quad (31)$$

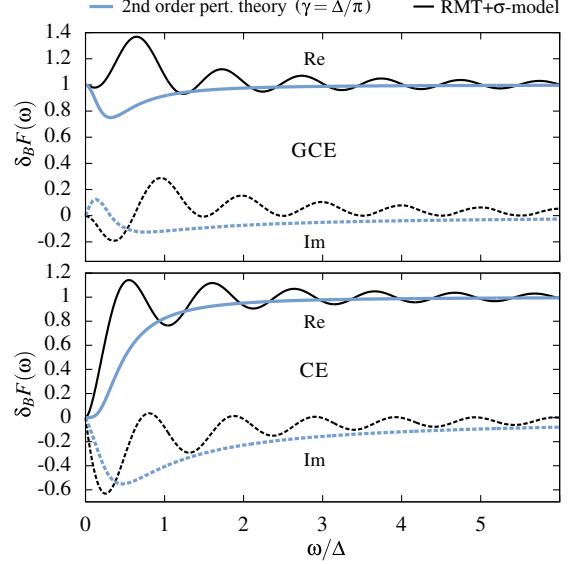


FIG. 7. (color online) The quantum corrections to the polarizability in the limit $E_{\text{Th}}(L) \gg \max(\Delta, \omega, \gamma)$ for the GCE (upper panel) and the CE (lower panel). We compare real (solid lines) and imaginary (dashed lines) parts the function $\delta_B F$ obtained from 2nd order perturbation theory, Eq. (30), and from the RMT+ σ -model, Eq. (31).

Here $R_{2,3}$ are the usual (dimensionless) two- and three-level spectral correlation functions, $\tilde{R}_3(\varepsilon, \varepsilon_1) = R_3(\varepsilon, \varepsilon_1) - R_2(\varepsilon)$, and $\delta_B R_{2,3}$ denotes the difference of the correlation functions without and with time-reversal symmetry. We have marked in Eq. (31) the relevance of different terms for the GCE and the CE.

We remind the reader that the RMT+ σ -model results are valid for $\gamma = 0$ and cannot straightforwardly describe a γ -dependence, while our perturbative result, Eq. (30), is valid only if $\Delta \lesssim \max(\gamma, \omega)$. To resolve this issue, one should set in Eq. (30) $\gamma \sim \Delta$. Eq. (30) yields $\delta_B F(\omega \rightarrow 0, g \rightarrow \infty) = \Delta/(\pi\gamma)$ for the GCE. Therefore, we have chosen $\gamma = \Delta/\pi$ to ensure the correct limit $\delta_B F(\omega \rightarrow 0, g \rightarrow \infty)|_{\text{GCE}} = 1$.

The comparison of the results obtained from RMT+ σ -model and from the perturbative calculations are shown in Fig. 7 for the GCE and the CE. Apart from the oscillations in the RMT+ σ -curves, whose origin is non-perturbative, the agreement is excellent. The asymptotic limits are fully recovered in the perturbative calculations: (i) $\delta_B F(\omega \gg \Delta, g \rightarrow \infty) \rightarrow 1$ for the both ensembles; (ii) $\delta_B F(\omega \rightarrow 0, g \rightarrow \infty) \rightarrow 0$ in the CE due to cancellation of $\delta\chi_{\text{GCE}}^{(2)}$ and $\delta\chi_{\text{CE}}^{(1)}$. The latter property of the CE holds true at any γ in 1st and 2nd order perturbation theory.

We conclude this section by noting that the perturbation theory is able to reproduce the results of the RMT+ σ -model with good qualitative agreement, which is the second major result of our work.

VI. POLARIZABILITY OF AN ENSEMBLE OF RINGS

The experiments described in Ref. [18] and [19] were done on a large number of disordered metallic rings. The rings were etched on a 2D substrate and were placed on the capacitive part of a superconducting resonator, where a spatially homogeneous in-plane electric field $\mathbf{E}(\omega)$ acted on them. In terms of the coordinate along the ring, $x \in [0, 2\pi R]$, where R is the ring radius, the external electric potential of this field is $\phi_{\text{ext}}(x, \omega) = |\mathbf{E}(\omega)|R \cos(x/R) + \phi_{\text{ext}}^{(0)}$, and its Fourier transform reads

$$\phi_{\text{ext}}(q, \omega) = -|\mathbf{E}(\omega)|R^2\pi [\delta_{q,1/R} + \delta_{q,-1/R}] + \phi_{\text{ext}}^{(0)} \cdot \delta_{q,0}. \quad (32)$$

The constant shift of the potential $\phi_{\text{ext}}^{(0)}$ does not contribute to the polarizability. Therefore, the sum in Eq. (5) involves only two modes, $q = 1/R$ and $q = -1/R$, which yield

$$\begin{aligned} \alpha(\omega) &= \frac{4e^2}{|\mathbf{E}(\omega)|^2} \frac{1}{2\pi R} \phi_{\text{ext}}^2(q, \omega) \frac{\chi(q, \omega)}{\varepsilon(q, \omega)} \Big|_{q=1/R} \\ &= 2\pi e^2 R^3 \frac{\chi(1/R, \omega)}{\varepsilon(1/R, \omega)}. \end{aligned} \quad (33)$$

In Eq. (33), we have taken into account the symmetry of the summand under the inversion $q \rightarrow -q$.

The Coulomb potential in quasi-1D is given by

$$U(q) = 2e^2 \ln(|qW|), \quad |qW| \ll 1; \quad (34)$$

where $W \ll R$ is the width of the ring. Inserting Eq. (34) into Eq. (27), we find the screening function of the quasi-1D ring at $q = 1/R$:

$$S(1/R, \omega) = \left(1 + (\kappa W) \ln(R/W) / \pi - \frac{i\omega}{E_{\text{Th}}(R)} \right)^{-1} \quad (35)$$

$$\frac{\kappa W \gg 1}{\approx} \frac{\pi}{(\kappa W) \ln(R/W)} \equiv S_0 \ll 1. \quad (36)$$

We have introduced the 2D Thomas-Fermi screening vector, $\kappa = 4\pi e^2 \rho_0 / W$ with ρ_0 being the *quasi-1D* density of states, see e.g. Ref. [9], and assumed sufficiently strong screening, $\kappa W \gg 1$, such that S reduces to the ω -independent constant S_0 . This agrees with the experiment where one can estimate $(\kappa W) \ln(R/W) \approx 18$. Therefore, we focus below only on the limit of strong screening. Note that in this limit, the product $U(1/R, \omega)S(1/R, \omega)$ can be also simplified

$$U(1/R, \omega)S(1/R, \omega) \approx -1/2\rho_0. \quad (37)$$

The classical part of the polarizability comes from inserting the leading term of the expansion (26) into Eq. (33):

$$\alpha_0 \simeq 2\pi e^2 R^3 \rho_0 S_0 = \frac{\pi R^3}{2 \ln(R/W)}. \quad (38)$$

Using Eqs. (13,37) in Eq. (26), and inserting the result into Eq. (33), we obtain the quantum corrections to the polarizability up to the term $\sim (F/g)^2$:

$$\frac{\Delta\alpha(\omega)}{2S_0\alpha_0} \approx \frac{F(R^{-1}, \omega)}{g(R)} - 2 \frac{E_{\text{Th}}(R)}{E_{\text{Th}}(R) - i\omega} \left(\frac{F(R^{-1}, \omega)}{g(R)} \right)^2. \quad (39)$$

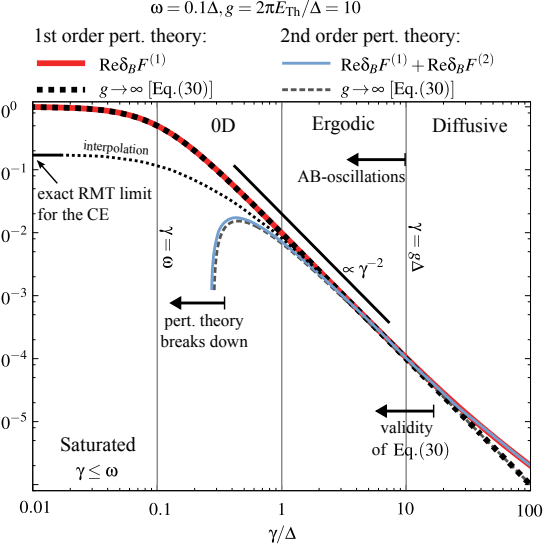


FIG. 8. (color online) Comparison of perturbative 1st order, $\delta_B F^{(1)}$, 2nd order, $\delta_B F^{(1)} + \delta_B F^{(2)}$, and interpolated (to the RMT+ σ -model limit) results for the quantum corrections to the polarizability in the parameter range $\omega < \Delta < E_{\text{Th}}$.

Let us regroup the terms in Eq. (39) to single out the terms of 1st and 2nd order perturbation theory:

$$\frac{\Delta\alpha(\omega)}{2S_0\alpha_0} \approx \frac{1}{g(R)} \left(F^{(1)}(1/R, \omega) + F^{(2)}(1/R, \omega) \right) \quad (40)$$

with

$$F^{(1)}(1/R, \omega) = (2\pi^2 R) \frac{(E_{\text{Th}}(R) - i\omega)^2}{E_{\text{Th}}(R)} \delta\chi_{\text{GCE}}^{(1)}(1/R, \omega), \quad (41)$$

and

$$\begin{aligned} F^{(2)}(1/R, \omega) &= \\ &= (2\pi^2 R) \frac{(E_{\text{Th}}(R) - i\omega)^2}{E_{\text{Th}}(R)} \left(\delta\chi_{\text{GCE}}^{(2)}(1/R, \omega) + \delta\chi_{\text{CE}}^{(1)}(1/R, \omega) \right) \\ &+ \frac{2}{g(R)} (2\pi^2 R)^2 \frac{(E_{\text{Th}}(R) - i\omega)^3}{E_{\text{Th}}(R)} \left(\delta\chi_{\text{GCE}}^{(1)}(1/R, \omega) \right)^2. \end{aligned} \quad (42)$$

We emphasize that all three parts of the density response function, $\delta\chi_{\text{GCE}}^{(1,2)}$ and $\delta\chi_{\text{CE}}^{(1)}$, are generically important for the theoretical description of the experimental data with the help of Eq. (40) if the rings are isolated. Having obtained Eqs. (17), (18) and (24) (and Eq. (30) for the limit $g \rightarrow \infty$) and Eqs. (39)-(42), we are now in the position to analyze different options to fit the experimental data. Ref. [18] and [19] focused on the T -dependence of the real part of the quantum corrections, thus, in the following we will concentrate on $\text{Re}\Delta\alpha$.

The crossover to 0D dephasing occurs when γ decreases below Δ . We expect that the ideal parameter range to study this

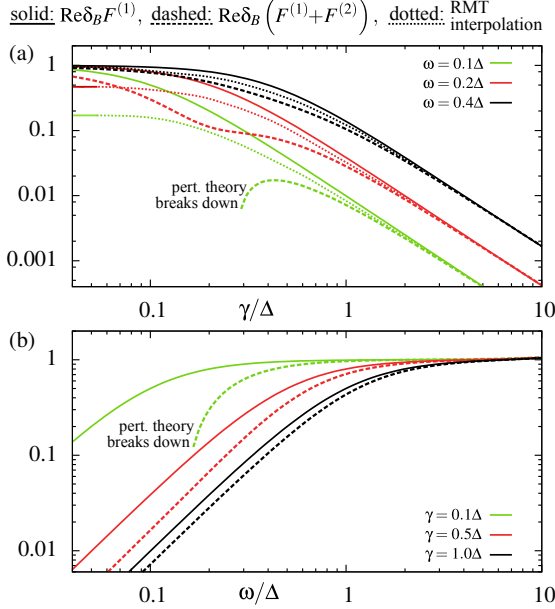


FIG. 9. (color online) Comparison of perturbative 1st order, $\delta_B F^{(1)}$, 2nd order, $\delta_B F^{(1)} + \delta_B F^{(2)}$, and interpolated (to the RMT+ σ -model limit) results for the quantum corrections to the polarizability (a) as a function of γ for different values of ω and (b) as a function of ω for different values of γ .

crossover experimentally in the CE is $\omega < \Delta < E_{\text{Th}}$. However, it is important that the conductance should be only moderately large, since $\Delta\alpha$ is suppressed in the case of extremely large g , cf. Eq. (39); and the frequency should not be too small, since the quantum corrections to the polarizability of isolated systems are suppressed in the static limit, see Fig. 7. Let us first discuss our general expectations for this parameter range, which are illustrated in Fig. 8. The simplest regime is $1 \lesssim \gamma/\Delta \lesssim g$ where the loop-expansion can be justified and the difference between the GCE and the CE is negligible. Keeping only the leading term, we obtain a power law for the dependence of $\Delta\alpha$ on γ . This power law can be derived straightforwardly after noting that, in the range $(\gamma, \omega)/\Delta \ll g$, one can use the approximation Eq. (30) and find $\text{Re}\Delta\alpha \sim \text{Re}\delta_B F(\omega) \sim \omega^2/\gamma^2$ for $\omega \ll \gamma$.

The subleading terms, which in particular describe the difference of the GCE and the CE, are able to improve the theoretical answer for γ being slightly smaller than Δ . However, $\text{Re}\delta_B F^{(2)}$ (and, correspondingly, the difference between the ensembles) is small at any γ for moderately small frequencies, see the example $\omega = 0.4\Delta$ in Fig. 9. Therefore, $\delta_B F^{(1)}$ suffices to fit the experiment at $\omega \gtrsim 0.4\Delta$. The T -dependence of $\Delta\alpha$ saturates to the value predicted by the RMT+ σ -model at $\gamma \lesssim \omega$ which makes the range of pronounced OD dephasing ($\omega \lesssim \gamma \lesssim \Delta$) too narrow even at $\omega \simeq 0.4\Delta$, thus, smaller frequencies are needed. Of course, the perturbation theory

is no longer valid if both ω and γ are small. In particular, when $F^{(2)}$ becomes of order of $F^{(1)}$ it can lead to changing the overall sign of $\text{Re}\delta_B(F^{(1)} + F^{(2)})$, see the cut of the lines in Fig. 8 marked “pert. theory breaks down”. We believe that this sign change is unphysical and, moreover, it contradicts the prediction of the RMT+ σ -model. Nevertheless, our calculations show that the power law, which is obtained in the perturbative region from the leading correction, can be extended well into the non-perturbative region $\omega \lesssim \gamma \lesssim \Delta$. This provides us with the unique possibility to detect the crossover to OD dephasing directly from the amplitude of $\Delta\alpha$. It is in sharp contrast to the quantum corrections to the conductivity, which always saturate at $\gamma \lesssim \Delta$.^{4,33}

Let us illustrate our unexpected statement with the help of Fig. 8: We know the exact value of $\Delta\alpha$ in the limit $\gamma \rightarrow 0$ from the RMT+ σ -model and the correct behavior of $\Delta\alpha$ for γ being of order of (and slightly below) Δ . Using these reference points, one can interpolate the dependence $\delta\alpha(\gamma)$ for the whole region $0 < \gamma \lesssim \Delta$. Since the slope of the interpolated curve is only slightly different from the perturbative one for $\gamma \geq 0.3\Delta$, the leading answer of perturbation theory can be used to detect the crossover to OD dephasing. If the range $\gamma \geq 0.3\Delta$ is not sufficient for unambiguously fitting the experiment, the whole interpolated curve can be used instead.

The authors of Ref. [18] and [19] used a superconducting resonator with fixed frequency $\omega \simeq 0.2\Delta \simeq 17\text{mK}$ to measure $\Delta\alpha(T)$ of the rings. In the following we will apply our theory to explain the experimental results of these papers. We note that the qualitative difference in the slope of the curves obtained from the three options for fitting – (i) the interpolated curve, (ii) the result of 2nd order perturbation theory, and (iii) the leading perturbative result – becomes rather insignificant at $\omega \simeq 0.2\Delta$ and $\gamma \gtrsim 0.3\Delta$, see Fig. 9(a). The main difference between (i) and (iii) is that the saturation originates at slightly larger γ than the leading perturbative result would suggest. Thus we can safely keep $F^{(1)}$ and neglect $F^{(2)}$ to fit the data, which makes our task simpler³².

The experimental results for the ring polarizability can be distorted because of a parasitic contribution from the resonator. The latter has been filtered out in the experiment with the help of an additional weak magnetic field B applied perpendicular to the rings, such that $\Delta\alpha$ becomes a periodic function of the magnetic flux through the ring. Measuring the T -dependence of the $\phi_0/2$ oscillations, cf. Fig. 9 of Ref. [19], allows one to focus purely on the response of the rings. Using Eq. (17) in Eq. (28), we find

$$\begin{aligned} \Delta\alpha &\propto F^{(1)}(1/R, \omega) = i\omega \sum_{\mathbf{Q}} P_{\mathbf{c}}(\mathbf{Q}, \omega) \\ &= i\omega L \int_0^\infty dt e^{i\omega t} \sum_n \frac{1}{\sqrt{4\pi Dt}} e^{-(nL)^2/4Dt} e^{i\theta n} e^{-\gamma t}, \end{aligned} \quad (43)$$

where $\theta = 4\pi\phi/\phi_0$ and ϕ is the flux through one ring, and $L = 2\pi R$. Taking the Fourier transform and selecting the $\phi_0/2$ signal gives:

$$\delta_{\phi_0/2} F^{(1)}(1/R, \omega) = \frac{i\omega \exp\left(-\sqrt{(\gamma - i\omega)/E_{\text{Th}}(L)}\right)}{\sqrt{E_{\text{Th}}(L)(\gamma - i\omega)}}. \quad (44)$$

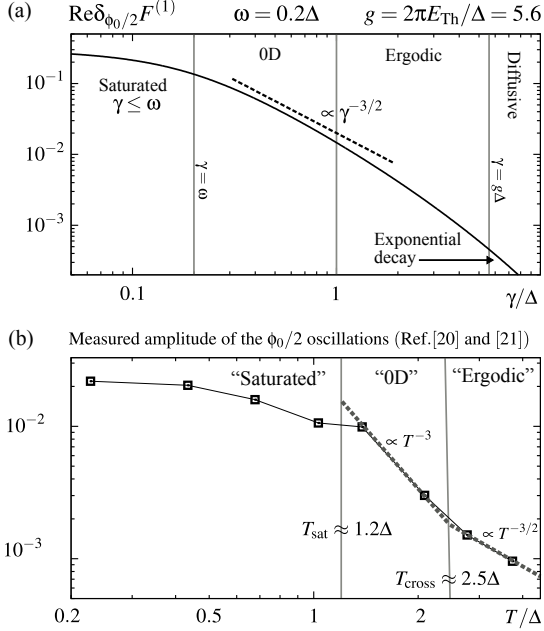


FIG. 10. Amplitude of the $\phi_0/2$ oscillations. (a) Expected dependence on γ from our theory, Eq. (44), for the parameter range $\omega \ll \Delta \ll E_{\text{Th}}$. (b) Experimentally measured data as a function of temperature and possible interpretation. Note that the theory (see e.g. Ref. [33] and [34]) predicts $\gamma_{\text{OD}} \propto T^2$ in the OD regime, and $\gamma_{\text{erg}} \propto T$ in the ergodic regime, therefore, the $\gamma^{-3/2}$ behavior indicated in (a) encompasses both the T^{-3} and $T^{-3/2}$ behavior seen in (b).

The function $\delta_{\phi_0/2} F^{(1)}$ is shown in Fig. 10(a). It is similar to $\delta_B F^{(1)}$, cf. Fig. 8, however, the dependence of $\delta_{\phi_0/2} F^{(1)}$ on γ is governed by a $\propto \gamma^{-3/2}$ power law in the regime $\omega \ll \gamma \ll g\Delta$, and in the regime $g\Delta \ll \gamma$, the $\phi_0/2$ oscillations are exponentially suppressed. The theory predicts a OD dephasing rate, $\gamma_{\text{OD}} = a\Delta T^2/E_{\text{Th}}^2$, at low temperatures and an ergodic dephasing rate, $\gamma_{\text{erg}} = b\Delta T/E_{\text{Th}}$, at higher temperatures, where a and b are system-specific, dimensionless coefficients of order ~ 1 , see Ref. [33] and [34]. The crossover between the two regimes occurs at a temperature $T_{\text{cross}} = \frac{b}{a} E_{\text{Th}}$. We expect that the saturation at $\gamma = \omega$ occurs in the OD regime, corresponding to a temperature $T_{\text{sat}} = \frac{1}{\sqrt{a}} E_{\text{Th}} \sqrt{\omega/\Delta}$. Note that the conductance of each ring was rather small, $g(L) \approx 5.6$, such that the Thouless energy $E_{\text{Th}}(L) \approx 0.9\Delta$. Thus, depending on the coefficients a and b , T_{cross} and T_{sat} can be relatively close to each other.

The experimental result for the T dependence of the $\phi_0/2$ oscillations is shown in Fig. 10(b). The measurements were done in the temperature interval $\omega \approx 0.2\Delta \leq T \leq 4\Delta$. Based on the preceding discussion, we offer the following interpretation of the data: At low temperatures $T \lesssim 1.2\Delta$, the quantum corrections depend only weakly on T and are almost sat-

urated. At intermediate temperatures $1.2\Delta \lesssim T \lesssim 2.5\Delta$ the slope of the data is steep and consistent with OD dephasing $\Delta\alpha(T) \propto \gamma_{\text{OD}}^{-3/2} \propto T^{-3}$. At higher temperatures $T \gtrsim 2.5\Delta$, the slope of $\Delta\alpha(T)$ decreases and is consistent with ergodic dephasing $\Delta\alpha \propto \gamma_{\text{erg}}^{-3/2} \propto T^{-3/2}$. The crossover temperatures, $T_{\text{sat}} \approx 1.2\Delta$ and $T_{\text{cross}} \approx 2.5\Delta$, correspond to coefficients $a \approx 0.1$ and $b \approx 0.3$, which are close to the values predicted in Ref. [33] ($a \approx 0.04$ and $b \approx 1$). However, we stress that this interpretation is based only on very few data points, and we do not claim that the experiment clearly shows a crossover to OD dephasing. Further experiments are needed to support this statement, see Section VII.

VII. CONCLUSIONS

Understanding interference phenomena and dephasing in mesoscopic systems at very low temperatures is a subtle issue which has provoked controversies between different theoretical approaches³⁵, as well as between theory and experiments³⁶. Quantum transport experiments cannot give a certain answer to all questions because of unavoidable distortions due to the coupling to the environment. The response of isolated disordered samples, on the other hand, provides a “cleaner” setup to study dephasing, and gives one the possibility to settle long-lasting open questions.

We have studied the quantum corrections to the polarizability of isolated disordered metallic samples aiming to improve the explanation of previous experiments (Ref. [18] and [19]), and to suggest new measurements, where the elusive OD regime of dephasing can be ultimately detected. Using the standard strategy of mesoscopic perturbation theory, i.e. the loop-expansion in diffusons and Cooperons, we have developed a theory, which (i) accounts for the difference between connected (GCE) and isolated (CE) systems, and (ii) is able to describe the low frequency response of disordered metals, taking into consideration weak dephasing induced by electron interactions. We have shown that the difference between the GCE and the CE appears only in the subleading terms, therefore, we have extended the calculations up to the second loop. An important by-product of these calculations is a systematic procedure to evaluate the Hikami boxes, see Fig. 2 and 4, which is based on a fundamental conservation law²⁴: electroneutrality of the density response function. Our main analytical results for the quantum corrections to the polarizability are presented in Eqs. (26)-(28) with Eqs. (17), (18) and (24).

We have demonstrated that, in the experimentally relevant parameter range, the difference between the statistical ensembles is unimportant and one can fit the measurements by using the leading term of the perturbation theory. The authors of Ref. [18] and [19] have tried to find OD dephasing with the help of an empirical fitting formula. By using the more rigorous and reliable Eq. (44), we have confirmed that OD dephasing might have manifested itself in the T -dependence of magneto-oscillations at $T \lesssim E_{\text{Th}}$. Unfortunately, the T -range of interest here is rather narrow, and only few experimental data points are available there. Therefore, we are unable to claim conclusively that OD dephasing has been observed in

the experiments. However, we can straightforwardly suggest several experiments which might yield conclusive evidence of 0D dephasing: Firstly, one can repeat the measurement of Ref. [18] and [19], but with a larger number of data points around the crossover temperature T_{cross} , see Fig. 10, while simultaneously improving the measurements precision. Since the theory predicts a drastic increase in slope of the $\phi_0/2$ -oscillations at the crossover (from $T^{-3/2}$ to T^{-3}), even such measurements should be able to reliably confirm the existence of 0D dephasing, thereby uncovering the role of the Pauli blocking at low T . Secondly, it is highly desirable to extend the T -range where the crossover to 0D dephasing is expected to appear, which can be achieved by decreasing ω and/or increasing g . However, a very large conductance and ultra-small frequencies are nevertheless undesirable, because in these limits the quantum corrections to the polarizability are reduced. Thus, improving the precision of the measurement is needed anyway. Besides, fitting with the help of the leading perturbative result fails at very small frequencies, see Fig. 9. This

difficulty can be overcome by taking into account our two-loop results and/or using an interpolation to the $\gamma \rightarrow 0$ limit from the RMT+ σ -model, see Fig. 8.

To summarize, we have shown that the quantum corrections to the polarizability are an ideal candidate to study dephasing at low T and the crossover to 0D dephasing. We very much hope that our theoretical results will stimulate new measurements in this direction.

ACKNOWLEDGMENTS

We acknowledge illuminating discussions with C. Texier, H. Bouchiat, G. Montambaux, and V. Kravtsov, and support from the DFG through SFB TR-12 (O. Ye.), DE 730/8-1 (M. T.) and the Cluster of Excellence, Nanosystems Initiative Munich. O. Ye. and M. T. acknowledge hospitality of the ICTP (Trieste) where part of the work for this paper was carried out.

-
- ¹ B. L. Altshuler, and A. G. Aronov, in *Electron-Electron Interactions in Disordered Systems*, edited by A. L. Efros and M. Pollak (North-Holland, Amsterdam, 1985), Vol. 1.
- ² B. L. Altshuler, A. G. Aronov, and D. E. Khmel'nitsky, *J. Phys. C* **15**, 7367 (1982).
- ³ U. Sivan and Y. Imry and A. G. Aronov, *Europhys. Lett.* **28**, 115 (1994).
- ⁴ M. Treiber, O. M. Yevtushenko, and J. von Delft, *Ann. Physik* **524**, 188 (2012).
- ⁵ B. L. Altshuler, Y. Gefen, A. Kamenev, and L. S. Levitov, *Phys. Rev. Lett.* **78**, 2803 (1997).
- ⁶ Ya. M. Blanter, *Phys. Rev. B* **54**, 12807 (1996).
- ⁷ V. E. Kravtsov, and A. D. Mirlin, *JETP Lett.* **60**, 656 (1994).
- ⁸ Ya. M. Blanter, and A. D. Mirlin, *Phys. Rev. B* **57**, 4566 (1998); *ibid* **63**, 113315 (2001).
- ⁹ G. Montambaux, and E. Akkermans, *Mesoscopic Physics of Electrons and Photons*, Cambridge University Press (2007).
- ¹⁰ A. Kamenev and Y. Gefen, *Phys. Rev. Lett.* **70**, 1976 (1993); *Phys. Rev. B* **56**, 1025 (1997); A. Kamenev, B. Reulet, H. Bouchiat, and Y. Gefen, *Europhys. Lett.* **28**, 391 (1994).
- ¹¹ W. Lehle, and A. Schmid, *Ann. Physik* **507**, 451 (1995).
- ¹² A. Altland and S. Iida and A. Müller-Groeling and H. A. Weidenmüller, *Europhys. Lett.* **20**, 155 (1992); *Ann. Phys. (N.Y.)* **219**, 148 (1992).
- ¹³ This approach has also been used in Ref. [8] to describe the polarizability in the non-perturbative regime.
- ¹⁴ L. P. Gorkov, and G. M. Eliashberg, *Sov. Phys. JETP* **21**, 940 (1965).
- ¹⁵ M. J. Rice, W. R. Schneider, and S. Strässler *Phys. Rev. B* **8**, 474 (1973).
- ¹⁶ A detailed discussion of the assumptions of Ref. [14] can be found in: Ya. M. Blanter, and A. D. Mirlin *Phys. Rev. B* **53**, 12601 (1996).
- ¹⁷ K. B. Efetov, *Phys. Rev. Lett.* **76**, 1908 (1996).
- ¹⁸ R. Deblock, Y. Noat, H. Bouchiat, B. Reulet, and D. Mailly, *Phys. Rev. Lett.* **84**, 5379 (2000).
- ¹⁹ R. Deblock, Y. Noat, B. Reulet, H. Bouchiat, and D. Mailly, *Phys. Rev. B* **65**, 075301 (2002).
- ²⁰ H. Bruus and K. Flensberg, *Many-Body Quantum Theory in Condensed Matter Physics*, Oxford graduate texts in mathematics (2004).
- ²¹ D. Vollhardt and P. Wölfle, *Phys. Rev. B* **22**, 4666 (1980).
- ²² S. Hikami, *Phys. Rev. B* **24**, 2671 (1981).
- ²³ K. B. Efetov, *Adv. Phys.* **32**, 53 (1983); B. L. Altshuler, V. E. Kravtsov, and I. V. Lerner, *Zh. Eksp. Teor. Fiz.* **91**, 2276 (1986).
- ²⁴ A similar idea has been discussed in the derivation of a current-conserving non-local conductivity: M. B. Hastings, A. D. Stone, and H. U. Baranger, *Phys. Rev. B* **50**, 8230 (1994).
- ²⁵ P. M. Ostrovsky, and V. Kravtsov, *unpublished*.
- ²⁶ G. Zala, B. N. Narozhny, and I. L. Aleiner, *Phys. Rev. B* **64**, 214204 (2001).
- ²⁷ L. P. Gorkov, A. I. Larkin, and D. E. Khmel'nitskii, *JETP Lett.* **30**, 228 (1979).
- ²⁸ R. A. Smith, I. V. Lerner, and B. L. Altshuler, *Phys. Rev. B* **58**, 10343 (1998).
- ²⁹ H. Bouchiat, *private communication*.
- ³⁰ T. Ludwig, and A. D. Mirlin, *Phys. Rev. B* **69**, 193306 (2004).
- ³¹ C. Texier, and G. Montambaux, *Phys. Rev. B* **72**, 115327 (2005).
- ³² The smallness of the contribution of 2nd order perturbation theory is also confirmed by the absence of ϕ_0 -periodic oscillations in the experimental data. We remind the reader that the ϕ_0 -periodic oscillations result from contributions of diffusons [see A. G. Aronov, and Yu. V. Sharvin, *Rev. Mod. Phys.* **59**, 755 (1987)] which exists only in $F^{(2)}$ due to $\delta\chi_{GCE}^{(2)}$ and $\delta\chi_{CE}^{(1)}$; For a discussion of this point, see A. Kamenev, and Y. Gefen, *Phys. Rev. B* **49**, 14474 (1994).
- ³³ M. Treiber, O. M. Yevtushenko, F. Marquardt, J. von Delft, and I. V. Lerner, *Phys. Rev. B* **80**, 201305(R) (2009).
- ³⁴ M. Treiber, C. Texier, O. M. Yevtushenko, J. von Delft, and I. V. Lerner, *Phys. Rev. B* **84**, 054204 (2011).
- ³⁵ F. Marquardt, J. von Delft, R. A. Smith, and V. Ambegaokar, *Phys. Rev. B* **76**, 195331 (2007); J. von Delft, F. Marquardt, R. A. Smith, and V. Ambegaokar, *ibid* **76**, 195332 (2007).
- ³⁶ A. G. Huibers, M. Switkes, C. M. Marcus, K. Campman, and A. C. Gossard, *Phys. Rev. Lett.* **81**, 200 (1998).

Chapter 5

Summary and conclusions

In this thesis we have contributed to the theory of dephasing in disordered mesoscopic systems. At low temperatures, Pauli blocking becomes important and limits the energy transfer ω of electron interactions to $\omega \ll T$ due to a lack of final scattering states. We have analyzed its effect on the interaction-induced dephasing rate γ , and discussed possible experiments to demonstrate the influence of Pauli blocking.

The thesis is divided into four main chapters, where we have reviewed the current state of research and presented a brief overview of our original results in the main text. More details on the original results can be found in the papers attached at the end of each chapter.

In Chapter 1, we have given a general introduction to the field, followed by a discussion of our motivation, and we have provided a brief outline of this thesis.

In Chapter 2, we have introduced the standard methods of mesoscopic physics, namely, the perturbative loop-expansion in diffusive propagators, and the non-perturbative random matrix theory. We have reviewed the usual derivations of the dephasing rate: (1) using a perturbation theory in the electron interactions and (2) using a path integral with an effective noise potential, and we have concluded that the temperature dependence of γ can be obtained from a self-consistent integral equation shown in Table 5 below. We have established that the so-called 0D regime of dephasing, reached at $T \ll E_{\text{Th}}$, is practically the only regime (in the relevant dimensions $d \leq 2$), where Pauli blocking significantly influences the temperature dependence of γ . Importantly, attempts to observe the 0D regime of dephasing experimentally have been unsuccessful so far, and we have concentrated on a possible experimental verification in the following. We have emphasized that the 0D regime is characterized by (1) a discreteness of the energy levels, accompanied with a breakdown of the perturbative loop-expansion, and (2) a relative weakness of the dephasing rate, such that electron trajectories, which probe the whole geometry of the system, become important. Our first main new result in this section has been the calculation of the two-loop expansion of the generalized diffusion propagator, where we have introduced a new method to calculate the short-range parts (so-called Hikami boxes) of the corresponding diagrams, which can be extended straightforwardly to more complicated diagrams, including higher loop corrections, and non-trivial physical problems. The second main result has been the derivation of a new dephasing rate functional, valid at arbitrary temperatures, which describes dephasing in non-trivial geometries, in particular, networks of quasi-1D wires.

In Chapter 3, we have considered the weak-localization correction Δg to the conductance, and discussed that Δg assumes a universal value ~ 1 in open systems, as soon as $\gamma \ll E_{\text{Th}}$, see Fig. 5.1(a) below. Since $T \ll \gamma$, the 0D regime occurs deep in the universal regime, where the weak-localization correction is practically independent of γ . However, a signature of 0D dephasing can still be extracted

$$\gamma = \frac{1}{\tau_\phi} \approx \frac{4E_{\text{Th}}T}{g} \int_{1/\tau_\phi}^T d\omega \sum_{\mathbf{q} \neq 0} \frac{1}{(D\mathbf{q}^2)^2 + \omega^2}, \quad E_{\text{Th}} = \frac{D}{L^2}, \quad g = 2\pi \frac{E_{\text{Th}}}{\Delta}$$

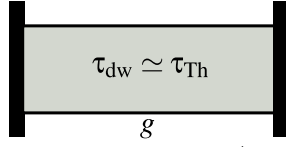
<div style="display: flex; align-items: center; justify-content: center;"> <div style="text-align: right; margin-right: 5px;">Temperature regime</div> <div style="text-align: left; margin-left: 5px;">Space dimension</div> </div>	<i>0D</i>	<i>ergodic</i>	<i>diffusive</i>
	$\gamma \ll T \ll E_{\text{Th}}$	$\gamma \ll E_{\text{Th}} \ll T$	$E_{\text{Th}} \ll \gamma \ll T$
(quasi-) 1D	$\gamma \simeq T^2/(E_{\text{Th}}g)$	$\gamma \simeq T/g$	$\gamma \simeq (\sqrt{E_{\text{Th}}}T/g)^{2/3}$
2D	$\gamma \simeq T^2/(E_{\text{Th}}g)$	$\gamma \simeq T \ln(T/E_{\text{Th}})/g$	$\gamma \simeq T \ln(g)/g$

Table 5.1: The formula for the dephasing time, see Section 2.2.5, and a table of possible regimes.

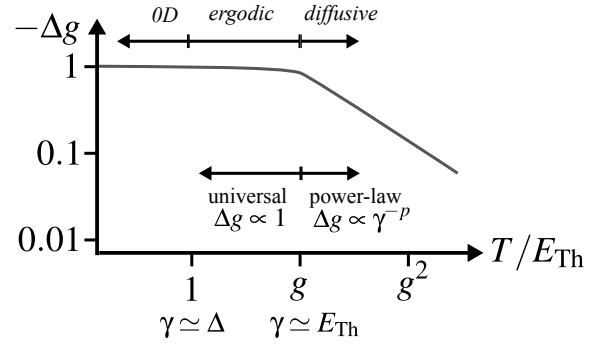
by subtracting the measured curve $\Delta g(T)$ from the universal value at $T \rightarrow 0$. We have argued that a low conductance, in combination with strongly absorbing leads, might suffice to find experimental evidence of 0D dephasing. Furthermore, we have discussed the random matrix theory of quantum transport, valid for strongly confined systems, where the electrons explore the whole system ergodically. In such systems, an additional time-scale can be introduced, the so-called dwelling time τ_{dw} , and we have proposed a simplified model, which is based on τ_{dw} , to study transport in almost isolated systems. Our first main result in this section has been a detailed description of the temperature dependence of Δg of an almost isolated ring. We have shown that the ring geometry is particularly well suited to study the 0D crossover, since the Aharonov-Bohm effect can be exploited to filter the response of the ring from distorting contributions of the leads. Our second main result has been the description of dephasing in a quantum dot model based on (1) the theory of diffusion in graphs, and (2) the dephasing rate functional derived in Chapter 2. Our model describes the weak-localization correction at arbitrary temperatures, and can be easily extended to more complicated geometries. We have concluded that confined systems are better suited to study the 0D crossover, however, 0D dephasing unavoidably occurs in the universal regime, see Fig. 5.1(b), as long as the conductance of the contacts is larger than 1.

In Chapter 4 we have focused on isolated systems, where $\tau_{\text{dw}} \rightarrow \infty$. In particular, we have considered the quantum corrections to the polarizability, $\Delta\alpha$, of an ensemble of isolated disordered metals. Previous descriptions of $\Delta\alpha$ were based on a combination of random matrix theory and the non-linear σ -model, and described the frequency dependence, however, they did not include dephasing at finite temperatures. Our main result has been a derivation of $\Delta\alpha$ using the loop-expansion, which allowed us to predict the full temperature dependence, and is valid for connected (grand-canonical ensemble) and isolated (canonical ensemble) systems. We have shown that, in contrast to Δg , the crossover to 0D dephasing occurs for $\Delta\alpha$ in a temperature range, where $\Delta\alpha$ is a power-law of γ , see Fig. 5.1(c). Our results are in good agreement with previous experiments, and suggest that 0D dephasing might have manifested itself in the observed magneto-oscillations. However, due to the small number of relevant data points, we have been unable to claim conclusively that 0D dephasing had been observed in the experiment. Nevertheless, we have concluded that the quantum corrections to the polarizability are an ideal candidate to study dephasing at low temperatures, and, in particular, the crossover to 0D dephasing and the influence of Pauli blocking. We hope that our theoretical results will stimulate new measurements in this direction.

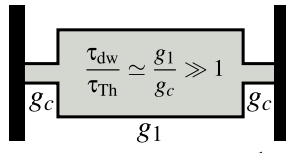
(a) open system



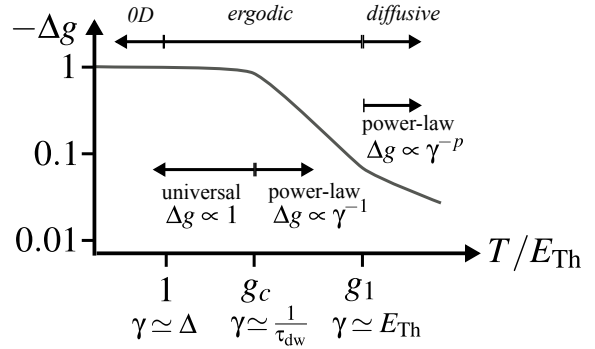
$$\Delta g \propto -E_{\text{Th}} \sum_{\mathbf{Q} \neq 0} \frac{1}{D\mathbf{Q}^2 + \gamma}$$



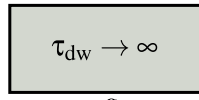
(b) confined system



$$\Delta g \propto -E_{\text{Th}} \frac{g_c}{g_1} \sum_{\text{all } \mathbf{Q}} \frac{1}{D\mathbf{Q}^2 + 1/\tau_{\text{dw}} + \gamma}$$



(c) closed system



$$\frac{\Delta\alpha(\omega)}{\alpha_0} \propto -i\omega \sum_{\text{all } \mathbf{Q}} \frac{1}{D\mathbf{Q}^2 - i\omega + \gamma}$$

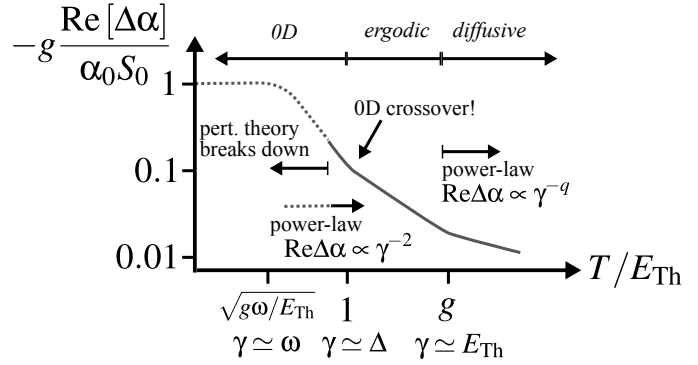


Figure 5.1: Comparison of (a) “open”, (b) “confined”, and (c) “closed” systems: The crossover between *ergodic* and *0D* dephasing occurs in (a) and (b) in the universal regime, where the quantum corrections to the conductance are practically independent of the dephasing rate γ . In (c), on the other hand, the crossover can be detected directly from the quantum corrections to the polarizability. [$p, q > 0$ are exponents depending on dimensionality; $S_0 \ll 1$ is a screening constant; We have assumed in (c) that ω is not *much* smaller than Δ , e.g. $\omega \simeq 0.3\Delta$, cf. Section 4.5.]

Appendix A

Source code listings

A.1 Calculation of the two-loop Hikami boxes

In this Appendix, we present the source code of a “Mathematica” script, which evaluates the Hikami boxes relevant for the two-loop correction to the generalized diffusion propagator, using ballistic regularization. All labels are consistent with the figures of Section 2.3.2.

```

1  (*
2
3  HOW TO USE THIS FILE:
4
5  Either
6
7  (1) Copy and paste the whole text into the Mathematica GUI and press
8      Shift-Enter,
9
10 or
11
12 (2) Pipe this file into the command line utility "math", e.g.
13     "cat this_file | /path/to/Mathematica/bin/math".
14
15 Tested with Mathematica 8.0.1
16
17 *)
18
19 (* === === === === === === === Helpful functions === === === === *)
20
21 (*
22   Imp: Value of one impurity line
23 *)
24 Imp:=1/(2*Pi*Rho*t)
25
26 (*
27   DL: Impurity ladder, expanded in excess momentum and energy
28 *)
29 DL[q_,w_]:=1+I*t*w-t*D*q^2
30
31 (*
32   GR and GA: Retarded and advanced Greens functions
33   expanded in excess momentum (q) and energy (e)
34 *)
35 GR[q_,e_]:=R-e*R^2+v*q*R^2+(v*q)^2*R^3
36 GA[q_,e_]:=A-e*A^2+v*q*A^2+(v*q)^2*A^3
37
38 (*
39   f[m,n]: Calculates the momentum sum over a product of "m" retarded and "n"
40   advanced Greens function with equal momenta and energies.
41 *)
42 f[m_,n_]:=2*Pi*Rho*t*I^(n-m)*t^(n+m-2)*((n+m-2)!)/(((n-1)!)*((m-1)!))

```

```

43
44 (*
45   GFSum: Evaluates the momentum sum over arbitrary powers of Greens function
46   with small momentum and energy differences. (Argument should be a product of GR[]/GA[.]
47   *)
48 GFSum[GFS_]:=Module[{x=GFS,CList,Dims,Res},
49   x=ZeroAndSecondOrderInv[x];
50   CList=CoefficientList[x,{R,A}];
51   Dims=Dimensions[CList];
52   Res=0;
53   Do[Do[Res=Res+CList[[iR]][[iA]]*f[iR-1,iA-1];,{iR,2,Dims[[1]]},{iA,2,Dims[[2]]}];
54   LowT[Res]
55 ]
56
57 (*
58   ZeroAndSecondOrderInv: Expand Expression in v and sum zero-order and second-order.
59   (First order gives zero.) Then replace v^2 by D/t.
60   *)
61 ZeroAndSecondOrderInv[GFS_]:=Module[{x=GFS},
62   Series[x,{v,0,4}][[3]][[1]]+(D/t)*Series[x,{v,0,4}][[3]][[3]]
63 ]
64
65 (*
66   LowT: Expand Expression to lowest and next-to lowest order in "t".
67   *)
68 LowT[GFS_]:=Module[{x=GFS,Ser,CList,AC,Dims,Ret},
69   Ser=Series[x,{t,0,100}];
70   CList=CoefficientList[x,t];
71   Dims=Dimensions[CList][[1]];
72   Ret = 0;
73   AC = 0;
74   Do[Ret=Ret+CList[[i]]*t^(i-1);If[ToString[CList[[i]]]!="0",AC=AC+1]; If[AC>1,Break[]],
75   {i,1,Dims}
76   ];
77   Ret
78 ]
79
80 (*
81   NextT: Expand Expression to lowest, next-to lowest
82   and next-to-next-to lowest order in "t".
83   *)
84 NextT[GFS_]:=Module[{x=GFS,Ser,CList,AC,Dims,Ret},
85   Ser=Series[x,{t,0,100}];
86   CList=CoefficientList[x,t];
87   Dims=Dimensions[CList][[1]];
88   Ret = 0;
89   AC = 0;
90   Do[Ret=Ret+CList[[i]]*t^(i-1); If[ToString[CList[[i]]]!="0",AC=AC+1]; If[AC>2,Break[]],
91   {i,1,Dims}
92   ];
93   Ret
94 ]
95
96 (*
97   === === === === === Generic 4-point box === === === === ===
98   R1
99   ===
100  A4 /   / A2
101   ===
102  R3
103   *)
104
105 H4UnDr[q1_,q2_,q3_,q4_,e1_,e2_,e3_,e4_] :=
106   LowT[GFSum[GR[q1,e1]*GA[q2,e2]*GR[q3,e3]*GA[q4,e4]]]
107 H4Dr13[q1_,q2_,q3_,q4_,e1_,e2_,e3_,e4_] :=
108   LowT[GFSum[GR[q1,e1]*GA[q2,e2]*GR[q3,e3]]*GFSum[GR[q3,e3]*GA[q4,e4]*GR[q1,e1]]*Imp]
109 H4Dr24[q1_,q2_,q3_,q4_,e1_,e2_,e3_,e4_] :=
110   LowT[GFSum[GA[q4,e4]*GR[q1,e1]*GA[q2,e2]]*GFSum[GA[q2,e2]*GR[q3,e3]*GA[q4,e4]]*Imp]

```

```

111
112 Print["Generic 4-point Hikami box:"]
113 FullSimplify[
114   H4UnDr[q1, q2, q3, q4, e1, e2, e3, e4]+
115   H4Dr13[q1, q2, q3, q4, e1, e2, e3, e4]+
116   H4Dr24[q1, q2, q3, q4, e1, e2, e3, e4]
117 ]
118
119 (*
120 === === === === === === === Generic 6-point box === === === === === ===
121
122   A2
123   -----
124   R1//      \\ R3
125   //        \\
126   \         /
127   A6\      /A4
128   =====
129   R5
130 *)
131 H6UnDr[q1_, q2_, q3_, q4_, q5_, q6_, e1_, e2_, e3_, e4_, e5_, e6_] :=
132   LowT[GFSum[GR[q1, e1]*GA[q2, e2]*GR[q3, e3]*GA[q4, e4]*GR[q5, e5]*GA[q6, e6]]]
133 H6Dr24[q1_, q2_, q3_, q4_, q5_, q6_, e1_, e2_, e3_, e4_, e5_, e6_] :=
134   LowT[Imp*GFSum[GA[q2, e2]*GR[q3, e3]*GA[q4, e4]]*
135     GFSum[GR[q1, e1]*GA[q2, e2]*GA[q4, e4]*GR[q5, e5]*GA[q6, e6]]]
136 H6Dr26[q1_, q2_, q3_, q4_, q5_, q6_, e1_, e2_, e3_, e4_, e5_, e6_] :=
137   LowT[Imp*GFSum[GA[q6, e6]*GR[q1, e1]*GA[q2, e2]]*
138     GFSum[GA[q2, e2]*GR[q3, e3]*GA[q4, e4]*GR[q5, e5]*GA[q6, e6]]]
139 H6Dr46[q1_, q2_, q3_, q4_, q5_, q6_, e1_, e2_, e3_, e4_, e5_, e6_] :=
140   LowT[Imp*GFSum[GA[q4, e4]*GR[q5, e5]*GA[q6, e6]]*
141     GFSum[GA[q6, e6]*GR[q1, e1]*GA[q2, e2]*GR[q3, e3]*GA[q4, e4]]]
142 H6Dr13[q1_, q2_, q3_, q4_, q5_, q6_, e1_, e2_, e3_, e4_, e5_, e6_] :=
143   LowT[Imp*GFSum[GR[q1, e1]*GA[q2, e2]*GR[q3, e3]]*
144     GFSum[GR[q1, e1]*GR[q3, e3]*GA[q4, e4]*GR[q5, e5]*GA[q6, e6]]]
145 H6Dr15[q1_, q2_, q3_, q4_, q5_, q6_, e1_, e2_, e3_, e4_, e5_, e6_] :=
146   LowT[Imp*GFSum[GR[q5, e5]*GA[q6, e6]*GR[q1, e1]]*
147     GFSum[GR[q1, e1]*GA[q2, e2]*GR[q3, e3]*GA[q4, e4]*GR[q5, e5]]]
148 H6Dr35[q1_, q2_, q3_, q4_, q5_, q6_, e1_, e2_, e3_, e4_, e5_, e6_] :=
149   LowT[Imp*GFSum[GR[q3, e3]*GA[q4, e4]*GR[q5, e5]]*
150     GFSum[GR[q1, e1]*GA[q2, e2]*GR[q3, e3]*GR[q5, e5]*GA[q6, e6]]]
151 H6Dr1315[q1_, q2_, q3_, q4_, q5_, q6_, e1_, e2_, e3_, e4_, e5_, e6_] :=
152   LowT[Imp^2*GFSum[GR[q1, e1]*GA[q2, e2]*GR[q3, e3]]*
153     GFSum[GR[q1, e1]*GR[q3, e3]*GA[q4, e4]*GR[q5, e5]]*
154     GFSum[GR[q5, e5]*GA[q6, e6]*GR[q1, e1]]]
155 H6Dr3135[q1_, q2_, q3_, q4_, q5_, q6_, e1_, e2_, e3_, e4_, e5_, e6_] :=
156   LowT[Imp^2*GFSum[GR[q1, e1]*GA[q2, e2]*GR[q3, e3]]*
157     GFSum[GR[q3, e3]*GR[q5, e5]*GA[q6, e6]*GR[q1, e1]]*
158     GFSum[GR[q3, e3]*GA[q4, e4]*GR[q5, e5]]]
159 H6Dr5153[q1_, q2_, q3_, q4_, q5_, q6_, e1_, e2_, e3_, e4_, e5_, e6_] :=
160   LowT[Imp^2*GFSum[GR[q3, e3]*GA[q4, e4]*GR[q5, e5]]*
161     GFSum[GR[q5, e5]*GR[q1, e1]*GA[q2, e2]*GR[q3, e3]]*
162     GFSum[GR[q5, e5]*GA[q6, e6]*GR[q1, e1]]]
163 H6Dr2426[q1_, q2_, q3_, q4_, q5_, q6_, e1_, e2_, e3_, e4_, e5_, e6_] :=
164   LowT[Imp^2*GFSum[GA[q6, e6]*GR[q1, e1]*GA[q2, e2]]*
165     GFSum[GA[q2, e2]*GA[q4, e4]*GR[q5, e5]*GA[q6, e6]]*
166     GFSum[GA[q2, e2]*GR[q3, e3]*GA[q4, e4]]]
167 H6Dr6264[q1_, q2_, q3_, q4_, q5_, q6_, e1_, e2_, e3_, e4_, e5_, e6_] :=
168   LowT[Imp^2*GFSum[GA[q6, e6]*GR[q1, e1]*GA[q2, e2]]*
169     GFSum[GA[q6, e6]*GA[q2, e2]*GR[q3, e3]*GA[q4, e4]]*
170     GFSum[GA[q4, e4]*GR[q5, e5]*GA[q6, e6]]]
171 H6Dr4246[q1_, q2_, q3_, q4_, q5_, q6_, e1_, e2_, e3_, e4_, e5_, e6_] :=
172   LowT[Imp^2*GFSum[GA[q2, e2]*GR[q3, e3]*GA[q4, e4]]*
173     GFSum[GA[q4, e4]*GA[q6, e6]*GR[q1, e1]*GA[q2, e2]]*
174     GFSum[GA[q4, e4]*GR[q5, e5]*GA[q6, e6]]]
175 H6Dr1346[q1_, q2_, q3_, q4_, q5_, q6_, e1_, e2_, e3_, e4_, e5_, e6_] :=
176   LowT[Imp^2*GFSum[GR[q1, e1]*GA[q2, e2]*GR[q3, e3]]*
177     GFSum[GA[q6, e6]*GR[q1, e1]*GR[q3, e3]*GA[q4, e4]]*
178     GFSum[GA[q4, e4]*GR[q5, e5]*GA[q6, e6]]]

```

```

179 H6Dr1524 [q1_, q2_, q3_, q4_, q5_, q6_, e1_, e2_, e3_, e4_, e5_, e6_] :=
180   LowT [Imp^2 * GFSum [GR [q5, e5] * GA [q6, e6] * GR [q1, e1]] *
181     GFSum [GA [q4, e4] * GR [q5, e5] * GR [q1, e1] * GA [q2, e2]] *
182     GFSum [GA [q2, e2] * GR [q3, e3] * GA [q4, e4]]]
183 H6Dr2635 [q1_, q2_, q3_, q4_, q5_, q6_, e1_, e2_, e3_, e4_, e5_, e6_] :=
184   LowT [Imp^2 * GFSum [GR [q3, e3] * GA [q4, e4] * GR [q5, e5]] *
185     GFSum [GA [q2, e2] * GR [q3, e3] * GR [q5, e5] * GA [q6, e6]] *
186     GFSum [GA [q6, e6] * GR [q1, e1] * GA [q2, e2]]]
187
188 Print ["Generic 6-point Hikami box:"]
189 FullSimplify[
190   H6UnDr [q1, q2, q3, q4, q5, q6, e1, e2, e3, e4, e5, e6] +
191   H6Dr24 [q1, q2, q3, q4, q5, q6, e1, e2, e3, e4, e5, e6] +
192   H6Dr26 [q1, q2, q3, q4, q5, q6, e1, e2, e3, e4, e5, e6] +
193   H6Dr46 [q1, q2, q3, q4, q5, q6, e1, e2, e3, e4, e5, e6] +
194   H6Dr13 [q1, q2, q3, q4, q5, q6, e1, e2, e3, e4, e5, e6] +
195   H6Dr15 [q1, q2, q3, q4, q5, q6, e1, e2, e3, e4, e5, e6] +
196   H6Dr35 [q1, q2, q3, q4, q5, q6, e1, e2, e3, e4, e5, e6] +
197   H6Dr1315 [q1, q2, q3, q4, q5, q6, e1, e2, e3, e4, e5, e6] +
198   H6Dr3135 [q1, q2, q3, q4, q5, q6, e1, e2, e3, e4, e5, e6] +
199   H6Dr5153 [q1, q2, q3, q4, q5, q6, e1, e2, e3, e4, e5, e6] +
200   H6Dr2426 [q1, q2, q3, q4, q5, q6, e1, e2, e3, e4, e5, e6] +
201   H6Dr6264 [q1, q2, q3, q4, q5, q6, e1, e2, e3, e4, e5, e6] +
202   H6Dr4246 [q1, q2, q3, q4, q5, q6, e1, e2, e3, e4, e5, e6] +
203   H6Dr1346 [q1, q2, q3, q4, q5, q6, e1, e2, e3, e4, e5, e6] +
204   H6Dr1524 [q1, q2, q3, q4, q5, q6, e1, e2, e3, e4, e5, e6] +
205   H6Dr2635 [q1, q2, q3, q4, q5, q6, e1, e2, e3, e4, e5, e6]
206 ]
207
208 (* === === === === === Calculation of 2-loop diagram Hikami boxes === === === === *)
209
210 Print ["=== Results for diagram (b) ==="]
211
212 Print ["(b1) = "]
213 FullSimplify[
214   LowT [H6UnDr [q, q-Q1, q-Q1+Q2, -Q1+Q2, Q2, 0, w, 0, w, 0, w, 0] * DL [Q1, w]^2 * DL [Q2, w]^2] +
215   LowT [H6Dr15 [q, q-Q1, q-Q1+Q2, -Q1+Q2, Q2, 0, w, 0, w, 0, w, 0] * DL [Q1, w]^2 * DL [Q2, w]^1] +
216   LowT [H6Dr35 [q, q-Q1, q-Q1+Q2, -Q1+Q2, Q2, 0, w, 0, w, 0, w, 0] * DL [Q1, w]^1 * DL [Q2, w]^2] +
217   LowT [H6Dr26 [q, q-Q1, q-Q1+Q2, -Q1+Q2, Q2, 0, w, 0, w, 0, w, 0] * DL [Q1, w]^1 * DL [Q2, w]^2] +
218   LowT [H6Dr24 [q, q-Q1, q-Q1+Q2, -Q1+Q2, Q2, 0, w, 0, w, 0, w, 0] * DL [Q1, w]^2 * DL [Q2, w]^1] +
219   LowT [H6Dr5153 [q, q-Q1, q-Q1+Q2, -Q1+Q2, Q2, 0, w, 0, w, 0, w, 0] * DL [Q1, w]^1 * DL [Q2, w]^1] +
220   LowT [H6Dr2426 [q, q-Q1, q-Q1+Q2, -Q1+Q2, Q2, 0, w, 0, w, 0, w, 0] * DL [Q1, w]^1 * DL [Q2, w]^1] +
221   LowT [H6Dr1524 [q, q-Q1, q-Q1+Q2, -Q1+Q2, Q2, 0, w, 0, w, 0, w, 0] * DL [Q1, w]^2 * DL [Q2, w]^0] +
222   LowT [H6Dr2635 [q, q-Q1, q-Q1+Q2, -Q1+Q2, Q2, 0, w, 0, w, 0, w, 0] * DL [Q1, w]^0 * DL [Q2, w]^2]
223 ]
224
225 Print ["(b2) = "]
226 FullSimplify[
227   LowT [H6Dr13 [q, q-Q1, q-Q1+Q2, -Q1+Q2, Q2, 0, w, 0, w, 0, w, 0] * DL [Q1, w]^2 * DL [Q2, w]^2] +
228   LowT [H6Dr1315 [q, q-Q1, q-Q1+Q2, -Q1+Q2, Q2, 0, w, 0, w, 0, w, 0] * DL [Q1, w]^2 * DL [Q2, w]^1] +
229   LowT [H6Dr3135 [q, q-Q1, q-Q1+Q2, -Q1+Q2, Q2, 0, w, 0, w, 0, w, 0] * DL [Q1, w]^1 * DL [Q2, w]^2] +
230   LowT [H6Dr46 [q, q-Q1, q-Q1+Q2, -Q1+Q2, Q2, 0, w, 0, w, 0, w, 0] * DL [Q1, w]^2 * DL [Q2, w]^2] +
231   LowT [H6Dr6264 [q, q-Q1, q-Q1+Q2, -Q1+Q2, Q2, 0, w, 0, w, 0, w, 0] * DL [Q1, w]^1 * DL [Q2, w]^2] +
232   LowT [H6Dr4246 [q, q-Q1, q-Q1+Q2, -Q1+Q2, Q2, 0, w, 0, w, 0, w, 0] * DL [Q1, w]^2 * DL [Q2, w]^1] +
233   LowT [Imp * H4UnDr [q, Q2-Q1, Q2, 0, w, 0, w, 0] *
234     H4UnDr [q, q-Q1, q-Q1+Q2, Q2-Q1, w, 0, w, 0] * DL [Q1, w]^2 * DL [Q2, w]^2] +
235   LowT [Imp * H4Dr13 [q, Q2-Q1, Q2, 0, w, 0, w, 0] *
236     H4UnDr [q, q-Q1, q-Q1+Q2, Q2-Q1, w, 0, w, 0] * DL [Q1, w]^2 * DL [Q2, w]^1] +
237   LowT [Imp * H4UnDr [q, Q2-Q1, Q2, 0, w, 0, w, 0] *
238     H4Dr24 [q, q-Q1, q-Q1+Q2, Q2-Q1, w, 0, w, 0] * DL [Q1, w]^2 * DL [Q2, w]^1] +
239   LowT [Imp * H4Dr13 [q, Q2-Q1, Q2, 0, w, 0, w, 0] *
240     H4Dr24 [q, q-Q1, q-Q1+Q2, Q2-Q1, w, 0, w, 0] * DL [Q1, w]^2 * DL [Q2, w]^0] +
241   LowT [Imp * H4UnDr [q, q-Q1, q-Q1+Q2, 0, w, 0, w, 0] *
242     H4UnDr [q-Q1+Q2, Q2-Q1, Q2, 0, w, 0, w, 0] * DL [Q1, w]^2 * DL [Q2, w]^2] +
243   LowT [Imp * H4Dr24 [q, q-Q1, q-Q1+Q2, 0, w, 0, w, 0] *
244     H4UnDr [q-Q1+Q2, Q2-Q1, Q2, 0, w, 0, w, 0] * DL [Q1, w]^1 * DL [Q2, w]^2] +
245   LowT [Imp * H4UnDr [q, q-Q1, q-Q1+Q2, 0, w, 0, w, 0] *
246     H4Dr13 [q-Q1+Q2, Q2-Q1, Q2, 0, w, 0, w, 0] * DL [Q1, w]^1 * DL [Q2, w]^2] +

```

```

247   LowT [ Imp*H4Dr24 [q, q-Q1, q-Q1+Q2, 0, w, 0, w, 0] *
248       H4Dr13 [q-Q1+Q2, Q2-Q1, Q2, 0, w, 0, w, 0] *DL [Q1, w]^0*DL [Q2, w]^2]
249 ]
250
251 Print ["(b3) = "]
252 FullSimplify [
253   LowT [H6Dr1346 [q, q-Q1, q-Q1+Q2, -Q1+Q2, Q2, 0, w, 0, w, 0, w, 0] *DL [Q1, w]^2*DL [Q2, w]^2] +
254   LowT [ Imp*H4Dr24 [q, Q2-Q1, Q2, 0, w, 0, w, 0] *
255       H4UnDr [q, q-Q1, q-Q1+Q2, Q2-Q1, w, 0, w, 0] *DL [Q1, w]^2*DL [Q2, w]^2] +
256   LowT [ Imp*H4Dr24 [q, Q2-Q1, Q2, 0, w, 0, w, 0] *
257       H4Dr24 [q, q-Q1, q-Q1+Q2, Q2-Q1, w, 0, w, 0] *DL [Q1, w]^2*DL [Q2, w]^1] +
258   LowT [ Imp*H4UnDr [q, Q2-Q1, Q2, 0, w, 0, w, 0] *
259       H4Dr13 [q, q-Q1, q-Q1+Q2, Q2-Q1, w, 0, w, 0] *DL [Q1, w]^2*DL [Q2, w]^2] +
260   LowT [ Imp*H4Dr13 [q, Q2-Q1, Q2, 0, w, 0, w, 0] *
261       H4Dr13 [q, q-Q1, q-Q1+Q2, Q2-Q1, w, 0, w, 0] *DL [Q1, w]^2*DL [Q2, w]^1] +
262   LowT [ Imp*H4UnDr [q, Q2-Q1, Q2, 0, w, 0, w, 0] *
263       H4UnDr [q, q-Q1, q-Q1+Q2, Q2-Q1, w, 0, w, 0] *DL [Q1, w]^2*DL [Q2, w]^2*DL [q-Q2+Q1, w]] +
264   LowT [ Imp*H4Dr13 [q, Q2-Q1, Q2, 0, w, 0, w, 0] *
265       H4UnDr [q, q-Q1, q-Q1+Q2, Q2-Q1, w, 0, w, 0] *DL [Q1, w]^2*DL [Q2, w]^1*DL [q-Q2+Q1, w]] +
266   LowT [ Imp*H4UnDr [q, Q2-Q1, Q2, 0, w, 0, w, 0] *
267       H4Dr24 [q, q-Q1, q-Q1+Q2, Q2-Q1, w, 0, w, 0] *DL [Q1, w]^2*DL [Q2, w]^1*DL [q-Q2+Q1, w]] +
268   LowT [ Imp*H4Dr13 [q, Q2-Q1, Q2, 0, w, 0, w, 0] *
269       H4Dr24 [q, q-Q1, q-Q1+Q2, Q2-Q1, w, 0, w, 0] *DL [Q1, w]^2*DL [Q2, w]^0*DL [q-Q2+Q1, w]] +
270   LowT [ Imp*H4Dr13 [q, q-Q1, q-Q1+Q2, 0, w, 0, w, 0] *
271       H4UnDr [q-Q1+Q2, Q2-Q1, Q2, 0, w, 0, w, 0] *DL [Q1, w]^2*DL [Q2, w]^2] +
272   LowT [ Imp*H4Dr13 [q, q-Q1, q-Q1+Q2, 0, w, 0, w, 0] *
273       H4Dr13 [q-Q1+Q2, Q2-Q1, Q2, 0, w, 0, w, 0] *DL [Q1, w]^1*DL [Q2, w]^2] +
274   LowT [ Imp*H4UnDr [q, q-Q1, q-Q1+Q2, 0, w, 0, w, 0] *
275       H4Dr24 [q-Q1+Q2, Q2-Q1, Q2, 0, w, 0, w, 0] *DL [Q1, w]^2*DL [Q2, w]^2] +
276   LowT [ Imp*H4Dr24 [q, q-Q1, q-Q1+Q2, 0, w, 0, w, 0] *
277       H4Dr24 [q-Q1+Q2, Q2-Q1, Q2, 0, w, 0, w, 0] *DL [Q1, w]^1*DL [Q2, w]^2] +
278   LowT [ Imp*H4UnDr [q, q-Q1, q-Q1+Q2, 0, w, 0, w, 0] *
279       H4UnDr [q-Q1+Q2, Q2-Q1, Q2, 0, w, 0, w, 0] *DL [Q1, w]^2*DL [Q2, w]^2*DL [q-Q1+Q2, w]] +
280   LowT [ Imp*H4UnDr [q, q-Q1, q-Q1+Q2, 0, w, 0, w, 0] *
281       H4Dr13 [q-Q1+Q2, Q2-Q1, Q2, 0, w, 0, w, 0] *DL [Q1, w]^1*DL [Q2, w]^2*DL [q-Q1+Q2, w]] +
282   LowT [ Imp*H4Dr24 [q, q-Q1, q-Q1+Q2, 0, w, 0, w, 0] *
283       H4UnDr [q-Q1+Q2, Q2-Q1, Q2, 0, w, 0, w, 0] *DL [Q1, w]^1*DL [Q2, w]^2*DL [q-Q1+Q2, w]] +
284   LowT [ Imp*H4Dr24 [q, q-Q1, q-Q1+Q2, 0, w, 0, w, 0] *
285       H4Dr13 [q-Q1+Q2, Q2-Q1, Q2, 0, w, 0, w, 0] *DL [Q1, w]^0*DL [Q2, w]^2*DL [q-Q1+Q2, w]]
286 ]
287
288 Print ["=== Results for diagram (c) ==="]
289
290 Print ["(c1) = "]
291 FullSimplify [
292   LowT [H6UnDr [q, q-Q1, q-Q1+Q2, -Q1+Q2, -Q1, 0, w, 0, w, 0, w, 0] *DL [Q1, w]^2*DL [Q2, w]^2] +
293   LowT [H6Dr15 [q, q-Q1, q-Q1+Q2, -Q1+Q2, -Q1, 0, w, 0, w, 0, w, 0] *DL [Q1, w]^1*DL [Q2, w]^2] +
294   LowT [H6Dr35 [q, q-Q1, q-Q1+Q2, -Q1+Q2, -Q1, 0, w, 0, w, 0, w, 0] *DL [Q1, w]^2*DL [Q2, w]^1] +
295   LowT [H6Dr26 [q, q-Q1, q-Q1+Q2, -Q1+Q2, -Q1, 0, w, 0, w, 0, w, 0] *DL [Q1, w]^1*DL [Q2, w]^2] +
296   LowT [H6Dr24 [q, q-Q1, q-Q1+Q2, -Q1+Q2, -Q1, 0, w, 0, w, 0, w, 0] *DL [Q1, w]^2*DL [Q2, w]^1] +
297   LowT [H6Dr5153 [q, q-Q1, q-Q1+Q2, -Q1+Q2, -Q1, 0, w, 0, w, 0, w, 0] *DL [Q1, w]^1*DL [Q2, w]^1] +
298   LowT [H6Dr2426 [q, q-Q1, q-Q1+Q2, -Q1+Q2, -Q1, 0, w, 0, w, 0, w, 0] *DL [Q1, w]^1*DL [Q2, w]^1] +
299   LowT [H6Dr1524 [q, q-Q1, q-Q1+Q2, -Q1+Q2, -Q1, 0, w, 0, w, 0, w, 0] *DL [Q1, w]^1*DL [Q2, w]^1] +
300   LowT [H6Dr2635 [q, q-Q1, q-Q1+Q2, -Q1+Q2, -Q1, 0, w, 0, w, 0, w, 0] *DL [Q1, w]^1*DL [Q2, w]^1]
301 ]
302
303 Print ["(c2) = "]
304 FullSimplify [
305   LowT [H6Dr13 [q, q-Q1, q-Q1+Q2, -Q1+Q2, -Q1, 0, w, 0, w, 0, w, 0] *DL [Q1, w]^2*DL [Q2, w]^2] +
306   LowT [H6Dr1315 [q, q-Q1, q-Q1+Q2, -Q1+Q2, -Q1, 0, w, 0, w, 0, w, 0] *DL [Q1, w]^1*DL [Q2, w]^2] +
307   LowT [H6Dr3135 [q, q-Q1, q-Q1+Q2, -Q1+Q2, -Q1, 0, w, 0, w, 0, w, 0] *DL [Q1, w]^2*DL [Q2, w]^1] +
308   LowT [H6Dr46 [q, q-Q1, q-Q1+Q2, -Q1+Q2, -Q1, 0, w, 0, w, 0, w, 0] *DL [Q1, w]^2*DL [Q2, w]^2] +
309   LowT [H6Dr6264 [q, q-Q1, q-Q1+Q2, -Q1+Q2, -Q1, 0, w, 0, w, 0, w, 0] *DL [Q1, w]^1*DL [Q2, w]^2] +
310   LowT [H6Dr4246 [q, q-Q1, q-Q1+Q2, -Q1+Q2, -Q1, 0, w, 0, w, 0, w, 0] *DL [Q1, w]^2*DL [Q2, w]^1] +
311   LowT [ Imp*H4UnDr [q, Q2-Q1, -Q1, 0, w, 0, w, 0] *
312       H4UnDr [q, q-Q1, q-Q1+Q2, Q2-Q1, w, 0, w, 0] *DL [Q1, w]^2*DL [Q2, w]^2] +
313   LowT [ Imp*H4Dr13 [q, Q2-Q1, -Q1, 0, w, 0, w, 0] *
314       H4UnDr [q, q-Q1, q-Q1+Q2, Q2-Q1, w, 0, w, 0] *DL [Q1, w]^1*DL [Q2, w]^2] +

```

```

315 LowT [Imp*H4UnDr [q, Q2-Q1, -Q1, 0, w, 0, w, 0] *
316     H4Dr24 [q, q-Q1, q-Q1+Q2, Q2-Q1, w, 0, w, 0] *DL [Q1, w]^2*DL [Q2, w]^1]+
317 LowT [Imp*H4Dr13 [q, Q2-Q1, -Q1, 0, w, 0, w, 0] *
318     H4Dr24 [q, q-Q1, q-Q1+Q2, Q2-Q1, w, 0, w, 0] *DL [Q1, w]^1*DL [Q2, w]^1]+
319 LowT [Imp*H4UnDr [q, q-Q1, q-Q1+Q2, 0, w, 0, w, 0] *
320     H4UnDr [q-Q1+Q2, Q2-Q1, -Q1, 0, w, 0, w, 0] *DL [Q1, w]^2*DL [Q2, w]^2]+
321 LowT [Imp*H4Dr24 [q, q-Q1, q-Q1+Q2, 0, w, 0, w, 0] *
322     H4UnDr [q-Q1+Q2, Q2-Q1, -Q1, 0, w, 0, w, 0] *DL [Q1, w]^1*DL [Q2, w]^2]+
323 LowT [Imp*H4UnDr [q, q-Q1, q-Q1+Q2, 0, w, 0, w, 0] *
324     H4Dr13 [q-Q1+Q2, Q2-Q1, -Q1, 0, w, 0, w, 0] *DL [Q1, w]^2*DL [Q2, w]^1]+
325 LowT [Imp*H4Dr24 [q, q-Q1, q-Q1+Q2, 0, w, 0, w, 0] *
326     H4Dr13 [q-Q1+Q2, Q2-Q1, -Q1, 0, w, 0, w, 0] *DL [Q1, w]^1*DL [Q2, w]^1]
327 ]
328
329 Print ["(c3) = "]
330 FullSimplify[
331     LowT [H6Dr1346 [q, q-Q1, q-Q1+Q2, -Q1+Q2, -Q1, 0, w, 0, w, 0, w, 0] *DL [Q1, w]^2*DL [Q2, w]^2]+
332     LowT [Imp*H4Dr24 [q, Q2-Q1, -Q1, 0, w, 0, w, 0] *
333         H4UnDr [q, q-Q1, q-Q1+Q2, Q2-Q1, w, 0, w, 0] *DL [Q1, w]^2*DL [Q2, w]^2]+
334     LowT [Imp*H4Dr24 [q, Q2-Q1, -Q1, 0, w, 0, w, 0] *
335         H4Dr24 [q, q-Q1, q-Q1+Q2, Q2-Q1, w, 0, w, 0] *DL [Q1, w]^2*DL [Q2, w]^1]+
336     LowT [Imp*H4UnDr [q, Q2-Q1, -Q1, 0, w, 0, w, 0] *
337         H4Dr13 [q, q-Q1, q-Q1+Q2, Q2-Q1, w, 0, w, 0] *DL [Q1, w]^2*DL [Q2, w]^2]+
338     LowT [Imp*H4Dr13 [q, Q2-Q1, -Q1, 0, w, 0, w, 0] *
339         H4Dr13 [q, q-Q1, q-Q1+Q2, Q2-Q1, w, 0, w, 0] *DL [Q1, w]^1*DL [Q2, w]^2]+
340     LowT [Imp*H4UnDr [q, Q2-Q1, -Q1, 0, w, 0, w, 0] *
341         H4UnDr [q, q-Q1, q-Q1+Q2, Q2-Q1, w, 0, w, 0] *DL [Q1, w]^2*DL [Q2, w]^2*DL [q-Q2+Q1, w]]+
342     LowT [Imp*H4Dr13 [q, Q2-Q1, -Q1, 0, w, 0, w, 0] *
343         H4UnDr [q, q-Q1, q-Q1+Q2, Q2-Q1, w, 0, w, 0] *DL [Q1, w]^1*DL [Q2, w]^2*DL [q-Q2+Q1, w]]+
344     LowT [Imp*H4UnDr [q, Q2-Q1, -Q1, 0, w, 0, w, 0] *
345         H4Dr24 [q, q-Q1, q-Q1+Q2, Q2-Q1, w, 0, w, 0] *DL [Q1, w]^2*DL [Q2, w]^1*DL [q-Q2+Q1, w]]+
346     LowT [Imp*H4Dr13 [q, Q2-Q1, -Q1, 0, w, 0, w, 0] *
347         H4Dr24 [q, q-Q1, q-Q1+Q2, Q2-Q1, w, 0, w, 0] *DL [Q1, w]^1*DL [Q2, w]^1*DL [q-Q2+Q1, w]]+
348     LowT [Imp*H4Dr13 [q, q-Q1, q-Q1+Q2, 0, w, 0, w, 0] *
349         H4UnDr [q-Q1+Q2, Q2-Q1, -Q1, 0, w, 0, w, 0] *DL [Q1, w]^2*DL [Q2, w]^2]+
350     LowT [Imp*H4Dr13 [q, q-Q1, q-Q1+Q2, 0, w, 0, w, 0] *
351         H4Dr13 [q-Q1+Q2, Q2-Q1, -Q1, 0, w, 0, w, 0] *DL [Q1, w]^2*DL [Q2, w]^1]+
352     LowT [Imp*H4UnDr [q, q-Q1, q-Q1+Q2, 0, w, 0, w, 0] *
353         H4Dr24 [q-Q1+Q2, Q2-Q1, -Q1, 0, w, 0, w, 0] *DL [Q1, w]^2*DL [Q2, w]^2]+
354     LowT [Imp*H4Dr24 [q, q-Q1, q-Q1+Q2, 0, w, 0, w, 0] *
355         H4Dr24 [q-Q1+Q2, Q2-Q1, -Q1, 0, w, 0, w, 0] *DL [Q1, w]^1*DL [Q2, w]^2]+
356     LowT [Imp*H4UnDr [q, q-Q1, q-Q1+Q2, 0, w, 0, w, 0] *
357         H4UnDr [q-Q1+Q2, Q2-Q1, -Q1, 0, w, 0, w, 0] *DL [Q1, w]^2*DL [Q2, w]^2*DL [q-Q1+Q2, w]]+
358     LowT [Imp*H4UnDr [q, q-Q1, q-Q1+Q2, 0, w, 0, w, 0] *
359         H4Dr13 [q-Q1+Q2, Q2-Q1, -Q1, 0, w, 0, w, 0] *DL [Q1, w]^2*DL [Q2, w]^1*DL [q-Q1+Q2, w]]+
360     LowT [Imp*H4Dr24 [q, q-Q1, q-Q1+Q2, 0, w, 0, w, 0] *
361         H4UnDr [q-Q1+Q2, Q2-Q1, -Q1, 0, w, 0, w, 0] *DL [Q1, w]^1*DL [Q2, w]^2*DL [q-Q1+Q2, w]]+
362     LowT [Imp*H4Dr24 [q, q-Q1, q-Q1+Q2, 0, w, 0, w, 0] *
363         H4Dr13 [q-Q1+Q2, Q2-Q1, -Q1, 0, w, 0, w, 0] *DL [Q1, w]^1*DL [Q2, w]^1*DL [q-Q1+Q2, w]]
364 ]
365
366 Print ["=== Results for diagrams (d) ==="]
367
368 Print ["(d1) = "]
369 FullSimplify[
370     LowT [H6UnDr [q, q-Q1, -Q1, Q2-Q1, Q2, 0, w, 0, w, 0, w, 0] *DL [Q1, w]^2*DL [Q2, w]^2]+
371     LowT [H6Dr13 [q, q-Q1, -Q1, Q2-Q1, Q2, 0, w, 0, w, 0, w, 0] *DL [Q1, w]^1*DL [Q2, w]^2]+
372     LowT [H6Dr15 [q, q-Q1, -Q1, Q2-Q1, Q2, 0, w, 0, w, 0, w, 0] *DL [Q1, w]^2*DL [Q2, w]^1]+
373     LowT [H6Dr24 [q, q-Q1, -Q1, Q2-Q1, Q2, 0, w, 0, w, 0, w, 0] *DL [Q1, w]^2*DL [Q2, w]^1]+
374     LowT [H6Dr26 [q, q-Q1, -Q1, Q2-Q1, Q2, 0, w, 0, w, 0, w, 0] *DL [Q1, w]^1*DL [Q2, w]^2]+
375     LowT [H6Dr1315 [q, q-Q1, -Q1, Q2-Q1, Q2, 0, w, 0, w, 0, w, 0] *DL [Q1, w]^1*DL [Q2, w]^1]+
376     LowT [H6Dr2426 [q, q-Q1, -Q1, Q2-Q1, Q2, 0, w, 0, w, 0, w, 0] *DL [Q1, w]^1*DL [Q2, w]^1]+
377     LowT [H6Dr1524 [q, q-Q1, -Q1, Q2-Q1, Q2, 0, w, 0, w, 0, w, 0] *DL [Q1, w]^2*DL [Q2, w]^0]+
378     LowT [H6UnDr [q, q-Q2, q-Q1-Q2, q-Q1, -Q1, 0, w, 0, w, 0, w, 0] *DL [Q1, w]^2*DL [Q2, w]^2]+
379     LowT [H6Dr15 [q, q-Q2, q-Q1-Q2, q-Q1, -Q1, 0, w, 0, w, 0, w, 0] *DL [Q1, w]^1*DL [Q2, w]^2]+
380     LowT [H6Dr46 [q, q-Q2, q-Q1-Q2, q-Q1, -Q1, 0, w, 0, w, 0, w, 0] *DL [Q1, w]^1*DL [Q2, w]^2]+
381     LowT [H6Dr35 [q, q-Q2, q-Q1-Q2, q-Q1, -Q1, 0, w, 0, w, 0, w, 0] *DL [Q1, w]^2*DL [Q2, w]^1]+
382     LowT [H6Dr26 [q, q-Q2, q-Q1-Q2, q-Q1, -Q1, 0, w, 0, w, 0, w, 0] *DL [Q1, w]^2*DL [Q2, w]^1]+

```

```

383 LowT[H6Dr5153[q,q-Q2,q-Q1-Q2,q-Q1,-Q1,0,w,0,w,0,w,0]*DL[Q1,w]^1*DL[Q2,w]^1]+
384 LowT[H6Dr6264[q,q-Q2,q-Q1-Q2,q-Q1,-Q1,0,w,0,w,0,w,0]*DL[Q1,w]^1*DL[Q2,w]^1]+
385 LowT[H6Dr2635[q,q-Q2,q-Q1-Q2,q-Q1,-Q1,0,w,0,w,0,w,0]*DL[Q1,w]^2*DL[Q2,w]^0]+
386 LowT[Imp*H4UnDr[q,q-Q1,-Q1,0,w,0,w,0,w,0]*
387     H4UnDr[-Q1,0,Q2,Q2-Q1,w,0,w,0]*DL[Q1,w]^1*DL[Q2,w]^2]
388 ]
389
390 Print["(d2) = "]
391 FullSimplify[
392 LowT[H6Dr35[q,q-Q1,-Q1,Q2-Q1,Q2,0,w,0,w,0,w,0]*DL[Q1,w]^2*DL[Q2,w]^2]+
393 LowT[H6Dr5153[q,q-Q1,-Q1,Q2-Q1,Q2,0,w,0,w,0,w,0]*DL[Q1,w]^2*DL[Q2,w]^1]+
394 LowT[H6Dr2635[q,q-Q1,-Q1,Q2-Q1,Q2,0,w,0,w,0,w,0]*DL[Q1,w]^1*DL[Q2,w]^2]+
395 LowT[H6Dr3135[q,q-Q1,-Q1,Q2-Q1,Q2,0,w,0,w,0,w,0]*DL[Q1,w]^1*DL[Q2,w]^2]+
396 LowT[Imp*H4UnDr[q,q-Q1,Q2,0,w,0,w,0]*
397     H4UnDr[-Q1,Q2-Q1,Q2,q-Q1,w,0,w,0]*DL[Q1,w]^2*DL[Q2,w]^2]+
398 LowT[Imp*H4Dr13[q,q-Q1,Q2,0,w,0,w,0]*
399     H4UnDr[-Q1,Q2-Q1,Q2,q-Q1,w,0,w,0]*DL[Q1,w]^2*DL[Q2,w]^1]+
400 LowT[Imp*H4Dr24[q,q-Q1,Q2,0,w,0,w,0]*
401     H4UnDr[-Q1,Q2-Q1,Q2,q-Q1,w,0,w,0]*DL[Q1,w]^1*DL[Q2,w]^2]+
402 LowT[Imp*H4UnDr[q,q-Q1,Q2,0,w,0,w,0]*
403     H4Dr24[-Q1,Q2-Q1,Q2,q-Q1,w,0,w,0]*DL[Q1,w]^2*DL[Q2,w]^1]+
404 LowT[Imp*H4Dr13[q,q-Q1,Q2,0,w,0,w,0]*
405     H4Dr24[-Q1,Q2-Q1,Q2,q-Q1,w,0,w,0]*DL[Q1,w]^2*DL[Q2,w]^0]+
406 LowT[Imp*H4Dr24[q,q-Q1,Q2,0,w,0,w,0]*
407     H4Dr24[-Q1,Q2-Q1,Q2,q-Q1,w,0,w,0]*DL[Q1,w]^1*DL[Q2,w]^1]+
408 LowT[H6Dr13[q,q-Q2,q-Q1-Q2,q-Q1,-Q1,0,w,0,w,0,w,0]*DL[Q1,w]^2*DL[Q2,w]^2]+
409 LowT[H6Dr1315[q,q-Q2,q-Q1-Q2,q-Q1,-Q1,0,w,0,w,0,w,0]*DL[Q1,w]^1*DL[Q2,w]^2]+
410 LowT[H6Dr1346[q,q-Q2,q-Q1-Q2,q-Q1,-Q1,0,w,0,w,0,w,0]*DL[Q1,w]^1*DL[Q2,w]^2]+
411 LowT[H6Dr3135[q,q-Q2,q-Q1-Q2,q-Q1,-Q1,0,w,0,w,0,w,0]*DL[Q1,w]^2*DL[Q2,w]^1]+
412 LowT[Imp*H4UnDr[q,q-Q2,q-Q1-Q2,0,w,0,w,0]*
413     H4UnDr[q-Q1-Q2,q-Q1,-Q1,0,w,0,w,0]*DL[Q1,w]^2*DL[Q2,w]^2]+
414 LowT[Imp*H4UnDr[q,q-Q2,q-Q1-Q2,0,w,0,w,0]*
415     H4Dr13[q-Q1-Q2,q-Q1,-Q1,0,w,0,w,0]*DL[Q1,w]^2*DL[Q2,w]^1]+
416 LowT[Imp*H4UnDr[q,q-Q2,q-Q1-Q2,0,w,0,w,0]*
417     H4Dr24[q-Q1-Q2,q-Q1,-Q1,0,w,0,w,0]*DL[Q1,w]^1*DL[Q2,w]^2]+
418 LowT[Imp*H4Dr24[q,q-Q2,q-Q1-Q2,0,w,0,w,0]*
419     H4UnDr[q-Q1-Q2,q-Q1,-Q1,0,w,0,w,0]*DL[Q1,w]^2*DL[Q2,w]^1]+
420 LowT[Imp*H4Dr24[q,q-Q2,q-Q1-Q2,0,w,0,w,0]*
421     H4Dr13[q-Q1-Q2,q-Q1,-Q1,0,w,0,w,0]*DL[Q1,w]^2*DL[Q2,w]^0]+
422 LowT[Imp*H4Dr24[q,q-Q2,q-Q1-Q2,0,w,0,w,0]*
423     H4Dr24[q-Q1-Q2,q-Q1,-Q1,0,w,0,w,0]*DL[Q1,w]^1*DL[Q2,w]^1]+
424 LowT[Imp*H4UnDr[q,q-Q1,-Q1,0,w,0,w,0]*
425     H4Dr13[-Q1,Q2-Q1,Q2,0,w,0,w,0]*DL[Q1,w]^1*DL[Q2,w]^2]
426 ]
427
428 Print["(d3) = "]
429 FullSimplify[
430 LowT[H6Dr46[q,q-Q1,-Q1,Q2-Q1,Q2,0,w,0,w,0,w,0]*DL[Q1,w]^2*DL[Q2,w]^2]+
431 LowT[H6Dr1346[q,q-Q1,-Q1,Q2-Q1,Q2,0,w,0,w,0,w,0]*DL[Q1,w]^1*DL[Q2,w]^2]+
432 LowT[H6Dr4246[q,q-Q1,-Q1,Q2-Q1,Q2,0,w,0,w,0,w,0]*DL[Q1,w]^2*DL[Q2,w]^1]+
433 LowT[H6Dr6264[q,q-Q1,-Q1,Q2-Q1,Q2,0,w,0,w,0,w,0]*DL[Q1,w]^1*DL[Q2,w]^2]+
434 LowT[Imp*H4UnDr[q,Q2-Q1,Q2,0,w,0,w,0]*
435     H4UnDr[q,q-Q1,-Q1,Q2-Q1,w,0,w,0]*DL[Q1,w]^2*DL[Q2,w]^2]+
436 LowT[Imp*H4UnDr[q,Q2-Q1,Q2,0,w,0,w,0]*
437     H4Dr13[q,q-Q1,-Q1,Q2-Q1,w,0,w,0]*DL[Q1,w]^1*DL[Q2,w]^2]+
438 LowT[Imp*H4UnDr[q,Q2-Q1,Q2,0,w,0,w,0]*
439     H4Dr24[q,q-Q1,-Q1,Q2-Q1,w,0,w,0]*DL[Q1,w]^2*DL[Q2,w]^1]+
440 LowT[Imp*H4Dr13[q,Q2-Q1,Q2,0,w,0,w,0]*
441     H4UnDr[q,q-Q1,-Q1,Q2-Q1,w,0,w,0]*DL[Q1,w]^2*DL[Q2,w]^1]+
442 LowT[Imp*H4Dr13[q,Q2-Q1,Q2,0,w,0,w,0]*
443     H4Dr13[q,q-Q1,-Q1,Q2-Q1,w,0,w,0]*DL[Q1,w]^1*DL[Q2,w]^1]+
444 LowT[Imp*H4Dr13[q,Q2-Q1,Q2,0,w,0,w,0]*
445     H4Dr24[q,q-Q1,-Q1,Q2-Q1,w,0,w,0]*DL[Q1,w]^2*DL[Q2,w]^0]+
446 LowT[H6Dr24[q,q-Q2,q-Q1-Q2,q-Q1,-Q1,0,w,0,w,0,w,0]*DL[Q1,w]^2*DL[Q2,w]^2]+
447 LowT[H6Dr1524[q,q-Q2,q-Q1-Q2,q-Q1,-Q1,0,w,0,w,0,w,0]*DL[Q1,w]^1*DL[Q2,w]^2]+
448 LowT[H6Dr2426[q,q-Q2,q-Q1-Q2,q-Q1,-Q1,0,w,0,w,0,w,0]*DL[Q1,w]^2*DL[Q2,w]^1]+
449 LowT[H6Dr4246[q,q-Q2,q-Q1-Q2,q-Q1,-Q1,0,w,0,w,0,w,0]*DL[Q1,w]^1*DL[Q2,w]^2]+
450 LowT[Imp*H4UnDr[q,q-Q2,-Q1,0,w,0,w,0]*

```

```

451     H4UnDr [q-Q1-Q2, q-Q1, -Q1, q-Q2, w, 0, w, 0] * DL [Q1, w]^2 * DL [Q2, w]^2 +
452 LowT [Imp*H4Dr13 [q, q-Q2, -Q1, 0, w, 0, w, 0] *
453     H4UnDr [q-Q1-Q2, q-Q1, -Q1, q-Q2, w, 0, w, 0] * DL [Q1, w]^1 * DL [Q2, w]^2 +
454 LowT [Imp*H4Dr24 [q, q-Q2, -Q1, 0, w, 0, w, 0] *
455     H4UnDr [q-Q1-Q2, q-Q1, -Q1, q-Q2, w, 0, w, 0] * DL [Q1, w]^2 * DL [Q2, w]^1 +
456 LowT [Imp*H4UnDr [q, q-Q2, -Q1, 0, w, 0, w, 0] *
457     H4Dr13 [q-Q1-Q2, q-Q1, -Q1, q-Q2, w, 0, w, 0] * DL [Q1, w]^2 * DL [Q2, w]^1 +
458 LowT [Imp*H4Dr13 [q, q-Q2, -Q1, 0, w, 0, w, 0] *
459     H4Dr13 [q-Q1-Q2, q-Q1, -Q1, q-Q2, w, 0, w, 0] * DL [Q1, w]^1 * DL [Q2, w]^1 +
460 LowT [Imp*H4Dr24 [q, q-Q2, -Q1, 0, w, 0, w, 0] *
461     H4Dr13 [q-Q1-Q2, q-Q1, -Q1, q-Q2, w, 0, w, 0] * DL [Q1, w]^2 * DL [Q2, w]^0 +
462 LowT [Imp*H4UnDr [q, q-Q1, -Q1, 0, w, 0, w, 0] *
463     H4Dr24 [-Q1, Q2-Q1, Q2, 0, w, 0, w, 0] * DL [Q1, w]^1 * DL [Q2, w]^2]
464 ]
465
466 Print["=== Results for diagrams (e) ==="]
467
468 Print["(e) = "]
469 FullSimplify[
470   NextT [Imp*H4UnDr [q, q-Q1, Q2, 0, w, 0, w, 0] *
471     H4UnDr [Q1, 0, q, q-Q2, w, 0, w, 0] * DL [Q1, w]^2 * DL [Q2, w]^2 +
472   NextT [Imp*H4UnDr [q, q-Q1, Q2, 0, w, 0, w, 0] *
473     H4Dr13 [Q1, 0, q, q-Q2, w, 0, w, 0] * DL [Q1, w]^1 * DL [Q2, w]^2 +
474   NextT [Imp*H4UnDr [q, q-Q1, Q2, 0, w, 0, w, 0] *
475     H4Dr24 [Q1, 0, q, q-Q2, w, 0, w, 0] * DL [Q1, w]^2 * DL [Q2, w]^1 +
476   NextT [Imp*H4Dr13 [q, q-Q1, Q2, 0, w, 0, w, 0] *
477     H4UnDr [Q1, 0, q, q-Q2, w, 0, w, 0] * DL [Q1, w]^2 * DL [Q2, w]^1 +
478   NextT [Imp*H4Dr13 [q, q-Q1, Q2, 0, w, 0, w, 0] *
479     H4Dr13 [Q1, 0, q, q-Q2, w, 0, w, 0] * DL [Q1, w]^1 * DL [Q2, w]^1 +
480   NextT [Imp*H4Dr13 [q, q-Q1, Q2, 0, w, 0, w, 0] *
481     H4Dr24 [Q1, 0, q, q-Q2, w, 0, w, 0] * DL [Q1, w]^2 * DL [Q2, w]^0 +
482   NextT [Imp*H4Dr24 [q, q-Q1, Q2, 0, w, 0, w, 0] *
483     H4UnDr [Q1, 0, q, q-Q2, w, 0, w, 0] * DL [Q1, w]^1 * DL [Q2, w]^2 +
484   NextT [Imp*H4Dr24 [q, q-Q1, Q2, 0, w, 0, w, 0] *
485     H4Dr13 [Q1, 0, q, q-Q2, w, 0, w, 0] * DL [Q1, w]^0 * DL [Q2, w]^2 +
486   NextT [Imp*H4Dr24 [q, q-Q1, Q2, 0, w, 0, w, 0] *
487     H4Dr24 [Q1, 0, q, q-Q2, w, 0, w, 0] * DL [Q1, w]^1 * DL [Q2, w]^1]
488 ]
489
490 Print["=== Results for diagrams (f) ==="]
491
492 Print["(f1) = "]
493 FullSimplify[
494   NextT [Imp*H4UnDr [q, Q2-Q1, -Q1, 0, w, 0, w, 0] *
495     H4UnDr [q+Q1-Q2, 0, q, q-Q2, w, 0, w, 0] * DL [Q1, w]^1 * DL [Q2, w]^1 * DL [q+Q1-Q2, w]^2 +
496   NextT [Imp*H4Dr13 [q, Q2-Q1, -Q1, 0, w, 0, w, 0] *
497     H4UnDr [q+Q1-Q2, 0, q, q-Q2, w, 0, w, 0] * DL [Q1, w]^0 * DL [Q2, w]^1 * DL [q+Q1-Q2, w]^2 +
498   NextT [Imp*H4Dr24 [q, Q2-Q1, -Q1, 0, w, 0, w, 0] *
499     H4UnDr [q+Q1-Q2, 0, q, q-Q2, w, 0, w, 0] * DL [Q1, w]^1 * DL [Q2, w]^1 * DL [q+Q1-Q2, w]^1 +
500   NextT [Imp*H4UnDr [q, Q2-Q1, -Q1, 0, w, 0, w, 0] *
501     H4Dr13 [q+Q1-Q2, 0, q, q-Q2, w, 0, w, 0] * DL [Q1, w]^1 * DL [Q2, w]^1 * DL [q+Q1-Q2, w]^1 +
502   NextT [Imp*H4Dr13 [q, Q2-Q1, -Q1, 0, w, 0, w, 0] *
503     H4Dr13 [q+Q1-Q2, 0, q, q-Q2, w, 0, w, 0] * DL [Q1, w]^0 * DL [Q2, w]^1 * DL [q+Q1-Q2, w]^1 +
504   NextT [Imp*H4Dr24 [q, Q2-Q1, -Q1, 0, w, 0, w, 0] *
505     H4Dr13 [q+Q1-Q2, 0, q, q-Q2, w, 0, w, 0] * DL [Q1, w]^1 * DL [Q2, w]^1 * DL [q+Q1-Q2, w]^0 +
506   NextT [Imp*H4UnDr [q, Q2-Q1, -Q1, 0, w, 0, w, 0] *
507     H4Dr24 [q+Q1-Q2, 0, q, q-Q2, w, 0, w, 0] * DL [Q1, w]^1 * DL [Q2, w]^0 * DL [q+Q1-Q2, w]^2 +
508   NextT [Imp*H4Dr13 [q, Q2-Q1, -Q1, 0, w, 0, w, 0] *
509     H4Dr24 [q+Q1-Q2, 0, q, q-Q2, w, 0, w, 0] * DL [Q1, w]^0 * DL [Q2, w]^0 * DL [q+Q1-Q2, w]^2 +
510   NextT [Imp*H4Dr24 [q, Q2-Q1, -Q1, 0, w, 0, w, 0] *
511     H4Dr24 [q+Q1-Q2, 0, q, q-Q2, w, 0, w, 0] * DL [Q1, w]^1 * DL [Q2, w]^0 * DL [q+Q1-Q2, w]^1]
512 ]
513
514 Print["(f2) = "]
515 FullSimplify[
516   NextT [Imp*H4UnDr [q, q-Q1, q+Q2-Q1, 0, w, 0, w, 0] *
517     H4UnDr [-Q2, 0, q, Q1-Q2, w, 0, w, 0] * DL [Q1, w]^1 * DL [Q2, w]^1 * DL [q-Q1+Q2, w]^2 +
518   NextT [Imp*H4Dr13 [q, q-Q1, q+Q2-Q1, 0, w, 0, w, 0] *

```

```

519     H4UnDr[-Q2,0,q,Q1-Q2,w,0,w,0]*DL[Q1,w]^1*DL[Q2,w]^1*DL[q-Q1+Q2,w]^1)+
520 NextT[Imp*H4Dr24[q,q-Q1,q+Q2-Q1,0,w,0,w,0]*
521     H4UnDr[-Q2,0,q,Q1-Q2,w,0,w,0]*DL[Q1,w]^0*DL[Q2,w]^1*DL[q-Q1+Q2,w]^2)+
522 NextT[Imp*H4UnDr[q,q-Q1,q+Q2-Q1,0,w,0,w,0]*
523     H4Dr13[-Q2,0,q,Q1-Q2,w,0,w,0]*DL[Q1,w]^1*DL[Q2,w]^0*DL[q-Q1+Q2,w]^2)+
524 NextT[Imp*H4Dr13[q,q-Q1,q+Q2-Q1,0,w,0,w,0]*
525     H4Dr13[-Q2,0,q,Q1-Q2,w,0,w,0]*DL[Q1,w]^1*DL[Q2,w]^0*DL[q-Q1+Q2,w]^1)+
526 NextT[Imp*H4Dr24[q,q-Q1,q+Q2-Q1,0,w,0,w,0]*
527     H4Dr13[-Q2,0,q,Q1-Q2,w,0,w,0]*DL[Q1,w]^0*DL[Q2,w]^0*DL[q-Q1+Q2,w]^2)+
528 NextT[Imp*H4UnDr[q,q-Q1,q+Q2-Q1,0,w,0,w,0]*
529     H4Dr24[-Q2,0,q,Q1-Q2,w,0,w,0]*DL[Q1,w]^1*DL[Q2,w]^1*DL[q-Q1+Q2,w]^1)+
530 NextT[Imp*H4Dr13[q,q-Q1,q+Q2-Q1,0,w,0,w,0]*
531     H4Dr24[-Q2,0,q,Q1-Q2,w,0,w,0]*DL[Q1,w]^1*DL[Q2,w]^1*DL[q-Q1+Q2,w]^0)+
532 NextT[Imp*H4Dr24[q,q-Q1,q+Q2-Q1,0,w,0,w,0]*
533     H4Dr24[-Q2,0,q,Q1-Q2,w,0,w,0]*DL[Q1,w]^0*DL[Q2,w]^1*DL[q-Q1+Q2,w]^1)
534 ]
535
536
537 Print["=== Results for diagrams (g) ==="]
538
539 Print["(g) = "]
540 FullSimplify[
541     NextT[Imp*H4UnDr[q,q-Q1,-Q1,0,w,0,w,0]*
542         H4UnDr[-Q1,0,Q2,Q2-Q1,w,0,w,0]*DL[Q1,w]^1*DL[Q2,w]^1]+
543     NextT[Imp*H4UnDr[q,q-Q1,-Q1,0,w,0,w,0]*
544         H4Dr13[-Q1,0,Q2,Q2-Q1,w,0,w,0]*DL[Q1,w]^1*DL[Q2,w]^0]+
545     NextT[Imp*H4UnDr[q,q-Q1,-Q1,0,w,0,w,0]*
546         H4Dr24[-Q1,0,Q2,Q2-Q1,w,0,w,0]*DL[Q1,w]^1*DL[Q2,w]^0]+
547     NextT[Imp*H4Dr13[q,q-Q1,-Q1,0,w,0,w,0]*
548         H4UnDr[-Q1,0,Q2,Q2-Q1,w,0,w,0]*DL[Q1,w]^0*DL[Q2,w]^1]+
549     NextT[Imp*H4Dr13[q,q-Q1,-Q1,0,w,0,w,0]*
550         H4Dr13[-Q1,0,Q2,Q2-Q1,w,0,w,0]*DL[Q1,w]^0*DL[Q2,w]^0]+
551     NextT[Imp*H4Dr13[q,q-Q1,-Q1,0,w,0,w,0]*
552         H4Dr24[-Q1,0,Q2,Q2-Q1,w,0,w,0]*DL[Q1,w]^0*DL[Q2,w]^0]+
553     NextT[Imp*H4Dr24[q,q-Q1,-Q1,0,w,0,w,0]*
554         H4UnDr[-Q1,0,Q2,Q2-Q1,w,0,w,0]*DL[Q1,w]^0*DL[Q2,w]^1]+
555     NextT[Imp*H4Dr24[q,q-Q1,-Q1,0,w,0,w,0]*
556         H4Dr13[-Q1,0,Q2,Q2-Q1,w,0,w,0]*DL[Q1,w]^0*DL[Q2,w]^0]+
557     NextT[Imp*H4Dr24[q,q-Q1,-Q1,0,w,0,w,0]*
558         H4Dr24[-Q1,0,Q2,Q2-Q1,w,0,w,0]*DL[Q1,w]^0*DL[Q2,w]^0]
559 ]

```


Bibliography

- Abrahams, E., P. W. Anderson, P. A. Lee, and T. V. Ramakrishnan, 1981, *Quasiparticle lifetime in disordered two-dimensional metals*, [Phys. Rev. B](#) **24**, 6783.
- Abrahams, E., P. W. Anderson, D. C. Licciardello, and T. V. Ramakrishnan, 1979, *Scaling theory of localization: Absence of quantum diffusion in two dimensions*, [Phys. Rev. Lett.](#) **42**, 673.
- Abrikosov, A.A., I.E. Dzyaloshinski, and L.P. Gorkov, 1965, *Quantum Field Theoretical Methods in Statistical Physics*, International series of monographs in natural philosophy, v.4.
- Abrikosov, A.A., L.P. Gorkov, and I.E. Dzyaloshinski, 1975, *Methods of Quantum Field Theory in Statistical Physics*, Dover Books on Physics Series (Dover Publ.) ISBN 9780486632285.
- Akkermans, E., A. Comtet, J. Desbois, G. Montambaux, and C. Texier, 2000, *Spectral determinant on quantum graphs*, [Annals of Physics](#) **284** (1), 10, ISSN 0003-4916.
- Akkermans, E., and G. Montambaux, 2007, *Mesoscopic Physics of Electrons and Photons* (Cambridge Univ. Press) ISBN 9780521855129.
- Aleiner, I. L., B. L. Altshuler, and M. E. Gershenson, 1999, *Interaction effects and phase relaxation in disordered systems*, [Waves in Random Media](#) **9** (2), 201.
- Aleiner, I. L., and Ya. M. Blanter, 2002, *Inelastic scattering time for conductance fluctuations*, [Phys. Rev. B](#) **65**, 115317.
- Aleiner, I.L., P.W. Brouwer, and L.I. Glazman, 2002, *Quantum effects in coulomb blockade*, [Physics Reports](#) **358** (5-6), 309.
- Altland, A., S. Iida, A. Müller-Groeling, and H. A. Weidenmüller, 1992a, *Persistent currents in an ensemble of isolated, mesoscopic rings at zero temperature: a nonperturbative approach*, *EPL (Europhysics Letters)* **20** (2), 155.
- Altland, A., S. Iida, A. Müller-Groeling, and H.A. Weidenmüller, 1992b, *Persistent currents in an ensemble of isolated mesoscopic rings*, [Annals of Physics](#) **219** (1), 148.
- Altland, A., and B. Simons, 2006, *Condensed Matter Field Theory* (Cambridge University Press) ISBN 9780521845083.
- Altshuler, B. L., 1985, *Fluctuations in the extrinsic conductivity of disordered conductors*, *Sov. Phys. JETP Lett.* **41**, 648.
- Altshuler, B. L., A. G. Aronov, and D. E. Khmel'nitsky, 1982a, *Effects of electron-electron collisions with small energy transfers on quantum localisation*, *Journal of Physics C: Solid State Physics* **15** (36), 7367.

- Altshuler, B. L., A. G. Aronov, and B. Z. Spivak, 1981a, *The aaronov-bohm effect in disordered conductors*, JETP Lett. **33**, 94.
- Altshuler, B. L., A. G. Aronov, and B. Z. Spivak, 1981b, *Magneto-resistance of thin films and of wires in a longitudinal magnetic field*, JETP Lett. **33**, 499.
- Altshuler, B. L., A. G. Aronov, B. Z. Spivak, D. Yu. Sharvin, and Yu. V. Sharvin, 1982b, *Observation of the aaronov-bohm effect in hollow metal cylinders*, JETP Lett. **35**, 588.
- Altshuler, B. L., Y. Gefen, A. Kamenev, and L. S. Levitov, 1997, *Quasiparticle lifetime in a finite system: A nonperturbative approach*, Phys. Rev. Lett. **78**, 2803.
- Altshuler, B. L., D. Khmel'nitzkii, A. I. Larkin, and P. A. Lee, 1980, *Magneto-resistance and hall effect in a disordered two-dimensional electron gas*, Phys. Rev. B **22**, 5142.
- Altshuler, B. L., and B. Shklovskii, 1986, *Repulsion of energy levels and conductivity of disordered conductors*, Sov. Phys. JETP Lett. **64**, 127.
- Altshuler, B.L., and A.G. Aronov, 1979, *Damping of one-electron excitations in metals*, JETP Lett. **30**, 482.
- Altshuler, B.L., and A.G. Aronov, 1985, *Electron-electron interactions in disordered systems*, Modern problems in condensed matter sciences (North-Holland) ISBN 9780444869166.
- Altshuler, B.L., A.G. Aronov, and D.E. Khmel'nitsky, 1981c, *Suppression of localization effects by the high frequency field and the nyquist noise*, Solid State Communications **39** (5), 619 .
- Anderson, P. W., 1958, *Absence of diffusion in certain random lattices*, Phys. Rev. **109**, 1492.
- Aronov, A. G., and Yu. V. Sharvin, 1987, *Magnetic flux effects in disordered conductors*, Rev. Mod. Phys. **59**, 755.
- Baranger, H. U., and P. A. Mello, 1994, *Mesoscopic transport through chaotic cavities: A random s -matrix theory approach*, Phys. Rev. Lett. **73**, 142.
- Baranger, H. U., and P. A. Mello, 1995, *Effect of phase breaking on quantum transport through chaotic cavities*, Phys. Rev. B **51**, 4703.
- Beenakker, C. W. J., 1997, *Random-matrix theory of quantum transport*, Rev. Mod. Phys. **69**, 731.
- Bergmann, G., 1983, *Physical interpretation of weak localization: A time-of-flight experiment with conduction electrons*, Phys. Rev. B **28**, 2914.
- Bergmann, G., 1984, *Weak localization in thin films: a time-of-flight experiment with conduction electrons*, Physics Reports **107** (1), 1 .
- Blanter, Ya. M., 1996, *Electron-electron scattering rate in disordered mesoscopic systems*, Phys. Rev. B **54**, 12807.
- Blanter, Ya. M., and A. D. Mirlin, 1996, *Gor'kov and eliashberg linear-response theory: Rigorous derivation and limits of applicability*, Phys. Rev. B **53**, 12601.
- Blanter, Ya. M., and A. D. Mirlin, 1997, *Correlations of eigenfunctions in disordered systems*, Phys. Rev. E **55**, 6514.

- Blanter, Ya. M., and A. D. Mirlin, 1998, *Electron-electron interaction in disordered mesoscopic systems: Weak localization and mesoscopic fluctuations of polarizability and capacitance*, *Phys. Rev. B* **57**, 4566.
- Blanter, Ya. M., and A. D. Mirlin, 2001, *Frequency dependence of the magnetopolarizability of mesoscopic grains*, *Phys. Rev. B* **63**, 113315.
- Blanter, Ya. M., V. M. Vinokur, and L. I. Glazman, 2006, *Weak localization in metallic granular media*, *Phys. Rev. B* **73**, 165322.
- Bleszynski-Jayich, A. C., W. E. Shanks, B. Peaudecerf, E. Ginossar, F. von Oppen, L. Glazman, and J. G. E. Harris, 2009, *Persistent currents in normal metal rings*, *Science* **326** (5950), 272.
- Bluhm, Hendrik, Nicholas C. Koshnick, Julie A. Bert, Martin E. Huber, and Kathryn A. Moler, 2009, *Persistent currents in normal metal rings*, *Phys. Rev. Lett.* **102**, 136802.
- Blümel, R., and U. Smilansky, 1988, *Classical irregular scattering and its quantum-mechanical implications*, *Phys. Rev. Lett.* **60**, 477.
- Brezin, E., S. Hikami, and J. Zinn-Justin, 1980, *Generalized non-linear σ -models with gauge invariance*, *Nucl. Phys. B* **165**, 528.
- Brouwer, P. W., and C. W. J. Beenakker, 1995, *Effect of a voltage probe on the phase-coherent conductance of a ballistic chaotic cavity*, *Phys. Rev. B* **51**, 7739.
- Brouwer, P. W., and C. W. J. Beenakker, 1997, *Voltage-probe and imaginary-potential models for dephasing in a chaotic quantum dot*, *Phys. Rev. B* **55**, 4695.
- Brouwer, P.W., 1997, *On the Random-Matrix Theory of Quantum Transport*, Ph.D. thesis (Leiden University, Leiden, Netherlands).
- Bruus, H., and K. Flensberg, 2004, *Many-Body Quantum Theory in Condensed Matter Physics: An Introduction*, Oxford graduate texts in mathematics (OUP Oxford) ISBN 9780198566335.
- Bunder, J.E., K.B. Efetov, V.E. Kravtsov, O.M. Yevtushenko, and M.R. Zirnbauer, 2007, *Superbosonization formula and its application to random matrix theory*, *Journal of Statistical Physics* **129**, 809.
- Büttiker, M., 1986a, *Four-terminal phase-coherent conductance*, *Phys. Rev. Lett.* **57**, 1761.
- Büttiker, M., 1986b, *Role of quantum coherence in series resistors*, *Phys. Rev. B* **33**, 3020.
- Büttiker, M., Y. Imry, and R. Landauer, 1983, *Josephson behavior in small normal one-dimensional rings*, *Physics Letters A* **96** (7), 365 .
- Capron, T., C. Texier, G. Montambaux, D. Mailly, A. D. Wieck, and L. Saminadayar, 2013, *Ergodic versus diffusive decoherence in mesoscopic devices*, *Phys. Rev. B* **87**, 041307.
- Chakravarty, S., and A. Schmid, 1986, *Weak localization: The quasiclassical theory of electrons in a random potential*, *Physics Reports* **140** (4), 193.
- Chandrasekhar, V., R. A. Webb, M. J. Brady, M. B. Ketchen, W. J. Gallagher, and A. Kleinsasser, 1991, *Magnetic response of a single, isolated gold loop*, *Phys. Rev. Lett.* **67**, 3578.

- Cheung, H. F., Y. Gefen, E. K. Riedel, and W. H. Shih, 1988, *Persistent currents in small one-dimensional metal rings*, *Phys. Rev. B* **37**, 6050.
- Clarke, R. M., I. H. Chan, C. M. Marcus, C. I. Duruöz, J. S. Harris, K. Campman, and A. C. Gossard, 1995, *Temperature dependence of phase breaking in ballistic quantum dots*, *Phys. Rev. B* **52**, 2656.
- Cohen, Doron, Jan von Delft, Florian Marquardt, and Yoseph Imry, 2009, *Dephasing rate formula in the many-body context*, *Phys. Rev. B* **80**, 245410.
- Comtet, A., J. Desbois, and C. Texier, 2005, *Functionals of brownian motion, localization and metric graphs*, *Journal of Physics A: Mathematical and General* **38** (37), R341.
- Datta, S., 1997, *Electronic Transport in Mesoscopic Systems*, Cambridge Studies in Semiconductor Physics and Microelectronic Engineering (Cambridge University Press) ISBN 9780521599436.
- Deblock, R., R. Bel, B. Reulet, H. Bouchiat, and D. Mailly, 2002a, *Diamagnetic orbital response of mesoscopic silver rings*, *Phys. Rev. Lett.* **89**, 206803.
- Deblock, R., Y. Noat, H. Bouchiat, B. Reulet, and D. Mailly, 2000, *Measurements of flux-dependent screening in aharonov-bohm rings*, *Phys. Rev. Lett.* **84**, 5379.
- Deblock, R., Y. Noat, B. Reulet, H. Bouchiat, and D. Mailly, 2002b, *ac electric and magnetic responses of nonconnected aharonov-bohm rings*, *Phys. Rev. B* **65**, 075301.
- von Delft, J., F. Marquardt, R. A. Smith, and V. Ambegaokar, 2007, *Decoherence in weak localization. ii. bethe-salpeter calculation of the cooperon*, *Phys. Rev. B* **76**, 195332.
- Doucot, B., and R. Rammal, 1985, *Quantum oscillations in normal-metal networks*, *Phys. Rev. Lett.* **55**, 1148.
- Doucot, B., and R. Rammal, 1986, *Interference effects and magnetoresistance oscillations in normal-metal networks: I - weak localization approach*, *J. Phys. (Paris)* **47**, 973.
- Dressel, M., and M. Scheffler, 2006, *Verifying the drude response*, *Annalen der Physik* **15** (7-8), 535.
- Edwards, S. F., and P. W. Anderson, 1975, *Theory of spin glasses*, *Journal of Physics F: Metal Physics* **5** (5), 965.
- Efetov, K. B., 1995, *Temperature effects in quantum dots in the regime of chaotic dynamics*, *Phys. Rev. Lett.* **74**, 2299.
- Efetov, K. B., 1996, *Polarizability of small metal particles: "weak localization" effects*, *Phys. Rev. Lett.* **76**, 1908.
- Efetov, K. B., 1997, *Supersymmetry in Disorder and Chaos* (Cambridge Univ. Press) ISBN 9780521663823.
- Efetov, K. B., A. I. Larkin, and D. E. Khemlnitskii, 1980, *Interaction of diffusion modes in the theory of localization*, *Sov. Phys. JETP* **52**, 568.
- Efetov, K.B., 1983, *Supersymmetry and theory of disordered metals*, *Advances in Physics* **32** (1), 53.
- Ferrier, M., A. C. H. Rowe, S. Guéron, H. Bouchiat, C. Texier, and G. Montambaux, 2008, *Geometrical dependence of decoherence by electronic interactions in a GaAs/GaAlAs square network*, *Phys. Rev. Lett.* **100**, 146802.

- Fetter, A.L., and J.D. Walecka, 1971, *Quantum Theory of Many-Particle Systems*, Dover Books on Physics (Dover Publications) ISBN 9780486428277.
- Feynman, R. P., and A. R. Hibbs, 1965, *Quantum Mechanics and Path Integrals* (McGraw-Hill Companies) ISBN 0070206503.
- Fisher, Daniel S., and Patrick A. Lee, 1981, *Relation between conductivity and transmission matrix*, *Phys. Rev. B* **23**, 6851.
- Fukuyama, H., and E. Abrahams, 1983, *Inelastic scattering time in two-dimensional disordered metals*, *Phys. Rev. B* **27**, 5976.
- Fyodorov, Y. V., and A. D. Mirlin, 1991, *Scaling properties of localization in random band matrices: A σ -model approach*, *Phys. Rev. Lett.* **67**, 2405.
- García-García, A. M., and J. J. M. Verbaarschot, 2003, *Critical statistics in quantum chaos and calogero-sutherland model at finite temperature*, *Phys. Rev. E* **67**, 046104.
- Gell-Mann, M., and K. A. Brueckner, 1957, *Correlation energy of an electron gas at high density*, *Phys. Rev.* **106**, 364.
- Gorkov, L. P., and G. M. Eliashberg, 1965, *Minute metallic particles in an electromagnetic field*, *Sov. Phys. JETP* **21**, 940.
- Gorkov, L.P., A.I. Larkin, and D.E. Khmel'nitskii, 1979, *Particle conductivity in a two-dimensional random potential*, *JETP Lett.* **30**, 228.
- Hastings, M. B., A. D. Stone, and H. U. Baranger, 1994, *Inequivalence of weak localization and coherent backscattering*, *Phys. Rev. B* **50**, 8230.
- Hikami, S., 1981, *Anderson localization in a nonlinear- σ -model representation*, *Phys. Rev. B* **24**, 2671.
- Hikami, S., A. I. Larkin, and Y. Nagaoka, 1980, *Spin-orbit interaction and magnetoresistance in the two dimensional random system*, *Progress of Theoretical Physics* **63** (2), 707.
- Hubbard, J., 1959, *Calculation of partition functions*, *Phys. Rev. Lett.* **3**, 77.
- Huibers, A. G., J. A. Folk, S. R. Patel, C. M. Marcus, C. I. Duruöz, and J. S. Harris, 1999, *Low-temperature saturation of the dephasing time and effects of microwave radiation on open quantum dots*, *Phys. Rev. Lett.* **83**, 5090.
- Huibers, A. G., S. R. Patel, C. M. Marcus, P. W. Brouwer, C. I. Duruöz, and J. S. Harris, 1998a, *Distributions of the conductance and its parametric derivatives in quantum dots*, *Phys. Rev. Lett.* **81**, 1917.
- Huibers, A. G., M. Switkes, C. M. Marcus, K. Campman, and A. C. Gossard, 1998b, *Dephasing in open quantum dots*, *Phys. Rev. Lett.* **81**, 200.
- Imry, Y., 1986, *Directions in Condensed Matter Physics* (World Scientific) ISBN 9971978423.
- Imry, Y., 2002, *Introduction to Mesoscopic Physics* (Oxford University Press) ISBN 0198507380.
- Jackson, J.D., 1962, *Classical electrodynamics* (Wiley).

- Jalabert, R. A., J.-L. Pichard, and C. W. J. Beenakker, 1994, *Universal quantum signatures of chaos in ballistic transport*, EPL (Europhysics Letters) **27** (4), 255.
- Kamenev, A., 2005, *Many-body theory of non-equilibrium systems*, arXiv:cond-mat/0412296v2.
- Kamenev, A., 2011, *Field Theory of Non-Equilibrium Systems* (Cambridge University Press) ISBN 9781139500296.
- Kamenev, A., and Y. Gefen, 1997a, *Differences between statistical mechanics and thermodynamics on the mesoscopic scale*, *Phys. Rev. B* **56**, 1025.
- Kamenev, A., and Y. Gefen, 1997b, *Statistical ensembles and spectral correlations in mesoscopic systems*, *Chaos, Solitons & Fractals* **7/8**, 1229.
- Kamenev, A., B. Reulet, H. Bouchiat, and Y. Gefen, 1994, *Conductance of aharonov-bohm rings: From the discrete to the continuous spectrum limit*, EPL (Europhysics Letters) **28** (6), 391.
- Kamenev, Alex, and Yuval Gefen, 1993, *Static versus adiabatic response of mesoscopic systems: The role of the statistical ensemble*, *Phys. Rev. Lett.* **70**, 1976.
- Kane, C. L., R. A. Serota, and P. A. Lee, 1988, *Long-range correlations in disordered metals*, *Phys. Rev. B* **37**, 6701.
- Khmelnitskii, D.E., 1984, *Localization and coherent scattering of electrons*, *Physica B+C* **126** (1-3), 235 .
- Kravtsov, V. E., 2009, *Random Matrix Theory: Wigner-Dyson statistics and beyond. Lecture notes given at SISSA (Trieste, Italy)*, arXiv:0911.0639.
- Kravtsov, V. E., and A. D. Mirlin, 1994, *Level statistics in a metallic sample: corrections to the wigner-dyson distribution*, *JETP Lett.* **60**, 656.
- Kupferschmidt, J. N., and P. W. Brouwer, 2008, *Temperature and magnetic-field dependence of the quantum corrections to the conductance of a network of quantum dots*, *Phys. Rev. B* **78**, 125313.
- Kurland, I. L., I. L. Aleiner, and B. L. Altshuler, 2000, *Mesoscopic magnetization fluctuations for metallic grains close to the stoner instability*, *Phys. Rev. B* **62**, 14886.
- Landauer, R., 1957, *Spatial variation of currents and fields due to localized scatterers in metallic conduction*, *IBM Journal of Research and Development* **1** (3), 223 .
- Langer, J. S., and T. Neal, 1966, *Breakdown of the concentration expansion for the impurity resistivity of metals*, *Phys. Rev. Lett.* **16**, 984.
- Larkin, A.I., and Yu. N. Ovchinnikov, 1975, *Nonlinear conductivity of superconductors in the mixed state*, *Sov. Phys. JETP* **41**, 960.
- Lee, P. A., and T. V. Ramakrishnan, 1985, *Disordered electronic systems*, *Rev. Mod. Phys.* **57**, 287.
- Lee, P. A., A. D. Stone, and H. Fukuyama, 1987, *Universal conductance fluctuations in metals: Effects of finite temperature, interactions, and magnetic field*, *Phys. Rev. B* **35**, 1039.
- Lee, P. A., and A. Douglas Stone, 1985, *Universal conductance fluctuations in metals*, *Phys. Rev. Lett.* **55**, 1622.

- Lehle, W., and A. Schmid, 1995, *Mesoscopic systems with fixed number of electrons*, [Annalen der Physik](#) **507** (5), 451.
- Lerner, I.V., 1990, *Distribution functions of mesoscopic fluctuations and applicability of the one-parameter scaling*, [Physica A: Statistical Mechanics and its Applications](#) **167** (1), 1 .
- Lévy, L. P., G. Dolan, J. Dunsmuir, and H. Bouchiat, 1990, *Magnetization of mesoscopic copper rings: Evidence for persistent currents*, [Phys. Rev. Lett.](#) **64**, 2074.
- Ludwig, T., and A. D. Mirlin, 2004, *Interaction-induced dephasing of aharonov-bohm oscillations*, [Phys. Rev. B](#) **69**, 193306.
- Madelung, O., 1978, *Introduction to Solid-State Theory* (Springer-Verlag) ISBN 354060443X.
- Marquardt, F., J. von Delft, R. A. Smith, and V. Ambegaokar, 2007, *Decoherence in weak localization. i. pauli principle in influence functional*, [Phys. Rev. B](#) **76**, 195331.
- McCann, E., and I. V. Lerner, 1996, *Mesoscopic conductance fluctuations in dirty quantum dots with single channel leads*, [Journal of Physics: Condensed Matter](#) **8** (36), 6719.
- McCann, E., and I. V. Lerner, 1998, *Effect of dephasing on mesoscopic conductance fluctuations in quantum dots with single-channel leads*, [Phys. Rev. B](#) **57**, 7219.
- Mehta, M.L., 2004, *Random Matrices*, Pure and Applied Mathematics (Elsevier Science) ISBN 9780080474113.
- Mirlin, A. D., 2000, *Statistics of energy levels and eigenfunctions in disordered and chaotic systems: Supersymmetry approach*, arXiv:cond-mat/0006421.
- Noat, Y., R. Deblock, B. Reulet, and H. Bouchiat, 2002, *Magnetopolarizability of mesoscopic systems*, [Phys. Rev. B](#) **65**, 075305.
- Noat, Y., B. Reulet, and H. Bouchiat, 1996, *Magneto-polarisability of mesoscopic rings*, [EPL \(Europhysics Letters\)](#) **36**, 701.
- Ostrovsky, P. M., and V. E. Kravtsov, 2013, *unpublished*.
- Pascaud, M., and G. Montambaux, 1999, *Persistent currents on networks*, [Phys. Rev. Lett.](#) **82**, 4512.
- Pines, D., and P. Nozieres, 1989, *The Theory of Quantum Liquids* (Adison-Wesley) ISBN 0201094290.
- Rammer, J., 2007, *Quantum field theory of non-equilibrium states*, revised ed. (Cambridge Univ. Press) ISBN 9780486632285.
- Rammer, J., and H. Smith, 1986, *Quantum field-theoretical methods in transport theory of metals*, [Rev. Mod. Phys.](#) **58**, 323.
- Reulet, Bertrand, Michel Ramin, Hélène Bouchiat, and Dominique Mailly, 1995, *Dynamic response of isolated aharonov-bohm rings coupled to an electromagnetic resonator*, [Phys. Rev. Lett.](#) **75**, 124.
- Rice, M. J., W. R. Schneider, and S. Strässler, 1973, *Electronic polarizabilities of very small metallic particles and thin films*, [Phys. Rev. B](#) **8**, 474.

- Richardella, A., P. Roushan, S. Mack, B. Zhou, D. A. Huse, D. D. Awschalom, and A. Yazdani, 2010, *Visualizing critical correlations near the metal-insulator transition in $ga_1-xm_nx_s$* , [Science](#) **327** (5966), 665.
- Santhanam, P., 1989, *Weak localization in normal-metal loops: Influence of boundary conditions*, [Phys. Rev. B](#) **39**, 2541.
- dos Santos, J. M. B. Lopes, 1983, *Self-consistent calculation of the quasiparticle lifetime in two-dimensional disordered metals*, [Phys. Rev. B](#) **28**, 1189.
- Schäfer, L., and F. Wegner, 1980, *Disordered system with n orbitals per site: Lagrange formulation, hyperbolic symmetry, and goldstone modes*, [Zeitschrift für Physik B: Condensed Matter](#) **38**, 113.
- Schäffer, M., 2012, *Interactions-induced dephasing in AC-driven disordered normal metals*, Master's thesis (Ludwig-Maximilians-Universität München, Munich, Germany).
- Schmid, A., 1974, *On the dynamics of electrons in an impure metal*, [Zeitschrift für Physik](#) **271**, 251.
- Schmid, A., 1991, *Persistent currents in mesoscopic rings by suppression of charge fluctuations*, [Phys. Rev. Lett.](#) **66**, 80.
- Schwabl, F., 2002, *Quantum Mechanics*, Advanced Texts in Physics (Springer) ISBN 9783540431091.
- Serota, R. A., Shechao Feng, C. Kane, and P. A. Lee, 1987, *Conductance fluctuations in small disordered conductors: Thin-lead and isolated geometries*, [Phys. Rev. B](#) **36**, 5031.
- Sharvin, D. Yu., and Yu. V. Sharvin, 1981, *Magnetic-flux quantization in a cylindrical film of a normal metal*, [JETP Lett.](#) **34**, 272.
- Sivan, U., Y. Imry, and A. G. Aronov, 1994, *Quasi-particle lifetime in a quantum dot*, [EPL \(Europhysics Letters\)](#) **28** (2), 115.
- Smith, R. A., I. V. Lerner, and B. L. Altshuler, 1998, *Spectral statistics in disordered metals: A trajectories approach*, [Phys. Rev. B](#) **58**, 10343.
- Stone, A. Douglas, 1985, *Magnetoresistance fluctuations in mesoscopic wires and rings*, [Phys. Rev. Lett.](#) **54**, 2692.
- Texier, C., 2007, *Effect of connecting wires on the decoherence due to electron-electron interaction in a metallic ring*, [Phys. Rev. B](#) **76**, 153312.
- Texier, C., 2008, *On the spectrum of the laplace operator of metric graphs attached at a vertex-spectral determinant approach*, [Journal of Physics A: Mathematical and Theoretical](#) **41** (8), 085207.
- Texier, C., P. Delplace, and G. Montambaux, 2009, *Quantum oscillations and decoherence due to electron-electron interaction in metallic networks and hollow cylinders*, [Phys. Rev. B](#) **80**, 205413.
- Texier, C., and G. Montambaux, 2004, *Weak localization in multiterminal networks of diffusive wires*, [Phys. Rev. Lett.](#) **92**, 186801.
- Texier, C., and G. Montambaux, 2005, *Dephasing due to electron-electron interaction in a diffusive ring*, [Phys. Rev. B](#) **72**, 115327.

- Texier, C., and G. Montambaux, 2007, *Altshuler-aronov correction to the conductivity of a large metallic square network*, *Phys. Rev. B* **76**, 094202.
- Verbaarschot, J.J.M., H.A. Weidenmüller, and M.R. Zirnbauer, 1985, *Grassmann integration in stochastic quantum physics: The case of compound-nucleus scattering*, *Physics Reports* **129** (6), 367 .
- Vollhardt, D., and P. Wölfle, 1980a, *Anderson localization in $d \sim 2$ dimensions: A self-consistent diagrammatic theory*, *Phys. Rev. Lett.* **45**, 842.
- Vollhardt, D., and P. Wölfle, 1980b, *Diagrammatic, self-consistent treatment of the anderson localization problem in $d \leq 2$ dimensions*, *Phys. Rev. B* **22**, 4666.
- Webb, R. A., S. Washburn, C. P. Umbach, and R. B. Laibowitz, 1985, *Observation of $\frac{h}{e}$ aharonov-bohm oscillations in normal-metal rings*, *Phys. Rev. Lett.* **54**, 2696.
- Weidenmüller, H. A., 1990, *Scattering theory and conductance fluctuations in mesoscopic systems*, *Physica A: Statistical Mechanics and its Applications* **167** (1), 28 .
- Wigner, E. P., and L. Eisenbud, 1947, *Higher angular momenta and long range interaction in resonance reactions*, *Phys. Rev.* **72**, 29.
- Yevtushenko, Oleg, and Vladimir E Kravtsov, 2003, *Virial expansion for almost diagonal random matrices*, *Journal of Physics A: Mathematical and General* **36** (30), 8265.
- Yevtushenko, Oleg, and Alexander Ossipov, 2007, *A supersymmetry approach to almost diagonal random matrices*, *Journal of Physics A: Mathematical and Theoretical* **40** (18), 4691.
- Zagoskin, A.M., 1998, *Quantum Theory of Many-Body Systems: Techniques and Applications*, Graduate Texts in Contemporary Physics Series (Springer Verlag) ISBN 9780387983844.

Acknowledgments

Foremost, I would like to thank Oleg M. Yevtushenko, who guided me through most of this work. Without his patience and experience this would not have been possible.

Also, I want to thank Jan von Delft for the opportunity to pursue my Ph.D. in his group, and his constant support in every aspect of this work.

I owe my deepest gratitude to my collaborators, Igor V. Lerner, Christophe Texier, Pavel M. Ostrovski, and Florian Marquardt. It was a great pleasure working with you.

Many thanks to Bärbel, Dietmar, Matthias, Markus, Sandra, and all my colleagues at the Arnold Sommerfeld Center for Theoretical Physics.

Furthermore, I acknowledge the generous financial support from the DFG through DE 730/8-1, SFB-TR-12 and the Cluster of Excellence, Nanosystems Initiative Munich.

Curriculum Vitae

Dipl.-Phys. Maximilian Treiber

Date of Birth: 22.03.1981

Place of Birth: Göttingen, Germany

Academic Education

- 2009 – 2013 Ph. D. studies of theoretical solid state physics,
Ludwig-Maximilians-University, Munich
- 2008 Diploma in physics,
Technical University of Munich
- 2004 – 2005 ERASMUS student exchange program in Paris, France,
“University Paris 6: Pierre et Marie Curie”
- 2001 – 2008 Academic studies of physics,
Technical University of Munich
- 2000 – 2001 Compulsory community service in Hann. Münden,
“Mobile Kranken- und Seniorenpflege Salzmann”
- 2000 Allgemeine Hochschulreife
- 1993 – 2000 Grotefend-Gymnasium Münden, Hann. Münden
- 1992 – 1993 Orientierungsstufe 2., Hann. Münden
- 1991 – 1992 Orientierungsstufe Lutherschule, Göttingen
- 1990 – 1991 Hölty-Grundschule, Göttingen
- 1989 – 1990 Wilhelm-Busch-Grundschule, Göttingen
- 1987 – 1989 Hölty-Grundschule, Göttingen